CAPSTONE SCENARIO APPLICATIONS OF CONSEQUENCE-BASED RISK MANAGEMENT FOR THE MEMPHIS TESTBED

Joshua S. Steelman and Jerome F. Hajjar

A Report of the Mid-America Earthquake Center

Mid-America Earthquake Center
1241 Newmark Civil Engineering Laboratory
205 North Mathews Avenue
University of Illinois at Urbana-Champaign
Urbana, Illinois 61801

September 2008

ACKNOWLEDGEMENTS

This research was supported by the Mid-America Earthquake Center, headquartered at the University of Illinois at Urbana-Champaign, under NSF Grant No. EEC-97010785, and by the University of Illinois at Urbana-Champaign. The authors would like to thank the researchers throughout the MAE Center who have provided guidance and information for this research. Professors Glenn Rix and Junho Song, in particular, provided extensive assistance during the development of the analytical framework employed in this report. Any opinions, findings, and conclusions or recommendations expressed in this material are those of the authors and do not necessarily reflect the views of the National Science Foundation or other sponsors.

TABLE OF CONTENTS

1 INTRODUCTION

A capstone goal of the Memphis Testbed (MTB), and the MAE Center research program in consequence-based risk management, is to complete a detailed study of seismic event effects on the city of Memphis, Tennessee. The completion of this study relies heavily on the aggregated research results from the ten-year period of MAE Center research, culminating in implementation within MAEViz, the consequence-based risk management (CRM) software system developed by the MAE Center (Elnashai and Hajjar, 2006; Hajjar and Elnashai, 2006; Myers and Spencer, 2005; Spencer et al., 2005; MAEviz, 2008).

MAEViz has been developed to provide an open-source option for regional loss assessment research. Other research groups have also worked to develop programs with a similar goal, such as the Alliance for Global Open Risk Analysis (AGORA) (http://www.risk-agora.org/), and Open Seismic Hazard Analysis (OpenSHA) (http://www.opensha.org/). These programs all share the objectives of providing risk assessment tools which are both more transparent and more flexible in terms of analysis framework methodology and algorithms. The state-of-the-art in earthquake loss modeling programs has been investigated and documented recently for Europe (Strasser, 2008). Strasser (2008) compared five available loss estimation packages which are in use in Europe by employing a case study of Istanbul, which found that the results of the various packages are reasonably consistent.

Finally, Pinho et al. (2008) investigated uncertainties and discrepancies which occur in HAZUS as well as the three most well-established commercial risk assessment packages: AIR, EQECAT, and RMS. Pinho et al. (2008) emphasizes the need for greater transparency in commercial risk assessments and improved communication of inherent uncertainties to users, noting the availability of the aforementioned programs. Pinho et al. (2008) also promotes a fundamental shift in the prevailing paradigm within the loss assessment and insurance and reinsurance industries, which currently focuses on providing deterministic “best estimates”, to account for uncertainties as a component of operational decision-making. In closing, Pinho et al. (2008) recommends further development and collaboration among all interested parties with respect to open-source software to maximize transparency during loss estimation studies.

Several publications have been reviewed in preparation for developing the capstone scenario plan, including “Guidelines for Developing an Earthquake Scenario” (Pruess and Godfrey, 2006), “Comparative Analysis of HAZUS-MH Runs for Shelby County, TN and Tate County, MO” (Pezeshk, 1999), “An Assessment of Damage and Casualties for Six cities in the Central United States Resulting from Earthquakes in the New Madrid Seismic Zone” (CUSEC, 1985), “Comparison Study of the 1985 CUSEC Six Cities Study Using HAZUS” (CUSEC, 2003) , and “Loss Assessment of Memphis Buildings” (Abrams and Shinozuka, 1997), in addition to three reports that summarize loss assessment studies of other regions (Wong et al., 2005; Ballantyne et al., 2005; Reis et al., 2001).

Pruess and Godfrey (2006) provide an excellent general overview for the process of developing an earthquake scenario. The work of Pezeshk (2005) provides a general overview of expected losses for Shelby County, TN. Pezeshk (2005) is a risk assessment study using a Level 1 HAZUS Analysis (FEMA, 2005) for Shelby County, TN, considering probabilistic hazard with a 2500 year return period.

CUSEC (1985) reported results for a six-city region in and around the Mississippi Embayment, including Memphis, TN. CUSEC (1985) used maximum credible events of Ms 7.6 and 8.6. The report considered the six cities independently, with separate seismic events for each. When describing the location of the epicenters chosen for the scenarios, the locations were selected within the New Madrid Seismic Zone to be as close to each city as was reasonable. The study region was limited to incorporated areas (i.e., all assets outside "city limits" are neglected). CUSEC (2003) conducted a Level 1 HAZUS (FEMA, 2001) analysis, and compared the results with those obtained from CUSEC (1985). CUSEC (2003) used $\boldsymbol{M_w}$ 6.5 and 7.5, and located the events at the historic epicenters for the 1811-1812 events. CUSEC (2003) also used default HAZUS inventory for census tracts in the study region near Memphis. CUSEC (2003) included inventory in tracts that were not incorporated (i.e., outside city limits). Both studies provide insight into methodologies for performing comprehensive scenario analyses.

Abrams and Shinozuka (1997) performed a comprehensive loss assessment using rigorous modeling for hazard, inventory, and vulnerability. Ground hazard considered the effects of the Embayment geology, rather than using typical USGS and NEHRP methodology to estimate hazard. Abrams and Shinozuka (1997) also used Tax Assessor records to develop a refined inventory database, and advanced engineering analysis to develop fragility models for URM and reinforced concrete structures. The MAE Center research which is integrated in MAEViz closely follows the approach of Abrams and Shinozuka (1997).

Additionally, the MAE Center has published a report for a study of seismic hazards in the Central United States (US) sponsored by the Federal Emergency Management Agency (FEMA) (Elnashai et al., 2008) using HAZUS-MH MR2 (FEMA, 2006). The report focuses on the hazard originating from the New Madrid Seismic Zone (NMSZ), specifically based on a source moment magnitude, $\boldsymbol{M_w}$, of 7.7, and the associated rupture of the three segments of the New Madrid Fault. The estimated impacts of the seismic hazard are reported for the eight surrounding states: Alabama, Arkansas, Illinois, Indiana, Kentucky, Mississippi, Missouri, and Tennessee. The report also includes estimates of the impacts of seismic sources outside the NMSZ for Indiana and Alabama. In the case of Indiana, the seismic hazard originates from a source event with $\boldsymbol{M_w}$ 7.1 in the Wabash Valley Seismic Zone along the southern border of Illinois and Indiana. For Alabama, the seismic hazard originates from a source event with $\boldsymbol{M_w}$ 5.9 in the East Tennessee Seismic Zone which runs along the western side of the Appalachian Mountains.

The MAE Center study of the Central U.S. incorporated ground shaking intensity maps provided by the United States Geological Survey (USGS), and also employed the liquefaction

algorithms available in HAZUS-MH MR2. The default inventory data was updated for lifeline systems and critical facilities to reflect improved data available from the HSIP Gold Dataset (PMH, 2006) and a previous study performed for Illinois by the MAE Center (MAEC, 2007), while partnering with FEMA and the Illinois Emergency Management Agency. The study found that Tennessee was projected to be the most severely impacted by the NMSZ hazard, with a projected direct economic loss estimate in excess of $56 billion.

A number of other risk assessments have also been performed and documented recently, notably with concentrations in southern and southeastern Europe and Turkey. In Bal et al. (2008), the Displacement-Based Earthquake Loss Assessment (DBELA) approach (Crowley et al., 2004) is implemented first in a Monte Carlo simulation study and then in a regional loss assessment using refined inventory data, vulnerability estimation, and damage ratios (coefficients used to determine the economic loss associated with the physical damage state of a building as determined by displacement demands) focusing on concrete frame and unreinforced masonry buildings to project losses for a single earthquake scenario near Istanbul.

In Erdik et al. (2008), a range of loss assessment tiers are proposed with a focus on rapid loss assessment. Thus, to minimize computation time, rough approximations of building stock data and hazard would be used directly to estimate losses in terms of building damage and casualties, or if longer computation times are acceptable, or higher accuracy is required, refinements may be supplied for hazard and inventory components, and vulnerability may be evaluated by use of empirically based intensity measure formulations or by use of spectral displacements deemed to be consistent with the supplied hazard. The 1999 Kocaeli earthquake was used as a case study to demonstrate the application of the system.

Teramo et al. (2008) conducted a scenario investigation of Messina, Italy to estimate damage in the city based on a seismic event similar to the 1908 event which caused nearly complete destruction of the city at that time. The authors estimate that the losses of the 1908 earthquake, converted to present day value, would be more than 2 billion Euros, or more than about 2.5 billion US dollars. A simplified pushover-based set of stick-element models are used to estimate structural capacities of concrete and masonry structures in the building stock. The resulting damage estimate projected a large percentage of heavily damaged structures, including an estimate of almost 40% of buildings expected to collapse or to be near collapse. A secondary objective unique to this study is to project the building damage as a component of response planning with respect to availability of transportation routes, based on the assumption that heavily damaged structures will generate significant debris and that nearby roadways are therefore more likely to be congested or blocked as a consequence.

Finally, Spence et al. (2008) considered uncertainties originating within various earthquake loss estimation approaches in use in Europe were investigated with respect to projected losses in Istanbul. The study used two bedrock ground motion time histories: one record from the 1999 Kocaeli, Turkey earthquake, and one synthetic time history record developed specifically for

Istanbul. Various methods were employed for hazard modeling, vulnerability assessment, and loss correlation with physical damage, but the inventory set was held constant in each case with respect to building structure types, heights, counts, and occupancy rates. The study found significant variation across scenarios with increasing uncertainty from building damage estimates, to collapse rates, and finally with maximum variation associated with casualty rates.

2 OVERVIEW

The capstone scenarios presented in this document focus primarily on the more damaging of two potential seismic sources, both of which are located on the Blytheville Arch segment of the New Madrid fault system. A large magnitude source at a greater distance (M_w 7.9 at Blytheville, AR), and a moderate magnitude source nearer to the study region (M_w 6.2 at Marked Tree, AR) were considered. The large magnitude event was found to be the more significant of the two sources for the study region in this report. The analyses incorporate advanced hazard modeling appropriate for the local geology to represent ground shaking and ground failure hazards which act on high resolution building inventory data for the study region. The building stock is represented by point-wise entities throughout the study region, and total nearly 300,000 individual assets. The building and bridge inventory damage is estimated by applying vulnerability formulations that were developed specifically to represent the construction in the study region, and Mid-America in general, and that also implicitly consider ground motion characteristics for the study region through the application of synthetic ground motion records in nonlinear dynamic analyses. Probabilistic damage factors are applied to the damage predictions to estimate the direct economic loss for the buildings and bridges in the study region. In addition to these analyses, various other economic and social impacts are considered as extensions of the physical damage to the buildings in the study region, including business interruption losses, casualties, displaced population, and short term shelter requirements. Finally, decision support algorithms are applied to investigate optimum approaches for mitigation efforts. All of these components are synthesized and analyzed within the GIS environment of MAEViz.

3 INVENTORY COLLECTION

The inventory used in seismic risk assessments can generally be broken down into three subsets: building stock, transportation lifelines, and utility lifelines. Each of these can be further subdivided into other sub-groups, depending on the objective of the study. This section describes the available data and the provenance and reliability of the data for the capstone scenarios. All inventory data considered within the capstone scenarios is spatially bounded by the extents of Shelby County, Tennessee.

3.1 Building Stock Inventory

Building stock inventory for Shelby County is based primarily on data obtained from the Shelby County Tax Assessor's Database (French and Muthukumar, 2006). The MTB capstone scenarios consider point-wise inventory for all building stock assets. Essential facility inventory is also included in the point-wise building stock data. Building stock inventory data used for the capstone scenarios is derived from passing the Tax Assessor's Database through a neural network model (French and Muthukumar, 2006). The building stock dataset includes 292,438 records, and an exposed building replacement value totaling approximately $35.27 billion. For comparison, the building stock data included by default for HAZUS-MH MR2 (FEMA, 2006) studies of the same study region, which provides only aggregated information per census tract for earthquake scenarios, indicate that there are 293,443 buildings with a total replacement value of $58.63 billion.

Assignment of characteristics by the neural network model is not perfect, so the building data obtained in this way includes uncertainties in various data fields (e.g., structure type, occupancy type, replacement value) (French and Muthukumar, 2006). The primary source of uncertainty for the building stock is structure type, and the MTB capstone scenarios consider the effects of structure type uncertainty on the outcome of the regional risk assessments, based on the information available from the neural network model and corresponding validation surveys for the implemented building stock dataset.

Figure 1 through Figure 7 and Table 1 through Table 6 are provided to illustrate the building stock characteristics in the study region, both by count of individual structures and by dollar value exposure, as well as providing comparisons with the default data used by HAZUS-MH MR2 (FEMA, 2006) for the study region. Descriptions of structure types and occupancy classes are provided in Appendix A. The building stock in the study region is dominated by single family residences, which are typically one- or two-story wood frame structures within the Residential occupancy, as shown in Table 1 and Table 2. Table 1 shows the total exposure in terms of replacement value for the building stock of the study region, distributed by general occupancy and structure type. The terminology used here and in following sections typically follows conventions used by HAZUS. For example, the replacement value exposures are similar

to the sum of structural and nonstructural values in HAZUS, and neglect the values of building contents.

In accordance with guidance from French and Muthukumar (2006), appraised value is treated as approximately equivalent to replacement value. As shown in Table 1, the primary concentration of value for the study region is found in residential wood frame structures (73.8%), followed by commercial concrete (6.7%), steel (6.5%), and masonry (3.9%). Similarly, Table 2 shows building count for the building stock of the study region, also distributed by general occupancy and structure type. Since residential structures are generally smaller and have a lower replacement value per unit floor area, the concentration of building count in wood frame residential structures is even more pronounced than building exposure values. As shown in Table 2, the primary concentration of building count for the study region is found in residential wood frame structures (93.4%), followed by commercial steel (1.9%) and masonry (1.8%), and then residential masonry (1.0%).

The Residential General Occupancy is clearly the most significant, both in terms of exposure and building count, as a consequence of the large number of single-family residences, which constitute 91.2% of all buildings, and among those buildings, 98.9% are small wood frames (W1). The building exposure and count distributions are markedly different in the non-single family residence inventory relative to the wood frame dominated single-family residences, as shown in Table 3 and Table 4.

Table 1. Exposure Distribution by Structure and Occupancy Types

		GENERAL OCCUPANCY							
		RES	COM	IND	AGR	REL	GOV	EDU	Grand Total
GENERAL STRUCTURE TYPE	C	0.8%	6.7%	2.8%	0.0%	0.0%	0.0%	0.0%	10.4%
	M	2.4%	3.9%	0.5%	0.0%	0.0%	0.0%	0.0%	6.8%
	S	1.0%	6.5%	1.0%	0.0%	0.0%	0.0%	0.0%	8.5%
	W	73.8%	0.5%	0.0%	0.0%	0.0%	0.0%	0.0%	74.3%
	Grand Total	78.0%	17.6%	4.3%	0.0%	0.1%	0.0%	0.1%	100.0%

Table 2. Building Count Distribution by Structure and Occupancy Types

		GENERAL OCCUPANCY							
		RES	COM	IND	AGR	REL	GOV	EDU	Grand Total
GENERAL STRUCTURE TYPE	C	0.1%	0.4%	0.1%	0.0%	0.0%	0.0%	0.0%	0.6%
	M	1.0%	1.8%	0.2%	0.0%	0.0%	0.0%	0.0%	3.0%
	S	0.2%	1.9%	0.4%	0.0%	0.0%	0.0%	0.0%	2.5%
	W	93.4%	0.4%	0.0%	0.0%	0.0%	0.0%	0.0%	93.8%
	Grand Total	94.7%	4.5%	0.7%	0.0%	0.0%	0.0%	0.0%	100.0%

*See Appendix A for structure and occupancy types.

Table 3. Exposure Distribution by Structure and Occupancy Types Among Non-Single Family Residences

		GENERAL OCCUPANCY							
		RES	COM	IND	AGR	REL	GOV	EDU	Grand Total
GENERAL STRUCTURE TYPE	C	2.74%	23.02%	9.60%	0.00%	0.01%	0.00%	0.02%	35.39%
	M	8.10%	13.36%	1.76%	0.00%	0.03%	0.02%	0.11%	23.37%
	S	3.37%	22.20%	3.29%	0.00%	0.13%	0.01%	0.08%	29.07%
	W	10.32%	1.79%	0.04%	0.00%	0.02%	0.00%	0.01%	12.16%
	Grand Total	24.52%	60.37%	14.69%	0.00%	0.17%	0.03%	0.21%	100.00%

Table 4. Building Count Distribution by Structure and Occupancy Types Among Non-Single Family Residences

		GENERAL OCCUPANCY							
		RES	COM	IND	AGR	REL	GOV	EDU	Grand Total
GENERAL STRUCTURE TYPE	C	1.33%	4.52%	1.26%	0.00%	0.01%	0.01%	0.17%	7.30%
	M	11.32%	19.97%	2.58%	0.00%	0.07%	0.09%	0.26%	34.30%
	S	1.79%	21.99%	4.19%	0.00%	0.06%	0.04%	0.10%	28.17%
	W	25.01%	5.04%	0.13%	0.00%	0.03%	0.00%	0.02%	30.23%
	Grand Total	39.45%	51.52%	8.16%	0.01%	0.17%	0.14%	0.55%	100.00%

*See Appendix A for structure and occupancy types.

Further investigation of the single-family residence occupancy reveals that the distribution of structure types in the single-family residence class (HAZUS classification RES1) is different from the default HAZUS mapping would indicate. Figure 1 and Figure 2 show the distribution of contributing structure types to the RES1 occupancy. According to the HAZUS default mapping, W1 constitutes 90% of the RES1 structures, with the remaining 10% classified as URM. The data developed by French and Muthukumar (2006) showed concentrations of 93.9% of the RES1 exposure and 99.0% of the building count in RES1 were associated with W1 structures. W2 structures then accounted for 6.1% of the RES1 exposure and 1.0% of the building count.

The dataset from French and Muthukumar (2006) also included 18 URM, 11 RM, 6 S3, and 3 PC2 structures. Although the URM and RM may be reasonable for single family residences, light steel frames (S3) and precast concrete frames (PC2) are highly unusual choices for framing of single-family residential structures. The occurrence of such structure types and their frequencies of prediction by the neural network model are, however, consistent with expectations for the development of a large and detailed dataset, such as point-wise inventory for an entire county. Either the structure type assignments are accurate, or the assignments are anomalies generated by unusual circumstances within the neural network model. The dataset has been analyzed assuming the assignment was correct (while also accounting for structure type uncertainty, discussed later)

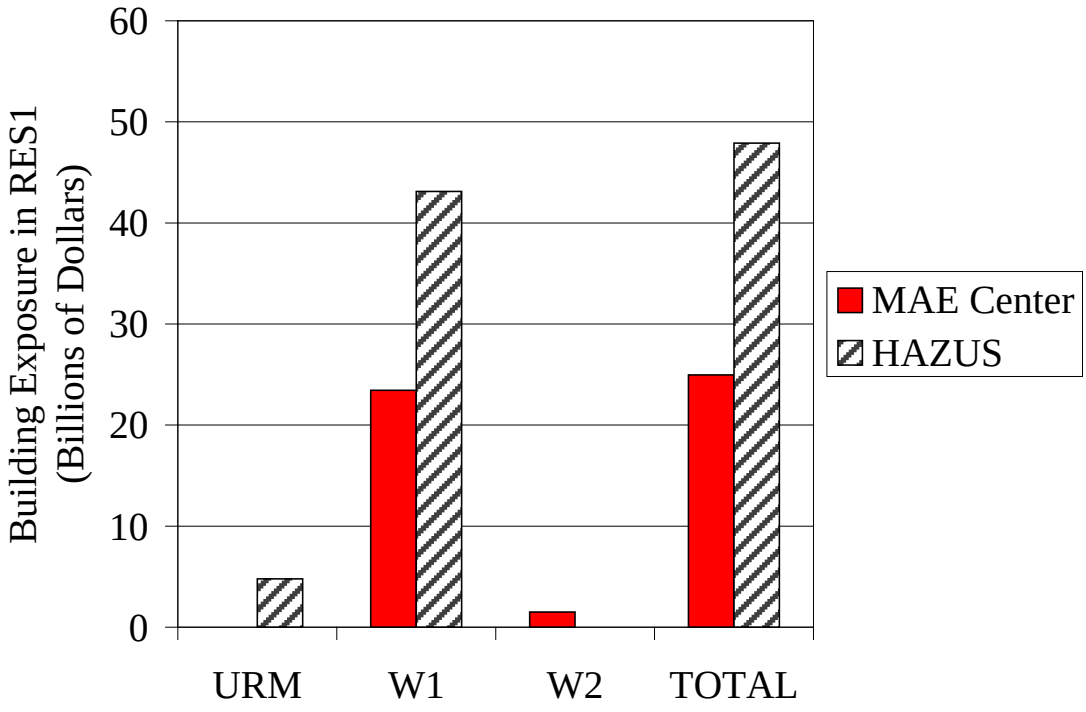

Figure 1. Single-Family Residence Exposure by Structure Type

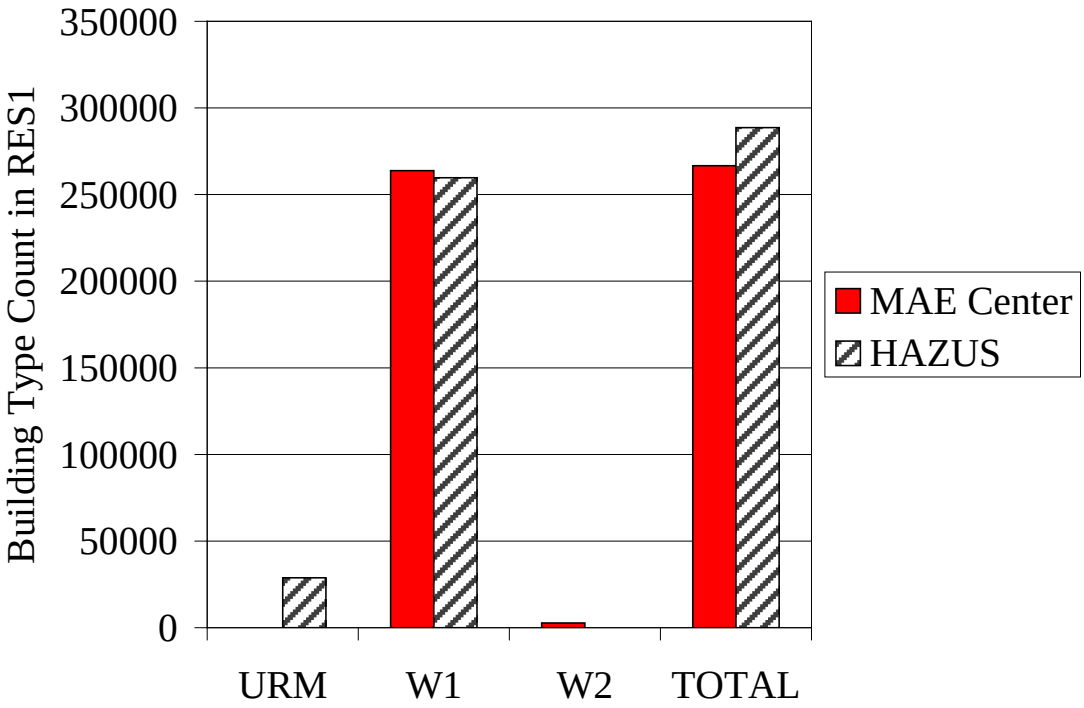

Figure 2. Single-Family Residence Building Count by Structure Type

Figure 3 and Figure 4 show the distribution of non-single-family buildings by exposure and building count, respectively, sorted by general occupancy. In these charts, the Residential occupancy does not include RES1. Even without including the single-family residences, the general residential occupancy, primarily constituted by multi-family residences, accounts for 23% of the remaining exposure and 39% of the remaining buildings by count. The other significant influence in the study region is the Commercial general occupancy, which accounts for 60.4% of the exposure and 51.5% of the remaining buildings by count. The Industrial sector is not negligible, but is smaller than the Commercial sector, having only 14.7% of the exposure and 8.2% of the remaining building stock by count.

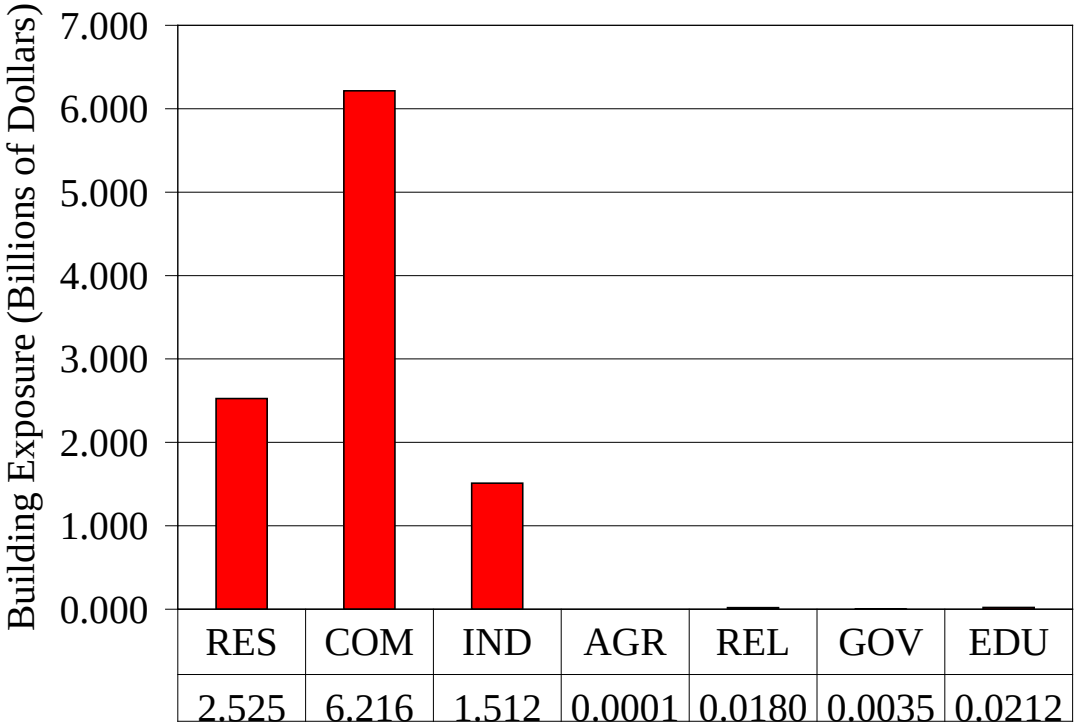

Figure 3. Non-Single-Family Residence Exposure by General Occupancy

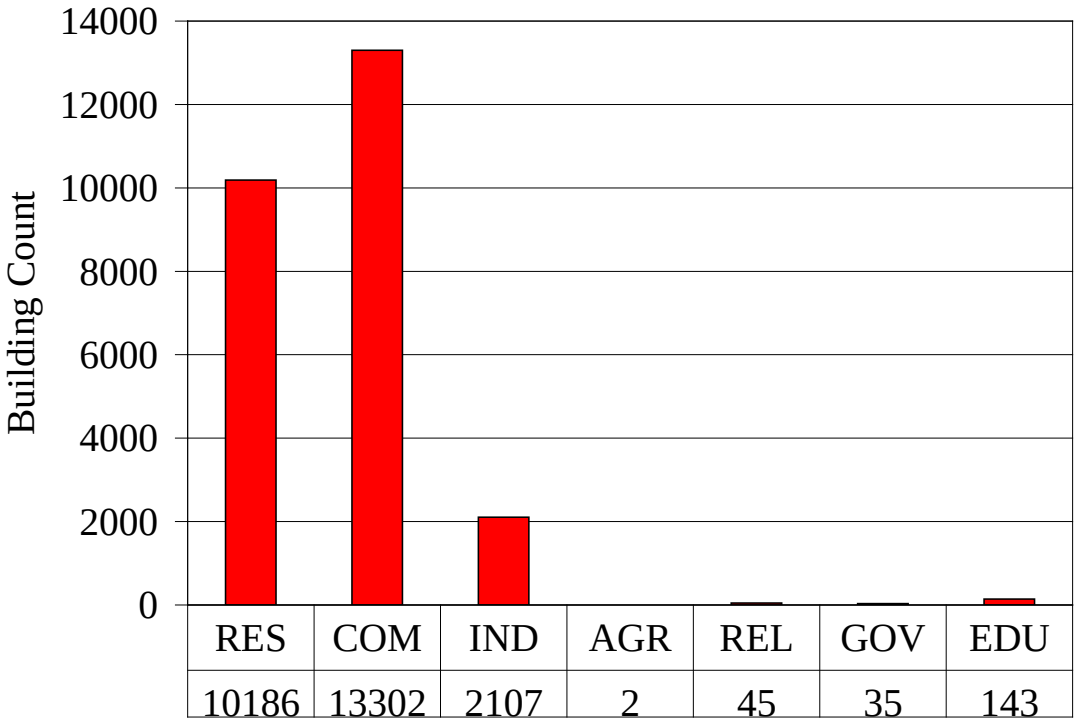

Figure 4. Non-Single-Family Residence Building Count by General Occupancy

Figure 5 and Figure 6 show the distribution of non-single-family buildings by exposure and building count, respectively, sorted by structure types. The building stock dataset excluding the single-family residences is characterized by relatively small residential structures, primarily wood frames or URM, together with larger buildings and facilities supporting commercial and industrial interests, constructed of steel and concrete. The mean cost per structure is markedly higher for the commercial and industrial structures, as shown in Figure 7, indicating the increased impact the failure of a single building poses in those sectors from a direct economic perspective.

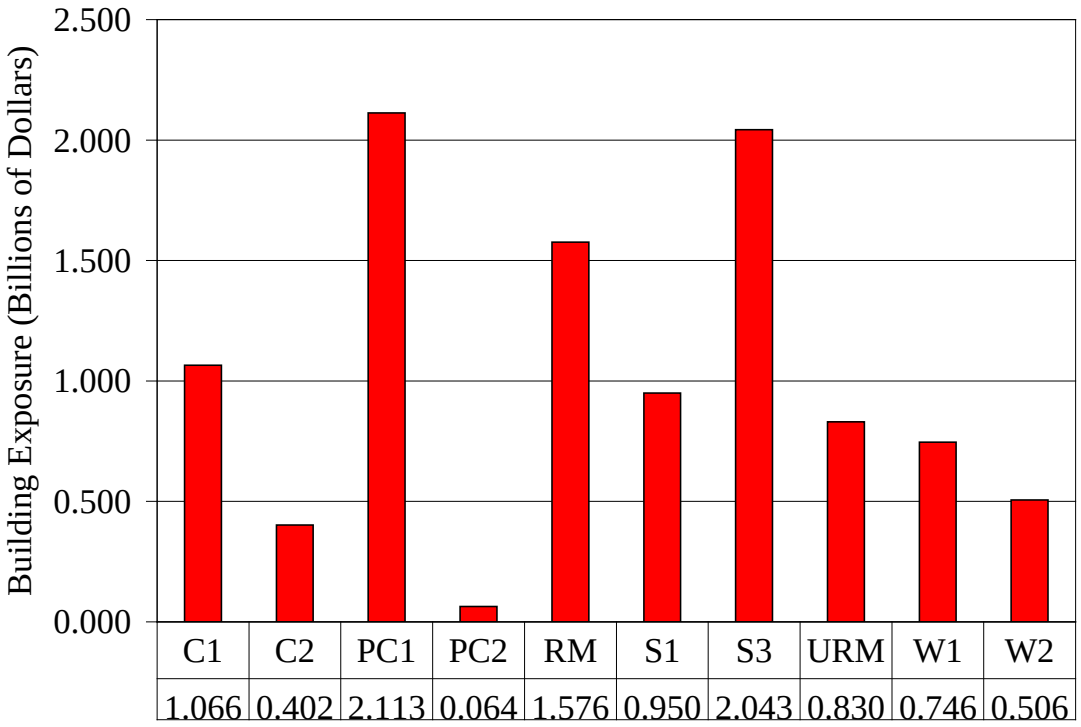

Figure 5. Non-Single-Family Residence Exposure by Structure Type

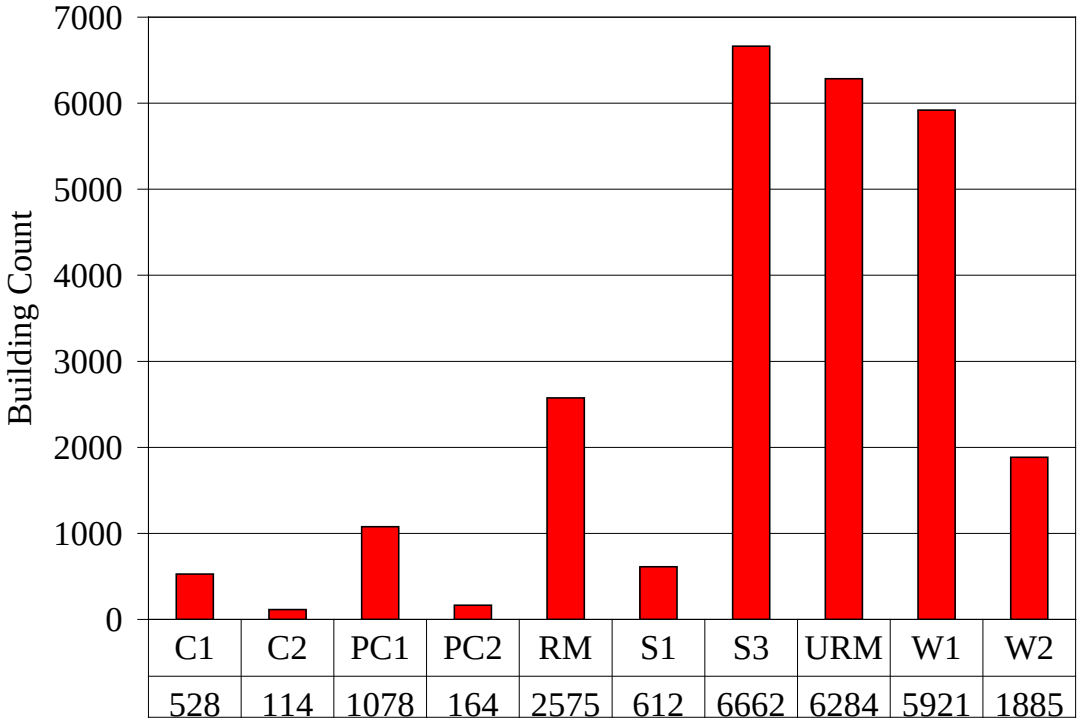

Figure 6. Non-Single-Family Residence Building Count by Structure Type

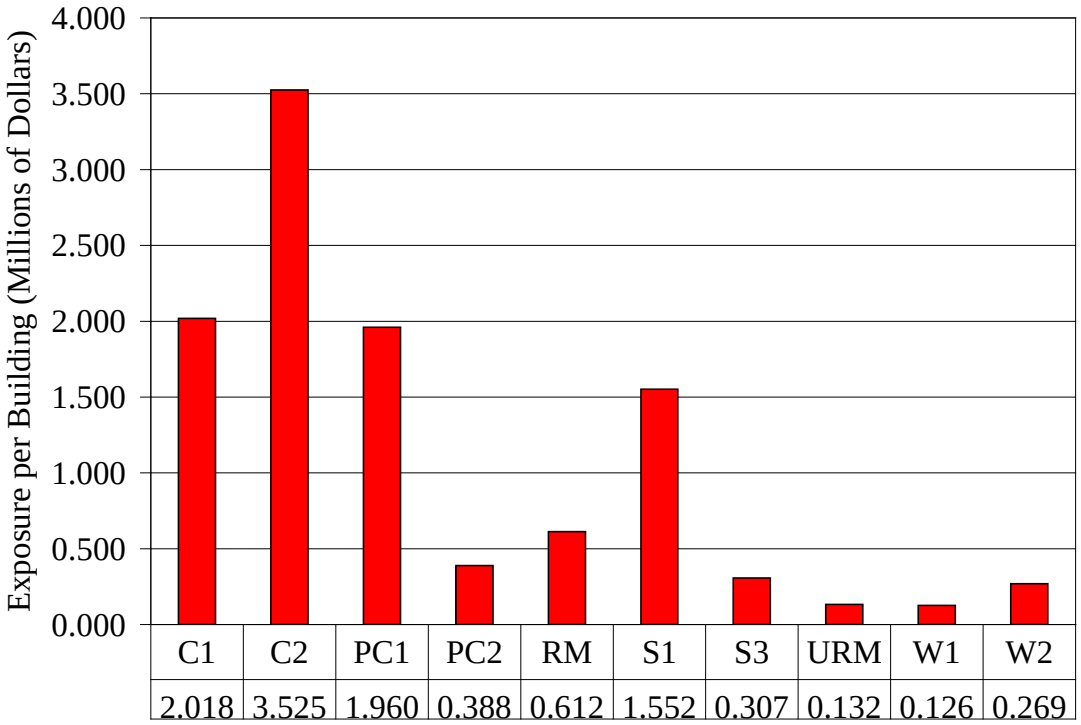

Figure 7. Non-Single-Family Residence Exposure per Building by Structure Type

The treatment of building stock uncertainty is premised on the assumptions that occupancy classifications and building heights in terms of number of stories have no uncertainty in the building stock dataset. Therefore, building stock uncertainty has negligible effect on the single family residences. Within the single family residence occupancy class, 98.9% of buildings are small wood frames (W1). In other occupancies, however, the neural network model may have assigned an incorrect structure type to particular assets. The neural network model can only be as reliable as the size and diversity of the calibration dataset will allow. To evaluate the accuracy of the model, a validation exercise was performed and the results were tabulated and submitted by French and Muthukumar (2006) as a component of the documentation for the building stock dataset, as shown in Table 5.

The vertical columns provide the critical information to provide insight to the user with respect to the reliability of the dataset. Each column indicates the prediction output from the neural network model. For example, in the given sample, the model predicted that 73 of the buildings would be URM, but when the individual buildings were investigated, it was determined that 60 of those buildings that were predicted to be URM were assigned the accurate structure type. The remaining 13 buildings included 7 wood frames, 3 concrete moment frames, 2 light steel frames, and 1 steel frame structure. Without taking some corrective action, these other structures would be analyzed as URM in error, which could then lead to a bias in the aggregate risk assessment for the region.

The implications of incorrect structure type assignments can be observed in Figure 8 through Figure 11. Figure 8, Figure 9, and Figure 10 show the variation in structural damage factors with respect to PGA for low-rise, mid-rise, and high-rise structures, respectively, as defined by HAZUS (FEMA, 2006). With respect to the regional loss estimates in this paper, the term “damage factor” refers to a coefficient used to correlate physical damage to economic loss. The damage factor typically ranges from 0 to 1, where 0 indicates no damage, and therefore no economic loss, and where 1 indicates complete damage, requiring demolition of any part of an existing structure which remained standing following the seismic event and reconstruction of the entire inventory asset. In some cases, the damage factor is also referred to as a percentage, which has the same meaning as the decimal equivalent, as in the axes of the following figures.

The plots were generated by using the Parameterized Fragility Method (Jeong and Elnashai, 2007), with the modifications outlined later regarding fragility assessment, together with the structural damage factors provided in Bai et al. (2007). The maximum differences between estimated structural damage factors of alternate structure types occurred between light steel frames (S3) and concrete frames with shear walls (C2), unreinforced masonry (URM) or light wood frames (W1) for low-rise; steel moment frames (S1) or steel braced frames (S2) and concrete shear walls (C2) for both mid- and high-rise. These differences highlight the different damage predictions that may occur if the structure type is inaccurately identified in the inventory for any particular structure. Although the mid- and high-rise structure types show less variation

relative to the low-rise results, the maximum difference between structure types is significant in each case. The importance of this source of uncertainty is compounded by the fact that the greatest variation exists for low-rise structures and that the vast majority of the building stock (99.8%) is comprised of low-rise buildings.

The general approach adopted for addressing the issue of structure type uncertainty was to analyze structures using alternate fragilities and weight the obtained results to account for likelihood of alternate structure types. Since the results shown in Table 5 are for only 416 out of 292438 buildings (0.14%), it was judged to be inappropriate to apply the specific results by structure type to the building stock in general when developing weighting factors. Instead, a general uncertainty of 30% was assumed with respect to structure type. Using the assumption that occupancy classifications and story quantities are accurate, an algorithm was implemented to capture the influence of likely alternate structure types.

The algorithm first grouped buildings into subpopulations by unique combinations of number of stories and occupancy classification. Building counts within each subpopulation were then used to determine weights for the contribution of alternate structure type candidates. A minimum limit is established to determine whether to include any given structure type in the list of prospective alternate structure types. For these analyses, the minimum value was taken as 1%. Table 6 is provided as an example to illustrate the process for consideration of structure type uncertainty. The values in Table 6 correspond to the 1-story COM1 subpopulation.

The Initial Fraction values are the ratio of the count for each building type to the total count of buildings in the subpopulation. The C1, C2, PC2, and S1 structure types are eliminated from consideration as alternate structure types because each represents less than 1% of the Initial Fraction. A Sum of Alternates is then taken to determine a total remaining fraction for the alternate structure types, neglecting those structures that did not meet the minimum tolerance, and also neglecting the contribution of the particular structure type associated with the calculation. For example, the value shown for PC1, 0.981, was determined by taking the sum of the values in the Adjust for Tolerance column, which accounts for those structure types that do not meet the minimum tolerance, and subtracting 0.013 to account for the 15 PC1 buildings. The Adjust for Tolerance values are then divided by the value of 0.981 to determine weights within the building stock uncertainty. For example, the URM value of 0.620 in the Adjust for Tolerance column is divided by 0.981 to arrive at a value of 0.632, which is shown as a percentage in the Table. When a 1-story, COM1, PC1 building is analyzed, 70% of the result is determined based on PC1 fragility parameters, but (30% * 63.2% = 19.0%) of the result is determined from URM fragility parameters, with the remaining components of the final analysis result for the building determined using RM, S3, W1, and W2 fragility parameters, and weighted as shown in Table 6, similarly to URM.

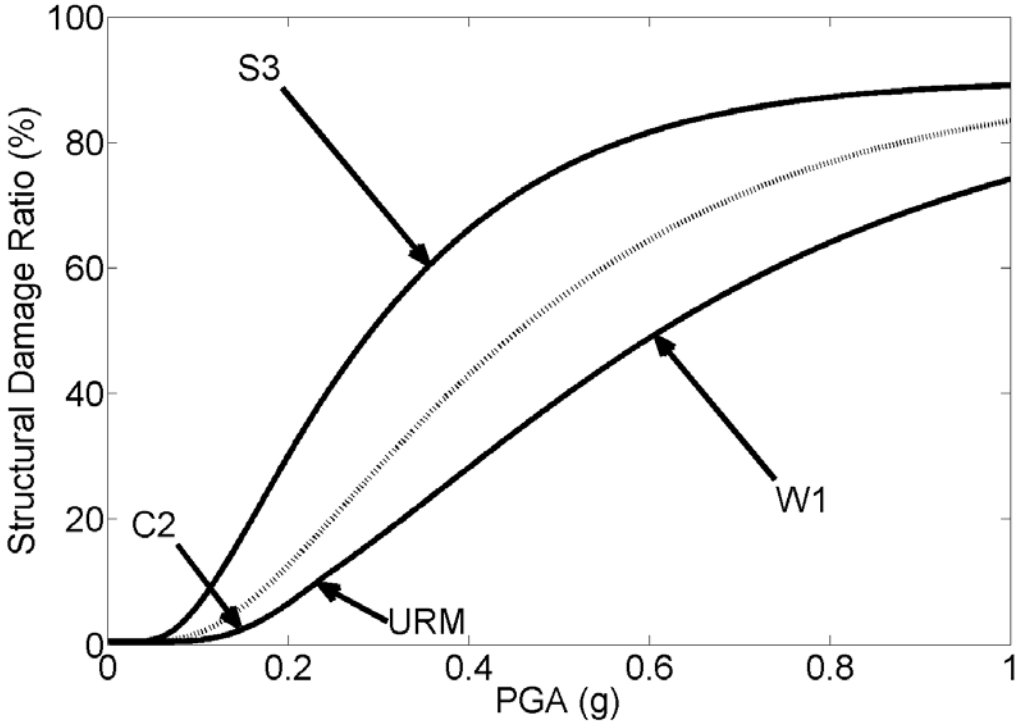

Figure 8. Variation of Low-Rise Structural Damage Factors with PGA

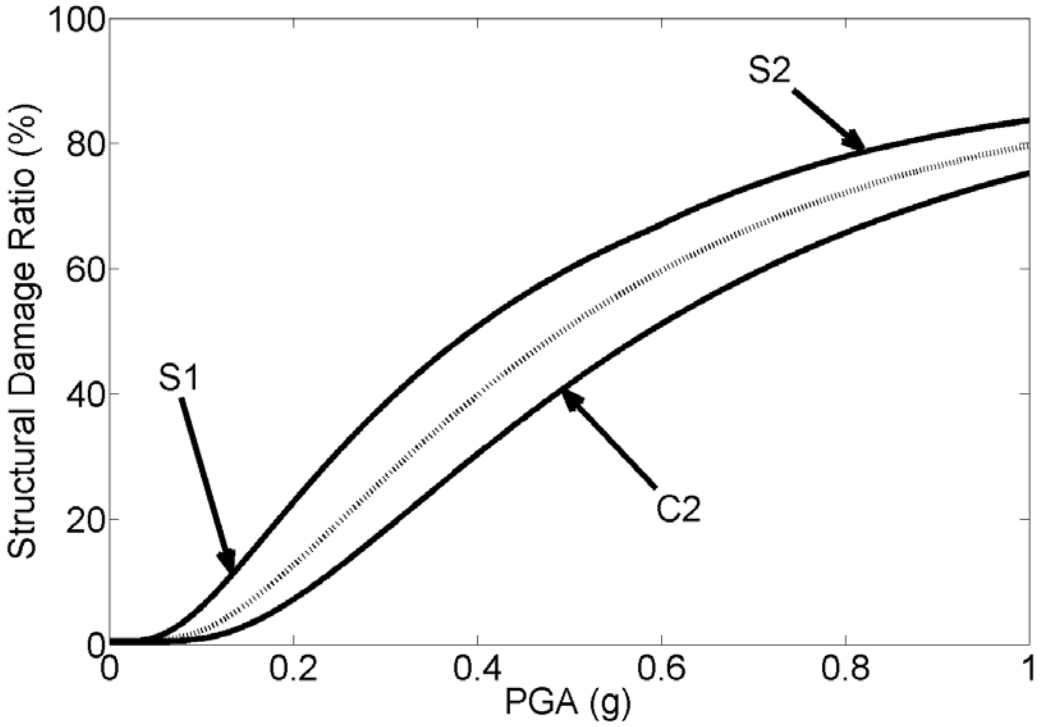

Figure 9. Variation of Mid-Rise Structural Damage Factors with PGA

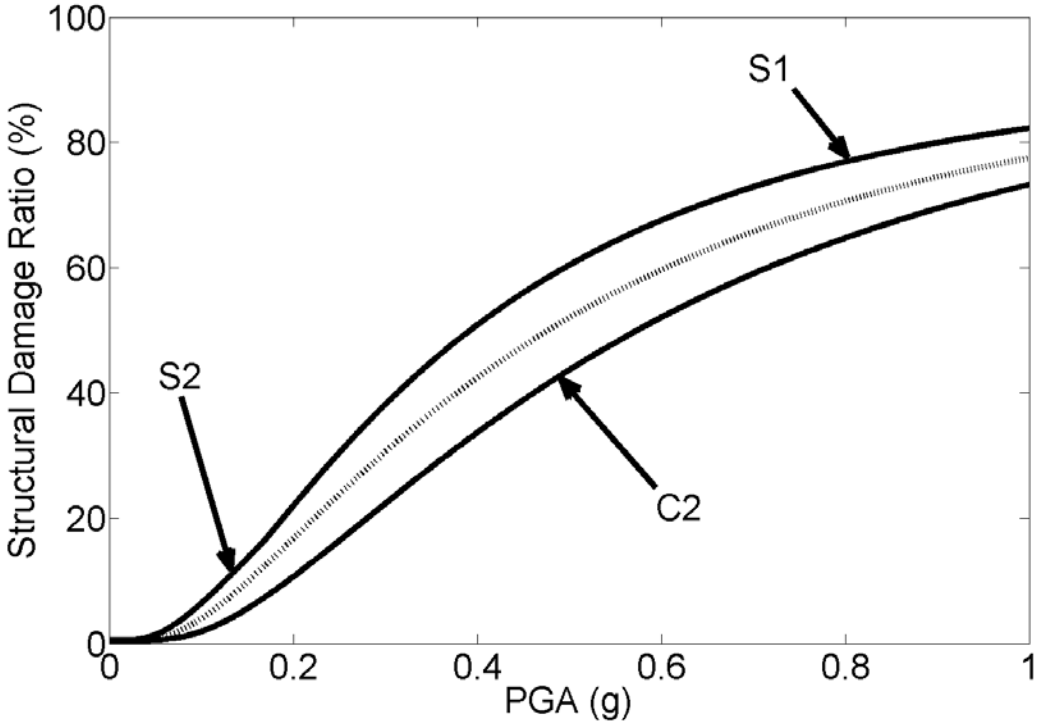

Figure 10. Variation of High-Rise Structural Damage Factors with PGA

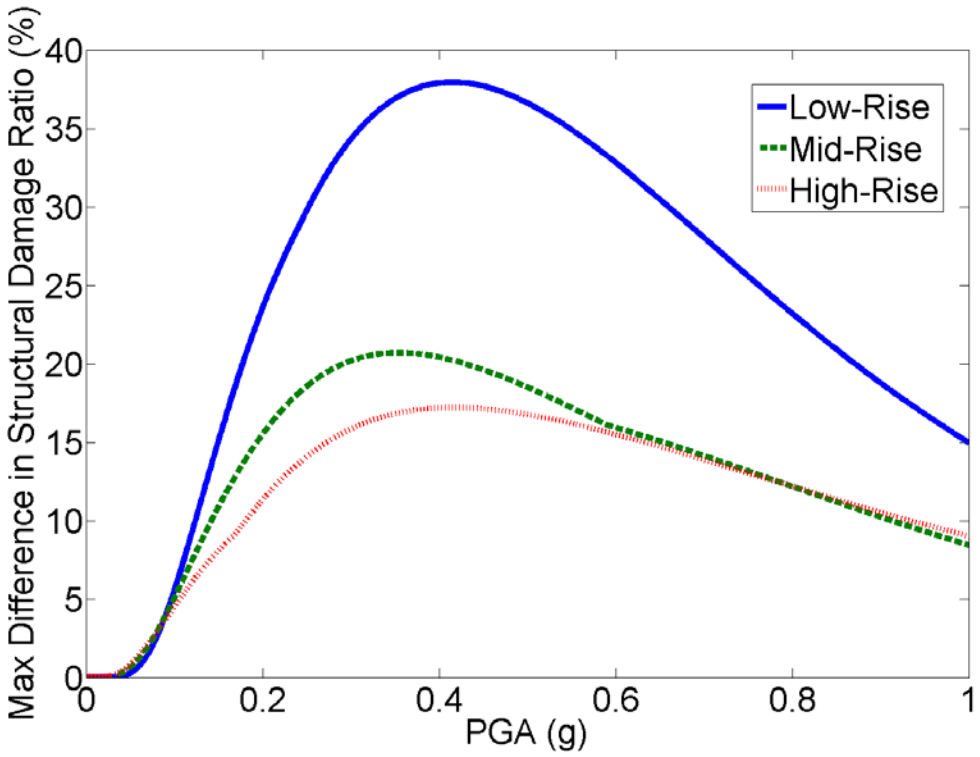

Figure 11. Variation of Maximum Difference in Structural Damage Factors with PGA

Table 5. Confusion Matrix of Artificial Neural Network Model Validation Exercise [from French and Muthukumar (2006)]

Structure Type	Code	Predicted									Survey Totals
		C1	C2	PC1	PC2	RM	S1	S3	URM	W	
Concrete Moment-resisting Frame	C1	**27**	9	0	2	0	2	1	3	0	**44**
Concrete Frame with Shear Wall	C2	1	**6**	0	0	0	0	0	0	0	**7**
Concrete Tilt-up	PC1	1	0	**32**	0	1	0	1	0	0	**35**
Precast Concrete Frame	PC2	2	1	0	**9**	1	2	0	0	0	**15**
Reinforced Masonry	RM	0	0	1	0	**19**	0	0	0	0	**20**
Steel Moment-resisting Frame	S1	7	1	0	0	5	**26**	2	1	0	**42**
Light Metal Frame	S3	4	2	4	0	1	9	**61**	2	0	**83**
Unreinforced Masonry	URM	9	1	2	2	1	1	8	**60**	0	**84**
Wood Frame	W	1	0	2	0	0	0	19	7	**57**	**86**
Totals		**52**	**20**	**41**	**13**	**28**	**40**	**92**	**73**	**57**	**416**
Prediction Accuracy		**51.92%**	**30.00%**	**78.05%**	**69.23%**	**67.86%**	**65.00%**	**66.30%**	**82.19%**	**100.0%**	**71.39%**

Table 6. Example Application of Inventory Uncertainty Adjustments

Structure Type	Count	Initial Fraction	Adjust for Tolerance	Sum of Alternates	0.000 C1	0.000 C2	0.013 PC1	0.000 PC2	0.075 RM	0.000 S1	0.205 S3	0.620 URM	0.064 W1	0.017 W2
C1	2	0.002	0.000	0.994	0.0%	0.0%	1.3%	0.0%	7.5%	0.0%	20.6%	62.4%	6.5%	1.7%
C2	0	0.000	0.000	0.994	0.0%	0.0%	1.3%	0.0%	7.5%	0.0%	20.6%	62.4%	6.5%	1.7%
PC1	15	0.013	0.013	0.981	0.0%	0.0%	0.0%	0.0%	7.6%	0.0%	20.9%	63.2%	6.6%	1.7%
PC2	4	0.003	0.000	0.994	0.0%	0.0%	1.3%	0.0%	7.5%	0.0%	20.6%	62.4%	6.5%	1.7%
RM	86	0.075	0.075	0.919	0.0%	0.0%	1.4%	0.0%	0.0%	0.0%	22.3%	67.5%	7.0%	1.8%
S1	1	0.001	0.000	0.994	0.0%	0.0%	1.3%	0.0%	7.5%	0.0%	20.6%	62.4%	6.5%	1.7%
S3	236	0.205	0.205	0.789	0.0%	0.0%	1.7%	0.0%	9.5%	0.0%	0.0%	78.6%	8.2%	2.1%
URM	713	0.620	0.620	0.374	0.0%	0.0%	3.5%	0.0%	20.0%	0.0%	54.9%	0.0%	17.2%	4.4%
W1	74	0.064	0.064	0.930	0.0%	0.0%	1.4%	0.0%	8.0%	0.0%	22.1%	66.7%	0.0%	1.8%
W2	19	0.017	0.017	0.977	0.0%	0.0%	1.3%	0.0%	7.7%	0.0%	21.0%	63.4%	6.6%	0.0%

3.2 Bridge Inventory

The bridge inventory used for the capstone scenarios has been obtained from the National Bridge Inventory compiled and maintained by the Federal Highway Administration for the year 2006, available at http://www.fhwa.dot.gov/bridge/nbi/ascii.cfm?year=2006, in conjunction with the Recording and Coding Guide for the Structure Inventory and Appraisal of the Nations Bridges, available at http://www.fhwa.dot.gov/bridge/mtguide.pdf. The key fields used for analysis were "Main Structure Type" (Item 43), which allowed classification of the bridges according to the types for which fragilities had been developed (Choi et al., 2004; DesRoches et al., 2003; DesRoches et al., 2006), as well as the number of spans, total length and width, and geographic coordinates. Modifications to the dataset included:

1. purging of bridges that are not addressed by the fragilities developed within the MAE Center (e.g., tunnels), which reduced the inventory set from 489 to 313 entries,
2. substitution of the mode of width (where "mode" is the most commonly observed value, 10.5 m) for bridge records lacking width data, which occurred 101 times in the remaining 313 entries,
3. substitution of 1 for the number of spans of simply-supported bridges and 3 for the number of spans of all other bridges where the number of spans is not included in the record , which occurred 96 times in the remaining 313 entries, and
4. conversion of latitude and longitude to decimal degrees, and setting all longitude values to negative values to reflect that the location is in the Western hemisphere.

The distribution of bridge count by type is shown in Figure 12. As shown in the Figure, the majority of bridges in the region are multi-span concrete, and most bridges within that subpopulation are simple spans. The distribution of mean estimates of replacement cost for the bridges in the study region are shown in Figure 13. Mean estimates of replacement cost are derived by multiplying bridge length and width by a replacement cost per square foot. The replacement costs per unit area match the values used in the Transportation Testbed Project of the MAE Center for the Charleston, SC area. The values were originally obtained from the South Carolina Department of Transportation (Padgett, personal communication, 2006).

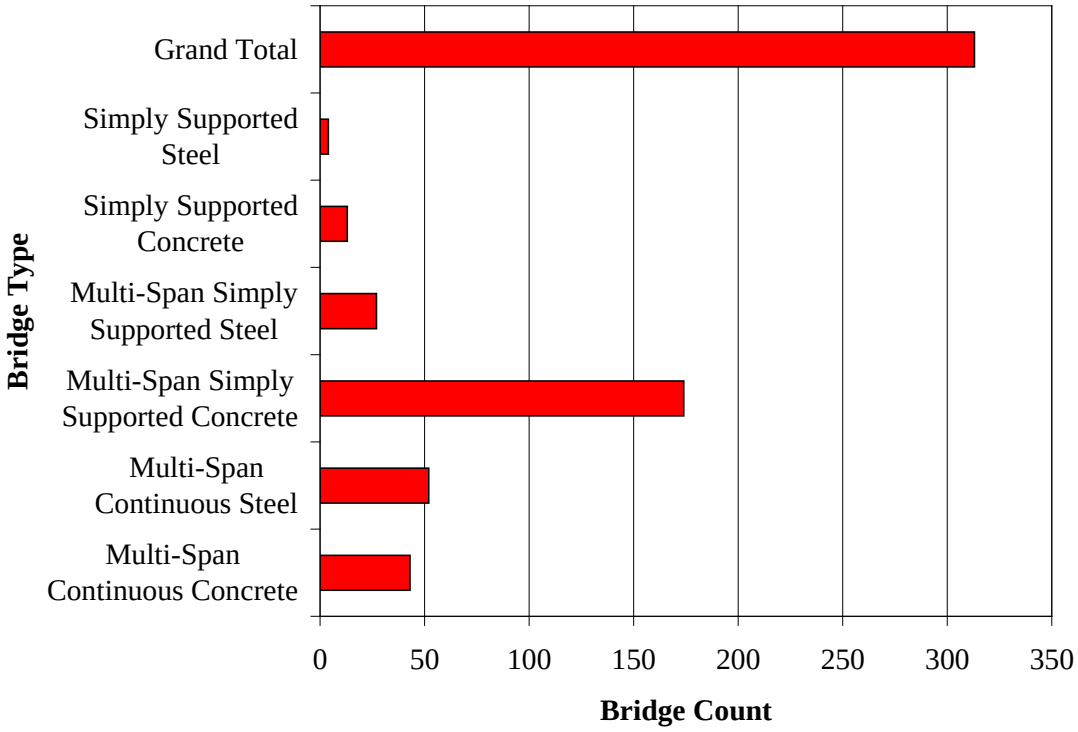

Figure 12. Distribution of Bridge Types by Count

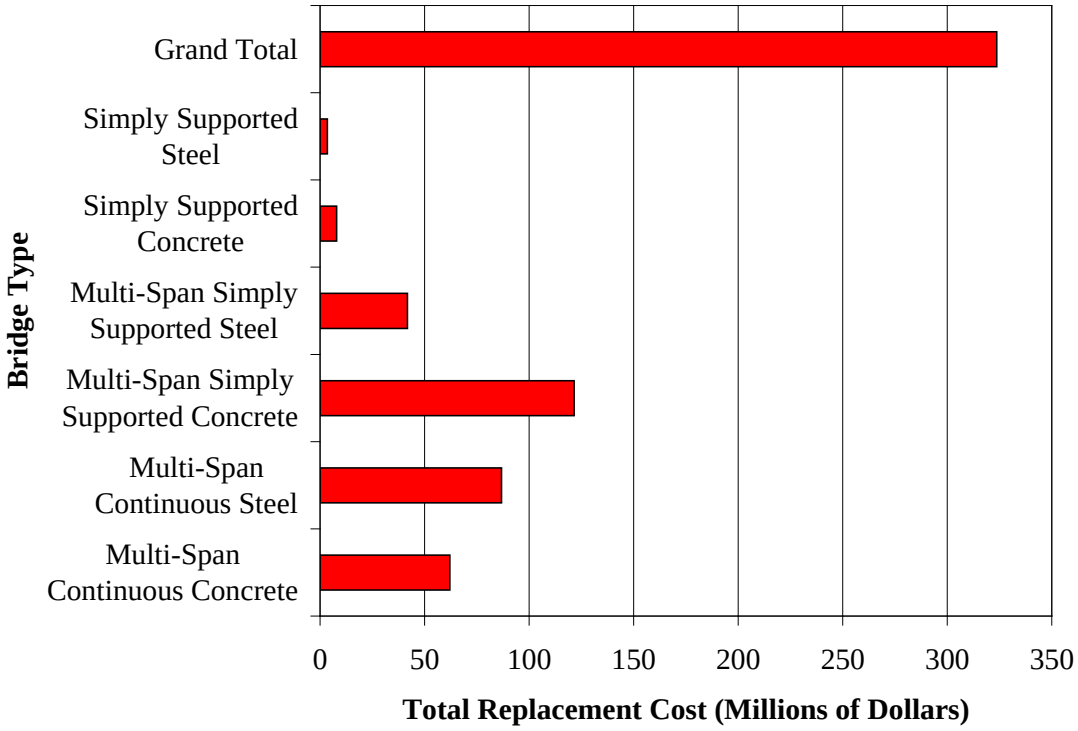

Figure 13. Distribution of Bridge Mean Estimated Replacement Value

3.3 Utility Network Inventory

Comprehensive detailed utility network data could not be obtained for use in the capstone scenarios. The data available within the Center was limited to a set of cast iron pipeline data, obtained during a previous project from Memphis Light Gas & Water (MLGW, 2005), and the HSIP Gold dataset (PMH, 2006), which provided only very low resolution data for a limited number of assets. Consequently, consideration of the impact of utility networks on the study region is extremely limited in the capstone scenarios.

4 HAZARD DEFINITION

The seismic sources were selected for the capstone scenarios to reflect known patterns of seismicity in the New Madrid Seismic Zone. Hazard is defined for the capstone scenarios based on two point sources: a M_w 7.9 centered near Blytheville, AR (35.927ºN, 89.919ºW), and a M_w 6.2 centered near Marked Tree, AR (35.535ºN, 90.430ºW). The point source epicenters are shown on a map with Shelby County in Figure 14. Point sources were selected rather than more detailed finite fault models as a consequence of the lack of data available for historical seismicity in the New Madrid Seismic Zone. The locations and magnitudes were selected based on disaggregation of USGS probabilistic seismic hazard maps to determine likely source characteristics, but also incorporate the expert opinions of researchers within the MAE Center to establish final positions and magnitudes.

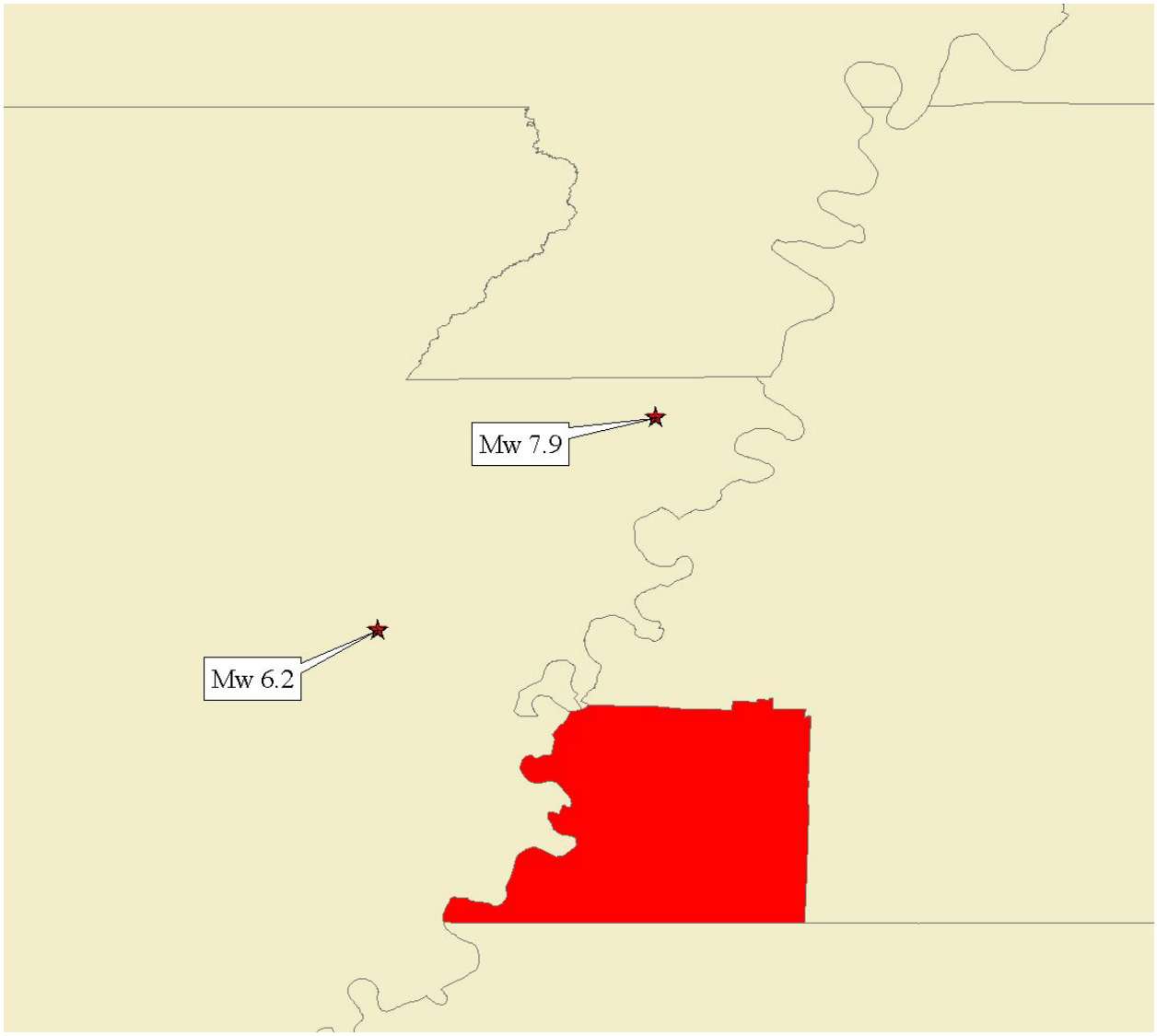

Figure 14. Epicenter Locations and Magnitudes

4.1 Ground Shaking Hazard Modeling

The ground shaking hazard employed in the capstone scenarios is based on the work of Fernandez and Rix (2006). This hazard model provides a composite representation of bedrock and overlying softer soils in the Mississippi Embayment with a goal of capturing the effects of the unique geology of the Embayment. Two key characteristics which must be defined for each asset are underlying soil type and soil depth. Fernandez and Rix (2006) consider two types of soil: Uplands (Pleistocene) and Lowlands (Holocene). Most of the study is underlain by Uplands soil (see Figure 15). The second key parameter required to estimate ground shaking hazard by Fernandez and Rix (2006) is soil depth. Seven depth bins were established, so each inventory item must be classified into one of the defined bins. The deepest bin considered in Fernandez and Rix (2006) is from 660 to 1220 meters of soil, and all of Shelby County is underlain by at least 1000 meters of soil (see Figure 16), so only the coefficients for the deepest soil are required to determine ground shaking hazard for the study region.

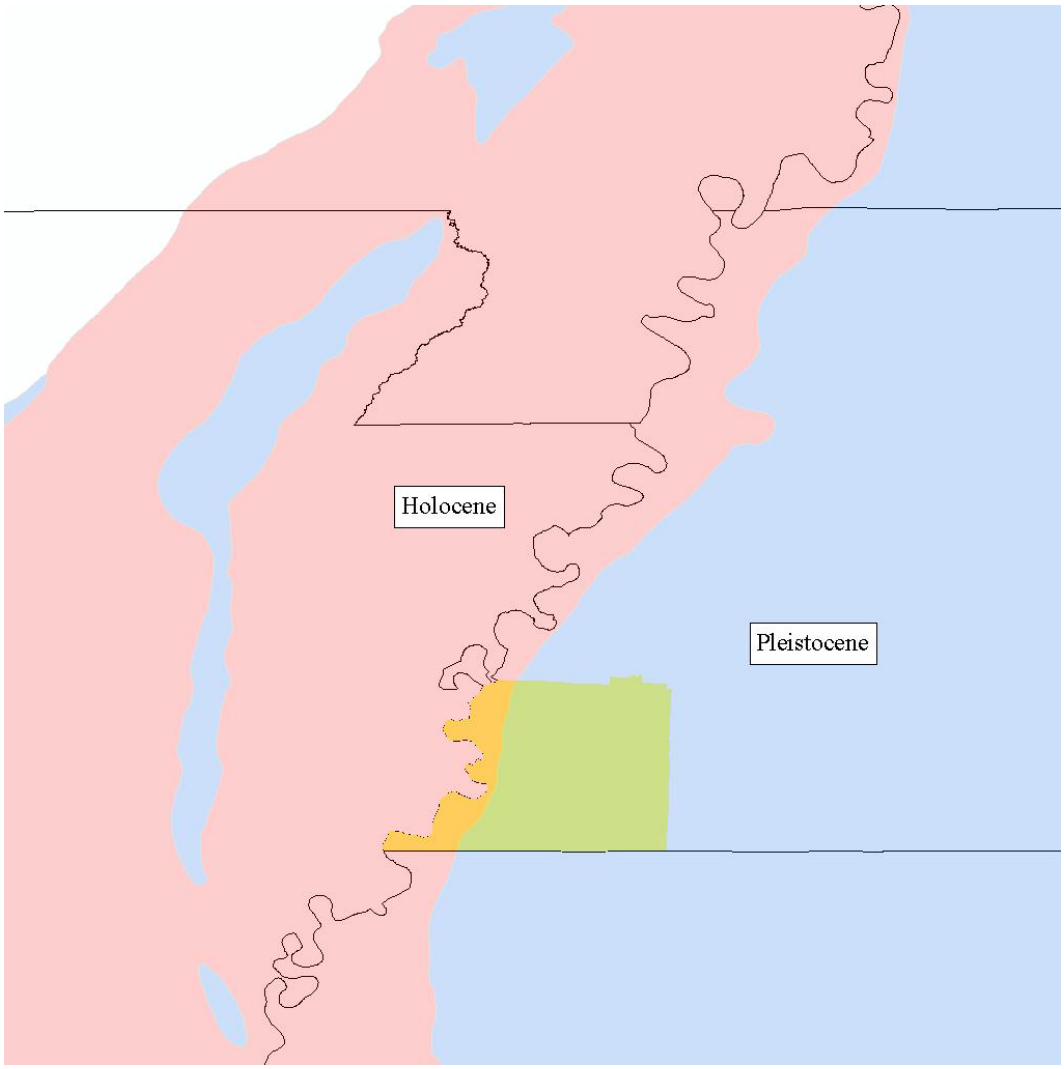

Figure 15. Study Region Geology

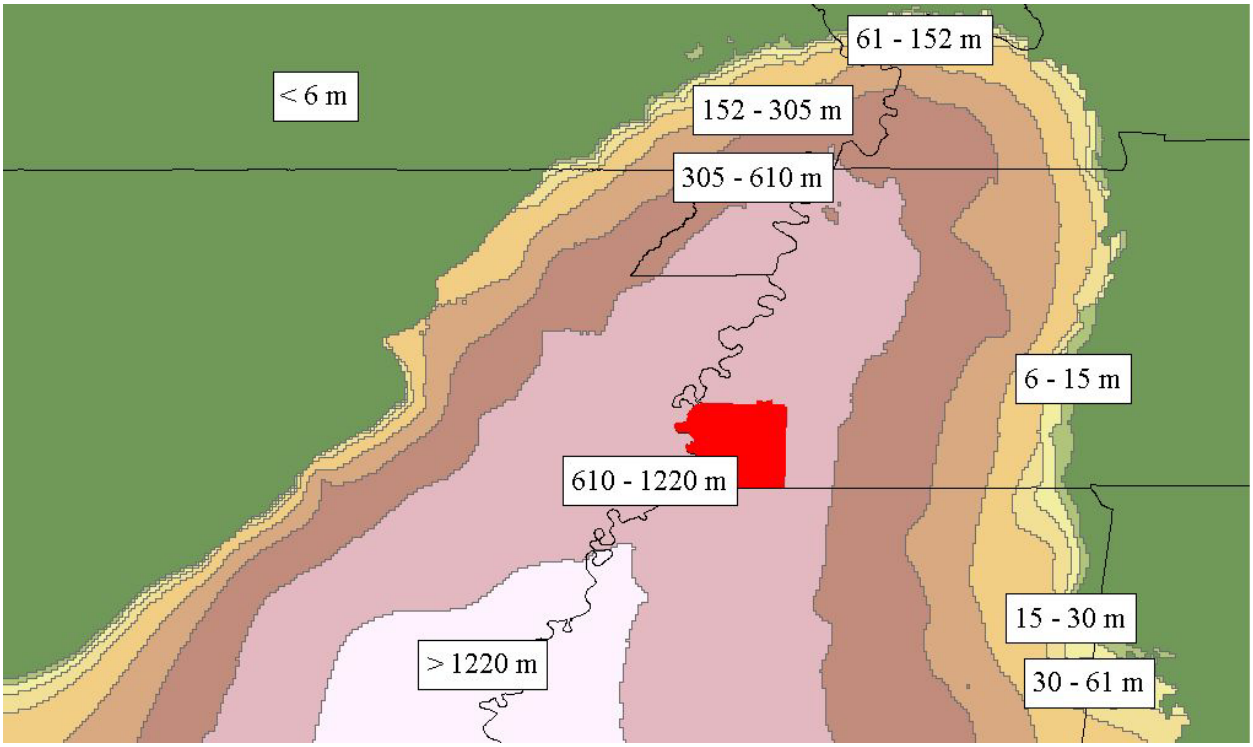

Figure 16. Study Region Soil Depth

The hazard determined in accordance with Fernandez and Rix (2006) tends to be lower than that generated by using the attenuation equations commonly employed by the United States Geological Survey (USGS) in conjunction with factors accounting for local soil effects obtained from the National Earthquake Hazards Reduction Program (NEHRP) documentation, in spite of the fact that the work of Fernandez and Rix (2006) also uses basic bedrock attenuation models from Atkinson and Boore (1995), Frankel et al. (1996), and Silva et al. (2003), similarly to USGS. The primary difference lies in the treatment of local soil effects. The NEHRP factors were developed to be used in areas of high seismicity in the U.S., primarily in California (Borcherdt, 1994; Dobry et al., 2000). As a consequence of the differences in local geology between the two locales, the local site effects tend to amplify ground motion accelerations in the NEHRP documentation and dampen accelerations in the Fernandez and Rix (2006) approach.

In Figure 17 and Figure 18, spectra are plotted based on point sources, with Figure 17 obtained by using a $\boldsymbol{M_w}$ 7.9 source at Blytheville, AR (35.927ºN, 89.919ºW), and Figure 18 obtained by using a $\boldsymbol{M_w}$ 6.2 source at Marked Tree, AR (35.535ºN, 90.430ºW). The site location was identical in each case, with a position near downtown Memphis, TN (35.1175ºN, 89.9711ºW). The spectra were developed to reflect the differences in hazard prediction for this study region between HAZUS Level I analyses, which employ USGS attenuation equations and NEHRP soil adjustment factors, and hazards calculated by applying Fernandez and Rix (2006).

For the spectra corresponding to "USGS/NEHRP", a 10 km depth was assumed for the hypocenter. The attenuations and corresponding weights for the "USGS/NEHRP" cases were selected based on the HAZUS Technical Manual for a Characteristic Event in the Central and Eastern United States. After the ground shaking hazard for bedrock motion had been determined from the attenuations, soil effects were included by using NEHRP factors for either Site Class D or E soil, as identified in the figure, which are generally meant to represent moderate and deep soft soils, respectively. The "USGS/NEHRP" hazard spectra are constructed by anchoring to spectral values at periods of 0.3 and 1.0 second, as indicated in the HAZUS Technical Manual. The sole difference between the two spectra determined by Fernandez and Rix (2006) is the use of Uplands versus Lowlands coefficients. Both spectra used the deepest soil bin coefficients.

There is a clear difference between the spectra obtained from the two different methodologies in the low period range. The nonlinear behavior in the soil, as predicted by Fernandez and Rix (2006), is expected to result in lower accelerations, but also generate larger displacements. Therefore, PGA and short period (approximately 0.3 second) spectral accelerations are expected to be relatively small, but moderate and longer period spectral accelerations may be magnified relative to values predicted by the USGS/NEHRP hazard estimation methodology. These differences are systematic, and embedded in the fundamental approach of the two methodologies. To illustrate the general form of ground motion prediction for each case, plots were developed as shown in Figure 19 through Figure 23. In each of the Figures, ground motions were calculated at increments of 0.2 in moment magnitude, from 5.5 to 8.5, and at increments of 5 km distance from the epicenter, from 5 to 100 km. In Figure 19 and Figure 20, the ground motion can be seen to remain level or, in some near-fault cases, decrease with increasing moment magnitude, especially when the magnitude becomes very large. This behavior is not observed in the models shown in Figure 21 and Figure 22.

The final plot, Figure 23, shows the ratio of predicted ground motion by the USGS/NEHRP approach with Site Class E and Fernandez and Rix (2006) using the deepest soil Uplands coefficients. The minimum ratio occurred at $\boldsymbol{M_w}$ = 6.1 and an epicenter distance of 5 km, with a ratio of 1.9, and the maximum ratio occurred at $\boldsymbol{M_w}$ = 8.5 and an epicenter distance of 5 km, with a ratio of 7.2. The mean calculated ratio for all sample combinations of moment magnitude and epicenter distance was 2.7. Thus, for any reasonable scenario, the average ground shaking PGA hazard obtained by Fernandez and Rix (2006) is expected to be no more than about half the value typically used in HAZUS. This discrepancy can lead to significant differences in projected losses for the study region as compared to other loss estimates for this study region performed using alternate hazard models. Collecting data from a major seismic event in the New Madrid Seismic Zone will help mitigate these differences in the future.

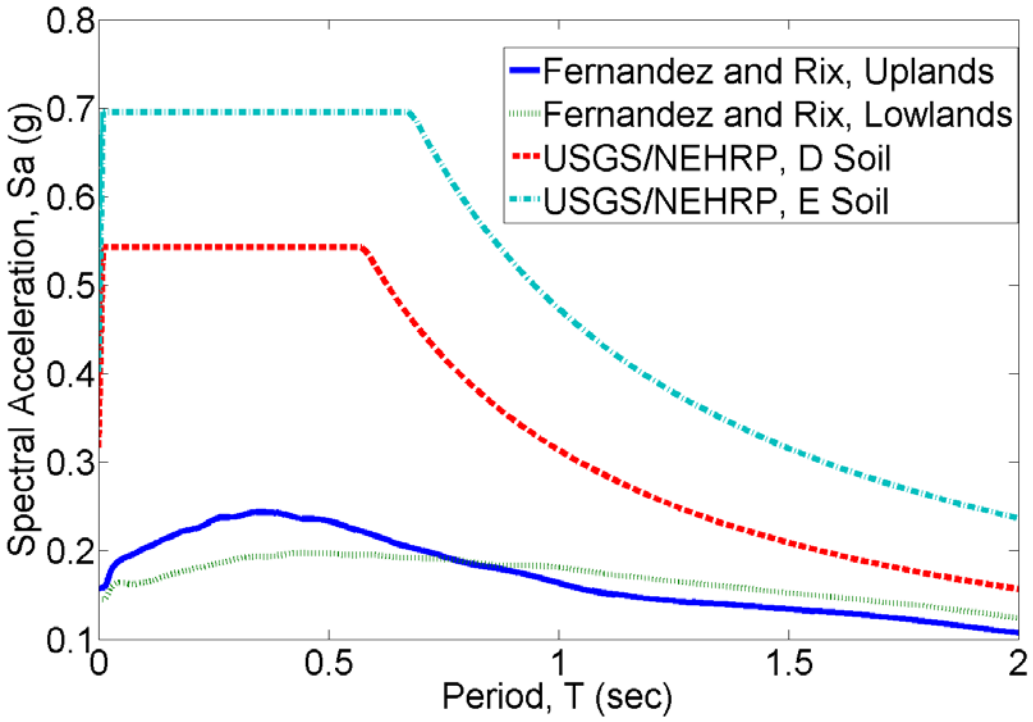

Figure 17. Spectra for Memphis, TN from Blytheville Source

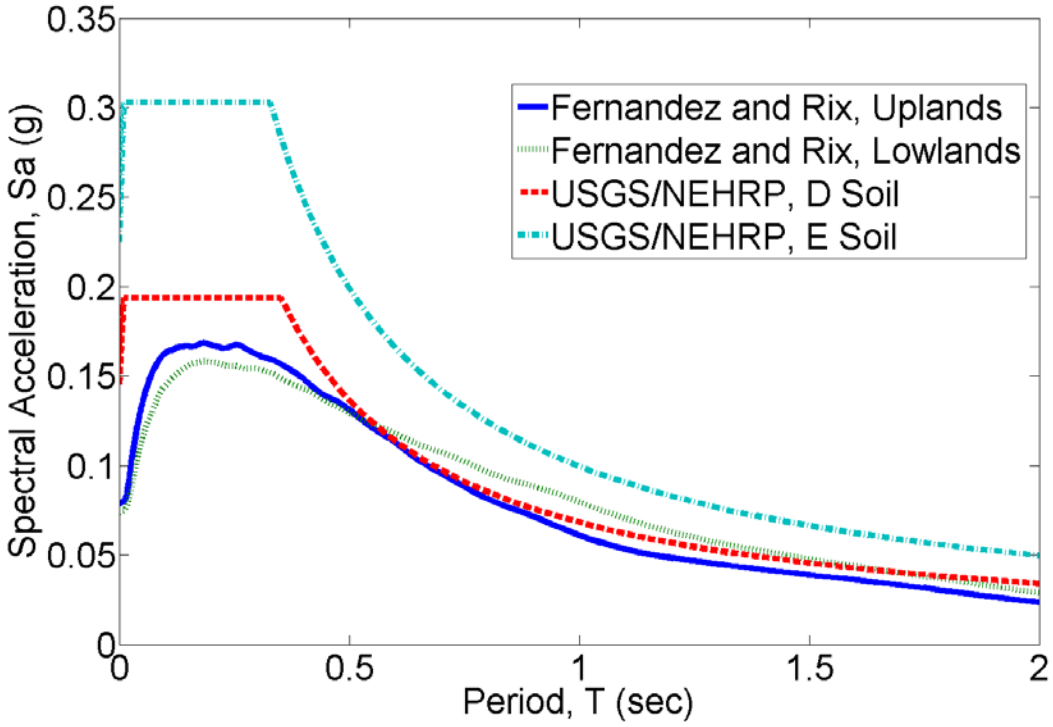

Figure 18. Spectra for Memphis, TN from Marked Tree Source

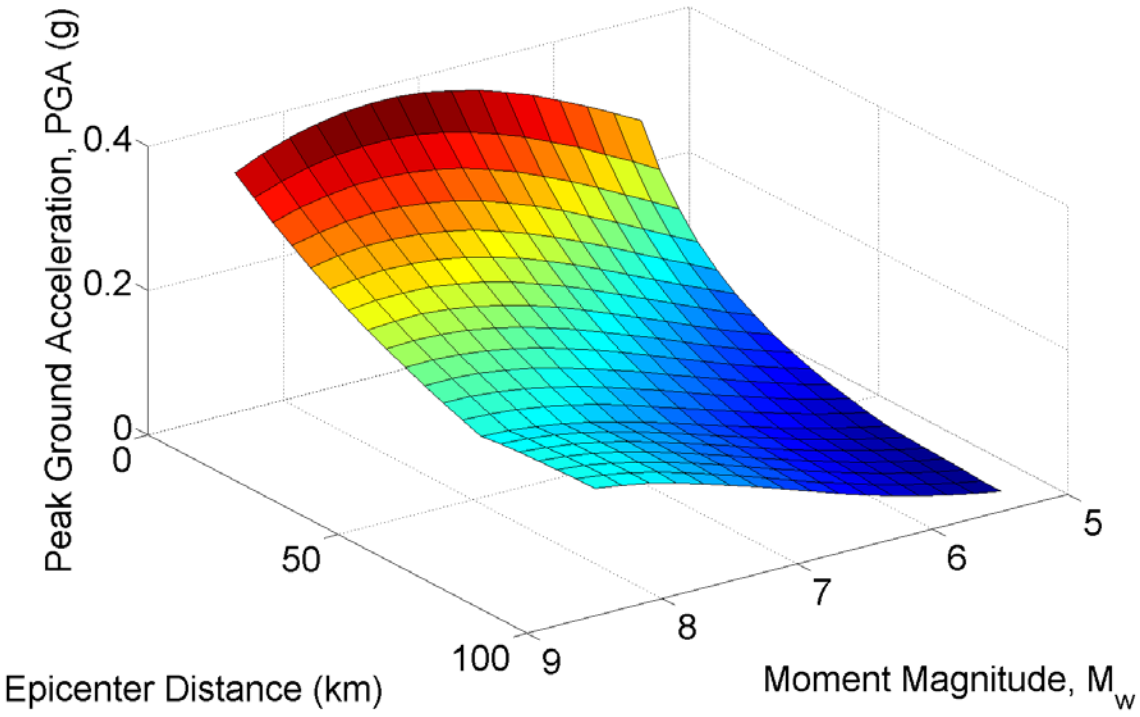

Figure 19. PGA Predicted by Fernandez and Rix (2006) for Uplands

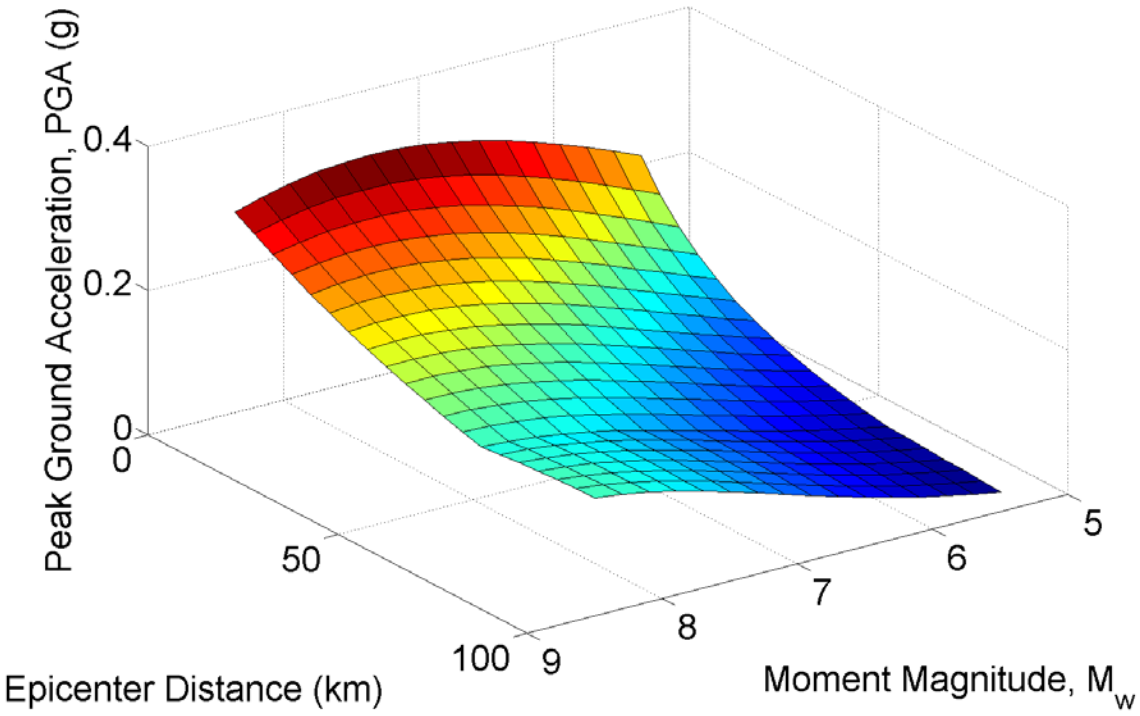

Figure 20. PGA Predicted by Fernandez and Rix (2006) for Lowlands

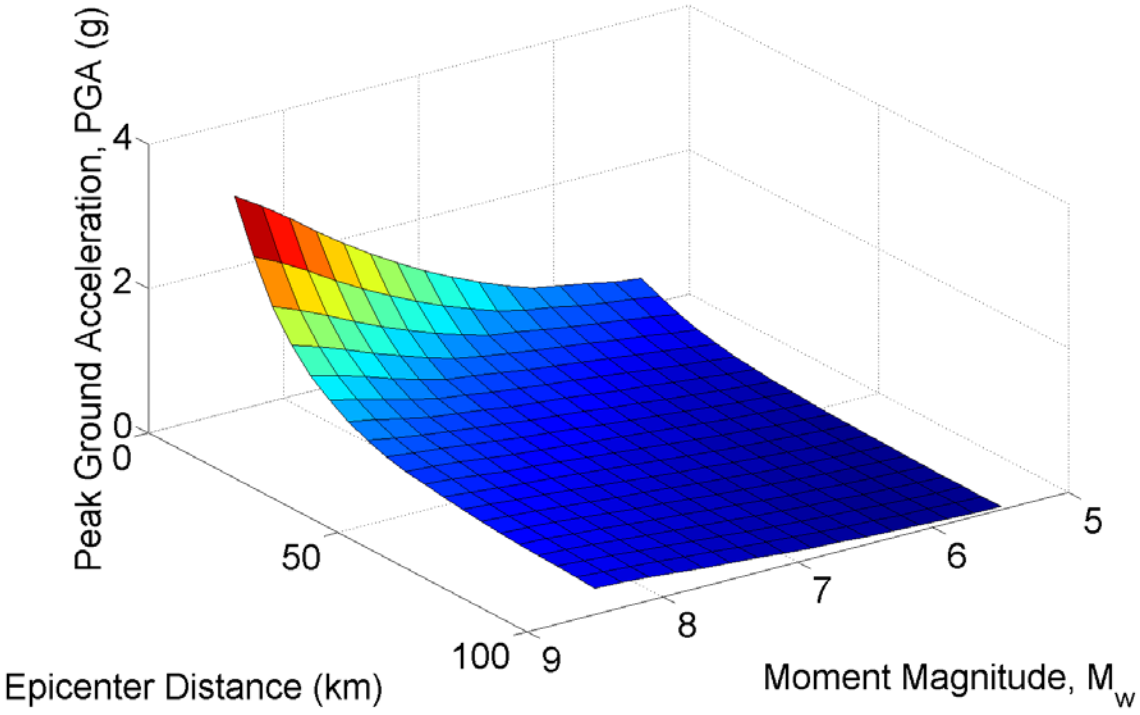

Figure 21. PGA Predicted by USGS/NEHRP for Site Class D

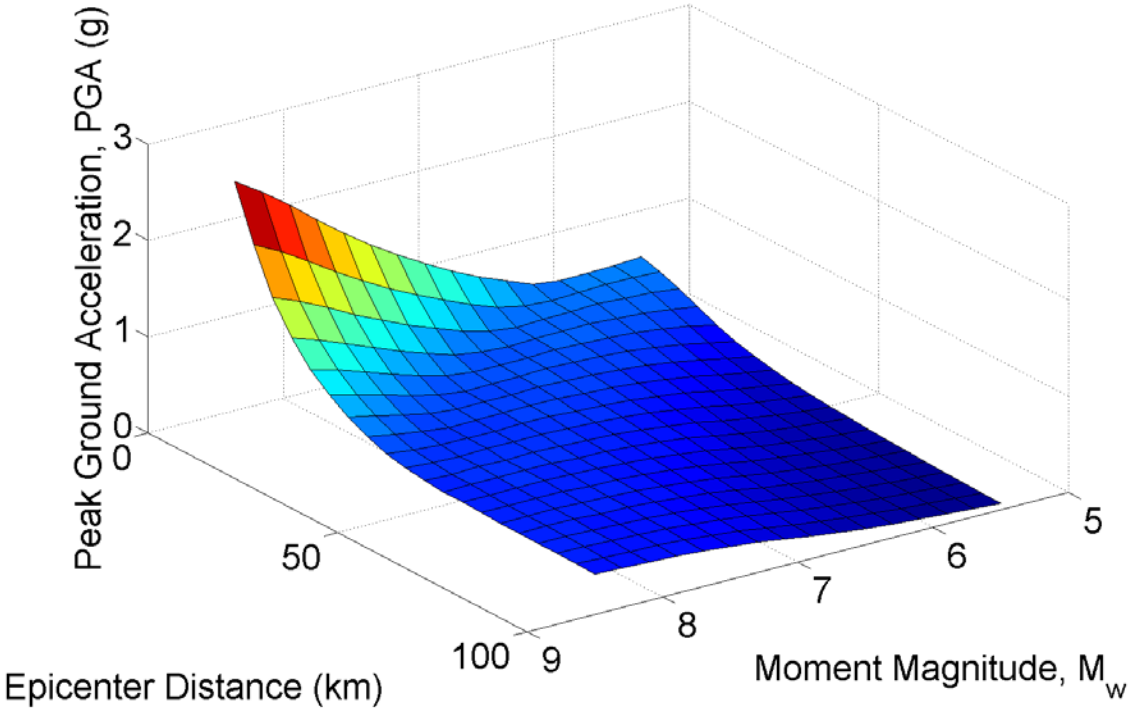

Figure 22. PGA Predicted by USGS/NEHRP for Site Class E

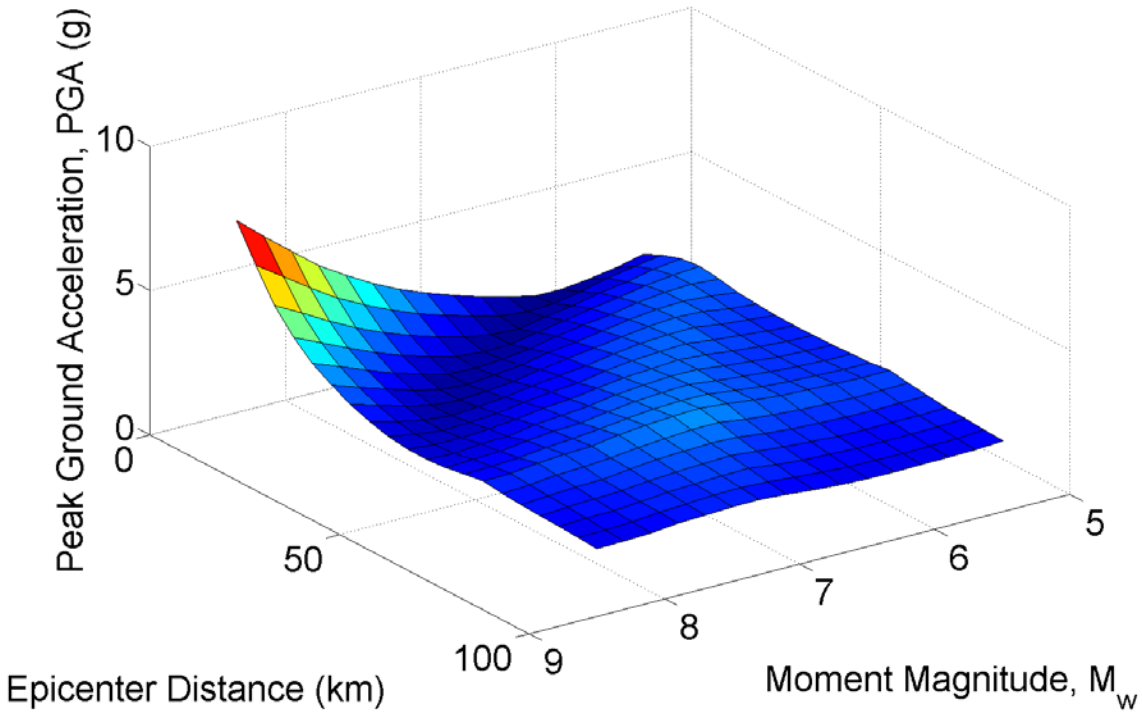

Figure 23. Ratio of PGA Predicted by USGS/NEHRP for Site Class E to Fernandez and Rix (2006) Uplands

4.2 Ground Failure Hazard Modeling

The ground failure hazard used in the capstone scenarios is based on work performed for the Memphis Hazard Mapping Project (USGS, 2006). Based on data provided within the MAE Center (Steelman and Hajjar, 2006), an algorithm was implemented in MAEViz to estimate probabilities of Liquefaction Potential Index (LPI) exceeding 5% and 15%. The probabilities for LPI exceeding 15% were then used as part of the damage and direct loss algorithms in MAEViz for the building stock. Maps of probabilities of LPI exceeding 15% are provided in Figure 24 and Figure 25. Correlation of liquefaction effects to building damage is based on the assumption that buildings subject to significant liquefaction effects are likely to be heavily damaged. To this end, the probability of having LPI > 15% was assumed to be equal to the probability of complete damage resulting from liquefaction.

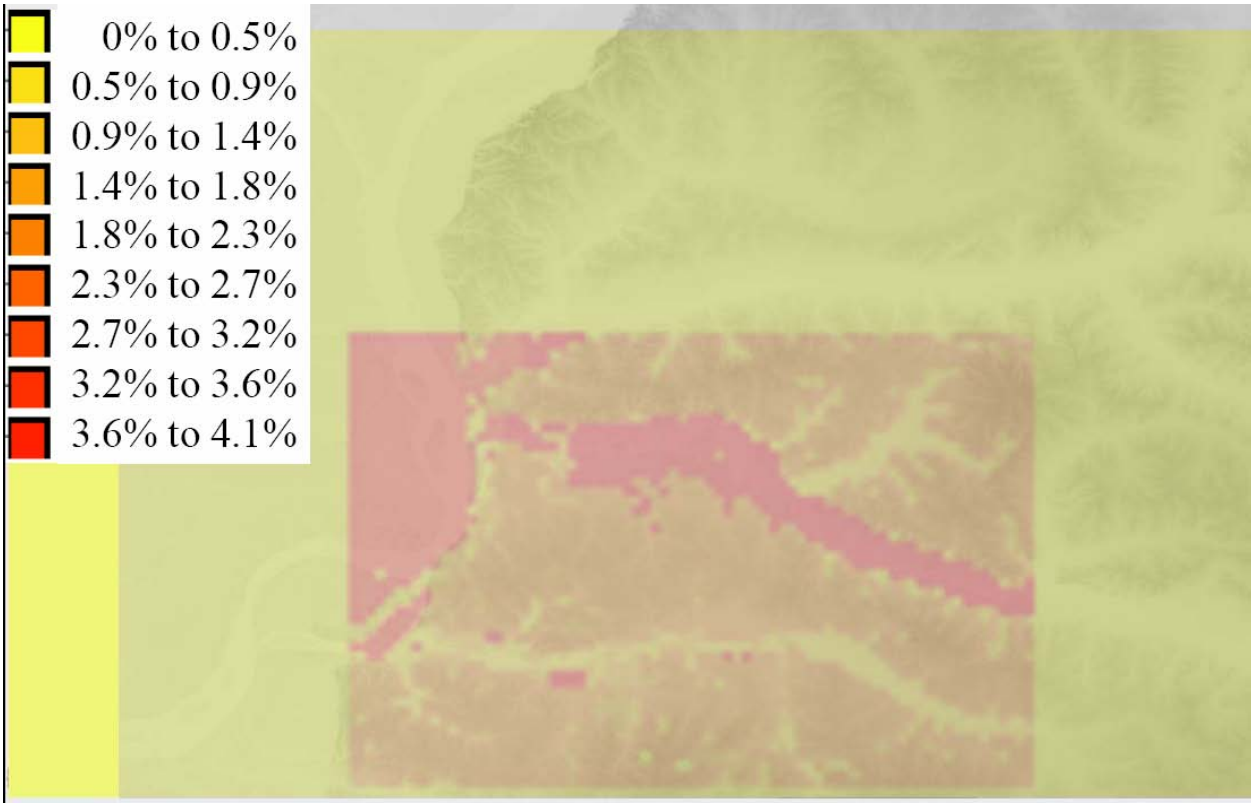

Figure 24. Probability of LPI > 15% for a Blytheville M_w 7.9 source

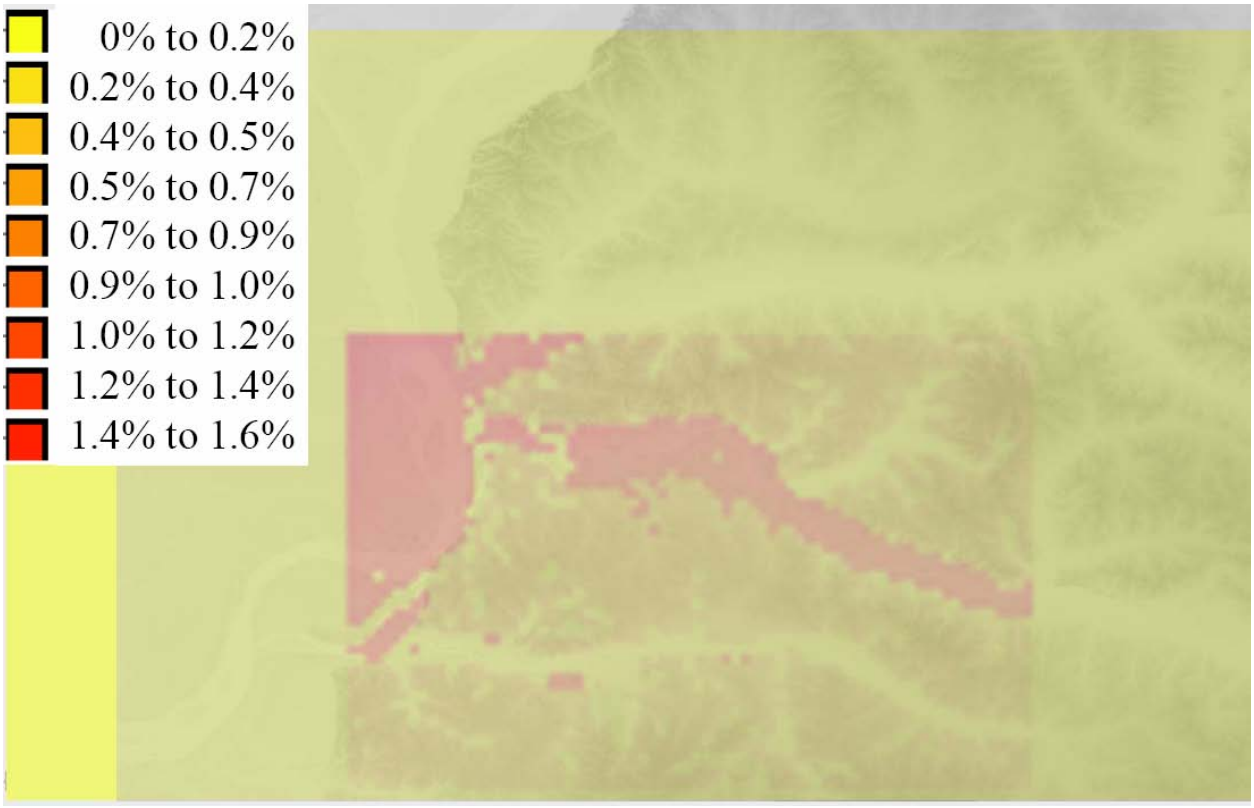

Figure 25. Probability of LPI > 15% for a Marked Tree M_w 6.2 source

5 VULNERABILITY FORMULATION

Vulnerability functions have been developed by a number of researchers affiliated with the Mid-America Earthquake Center to reflect the seismic demands and capacities for components of the built environment commonly found in Central and Eastern United States. This section describes the vulnerability formulations utilized in damage assessment for the capstone scenarios.

5.1 Building Stock Vulnerability

Building stock vulnerability for Shelby County has been investigated by a wide range of researchers. Fragility functions have been developed for light wood frame construction, both 1- and 2-story structures, and considering both slab-on-grade construction and frames constructed with crawl spaces (Ellingwood et al., 2008; Ellingwood, 2006). Fragility functions have also been developed to represent 2-story and 4-story partially restrained steel moment frames, 3-story fully restrained steel moment frames, and 6-story X-braced steel frames (Ellingwood, 2006). Extensive studies of concrete frames have also been conducted (Bai and Hueste, 2006; Erberik and Elnashai, 2006; Hueste and Bai, 2003; Ramamoorthy et al., 2006).

If a structure type occurred in the inventory, and a fragility set was not available (e.g., reinforced masonry), then a fragility set obtained from the parameterized fragility method (Jeong and Elnashai, 2007) was substituted, which incorporated the expected characteristics for the local ground motion in the study region (Fernandez, 2007). In addition to supplementing structural fragilities, the fragility functions for all nonstructural cases were developed by applying the parameterized fragility method. A number of modifications were made to the parameterized fragility method, as described in Steelman and Hajjar (2008). In addition to the adjustments made in that paper, several parameters were adjusted prior to invoking the parameterized fragility engine to develop fragilities for use in the capstone scenarios. There were two main adjustments to the analysis parameters: revision of elastic damping ratios and revision of uncertainty parameters.

The elastic damping ratios were generally reduced to reflect common estimates found in the literature. The most significant of these was the adjustment of the value for W1 structures. As described previously, W1 structures represent the extensive majority of the building stock for the region, so selection of parameters for these structures plays a critical role in developing estimates of consequences for the study region. The default value used by HAZUS is 15% of critical damping (FEMA, 2006). However, in accordance with the value referenced by Ellingwood et al. (2008), this value was reduced to 1%.

The uncertainty parameters provided in the HAZUS Technical Manual (FEMA, 2006) are the products of a convolution process which accounts for demand uncertainties. With the parameterized fragilities (Jeong and Elnashai, 2007), the demand uncertainty is obtained directly as a result of the regression correlating the hazard parameter used for indexing into fragilities with the structural response of the SDOF model. Therefore, only the modeling and capacity

uncertainty terms were obtained from the HAZUS Technical Manual (FEMA, 2006), and were combined by a square root of sum of squares (SRSS) method with demand uncertainties arising from variability in response to ground motion records.

An example set of fragilities is shown in Figure 26. Three sets of fragilities are shown, indicated as STR, NSDS, and NSAS for structural, drift-sensitive nonstructural, and acceleration-sensitive nonstructural, respectively. Each set includes three limit states, which represent the threshold of transitions between damage states. The damage states considered in the MAE Center and implemented in MAEViz for building stock are Insignificant (I), Moderate (M), Heavy (H), and Complete (C). Thus, a line identified in the legend with "DS>I", for example, represents the probability of exceeding the Insignificant damage state and transitioning from Insignificant to Moderate damage at a particular level of imposed hazard, which is taken as PGA in this plot.

It can be seen from the plot that both median values and the general shape of the vulnerability curves can be expected to vary depending on the type of damage and also the severity of damage. As a consequence of the fundamental constraint of lognormal distributions requiring zero probability for random variables values less than zero, the slope of the cumulative density function will become gradually more gentle as the median shifts farther from the origin, which coincidentally reflects an increased uncertainty of damage prediction for heavier damage states. For example, the structural curve representing the transition from Heavy to Complete damage (STR, DS>H) has a much gentler slope compared to the structural curve representing the transition from Insignificant to Moderate damage (STR, DS>I). This trend is consistent for all three damage types. Furthermore, the lines for transition of structural damage from Moderate to Heavy (STR, DS>M) and drift-sensitive nonstructural damage from Heavy to Complete (NSDS, DS>H) are almost identical, indicating that the drift-sensitive nonstructural components are naturally more prone to damage than the structural components of the building for the example building type.

One of the common challenges faced in a study of regional seismic risk is accurate selection of fragilities to represent vulnerability of the building stock. In HAZUS, the default mapping is based on judgment and implicitly assumes the use of the Uniform Building Code, which is clear by observing that the majority of structures are assigned to a Moderate code level. The assumed mapping applied by HAZUS was revisited as part of this study to determine if adjustments might be appropriate, considering the historical structural engineering practices in the region.

The first significant point to be considered relative to seismic engineering in Memphis, TN, is to note that there was no seismic code in effect until 1992 (Keuht, personal communication, 2006), at which point the seismic provisions in the Standard Building Code (1999) were implemented. According to the data recorded in the inventory dataset provided by French and Muthukumar (2006), 83.3% of buildings were constructed in 1992 or earlier, and these structures should be regarded as Pre-Code, since wind loads for the area are relatively low, and there were

no seismic provisions in place at the time these structures were designed. The HAZUS mapping, however, predicts 100% of Wood buildings and 70%-75% of Masonry buildings in the RES1 (single-family residence) and RES3 (multi-family residence) occupancy categories should be Moderate Code, with the remainder falling into the Pre-Code category. The dataset provided by French and Muthukumar (2006) was not adjusted to bring the construction dates into greater agreement with the HAZUS mapping because the values provided by French and Muthukumar (2006) reflected recorded data on a building-by-building basis, obtained directly from the Tax Assessor for Shelby County, whereas the HAZUS mapping scheme was a far more general and broadly intuitive assignment with less substantiating data to support the presumed distribution. Consequently, a rule for mapping of fragilities to inventory in the building stock was established so that buildings constructed in 1992 or earlier were presumed to be appropriately modeled with a Pre-Code level of vulnerability, and the remaining buildings were presumed to have some degree of seismic demand considered during design.

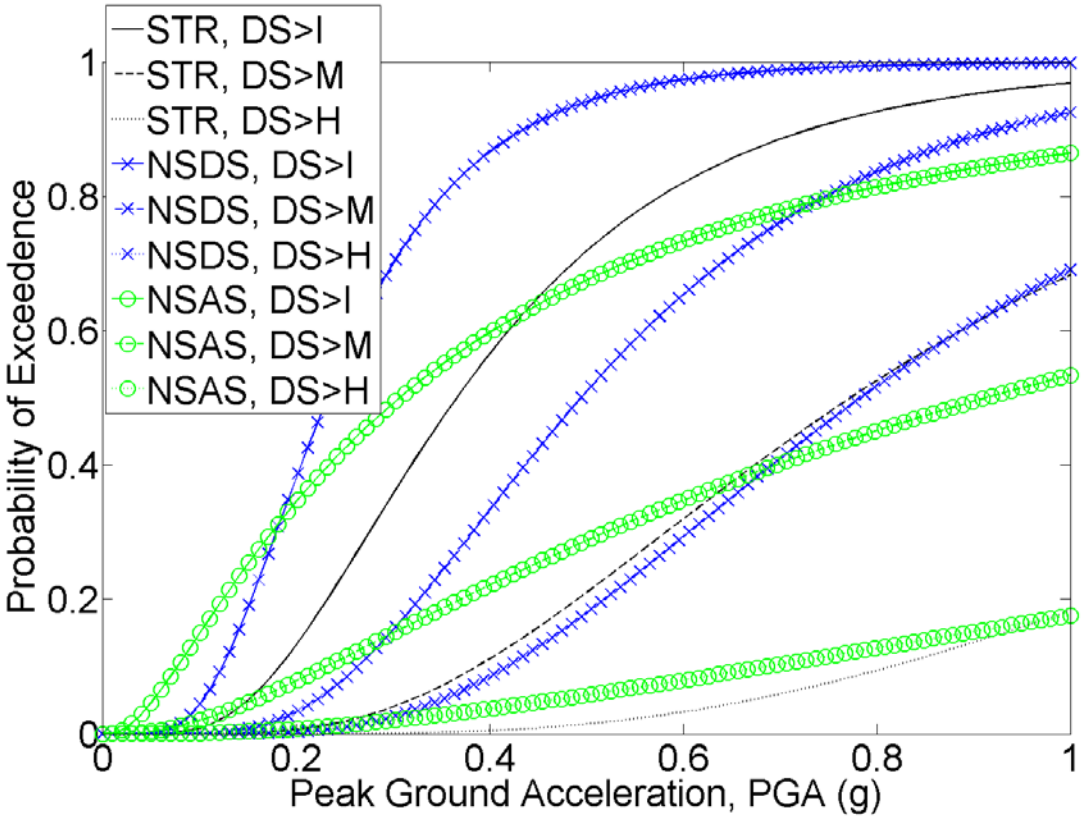

Figure 26. Example Fragilities for Wood Frame (W1)

The next required assessment was to determine an appropriate level of seismic demand presumed to be incorporated into buildings constructed after 1992. This assessment was made by reviewing the Uniform Building Code, which the HAZUS Technical Manual (FEMA, 2006) refers to as providing correlation for seismic design requirements and High, Moderate, Low, and Pre Code levels, and drawing comparisons between the elastic design requirements found therein

and in the Standard Building Code. The seismic provisions are not identical in their approaches, but they are conceptually consistent. Taking account of differences in the two methodologies (e.g., the use of a *Z* factor in the UBC and the use of A_a and A_v in the SBC, different values for *R* factors), spectra were developed and compared to determine an appropriate seismic design level for the region.

Example spectra are provided in Figure 27, plotting the elastic base shear coefficient versus natural structural period for a bearing wall system with light framed walls with shear panels and having three or fewer stories, which is a fitting description for typical wood frame residential structures that dominate the building stock. The spectra obtained from the two sets of provisions are not equivalent, but Low Code was conservatively assigned throughout the study region to structures built after 1992. This decision was influenced by the general lack of awareness of seismic hazard in the study region, as evidenced by the complete absence of any seismic design requirements prior to 1992, as well as the belief that although seismic design requirements were mandated, designers were not expected to rapidly accept and implement the new provisions, and would likely delay making adjustments to design practices and attempt to minimize the influence of the new provisions.

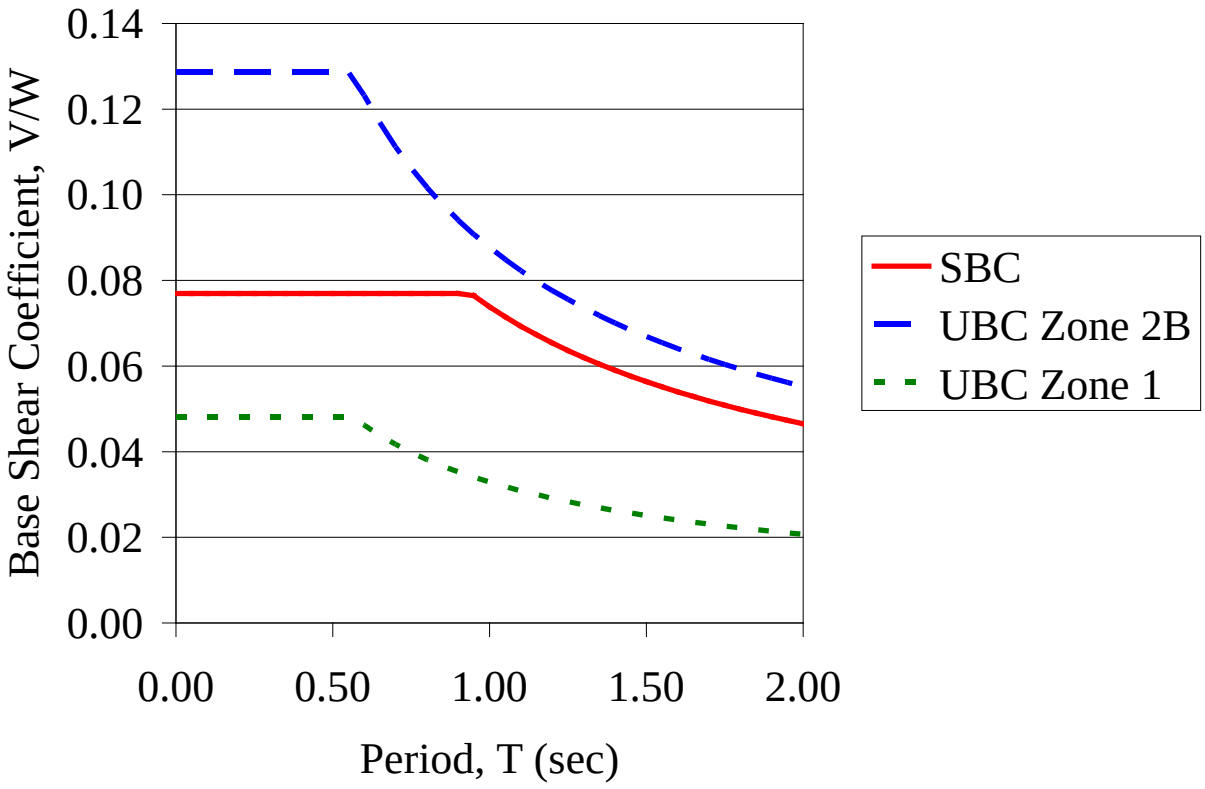

Figure 27. Example Elastic Design Spectra

Thus, the mapping scheme employed in the capstone scenarios was primarily driven by:

1. Structure Type (obtained from neural network model)
2. Number of Stories (obtained from Tax Assessor database)
3. Year of Construction (Pre-Code if constructed in 1992 or earlier, Low Code otherwise)

5.2 Bridge Vulnerability

Bridge vulnerability functions have been developed to reflect typical construction found in the Central and Eastern United States (DesRoches et al., 2006). The fragility sets include as-built cases as well as various retrofit schemes such as elastomeric bearings and seat extenders. No fragilities have been developed specifically to represent bridges constructed with seismic design, but this is because bridges in the region are generally not expected to have been designed with seismic considerations taken into account. The only procedural difference between evaluations of bridge damage relative to evaluation of building damage is that bridges are characterized by five damage states, similar to HAZUS, whereas buildings are characterized by four damage states.

5.3 Analytical Form of Vulnerability Functions and Treatment of Uncertainty

Vulnerability assessment of both building stock and bridge assets, with the exception of one set of building fragilities, takes the form of a lognormal cumulative density function (CDF), as shown in Equation (1).

$$P\left(DS > ds_i \mid S_a\right) = \Phi\left(\frac{\ln\left(S_a\right) - \lambda_i}{\beta_i}\right) \tag{1}$$

Where

$P(*)$	= probability of occurrence of (*)
DS	= actual damage state of structure
ds_i	= damage state "i"
S_a	= spectral acceleration
$\Phi(*)$	= cumulative normal distribution evaluated at (*)
λ_i	= lognormal median parameter defining the threshold of damage state "i"
β_i	= lognormal dispersion parameter defining the threshold of damage state "i"

In Equation (1), the S_a term is defined by the researcher providing the fragility set. The parameterized fragilities, for example, are provided in three groups, so that the user may select whether to use spectral acceleration at 0 seconds (PGA), 0.3 seconds, or 1 second period. Hazard uncertainty was propagated through the vulnerability assessment by calculating a

lognormal standard deviation of the ground shaking hazard, β_{Sa}, term for the ground shaking hazard, and replacing the β_i term with a $\overline{\beta}_i$ term, where

$$\overline{\beta}_i = \sqrt{\beta_i^2 + \beta_{Sa}^2} \tag{2}$$

The adjustment shown in Equation (2) results in a fragility curve with a gentler slope to reflect the increased uncertainty resulting from the use of an uncertain spectral acceleration input, while maintaining the same bounds of probability, from 0% to 100%.

5.4 Combination of Ground Shaking and Ground Failure Hazard Effects

The vulnerability formulation provided in the previous section describes the probability of exceeding a particular limit state, given lognormal distribution parameters for the limit state of interest, based on a specified level of ground shaking intensity, quantified by the S_a term. When a building is also subject to liquefaction hazard, the probability of exceeding limit state thresholds due to the combined effect of ground shaking and ground failure is determined by assuming that the probabilities of breeching limit state thresholds due to each of the two types of hazards are statistically independent (Steelman et al., 2006). Thus,

$$\hat{P}\left(DS > ds_i\right) = P_{GS}\left(DS > ds_i \mid S_a\right) + P_{GF}\left(DS > ds_i \mid P\left(LPI > 15\right)\right) - P_{GS}\left(DS > ds_i \mid S_a\right) * P_{GF}\left(DS > ds_i \mid P\left(LPI > 15\right)\right) \tag{3}$$

Where

$\hat{P}(*)$	= probability of occurrence of (*) as a result of combined effects of ground shaking and ground failure
$P_{GS}(*)$	= probability of occurrence of (*)
$P_{GF}(*)$	= probability of occurrence of (*)
$P(LPI>15)$	= probability of LPI exceeding 15
DS	= actual damage state of structure
ds_i	= damage state “i”
S_a	= spectral acceleration

According to the current implementation of the liquefaction-induced damage algorithm, damage resulting from liquefaction effects is assumed to generate Complete damage exclusively. Furthermore, as discussed in Section 4.2, the probability of damage occurring as a result of liquefaction effects is assumed equal to the probability of LPI exceeding 15. Therefore, the following simplification may be made in Equation (3),

$$P_{GF}\left(DS > ds_i \mid P\left(LPI > 15\right)\right) = P\left(LPI > 15\right) \tag{4}$$

5.5 Determination of Discrete Damage States

For both buildings and bridges, discrete damage state mean probabilities are determined by taking the differences of adjacent damage state exceedence probabilities. Therefore, for buildings, the mean probabilities are determined as follows:

$$\hat{P}\left(DS = ds_I\right) = 1 - \hat{P}\left(DS > ds_I\right) \tag{5}$$

$$\hat{P}\left(DS = ds_M\right) = \hat{P}\left(DS > ds_I\right) - \hat{P}\left(DS > ds_M\right) \tag{6}$$

$$\hat{P}\left(DS = ds_H\right) = \hat{P}\left(DS > ds_M\right) - \hat{P}\left(DS > ds_H\right) \tag{7}$$

$$\hat{P}\left(DS = ds_C\right) = \hat{P}\left(DS > ds_H\right) \tag{8}$$

where the subscripts on the *ds* terms indicate specific damage states: I, M, H, and C for Insignificant, Moderate, Heavy, and Complete, respectively. Damage states for bridges are similar, except that the damage states were selected to parallel those found in HAZUS, which are None, Slight, Moderate, Extensive, and Complete (FEMA, 2006).

6 CAPSTONE SCENARIO RESULTS: ECONOMIC AND SOCIAL IMPACTS

A number of economic and social consequence models are available and have been applied to the study region for the capstone scenarios. Generally, there is a direct correlation drawn from physical damage to social and economic consequences.

6.1 Direct Economic Loss

The most fundamental loss parameter provided in any regional seismic risk study is the direct cost required to repair and replace inventory assets damaged by the earthquake. For buildings, the process follows similarly to the approach adopted in the HAZUS methodology (FEMA, 2006). Damage factors were proposed by Bai et al. (2007) and implemented for the capstone predictions. The parameters proposed by Bai et al. (2007) are shown in Table 7 and Table 8, together with similar factors applied to drift-sensitive and acceleration-sensitive nonstructural economic loss (abbreviated as NSDS and NSAS, respectively) and contents losses. Plots are also provided in Figure 28 through Figure 31 to represent the probabilistic distribution of damage factors for each damage state in each damage type category. All damage factors were assumed to be uncorrelated beta distributed random variables. The nonstructural and contents damage factor means were selected to generally follow the approach in the HAZUS methodology (FEMA, 2006). Direct economic losses are calculated for each inventory item according to the following equation

$$E\left[L_i\right] = M_i \sum_{j=1}^{4} \alpha_j \mu_j \tag{9}$$

Where

$E[L_i]$ = expected direct economic loss ($) of inventory item i

M_i = replacement cost ($) of inventory item i

α_j = partitioning factor for damage type j (determined by occupancy)

μ_j = mean damage factor for damage type j

And the mean damage factor is determined by

$$\mu_j = \sum_{k=1}^{4} \hat{P}\left(DS = ds_k\right) * \mu_{DF_{k,j}} \tag{10}$$

Where

$\mu_{DF_{k,j}}$ = mean damage factor for damage state k of damage type j

Uncertainty is calculated by applying

$$VAR[L_i] = M_i^2 \sum_{j=1}^{4} \alpha_j^2 \sigma_j^2 \quad (11)$$

Where

$VAR[L_i]$ = variance of direct economic loss ($) of inventory item *i*

σ_j^2 = variance of damage factor for damage type *j*

And the variance of the damage factor is determined by

$$\sigma_j^2 = \sum_{k=1}^{4} \left[\hat{P}(DS = ds_k) * \left(\sigma_{DF_{k,j}}^2 + \mu_{DF_{k,j}}^2 \right) \right] - \mu_j^2 \quad (12)$$

Where

$\sigma_{DF_{k,j}}^2$ = variance of damage factor for damage state *k* of damage type *j*

The mean and variance of loss for an item, considering inventory uncertainty, is determined by a linear weighted combination of mean and variance calculated by assuming each of the potential alternate structure types during damage assessment.

Table 7. Damage Factor Mean Values (μ_{DF})

Damage State	Damage Type			
	Structural	NSDS	NSAS	Contents
Insignificant	0.005	0.03	0.03	0.015
Moderate	0.155	0.18	0.13	0.09
Heavy	0.55	0.525	0.425	0.2625
Complete	0.9	0.875	0.825	0.4375

Table 8. Damage Factor Standard Deviation Values (σ_{DF})

Damage State	Damage Type			
	Structural	NSDS	NSAS	Contents
Insignificant	0.002	0.02	0.02	0.01
Moderate	0.058	0.08	0.0467	0.04
Heavy	0.1	0.15	0.15	0.075
Complete	0.04	0.0833	0.117	0.0417

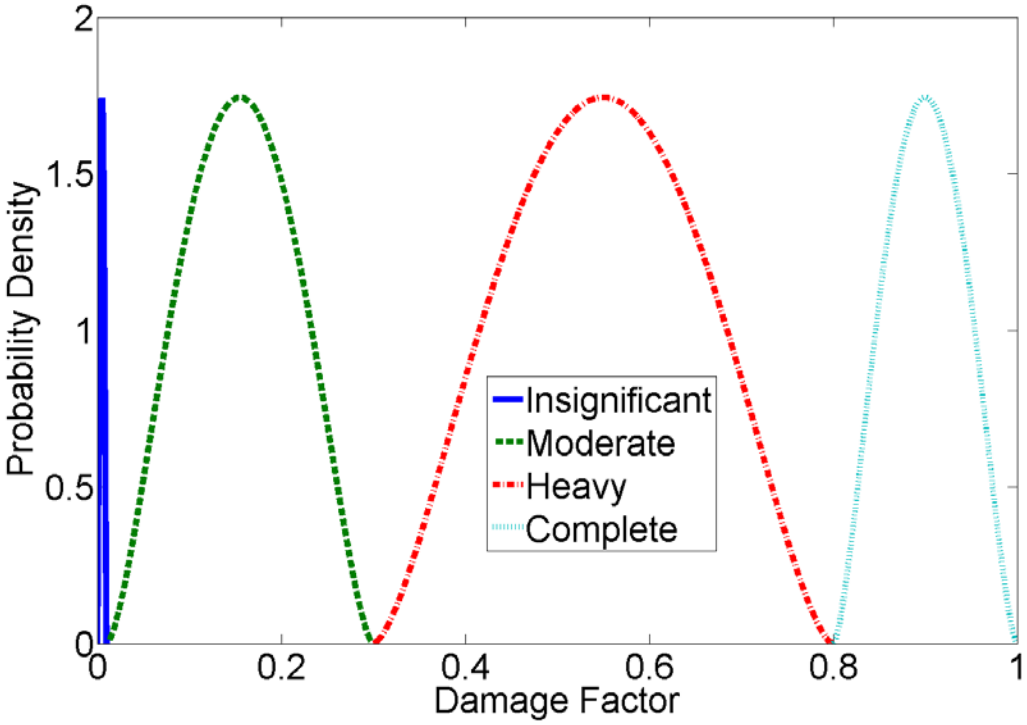

Figure 28. Damage Factor Probabilistic Distributions for Structural Damage

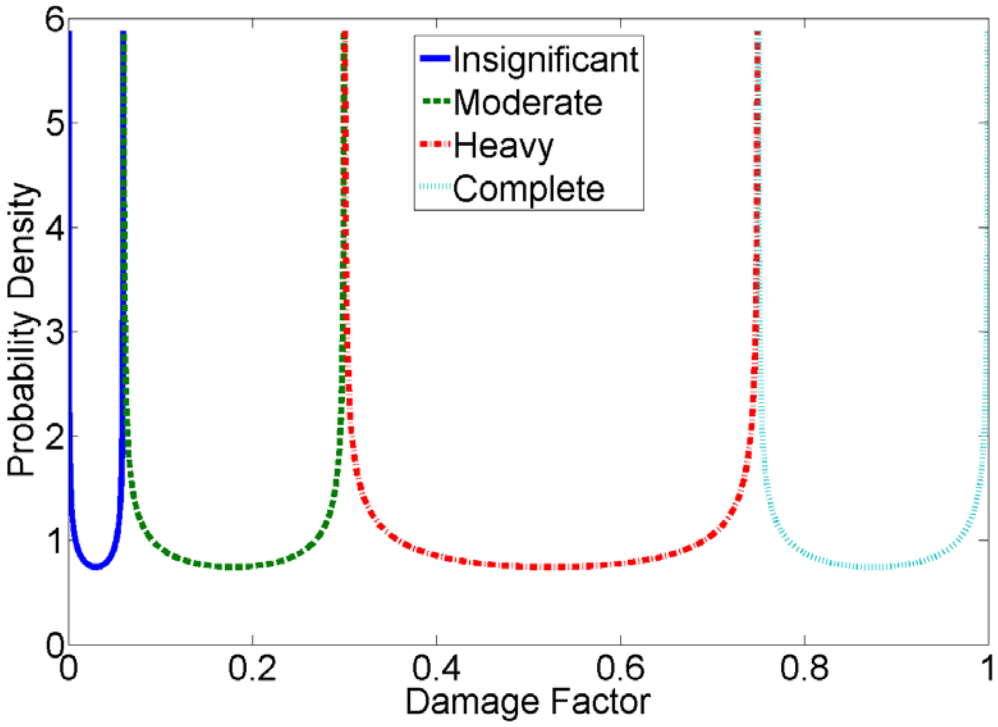

Figure 29. Damage Factor Probabilistic Distributions for Drift-Sensitive Nonstructural Damage

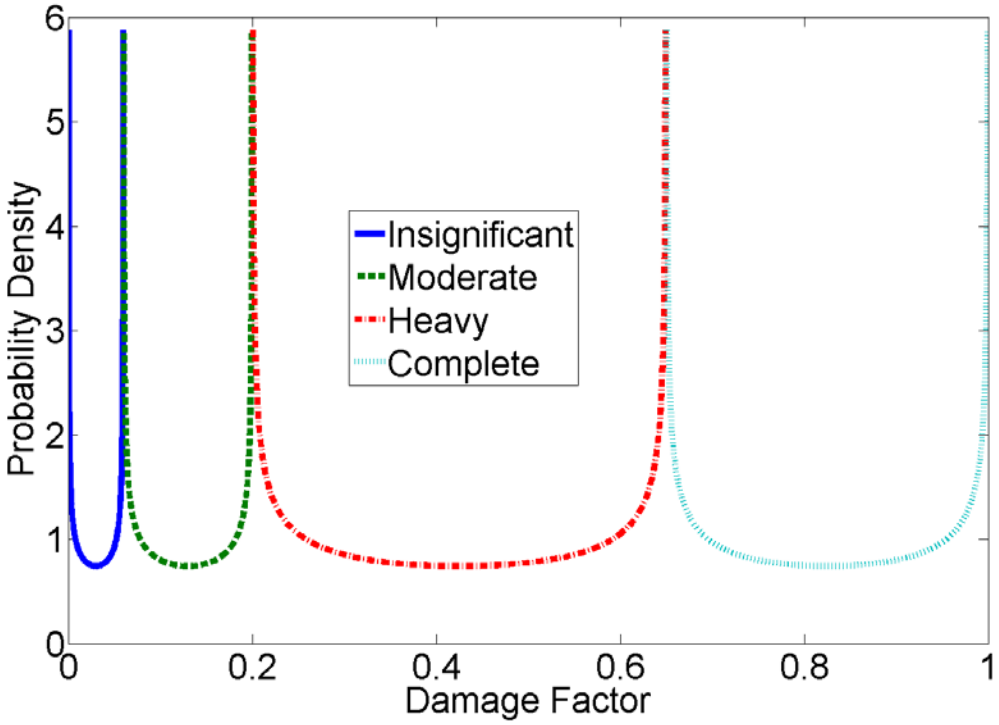

Figure 30. Damage Factor Probabilistic Distributions for Acceleration-Sensitive Nonstructural Damage

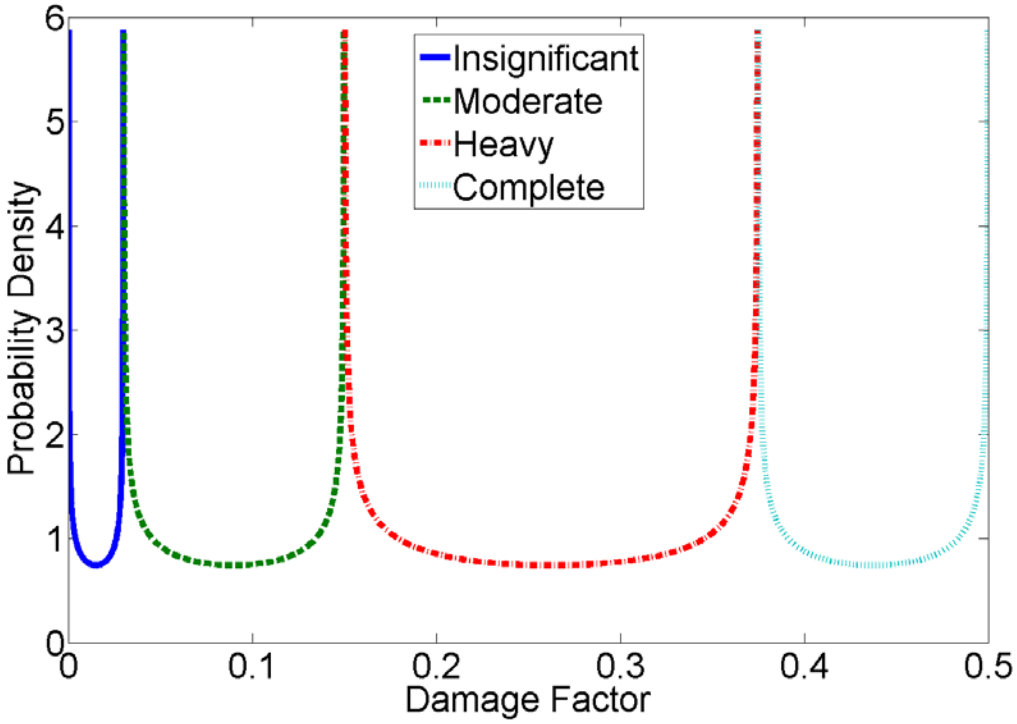

Figure 31. Damage Factor Probabilistic Distributions for Contents Damage

The damage estimation methodology for bridge repair costs is similar to buildings. Mean and standard deviation parameters for replacement costs of bridge types have been collected for the Transportation Testbed Project and implemented in this study. Estimated repair costs for bridges are determined by

$$E\left[L_i\right] = BRC_i L_i W_i \mu_i \tag{13}$$

Where

$E[L_i]$ = expected direct economic loss ($) of inventory item i

BRC_i = mean bridge replacement cost ($/ft^2) of inventory item i

L_i = plan length (ft) of inventory item i

W_i = plan width (ft) of inventory item i

μ_i = mean damage factor for inventory item i

Mean and standard deviation parameters correlating bridge damage to loss are shown in Table 9 and the probability density functions of the beta-distributed bridge damage factors are plotted in Figure 32 and Figure 33. Note in Table 9 that damage factor parameters for the complete damage state reflect the expectation that the Complete damage state is correlated with the unseating of at most two spans simultaneously. Therefore, as the number of spans increases, the damage proportionate to the entire structure decreases. This pattern is shown in Figure 33, as the mean shifts downward and the distribution becomes more concentrated near the mean with increasing spans, n.

Table 9. Bridge Damage Factor Distribution Parameters

Damage State	Spans (n)	Mean	Standard Deviation
None	any	0.005	0.00333
Slight	any	0.02	0.00667
Moderate	any	0.08	0.0433
Extensive	any	0.25	0.1
Complete	<= 2	0.65	0.233
Complete	>2	1.30/n	2/3n - 0.1

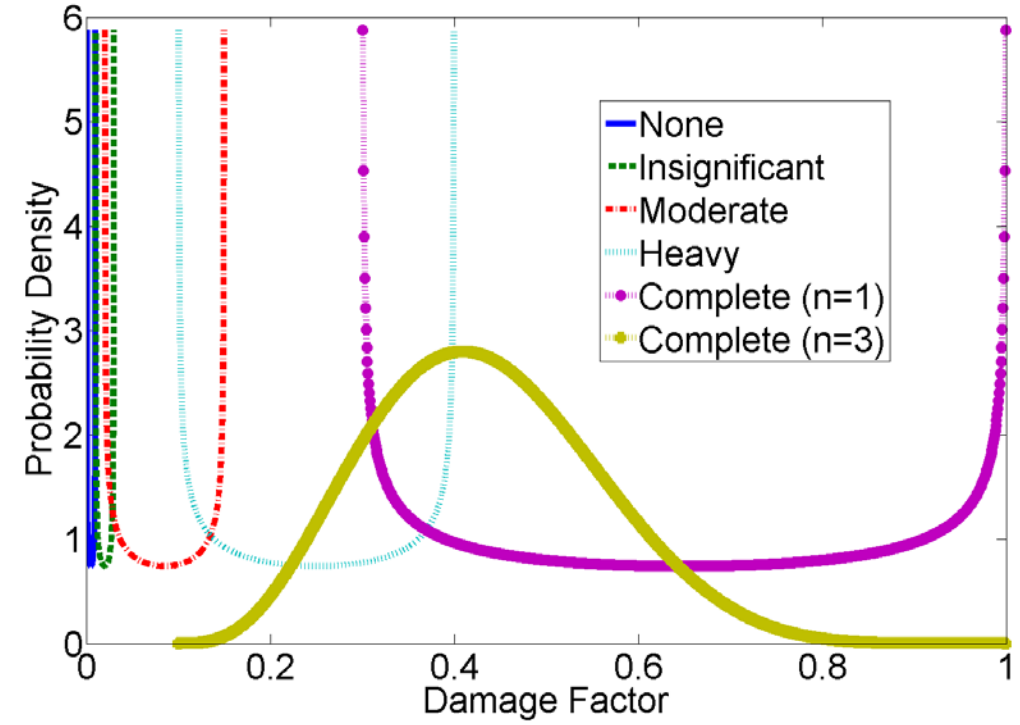

Figure 32. Damage Factor Probabilistic Distributions for Bridge Damage

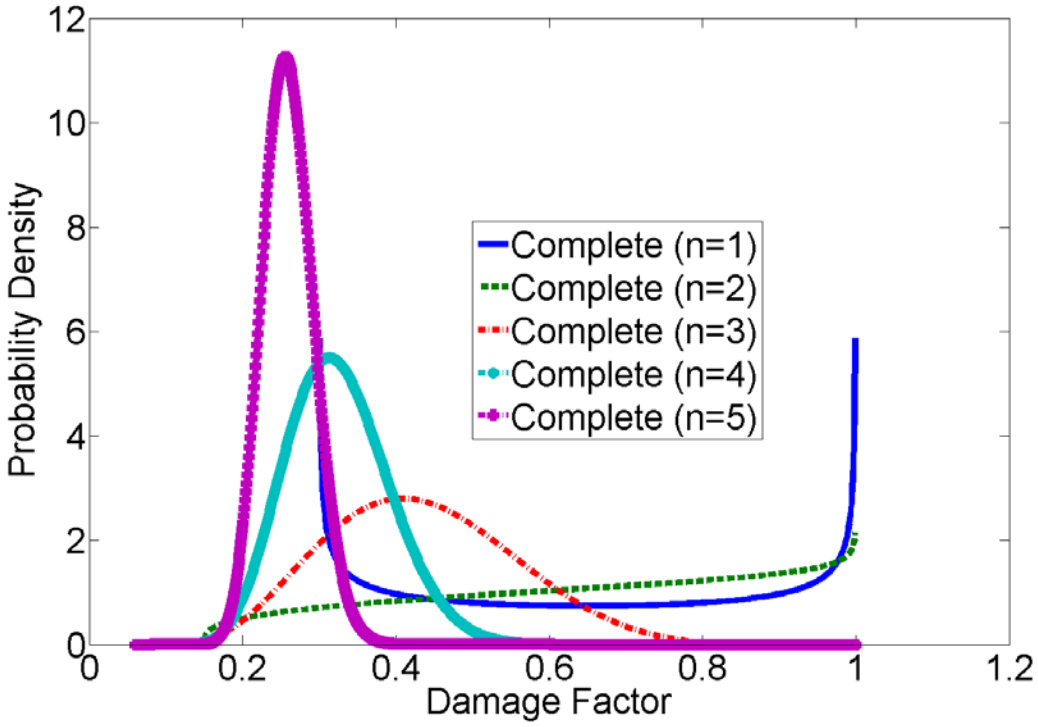

Figure 33. Damage Factor Probabilistic Distributions for Complete Bridge Damage, varying numbers of spans

By applying the algorithms and data described up to this point, direct economic losses from the Blytheville source scenario for buildings and bridges are estimated to be $4.80 billion and $10.6 million, respectively. Similar estimates for the Marked Tree source scenario are $2.48 billion and $2.82 million, respectively. Further detailed investigations focus on the consequences of the Blytheville source event since it clearly poses the greater risk. Total direct economic loss (the sum of structural, nonstructural, and contents repair and replacement costs) are shown aggregated to census tracts in Figure 34, and loss ratios are shown by nine quantiles (colors darkening with each increasing step of 11.1% of included tracts) in Figure 35. The representation of loss in Figure 34 is influenced by the mixture of structure and occupancy types, together with the total exposure of dollar value for each tract, as opposed to the distribution of loss shown in Figure 35, which represents only the relative loss for each tract normalized by its own exposure.

The mean loss ratio for the entire building stock subjected to the Blytheville source is 8.3%, calculated as the sum of direct economic losses for the study region building stock, divided by the sum of total appraised value and total contents value of the building stock. Uncertainty characteristics for the total direct economic loss are shown in Figure 36 and Figure 37. Coefficients of variation (cov's) are shown by structure type in Figure 36. The primary influences on the cov's are the uncertainty associated with particular damage states and types, the vulnerability of structure types and the associated likelihood of falling into damage state categories with more uncertain loss estimation parameters, and the total number of structures of each structure type in the inventory. Cov's are a normalized representation of uncertainty, calculated as the ratio of standard deviation to mean of a particular parameter, which is total direct economic loss in this case. With an increasing number of inventory items, the mean and the variance of the loss estimate grow proportionately with the exposed inventory. However, standard deviation is the square root of variance, so the growth of the mean will outpace the growth of the standard deviation.

The importance of this influence is evident by the fact that both the W1 and TOTAL cov's are clearly smaller than the other structure types, in spite of the fact that the W1 structures exhibit higher damage ratios, as shown in later figures. As the damage ratio increases, it would generally be expected that uncertainty would increase as well. There is greater uncertainty in higher damage states as opposed to very light damage states as a result of wider availability of data for losses associated with light damage and improved accuracy of prediction of building behavior when only light damage is sustained and linear analysis approaches remain reasonably accurate. For the W1 structure type, however, there is much less relative uncertainty, compared with the other structure types, and this outcome parallels the fact that the great majority of structures in the inventory are expected to be W1 structures.

Data is also presented in Figure 37 to illustrate the expected range of damage factors for general structure types. Data points are plotted at intervals of 0.0025 in the total damage factor.

Similarly to the description of cov for W1 structures, the wood (W) general structure type shows very little uncertainty in prediction, but that statement is only marginally more evident for wood structures when compared to any other general structure type. In all cases, the range of damage factor is observed to be limited to about 0.02.

The loss ratios are shown broken down by structure type and occupancy type, both as actual calculated loss ratios, and also as variations relative to the mean for the entire inventory in Figure 38 through Figure 41. The key feature in the figures shown can be traced to the distribution of value among building components, and the associated vulnerability of those components. The W1 and W2 structure types tend to have higher loss ratios, as does the RES1 occupancy. These structures tend to be more significantly influenced by drift-based vulnerability as compared to other structures, as a consequence of the proportion of exposure constituted by structural and drift-sensitive nonstructural elements. Only the COM10 (parking structures) occupancy category has a greater proportion of drift-sensitive vulnerability, at 52% versus 49% for RES1. Other RES occupancies are typically governed by drift-sensitive vulnerability by about 38-39%, while COM occupancies are about 20-30% and IND are about 11%.

Both acceleration-sensitive nonstructural components and contents are evaluated using acceleration-sensitive nonstructural component vulnerability, similarly to HAZUS (FEMA, 2006). The nonstructural fragility functions implemented in the capstone scenarios followed the vulnerability thresholds published in the HAZUS Technical Manual, but also were determined by applying the parameterized fragility method (Jeong and Elnashai, 2007) as modified in Steelman and Hajjar (2008). The greater influence of drift-sensitive vulnerability leads the W1 and W2 RES1 structures to dictate the core of the regional loss, while the other structures and occupancies tend to have lower predicted loss ratios and draw the average predicted loss ratio down.

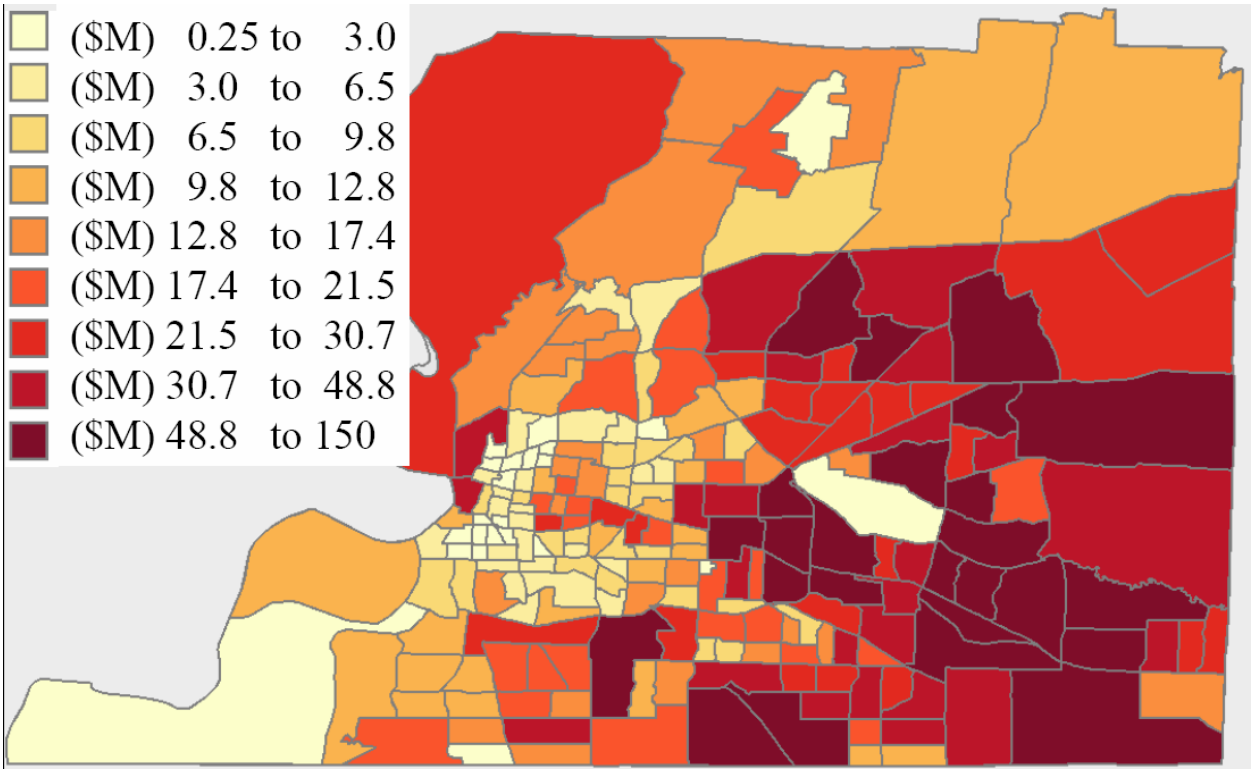

Figure 34. Total Loss Aggregated to Census Tracts (Quantile)

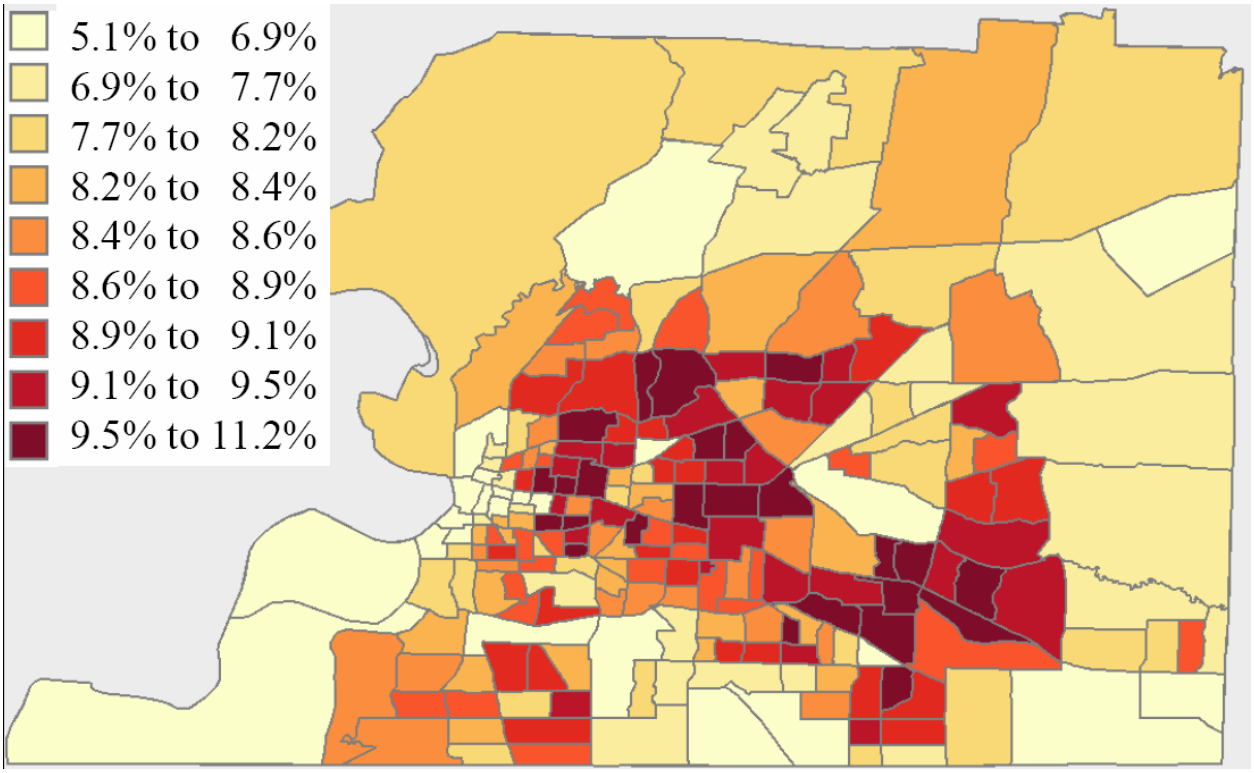

Figure 35. Total Loss Ratio by Census Tract (Quantile)

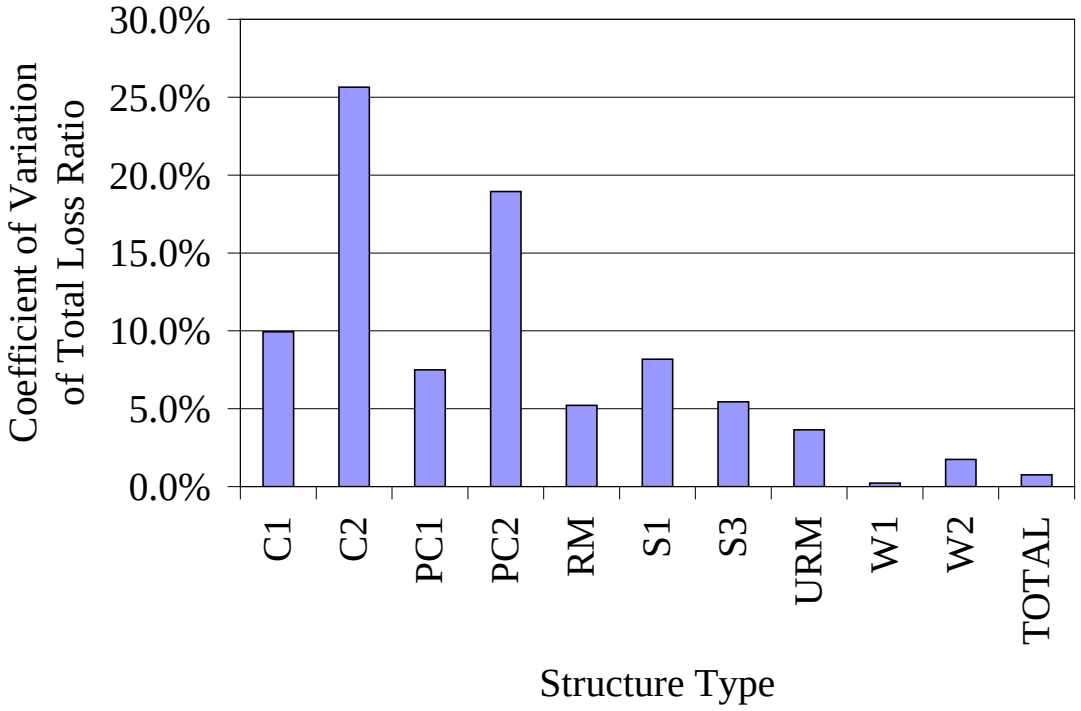

Figure 36. Coefficient of Variation of Total Direct Economic Loss Ratio by Structure Type

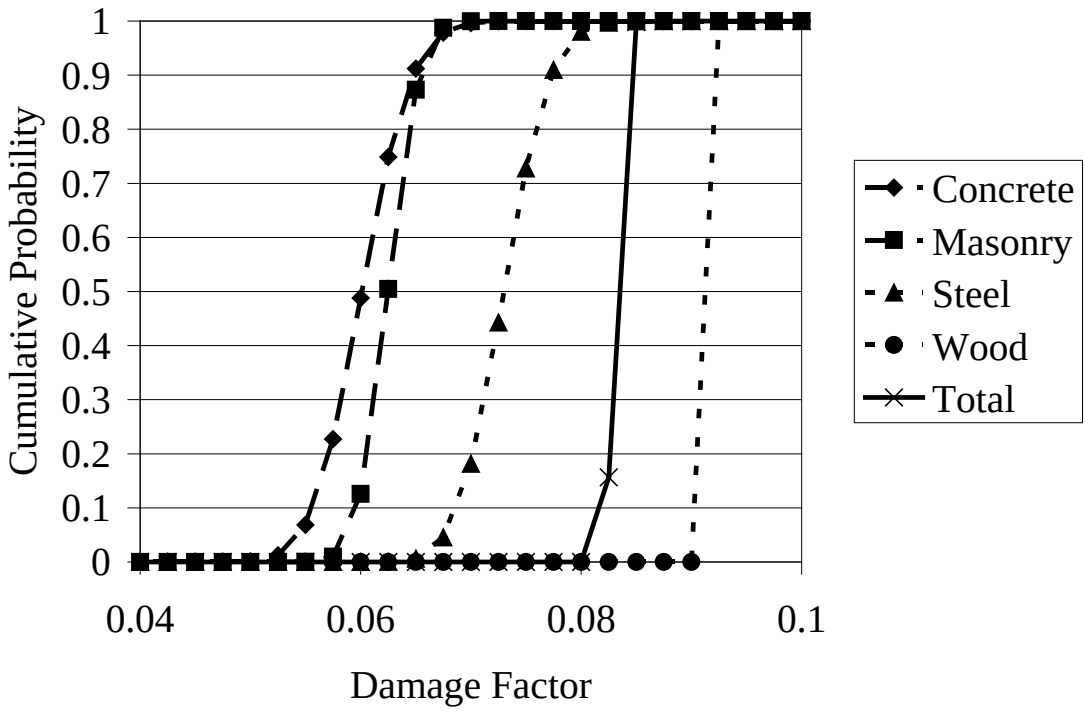

Figure 37. Cumulative Probabilities of Damage Factors by General Structure Type

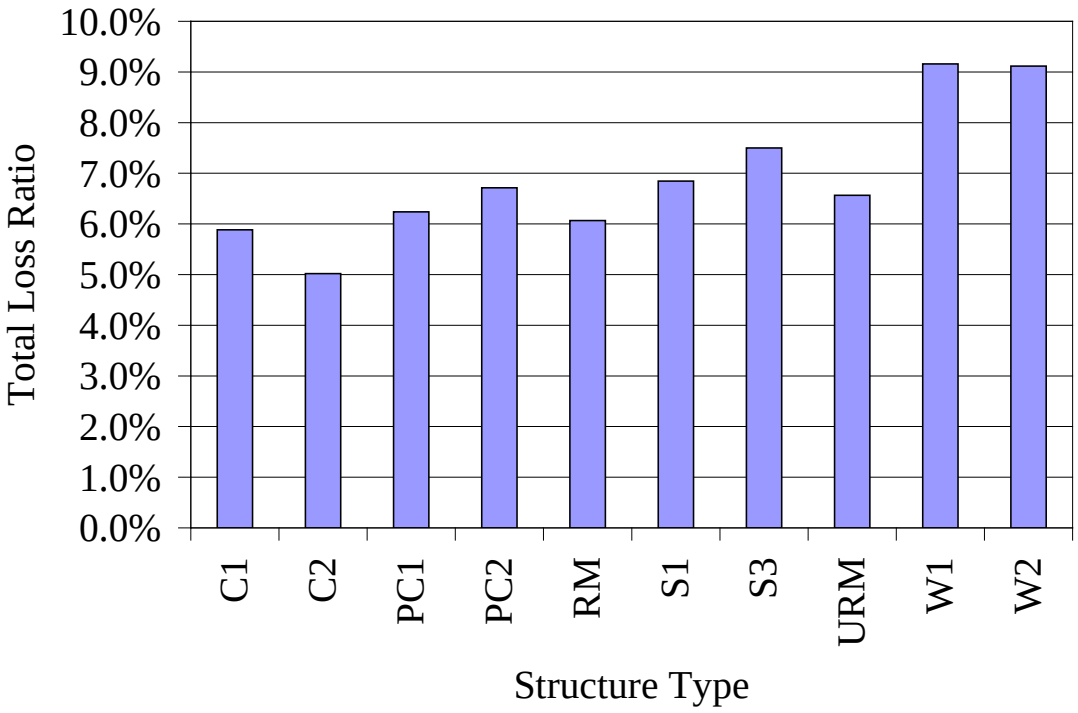

Figure 38. Total Direct Economic Loss Ratio by Structure Type

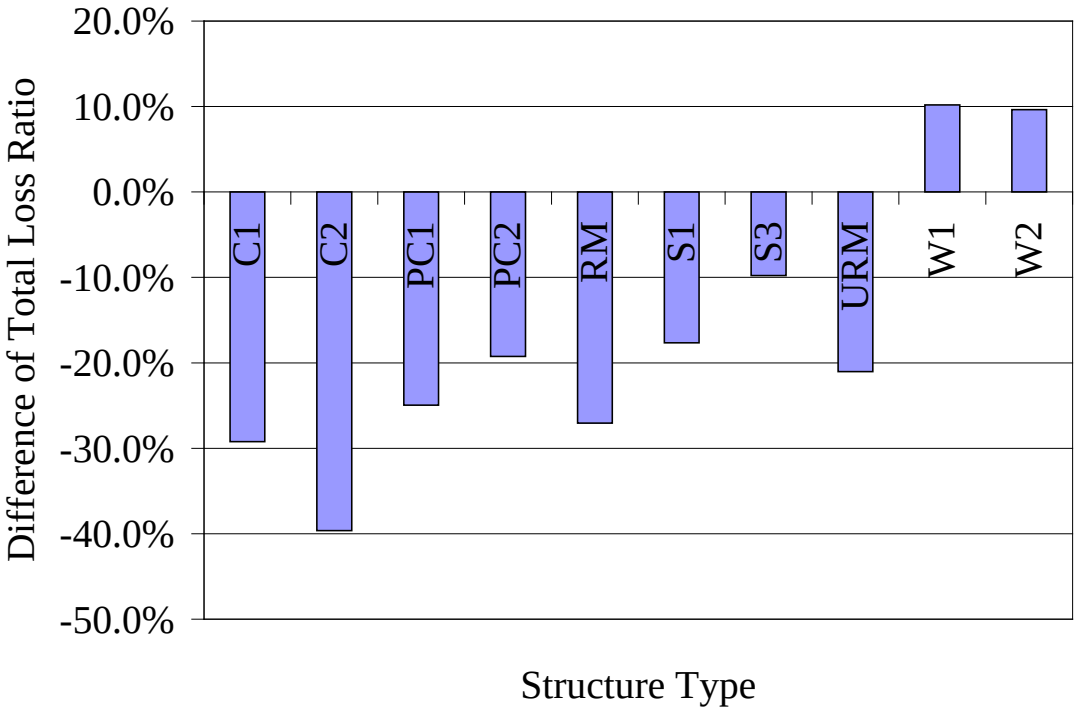

Figure 39. Variation of Total Direct Economic Loss Ratio by Structure Type (Relative to Mean Loss Ratio for Entire Inventory)

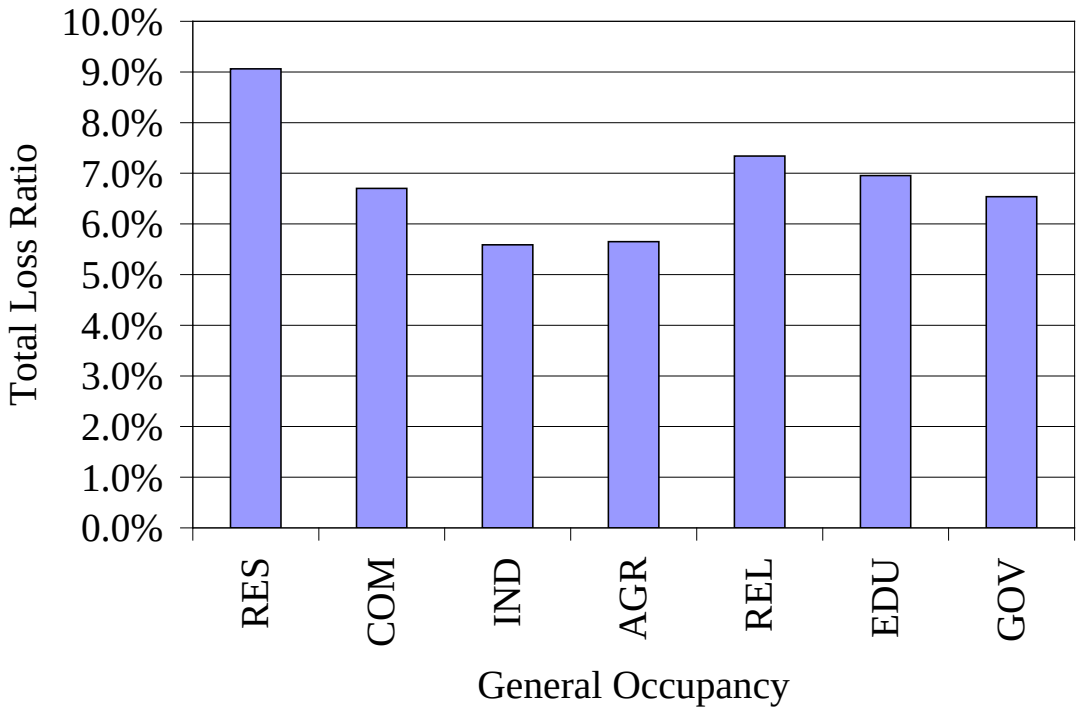

Figure 40. Total Direct Economic Loss Ratio by Occupancy Type

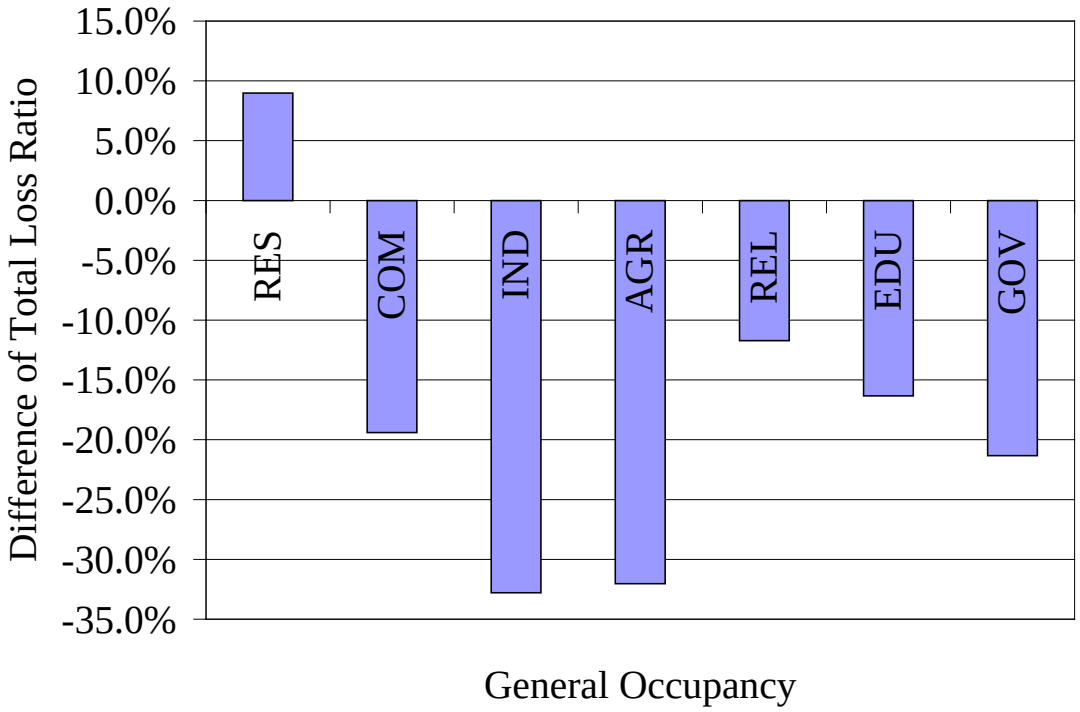

Figure 41. Variation of Total Direct Economic Loss Ratio by Occupancy Type (Relative to Mean Loss Ratio for Entire Inventory)

The reliability of economic loss prediction with respect to the influences of hazard and inventory uncertainty was also investigated. A subset of buildings neglecting the RES1 occupancy was analyzed subject to the Blytheville source, and results were obtained from the four combinations of considering or neglecting hazard and inventory uncertainty. A probabilistic loss ratio was determined for each combination by applying the structural damage factors to the appraised value of each building in the subset. The results are plotted in Figure 42.

The effect of hazard uncertainty is more noticeably pronounced than that of inventory uncertainty. When hazard uncertainty was considered, the expected loss ratio increased by approximately 64%. The range of 90% confidence also increased by about 63% to 73%, depending on whether inventory uncertainty was considered. The increase in expected loss is a combination of an increase in the vulnerability uncertainty and the fact that damage is relatively light. For a heavily damaged structure, hazard uncertainty may result in a decrease in expected loss. The increase in uncertainty of the loss estimate also includes a secondary result of the shift to higher expected damage, where the loss estimate is being increasingly more strongly influenced by damage factors with greater uncertainty than the Insignificant damage state. The general uncertainty remained relatively small, with a coefficient of variation of about 4.3% to 4.7% for all cases. In each case where inventory uncertainty was included and compared against a similar analysis with respect to hazard uncertainty, the case including inventory uncertainty experienced a relative decrease in expected loss of about 1.5%.

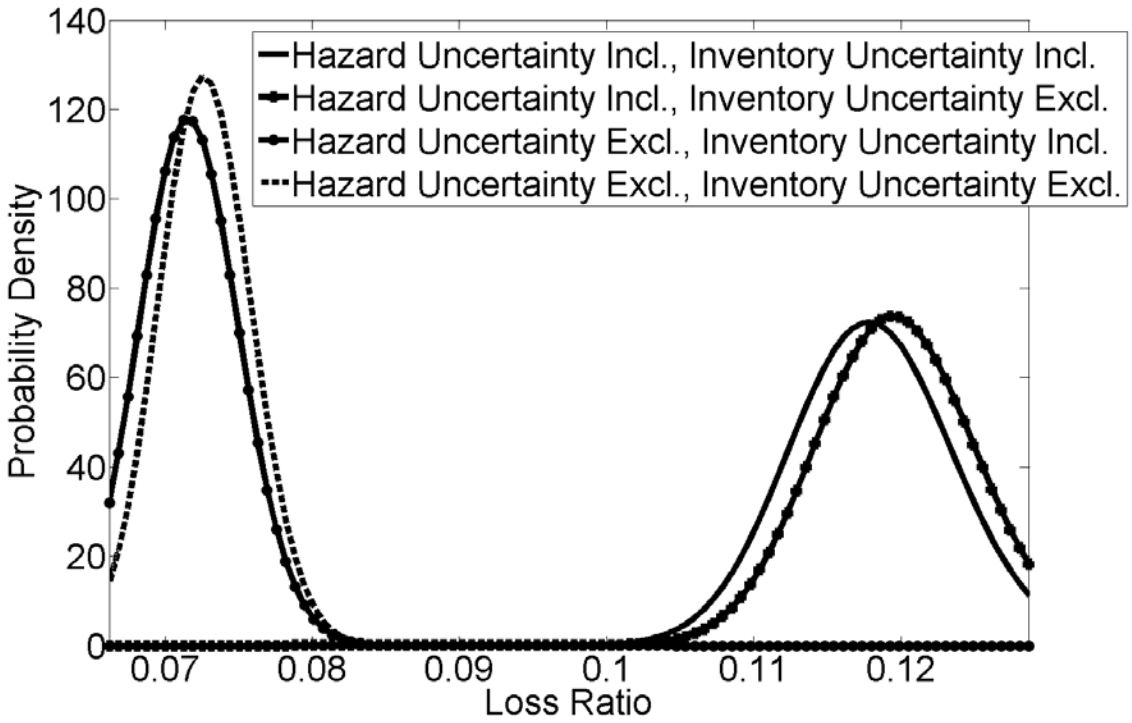

Figure 42. Beta-Distributed Loss Ratios

6.2 Bridge Functionality

Bridge functionality and restoration rates were investigated in the Transportation Testbed Project and documented in Padgett and DesRoches (2007). Bridge functionality is determined by first calculating an expected damage factor, as described previously. The expected damage state is then found by comparing the expected damage factor with the damage factor ranges for the various damage states, as shown in Table 10. Each damage state has an associated stepped restoration function, as shown in Figure 43. The count of bridges in each expected damage state is shown in Figure 44, and the progression of restoration for the study region is shown in Figure 45. The functionality of bridges in the study region immediately following the earthquake (day 0), as well as one, three, and seven days after the earthquake are shown in Figure 46 through Figure 48 for the Blytheville source scenario.

Although the data collected for Padgett and DesRoches (2007) is based on the expert opinions of practicing engineers in the region, and should therefore be reasonably reliable, the underlying premise of the survey responses was that sufficient resources in terms of manpower and equipment were available to perform work on damaged bridges. Further refinement in the results is thus possible due to lack of data to address the resources required to repair each damaged bridge type and damage level, together with a lack of data to indicate what resources could reasonably be expected to be available after a major seismic event. The expectation that within 24 hours, 89 Moderately damaged bridges can be brought from 0% to 50% functionality, while at the same time, 220 Slightly damaged bridges can be brought from 50% to 100% functionality, seems unlikely. Still, if the time scale were to be extended, the distribution of damage and bridge functionality is expected to be reasonably representative of expected seismic impacts on the region's transportation network.

Table 10. Correlation of Bridge Damage States to Damage Factor Ranges

Damage State	Damage Factor	
	Minimum	Maximum
None	0	0.99
Slight	1	2.99
Moderate	3	14.99
Extensive	15	39.99
Complete	40	100

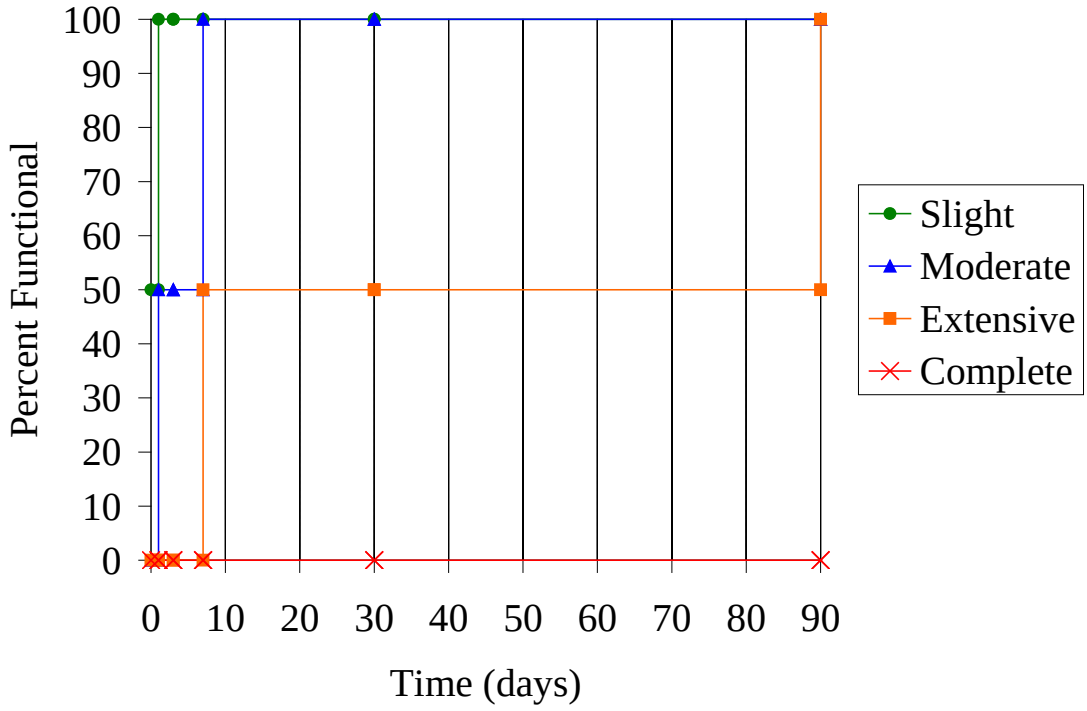

Figure 43. Bridge Restoration Functions [after Padgett and DesRoches (2007)]

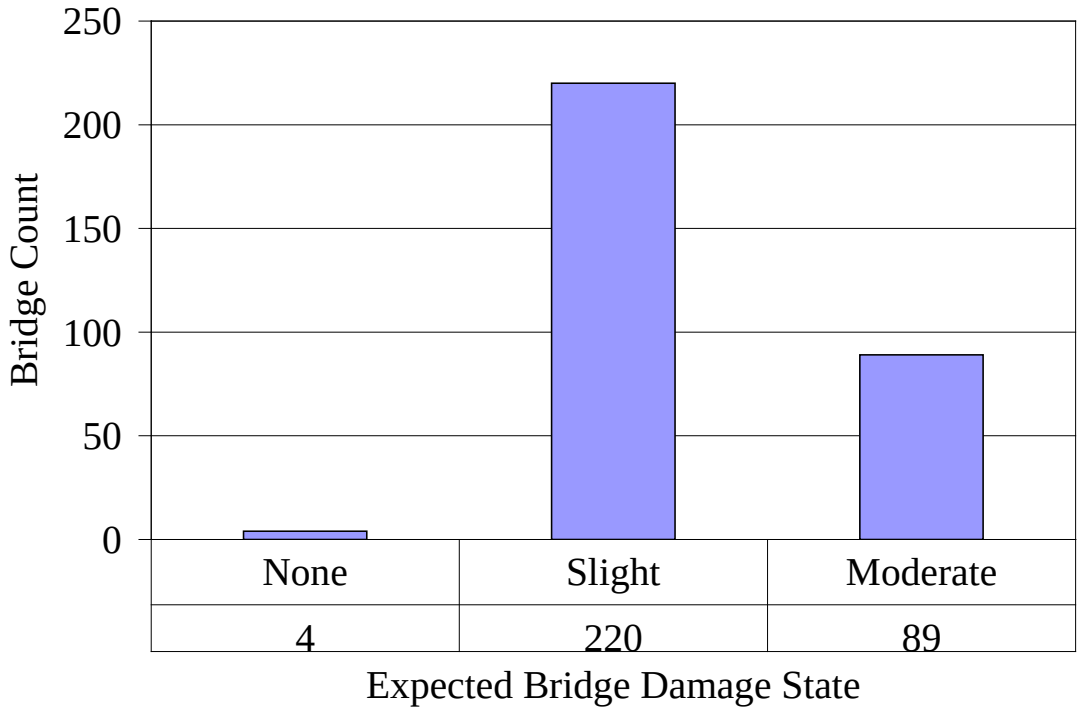

Figure 44. Bridge Expected Damage States for Blytheville Source

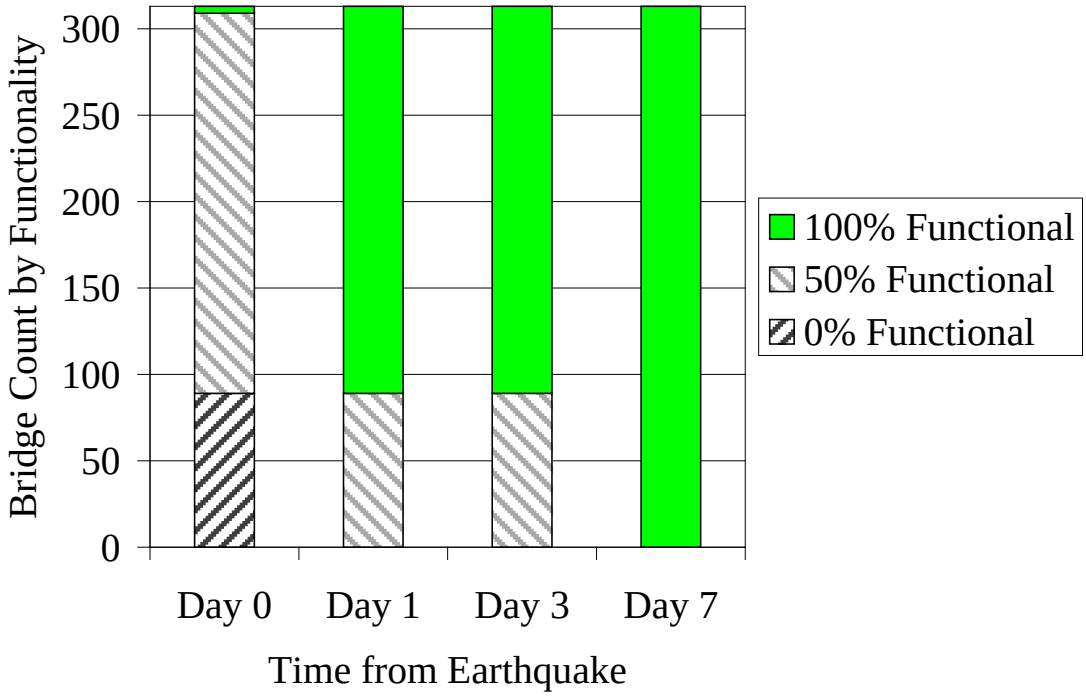

Figure 45. Bridge Counts by Functionality for Blytheville Source

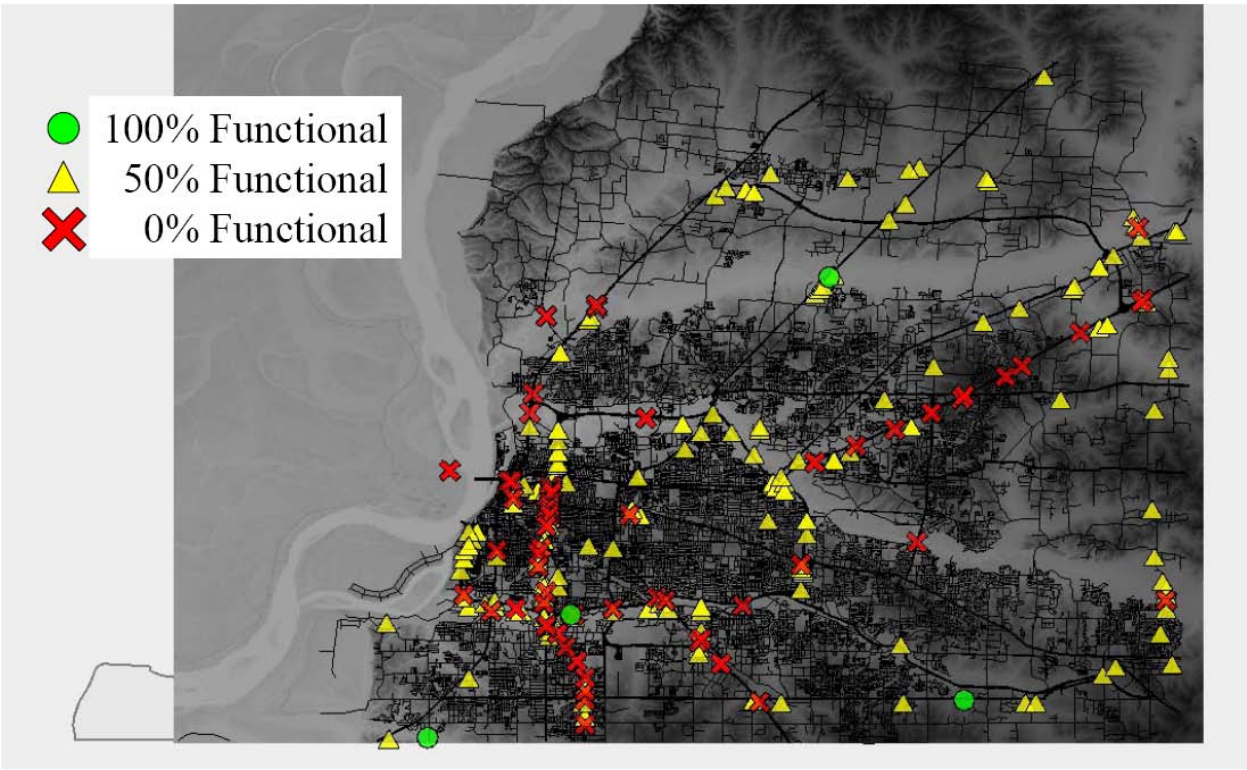

Figure 46. Bridge Functionality at Day 0 for Blytheville Source

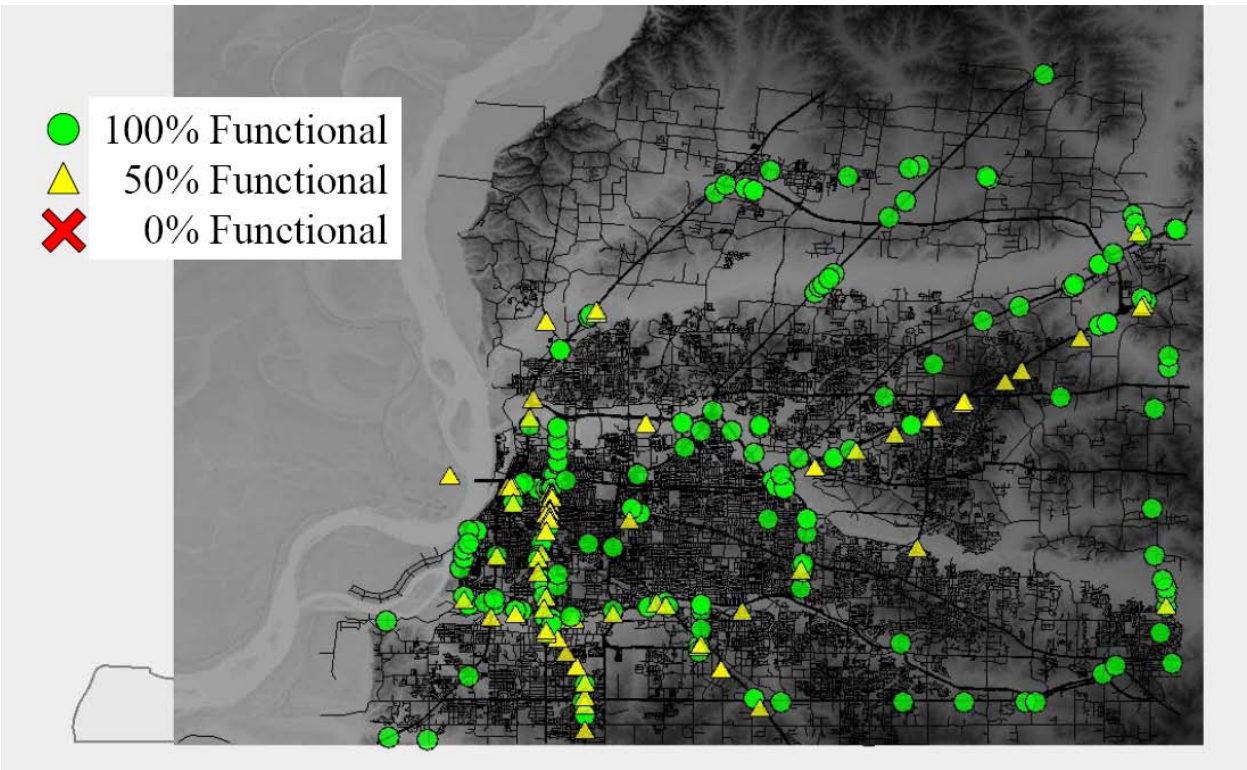

Figure 47. Bridge Functionality at Day 1 and Day 3 for Blytheville Source

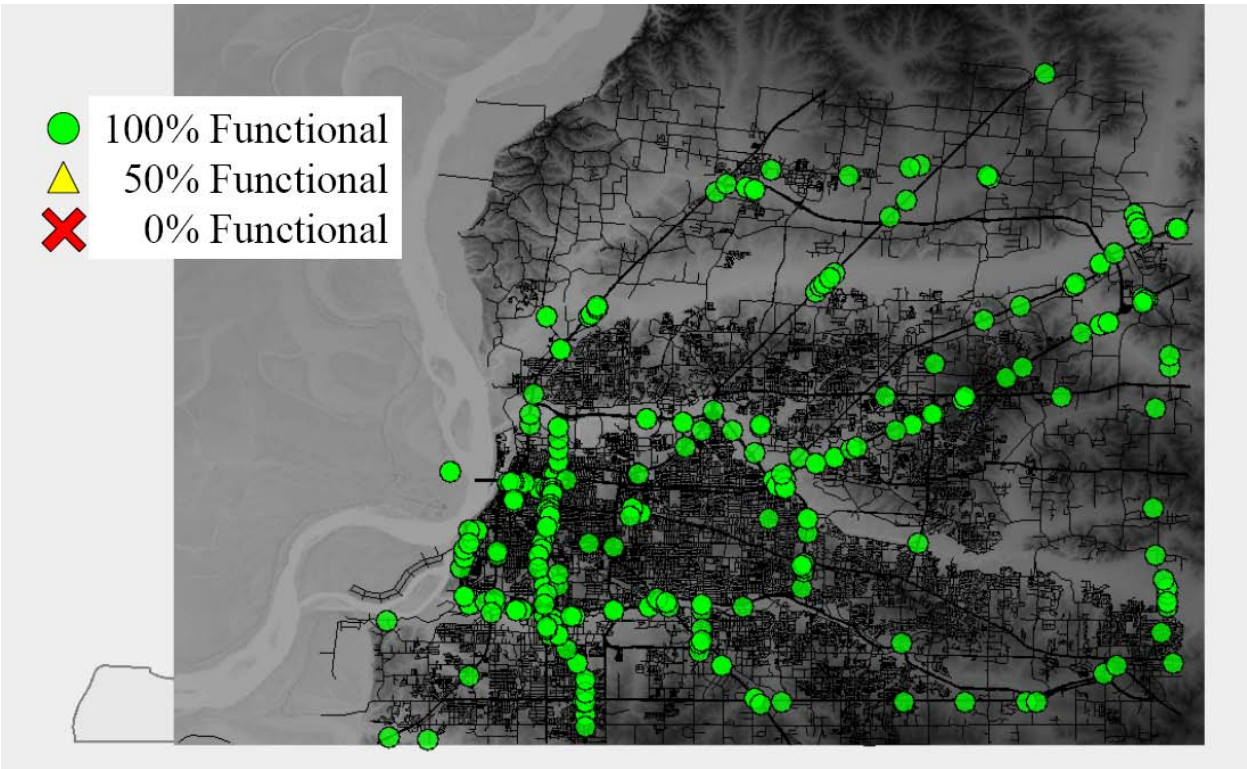

Figure 48. Bridge Functionality at Day 7 for Blytheville Source

6.3 Casualty Estimates

Casualty estimates for the capstone scenarios are determined based on an assumption of an average population density of 1.06 persons per 1000 ft^2. This figure was determined by dividing the total population, 897,472 persons, by the total square footage from the building dataset, 843,663 ft^2. Casualty rates implemented in the capstone scenarios are consistent with the values published in the HAZUS Technical Manual (FEMA, 2006), where the "injuries" and "deaths" reported for the capstone scenarios correspond to Level 2 and Level 4 casualties in HAZUS. The total estimated injuries and deaths in the study region as a result of the Blytheville source event are 984 and 188 persons, respectively. Injuries and deaths are shown aggregated to census tracts in Figure 49 and Figure 50, respectively. In each case, the aggregated data is shown colored according to nine quantiles, with darker colors representing greater numbers of casualties.

Distributions of injuries are provided in Figure 51 through Figure 54, and distributions of deaths are provided in Figure 55 through Figure 58. In each case, casualties are shown distributed by structure type and occupancy type, both as totals, and normalized by floor area. Algorithmically, injury and death estimates are dependent on population density, floor area, structure type, and predicted structural damage. The exposed population is determined from the multiplication of population density and floor area. An expected casualty rate is determined for each building, using an average of casualty rates by damage state, weighted by the probability of each damage state. The probability of collapse is determined as a subset of the Complete damage state, based on structure type.

Thus, Figure 52 and Figure 56 represent distillations of casualty estimates to reflect the direct effect of structure vulnerability on casualty estimation, whereas Figure 51 and Figure 55 reflect a combination of structure vulnerability with the prevalence of each structure type within the square footage distribution of the study region. Similarly, the data in Figure 54 and Figure 58 are driven by the structure types constituting the various occupancy classes, while Figure 53 and Figure 57 are influenced by the floor area for each occupancy in the study region in addition to the structure types constituting the occupancies.

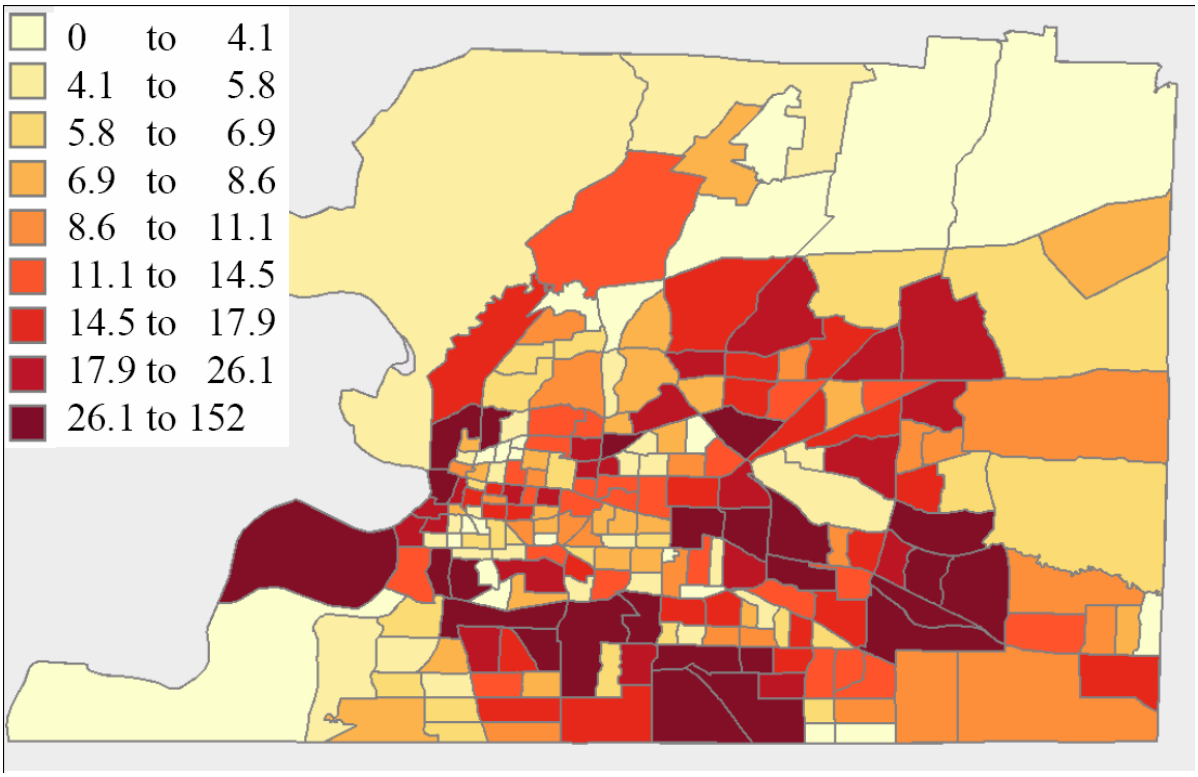

Figure 49. Injuries Aggregated to Census Tracts

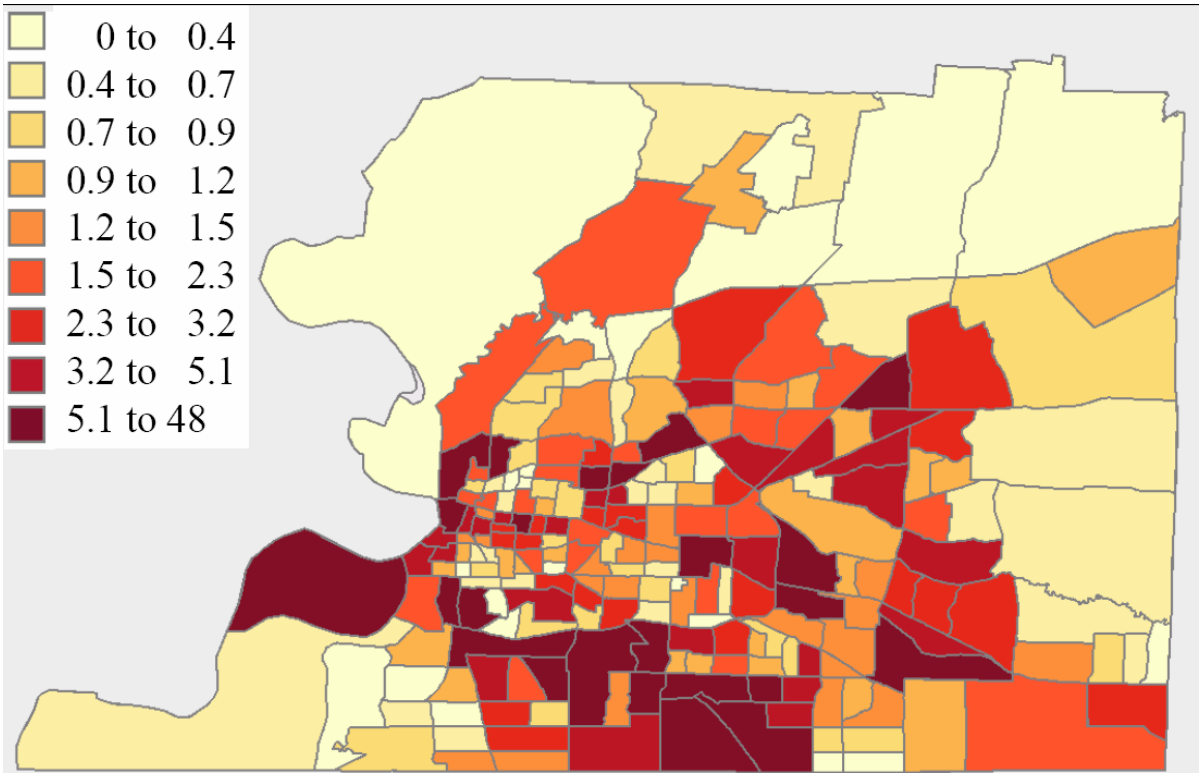

Figure 50. Deaths Aggregated to Census Tracts

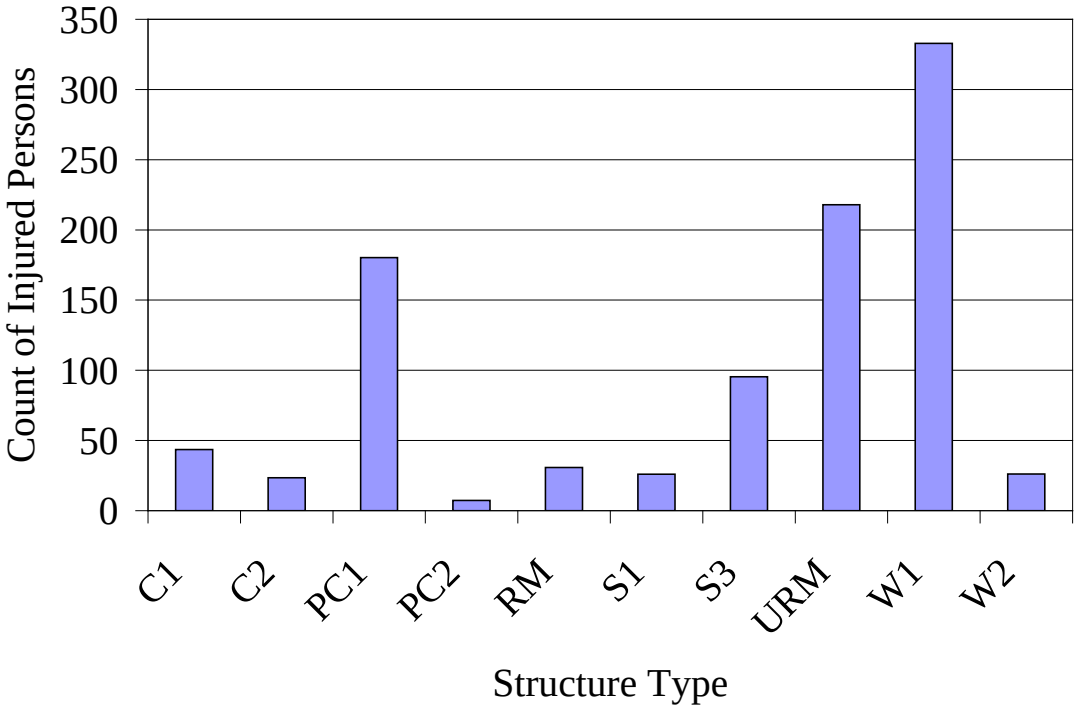

Figure 51. Estimated Injuries Requiring Hospitalization by Structure Type

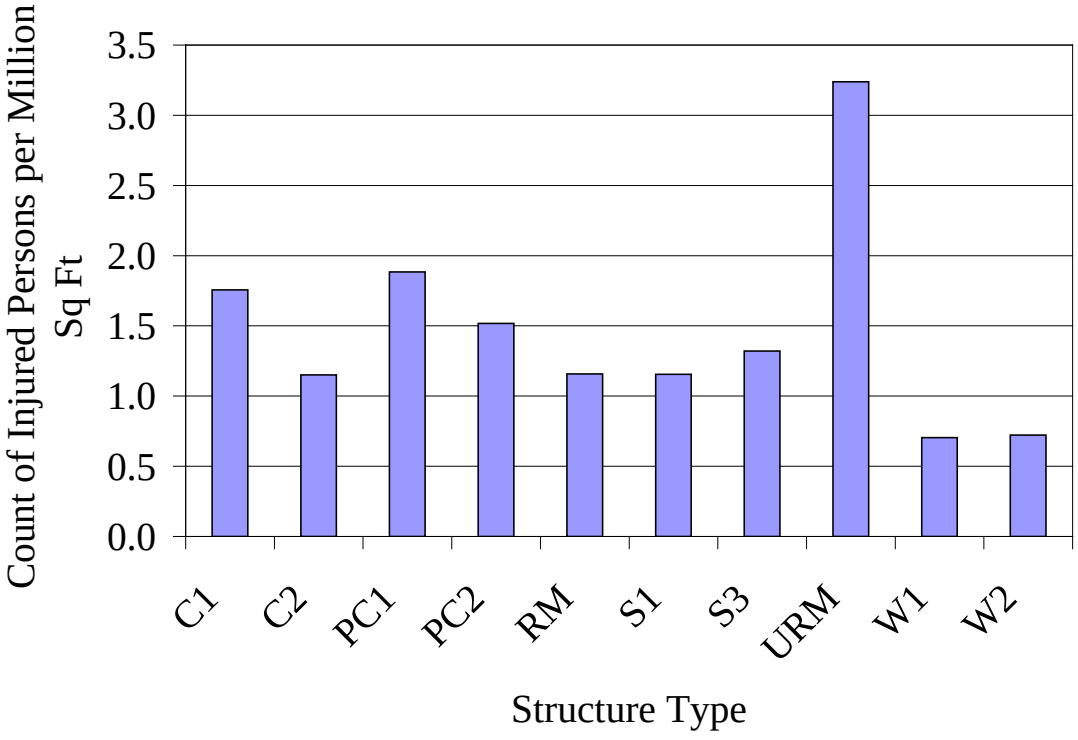

Figure 52. Estimated Injuries Requiring Hospitalization by Structure Type (Normalized by Floor Area)

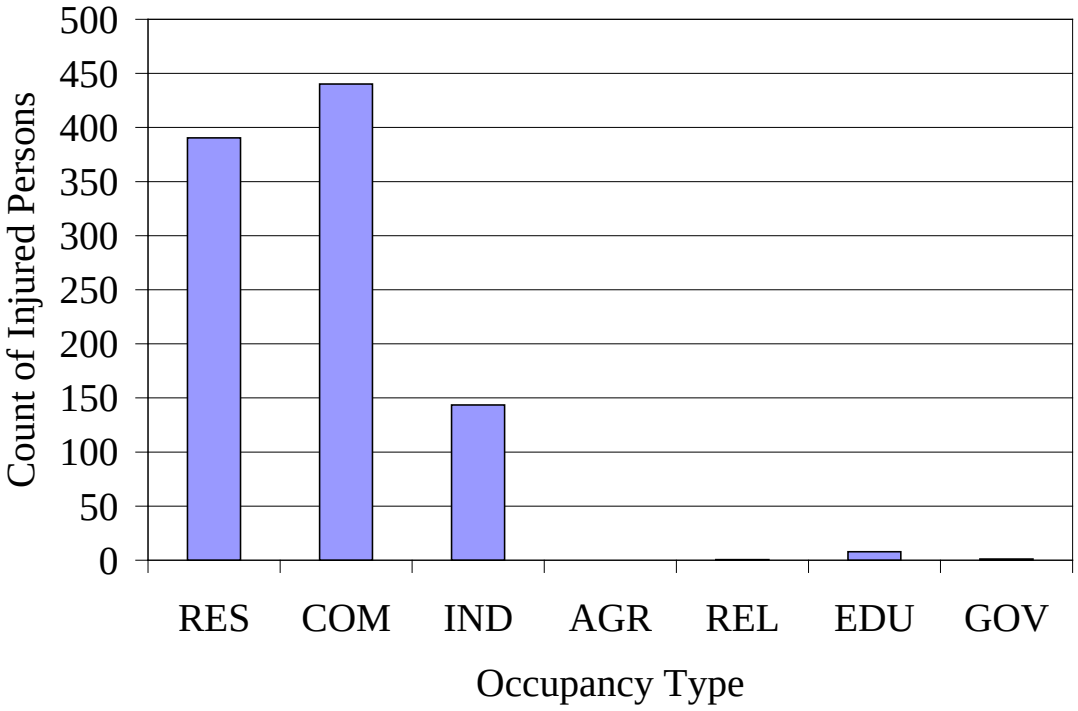

Figure 53. Estimated Injuries Requiring Hospitalization by Occupancy Type

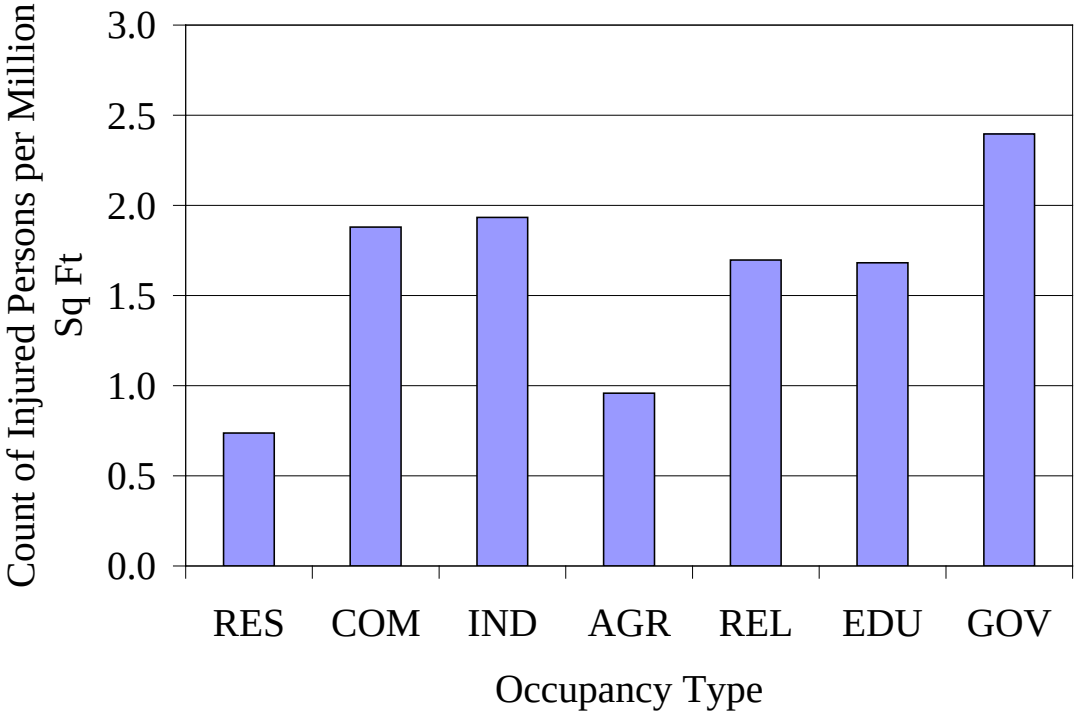

Figure 54. Estimated Injuries Requiring Hospitalization by Occupancy Type (Normalized by Floor Area)

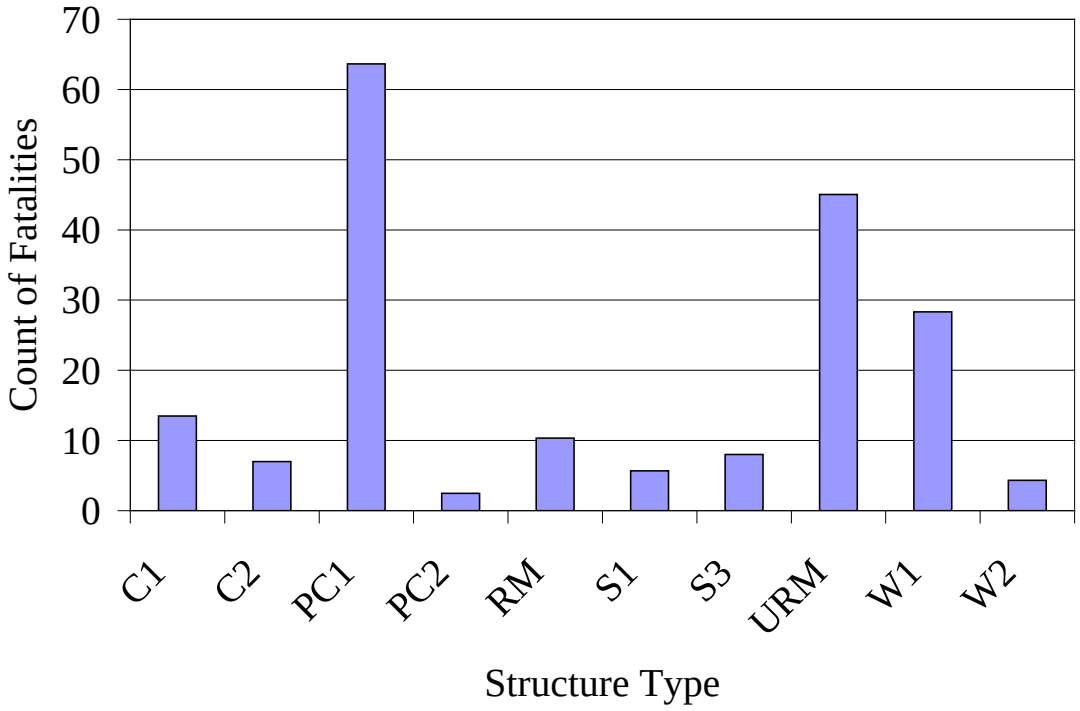

Figure 55. Estimated Deaths by Structure Type

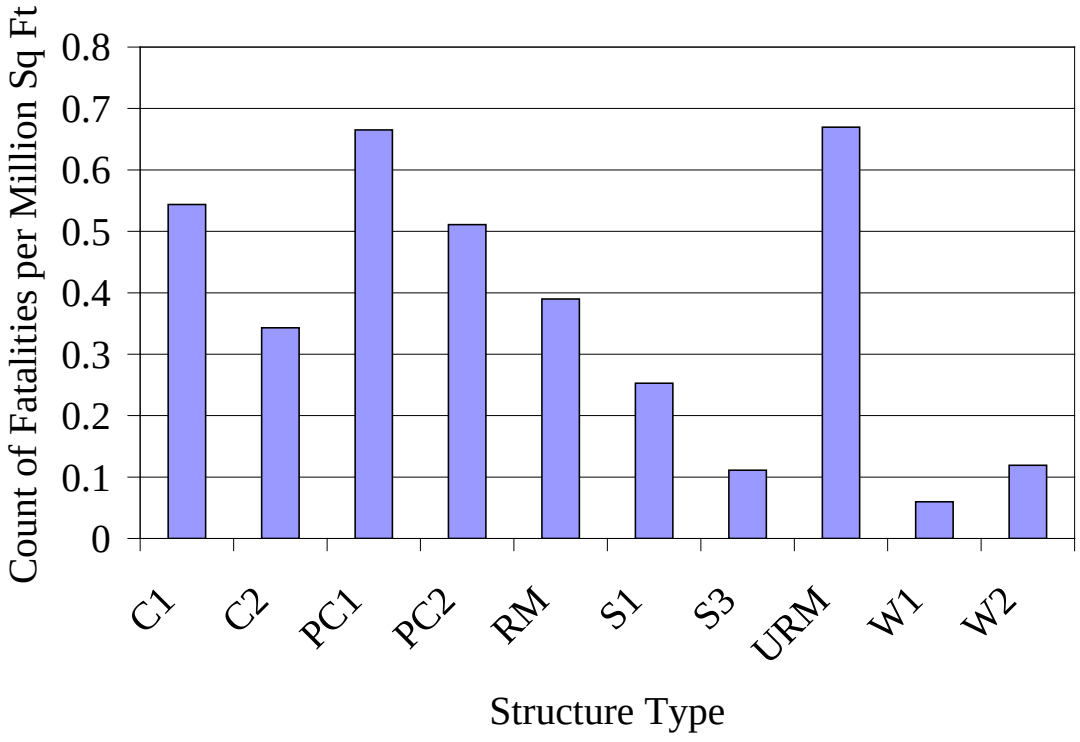

Figure 56. Estimated Deaths by Structure Type (Normalized by Floor Area)

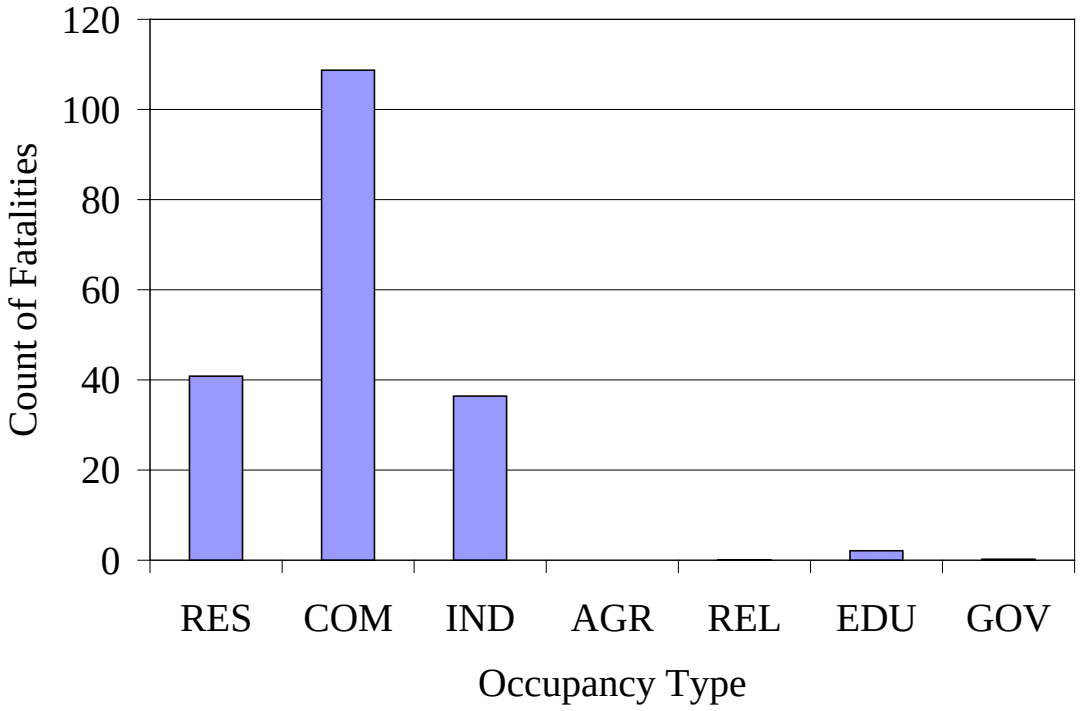

Figure 57. Estimated Deaths by Occupancy Type

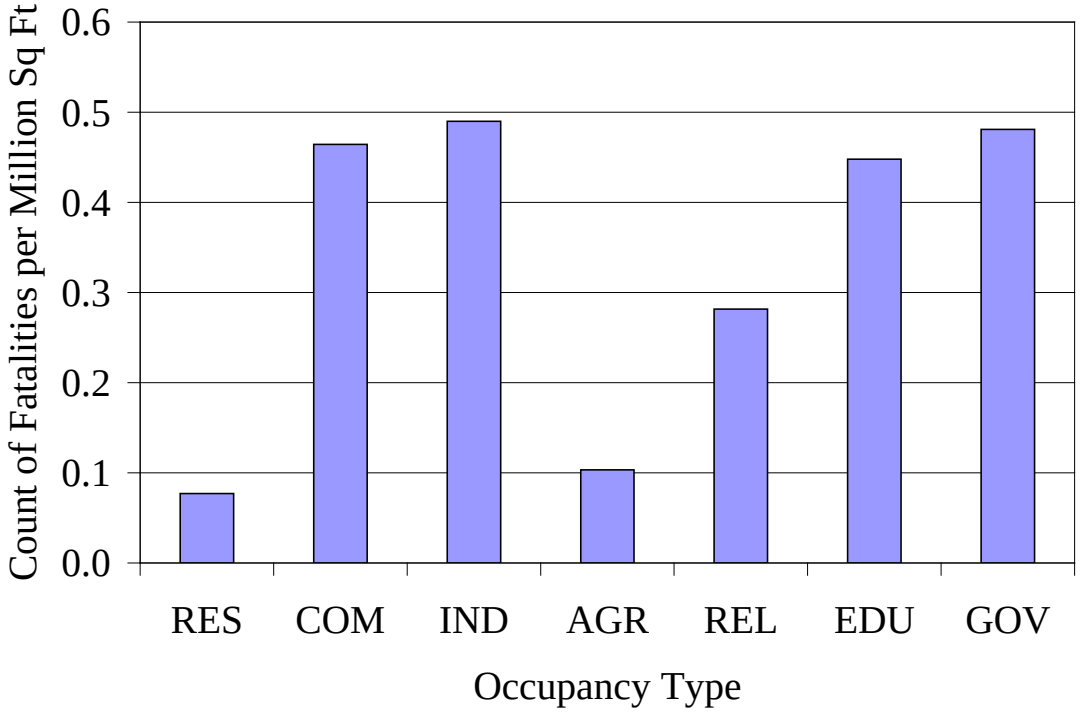

Figure 58. Estimated Deaths by Occupancy Type (Normalized by Floor Area)

6.4 Business Inventory Losses

Business inventory losses have been estimated for the building stock by a method which is algorithmically similar to the analysis in HAZUS-MH (FEMA, 2006; Green and Feser, 2007). Total business inventory losses for the Blytheville source event are estimated to be $83.8 million. The standard mapping of MAEViz to HAZUS acceleration-sensitive nonstructural damage states on a one-to-one basis, neglecting the None damage state, facilitated the implementation of the HAZUS methodology. Losses vary with respect to both structure and occupancy types, since business inventory losses resulting from physical damage are assumed to be correlated directly to acceleration-sensitive nonstructural damage, and characteristic business inventory parameters are dictated by occupancy categories. Thus, there are clear variations in Figure 59 through Figure 62 with respect to both structure and occupancy types. Heavy industrial facilities (IND1) incorporating tilt-up concrete frame systems (PC1) are seen to be the most vulnerable to inventory losses as a result of the scenario seismic hazard.

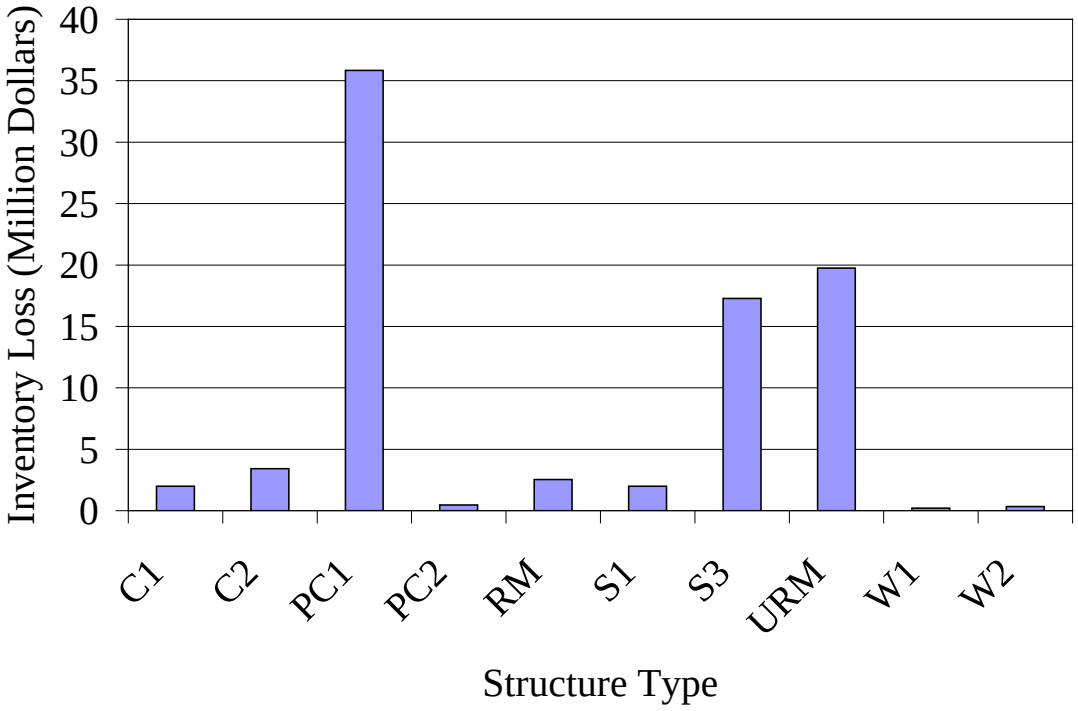

Figure 59. Business Inventory Losses by Structure Type

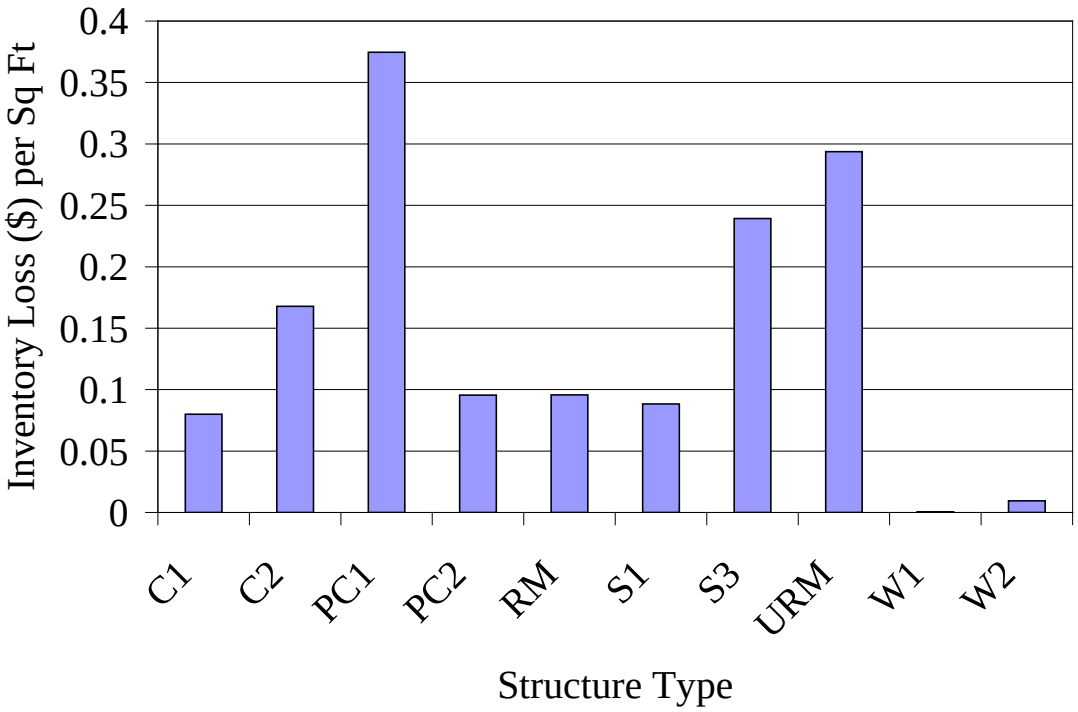

Figure 60. Business Inventory Losses by Structure Type (Normalized by Floor Area)

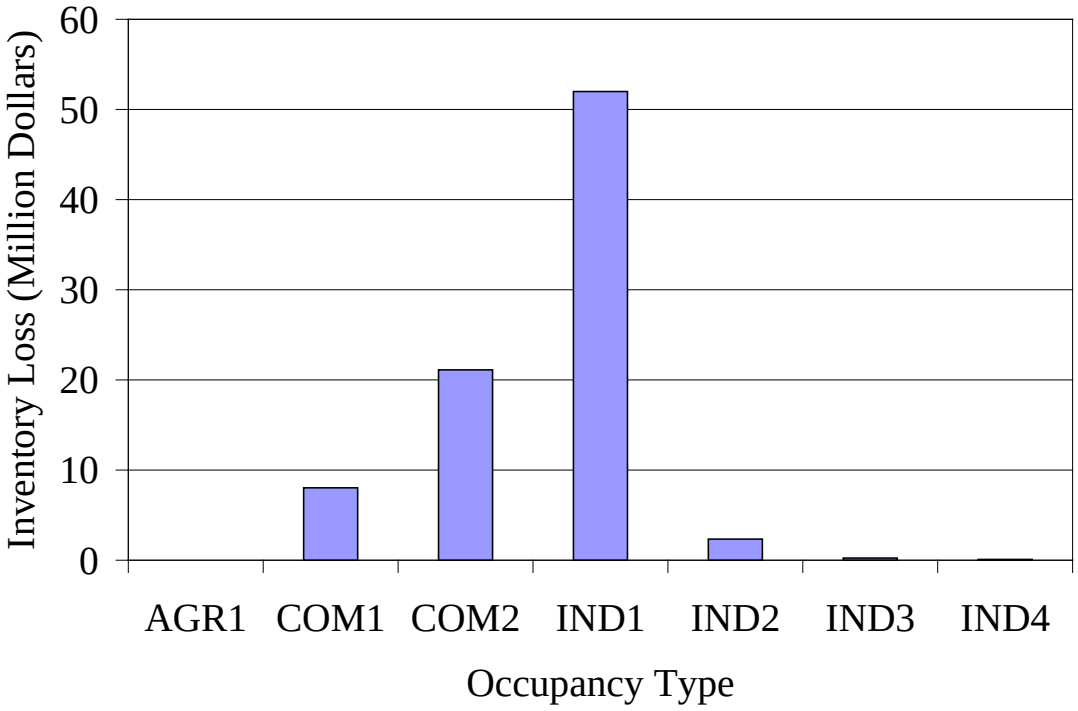

Figure 61. Business Inventory Losses by Occupancy Type

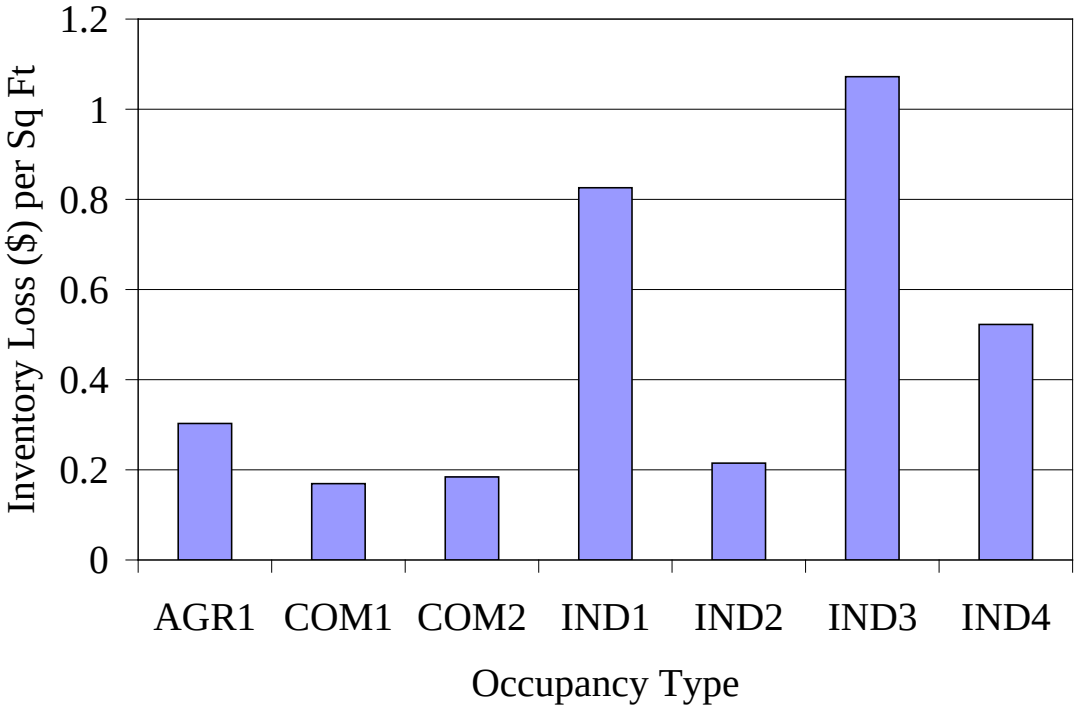

Figure 62. Business Inventory Losses by Occupancy Type (Normalized by Floor Area)

6.5 Business Interruption Losses

Business interruption losses have been estimated for the building stock by a method which is algorithmically similar to the analysis in HAZUS-MH (FEMA, 2006; Green and Feser, 2007). Total business interruption losses for the Blytheville source event are estimated to be $964 million, or about 20% of the estimated direct repair and replacement cost of buildings. The standard mapping of MAEViz to HAZUS structural damage states on a one-to-one basis, neglecting the None damage state, facilitated the implementation of the HAZUS methodology. Losses vary with respect to both structure and occupancy types, since business interruption is correlated directly to structural damage, and business operation parameters are dictated by occupancy categories. Thus, as with inventory losses, there are clear variations in Figure 63 through Figure 66 with respect to both structure and occupancy types.

With respect to structure types, business interruption losses are most significantly affected by steel structures, with the single greatest source of loss associated with steel frame structures (S1), and the greatest normalized source of loss associated with light steel frames (S3). With respect to occupancy types, there are noticeable differences between the non-normalized and normalized loss values. Warehouses (COM2) and heavy industrial facilities (IND1) both have significant impacts on the estimated business interruption loss, however, from a mitigation viewpoint, interruption losses associated with hospitals (COM6) and medical offices (COM7) would be expected to be more easily reduced, based on interruption loss per area. Those occupancies provide the additional benefit of being especially valuable after a major seismic event for the treatment of injuries.

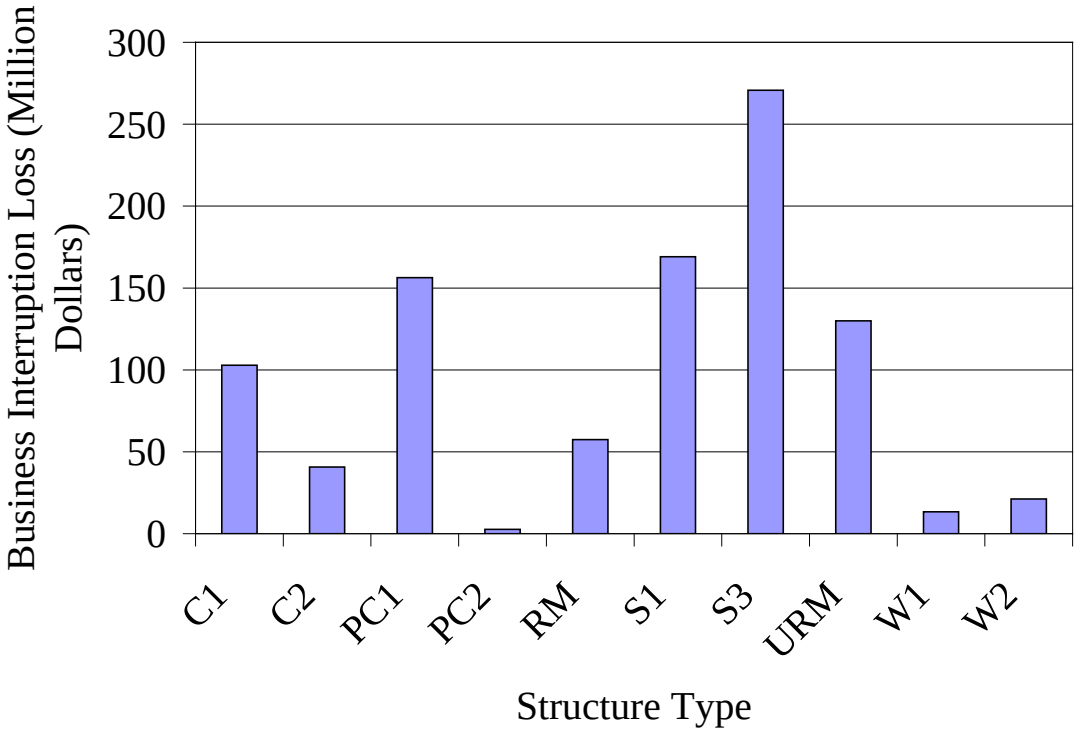

Figure 63. Business Interruption Losses by Structure Type

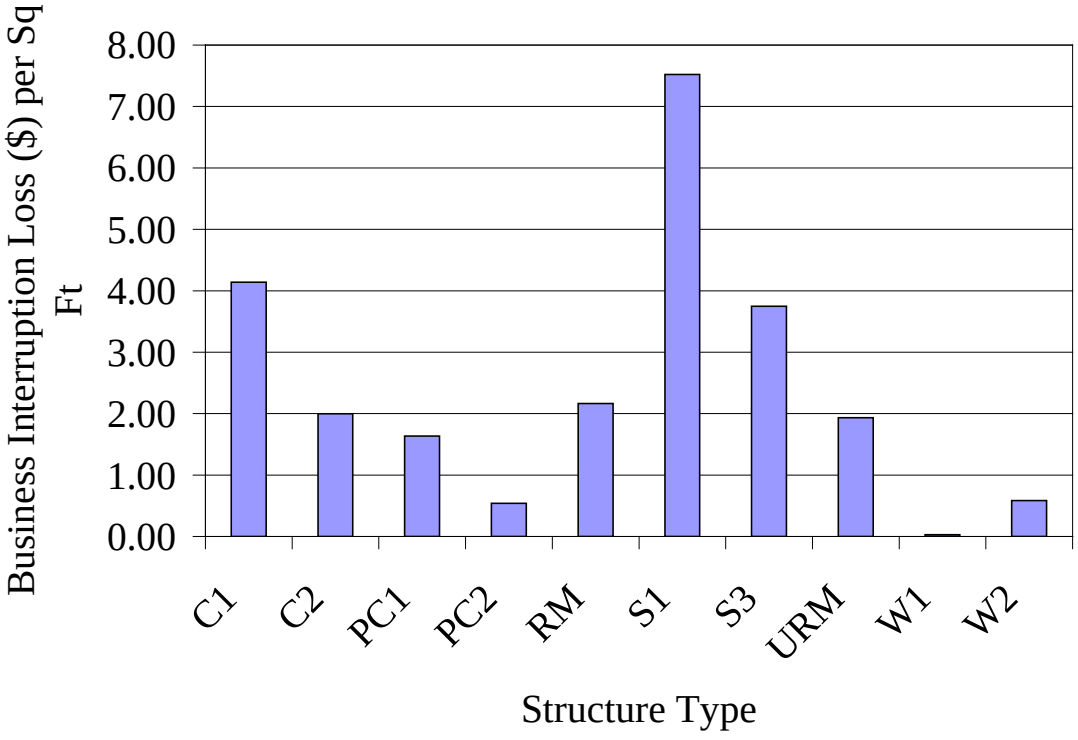

Figure 64. Business Interruption Losses by Structure Type (Normalized by Floor Area)

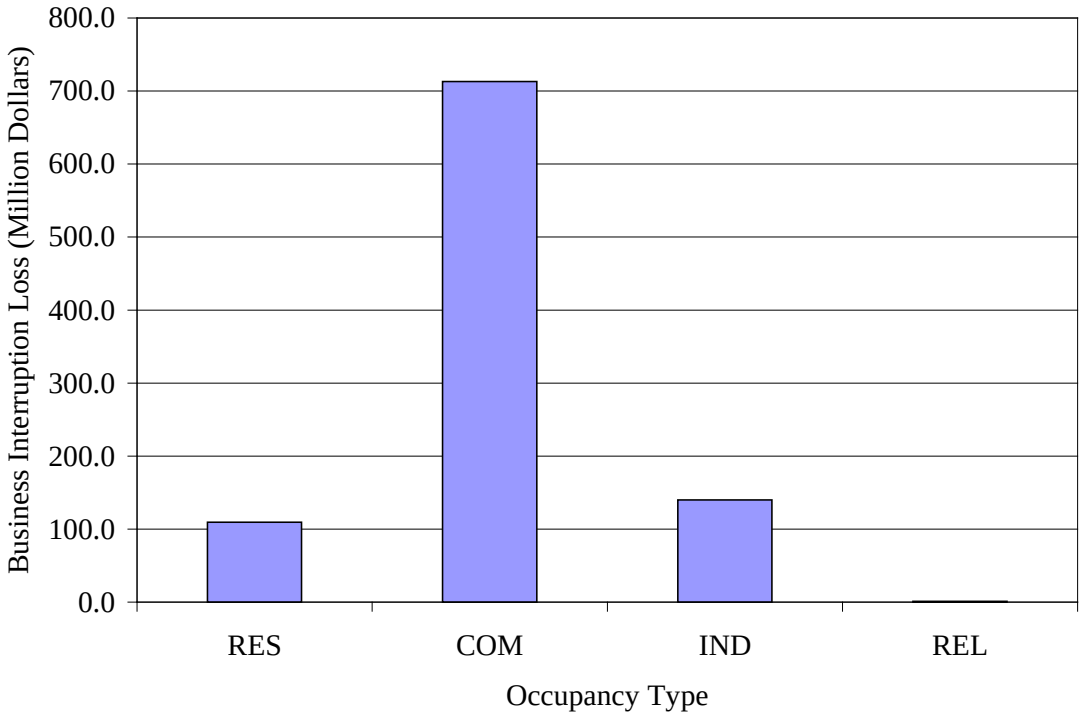

Figure 65. Business Interruption Losses by Occupancy Type

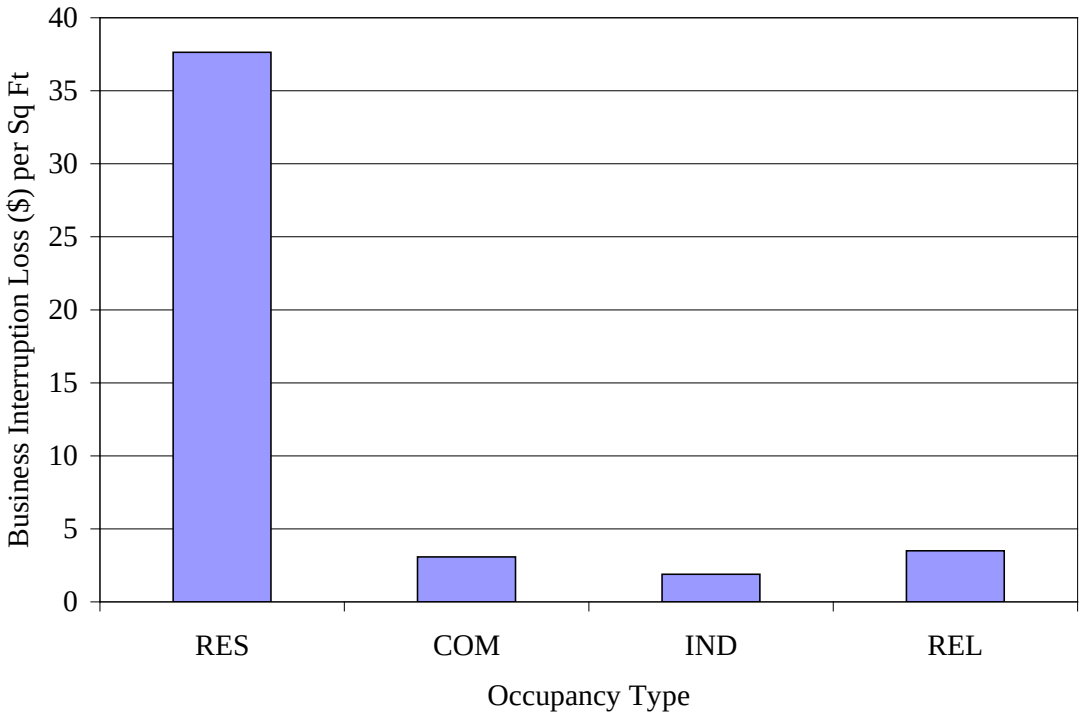

Figure 66. Business Interruption Losses by Occupancy Type (Normalized by Floor Area)

6.6 Household and Population Dislocation Estimates

Dislocation of population and households have been estimated for the building stock by a method which is algorithmically similar to the analysis in HAZUS-MH (FEMA, 2006; Peacock, 2007). The primary difference between the adapted HAZUS method implementation in MAEViz and the original algorithm in HAZUS originates from the substitution of MAE Center damage states for HAZUS damage states. The MAEViz results also represent higher resolution results, as MAEViz data is obtained from a point-wise treatment of building assets. Census data has been collected at the block group level, and is distributed to single- and multi-family housing units in each block group by distributing households and population proportionately with respect to the ratio of the number of dwelling units recorded in the building stock inventory to the total number of households in the census data. Similarly with the HAZUS methodology, an algorithmic predilection exists for single-family residence (occupancy RES1) structures to remain inhabited in spite of heavy damage. This trend may be observed in Figure 71 and Figure 76, where the dislocation per unit household is less for RES1 than RES3. This is valid on a normalized (per household) basis, although the total number of persons and household displaced is larger for RES1, as seen in Figure 70 and Figure 75, primarily as a result of the number of persons associated with RES1 as opposed to RES3, although structure types assigned to buildings in each occupancy also affect the dislocation projections.

The total number of displaced households and the displaced population for the Blytheville source event is estimated at 14,931 and 37,897, respectively. Most of these displaced households and persons are associated with the W1 structure type, as shown in Figure 67 and Figure 72. This trend is expected, since the vast majority of residences are single-family residences in the study region, and most single-family residences are associated with the W1 structure type. After W1, the residential structures of the commercial wood frame (W2), steel frame (S1), and reinforced masonry (RM) structure types represent the greatest impacts on dislocation, as seen in Figure 68 and Figure 73. This pattern appears to be significantly influenced by the representation of each of the structure types in the building stock, based on Figure 69 and Figure 74, since the pattern is not maintained, with the exception of S1 structures, when results are normalized by the total number of dwelling units.

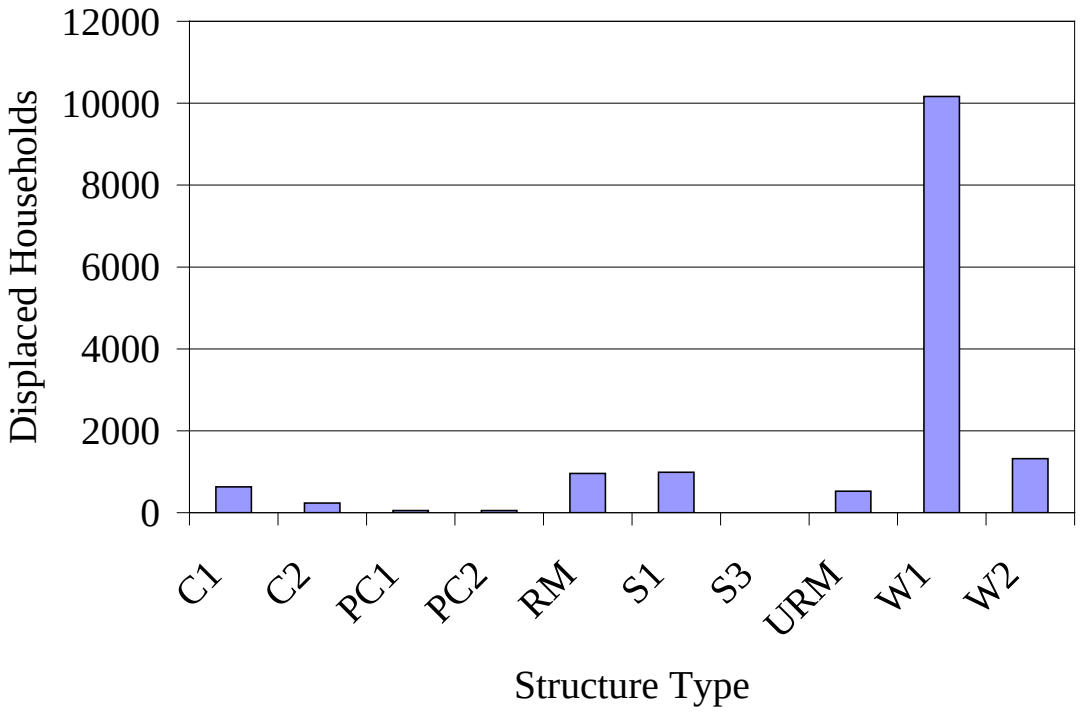

Figure 67. Displaced Households by Structure Type

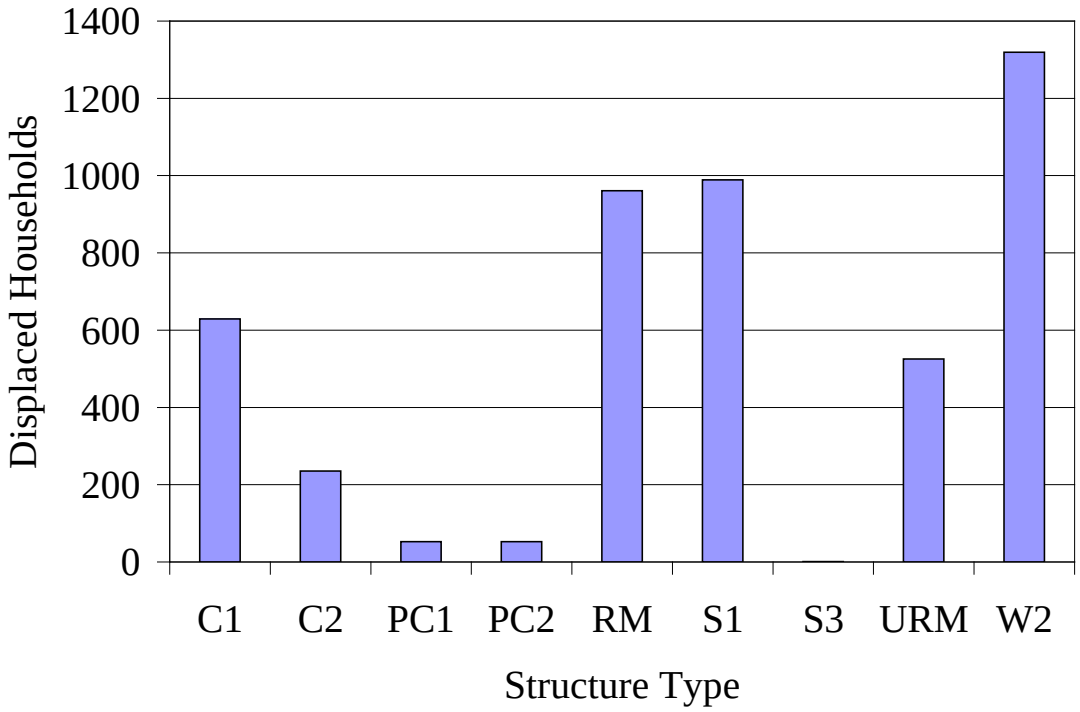

Figure 68. Displaced Households by Structure Type Neglecting W1

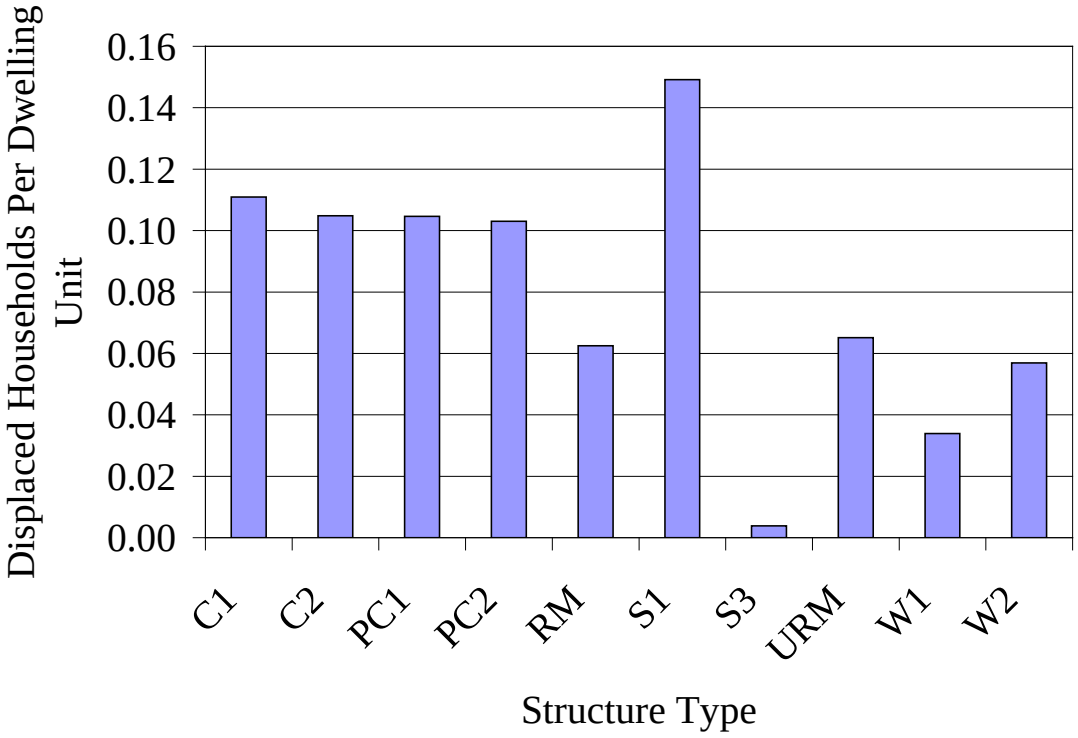

Figure 69. Displaced Households by Structure Type (Normalized by Dwelling Units)

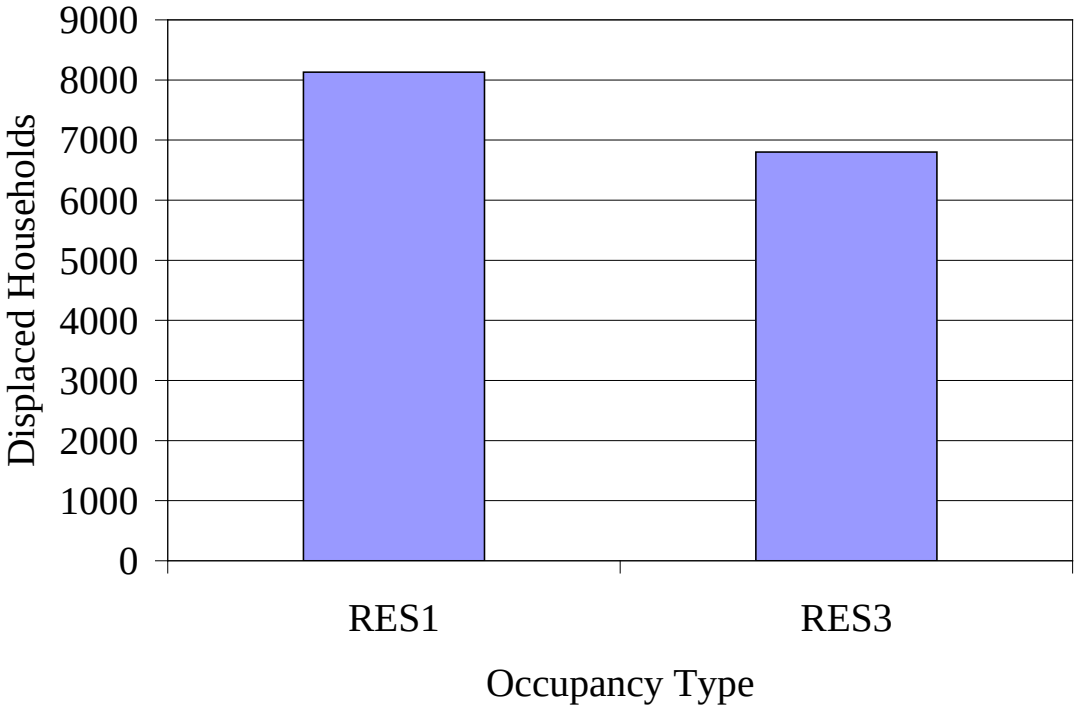

Figure 70. Displaced Households by Occupancy Type

Figure 71. Displaced Households by Occupancy Type (Normalized by Dwelling Units)

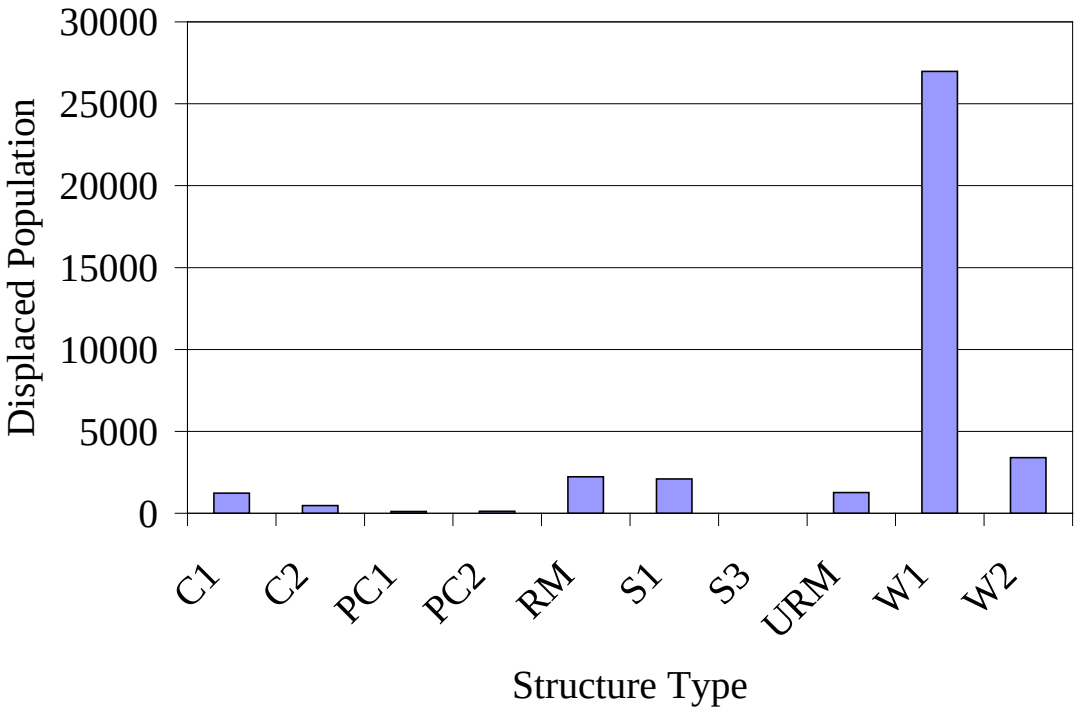

Figure 72. Displaced Population by Structure Type

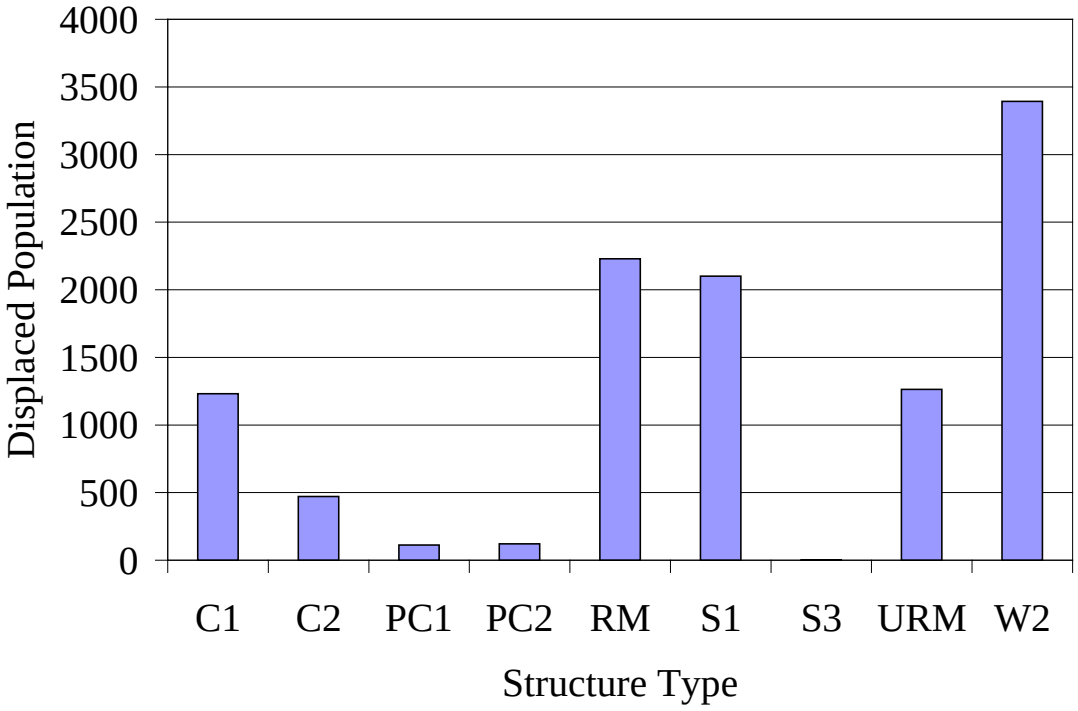

Figure 73. Displaced Population by Structure Type Neglecting W1

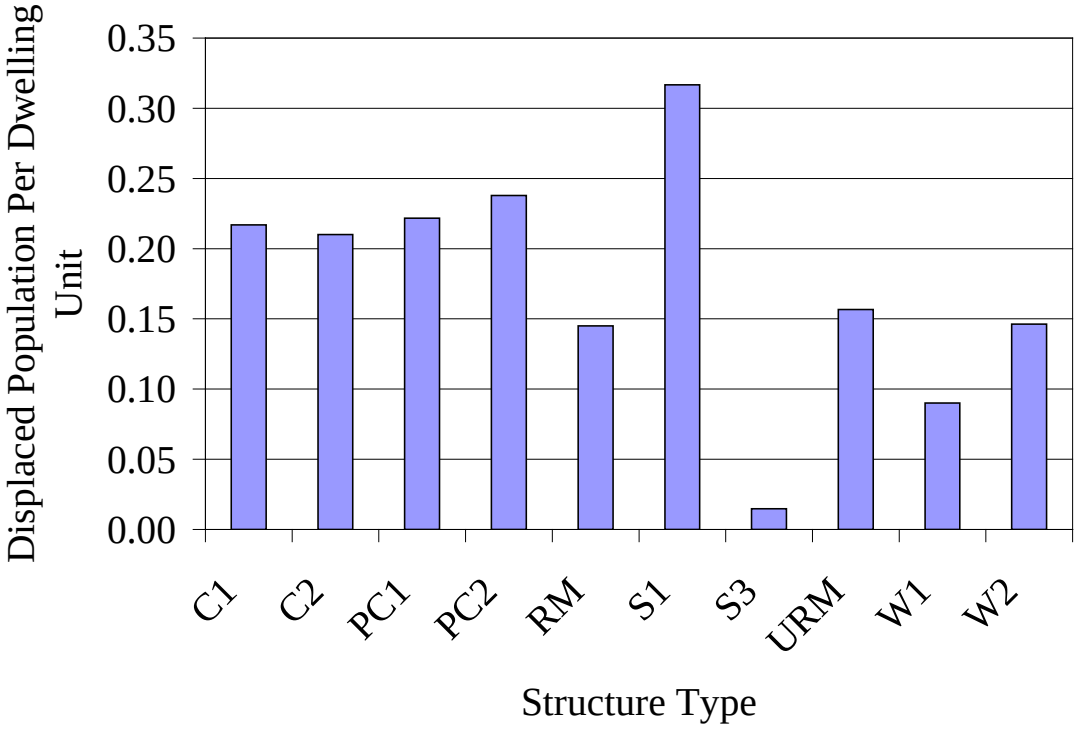

Figure 74. Displaced Population by Structure Type (Normalized by Dwelling Units)

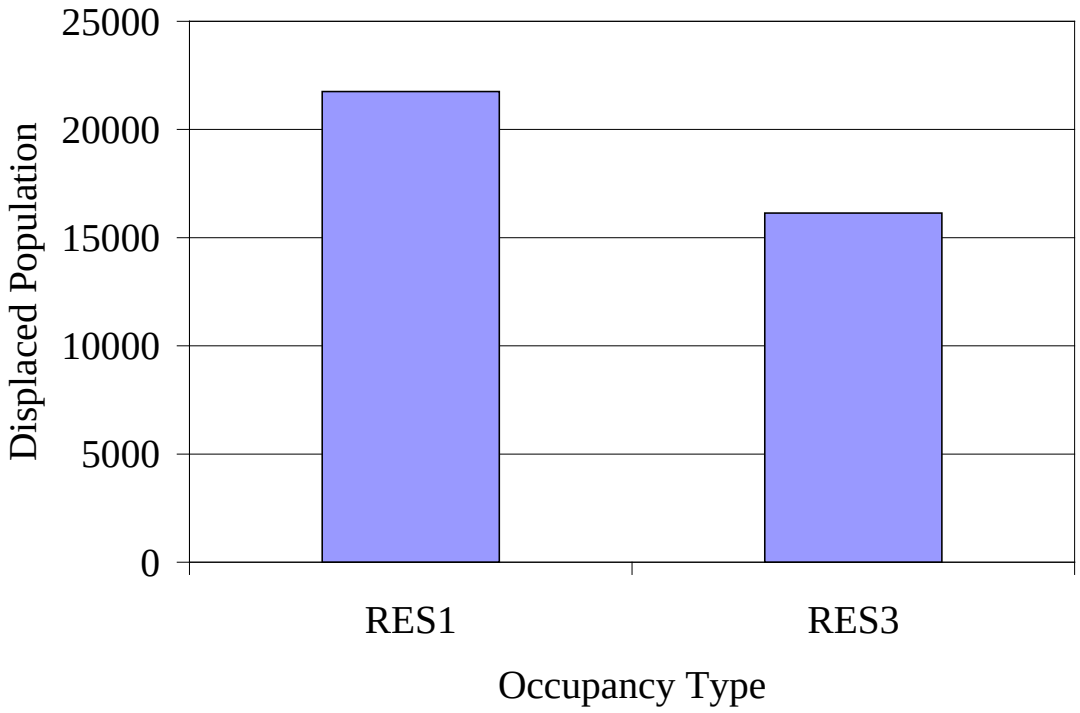

Figure 75. Displaced Population by Occupancy Type

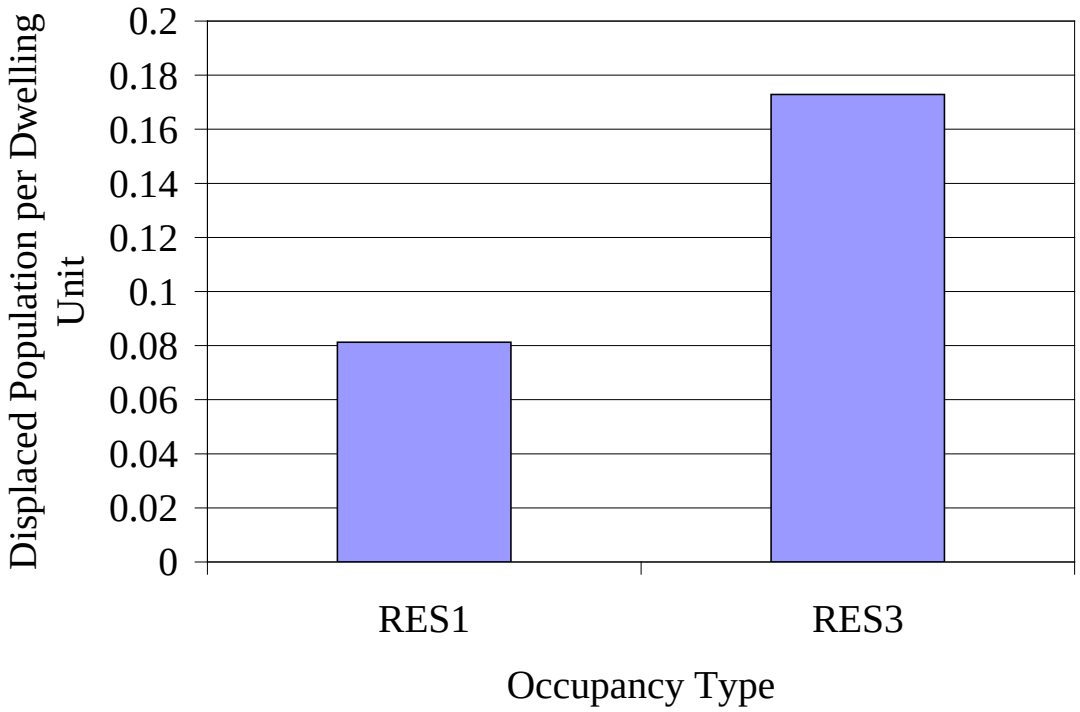

Figure 76. Displaced Population by Occupancy Type (Normalized by Dwelling Units)

6.7 Short Term Shelter Requirements

Short term shelter requirements have been estimated for the building stock by a method which is algorithmically similar to the analysis in HAZUS-MH (FEMA, 2006; Peacock, 2007). The standard mapping of MAEViz to HAZUS structural damage states on a one-to-one basis, neglecting the None damage state, facilitated the implementation of the HAZUS methodology. Demographic data, primarily focusing on income level and ethnicity, is employed at the block group level and combined with the point-wise population and household dislocation analysis output to estimate the number of persons requiring short term shelter immediately after the seismic event. The total number of persons requiring short term shelter is estimated to be 10,282 people, or 27.1% of the total displaced population. There are a total of 698 block groups in the study region, with a mean and standard deviation of 14.7 and 13.0 persons, respectively, requiring shelter. The total number of persons seeking shelter and the percentage within the block group are shown in Figure 77 and Figure 78, respectively. In each case, the data is shown colored according to nine quantiles, with darker colors representing greater numbers of displaced persons seeking shelter by count or percentage.

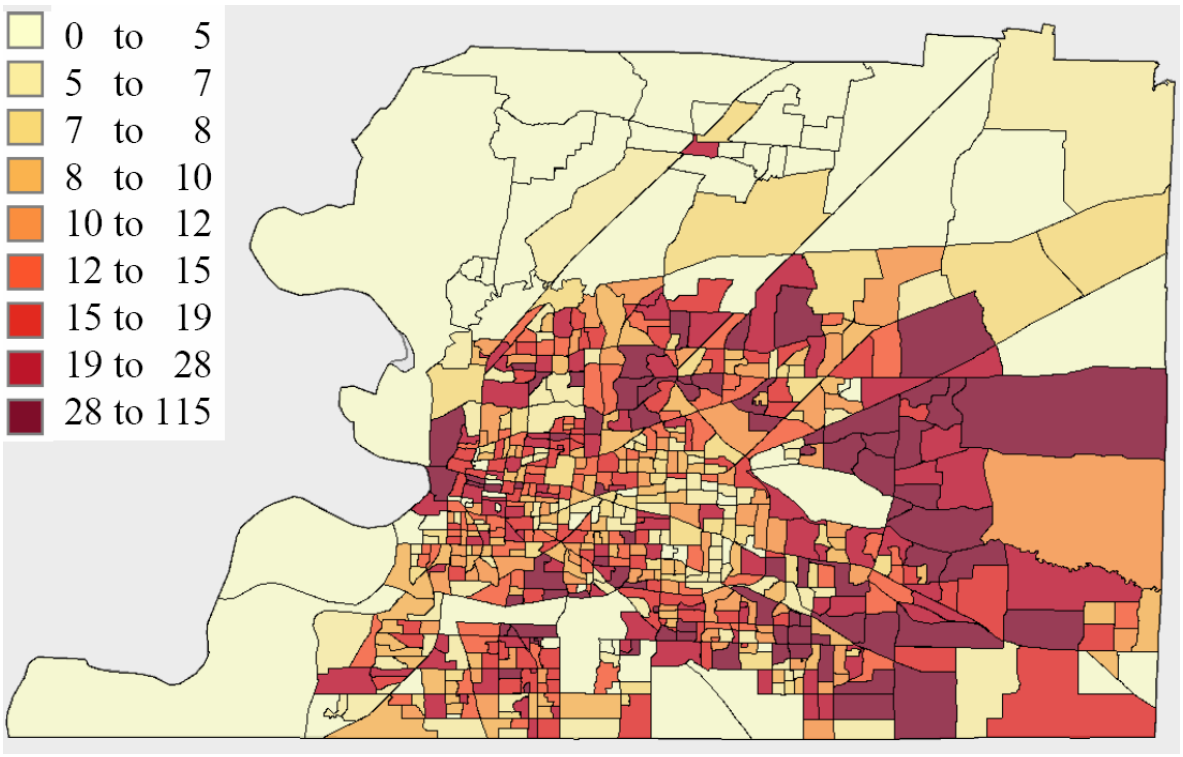

Figure 77. Quantile Representation of Number of Persons Expected to Seek Shelter per Block Group

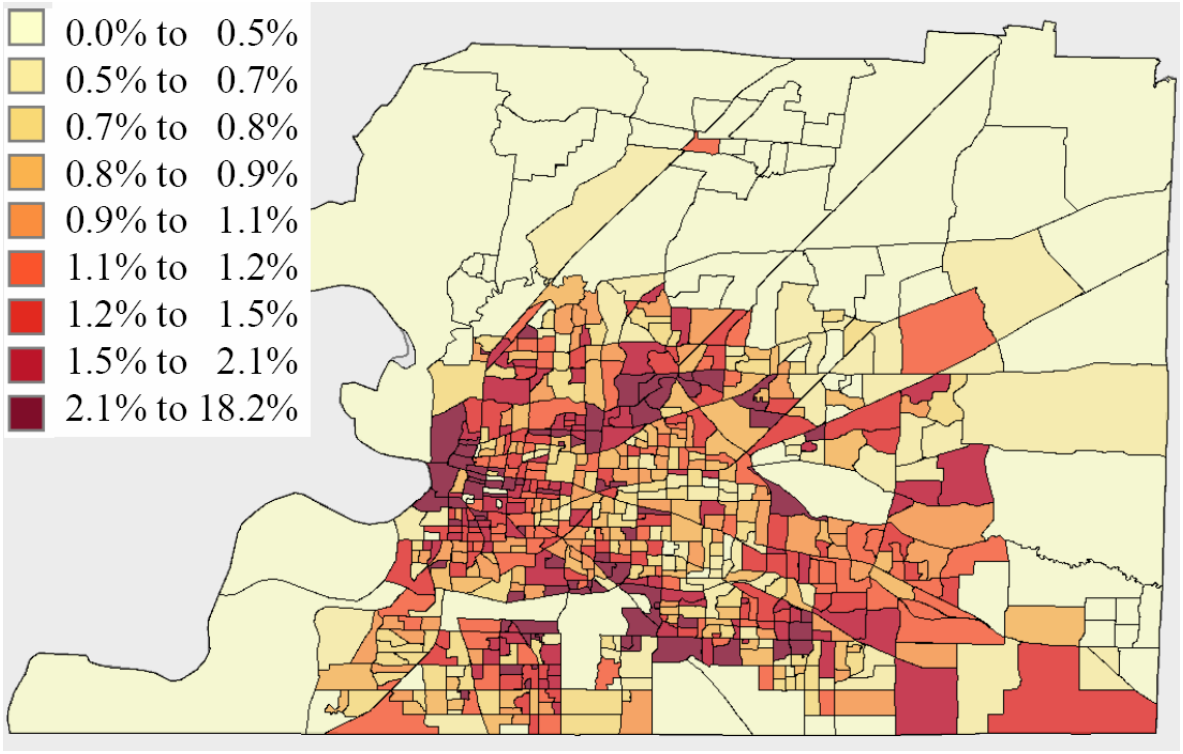

Figure 78. Quantile Representation of Percentage of Persons Expected to Seek Shelter per Block Group

6.8 Fiscal Impacts

The impact on tax revenue was investigated as a component of the capstone effort (French, 2007). To reflect the property taxes levied on the building stock, effective tax rates were applied to the estimated repair and replacement costs of structures in the building stock. In accordance with the tax structure in Shelby County, buildings in various occupancies were treated differently with respect to assessed value. Buildings classified as RES or AGR were assumed to be assessed at 25% of appraised value, while COM and IND buildings were assumed to be assessed at 40% of appraised value. Buildings in the REL, EDU, or GOV occupancy classes were assumed to be tax-exempt. The tax rate assumed to be applied to the assessed value for all buildings was 4%. Thus, an equivalent tax rate of 1% was applied to the estimated direct loss of RES and AGR buildings, which was in turn determined from appraised value. Similarly, an equivalent rate of 1.6% was applied to COM and IND buildings. The total fiscal impact, based on these parameters, is estimated to be $42.4 million. As expected, W1 RES1 structures dominate estimates of fiscal impact, based solely on the vast proportion of the building inventory constituted by that particular class of structures.

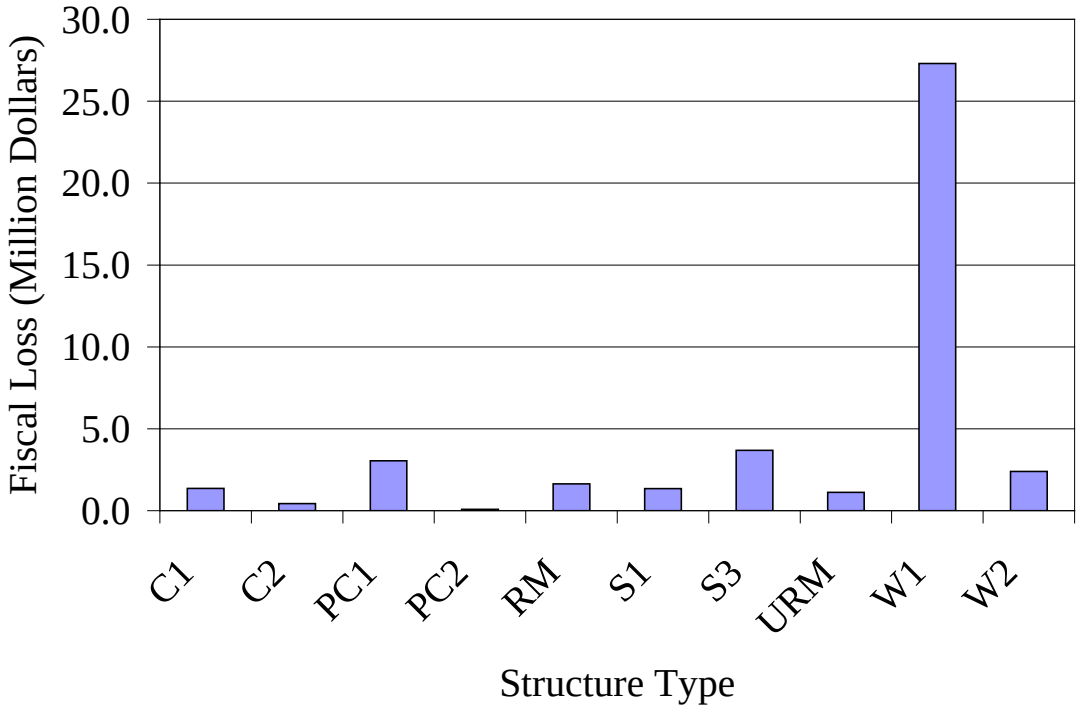

Figure 79. Fiscal Losses by Structure Type

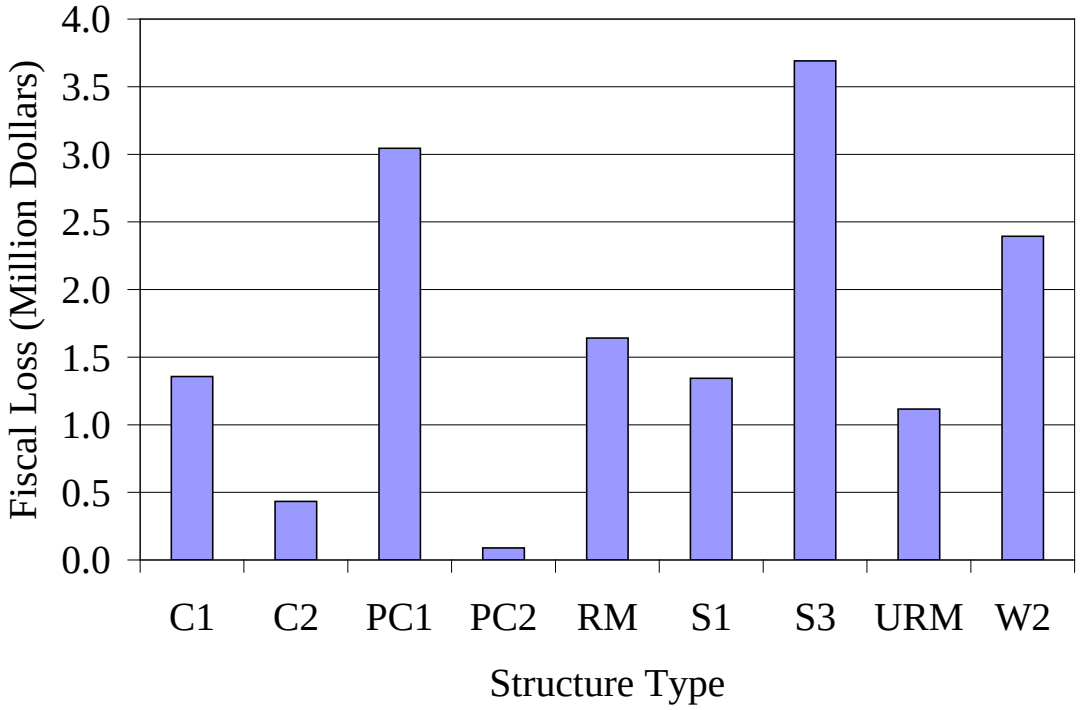

Figure 80. Fiscal Losses by Structure Type Neglecting W1

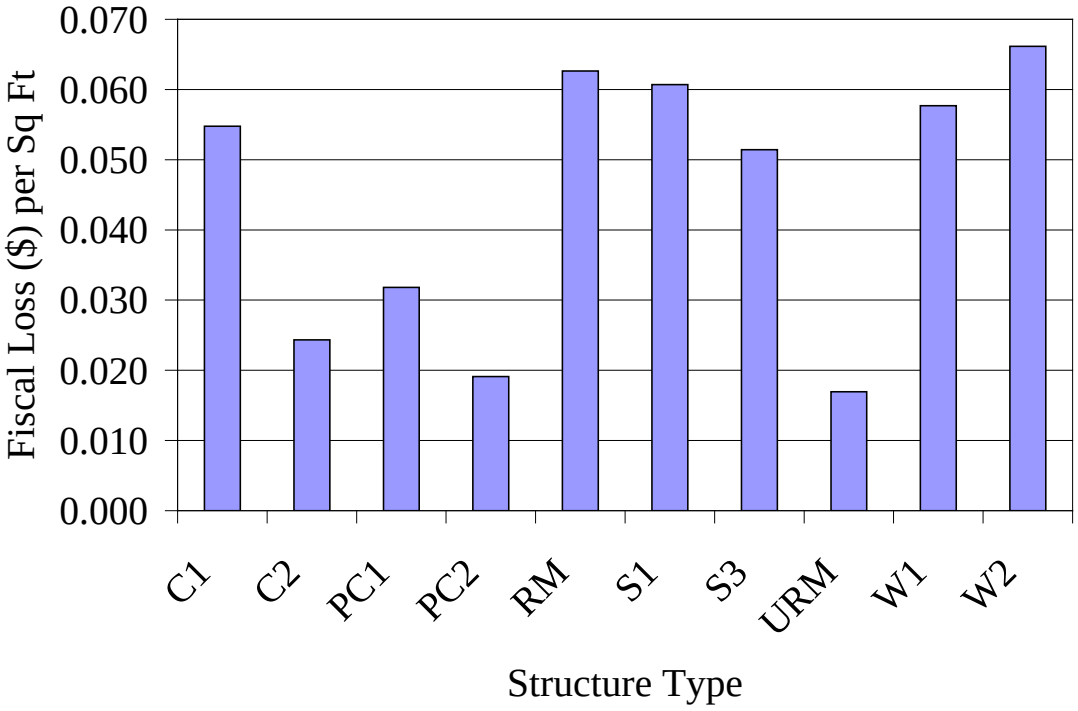

Figure 81. Fiscal Losses by Structure Type (Normalized by Floor Area)

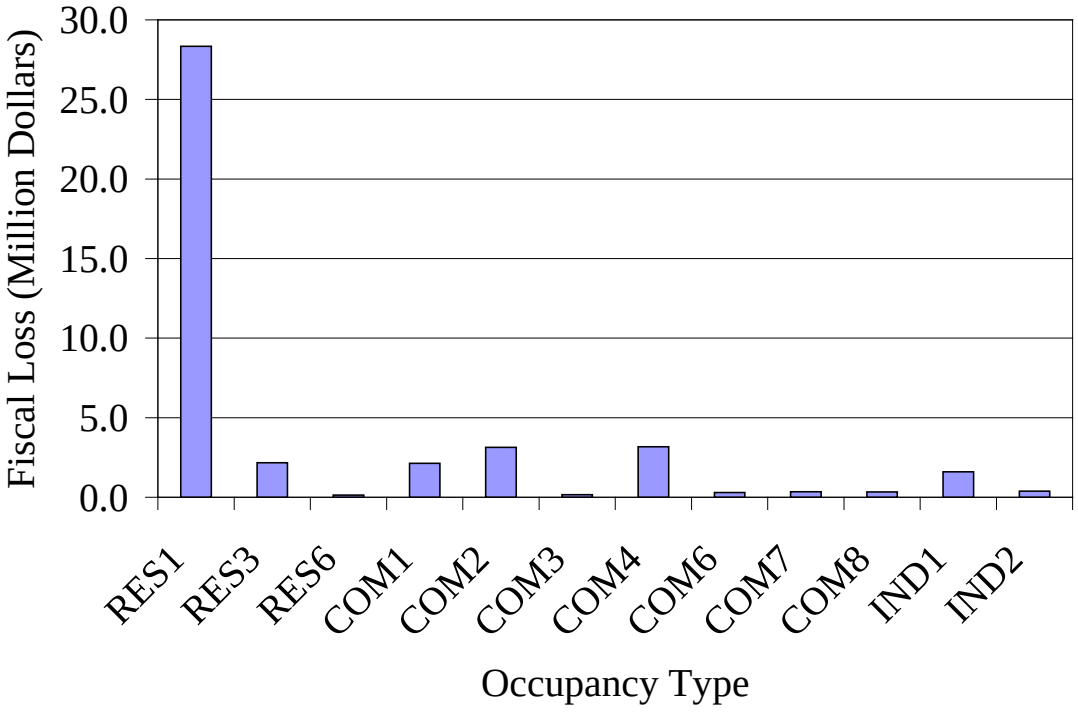

Figure 82. Fiscal Losses by Occupancy Type

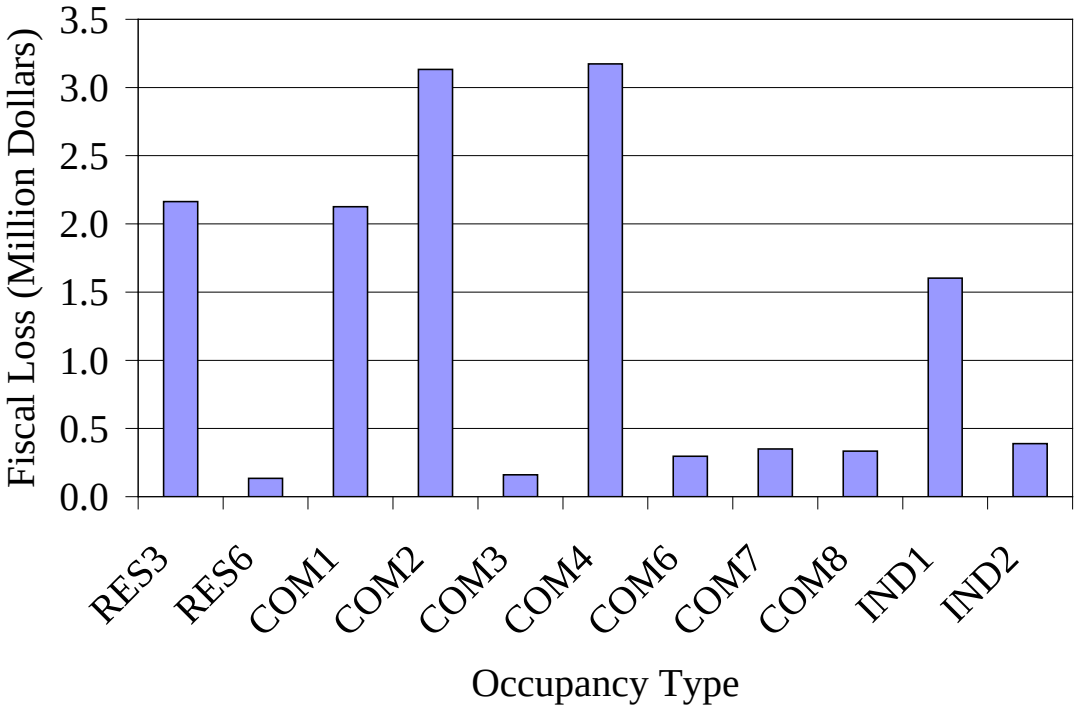

Figure 83. Fiscal Losses by Occupancy Type Neglecting RES1

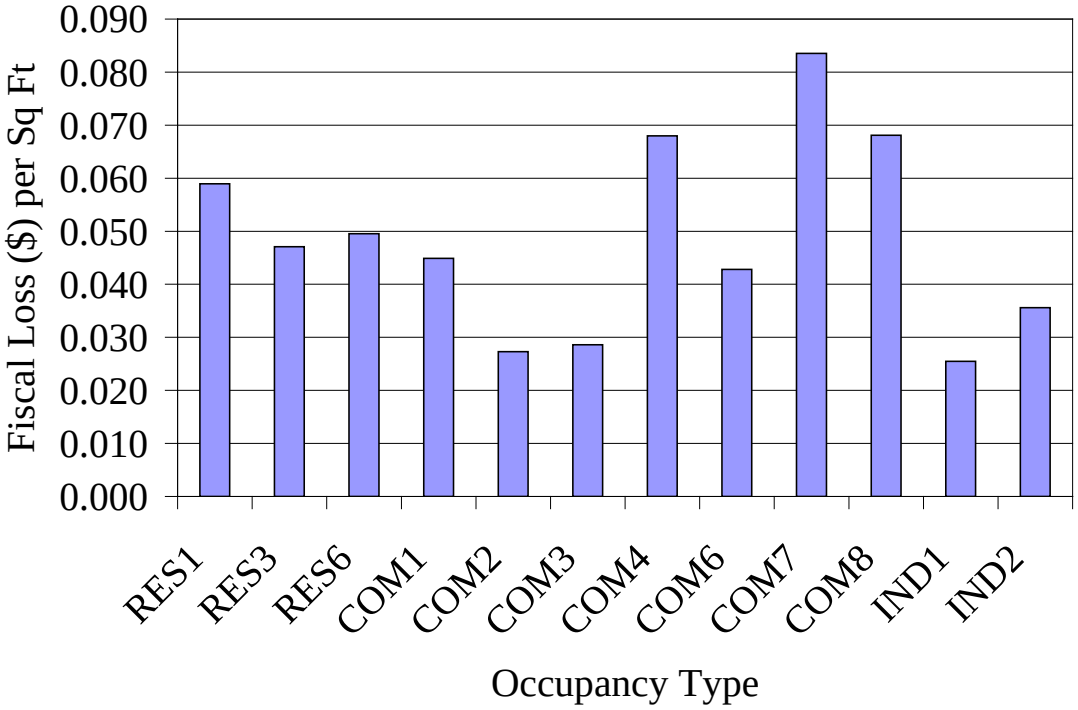

Figure 84. Business Interruption Losses by Occupancy Type (Normalized by Floor Area)

6.9 Social Vulnerability

Social vulnerability was evaluated for the study region, based solely on socio-economic parameters (i.e., without regard for any imposed hazard) (Peacock, 2007). The objective of this analysis is to determine areas where the population would have greater difficulty coping with the effects of a disaster, such as lower-income populations, or areas with large numbers of children or elderly. The algorithm performs a tiered analysis of social vulnerability, as shown in Table 11. Each 1st order variable is calculated, then ranked and classified by decile, so that the least to most vulnerable areas are assigned values of 1 to 10. The 1st order decile rankings are then rolled up to 2nd order classifications, and similarly the 2nd order rankings are rolled up to a 3rd order classification to represent social vulnerability in an aggregate global sense. The algorithm also includes calculation of weighted rankings, where weights are determined based on an estimate of population density. The output of the analysis is therefore a gradation of "hotspots" showing areas of greater or lesser social vulnerability, as shown in Figure 85, where the hotspots are weighted and classified by decile. Superimposing the social vulnerability maps with other maps provides a composite representation of the effects on the study region, representing not only physical hazard and vulnerability of the built environment, but also how the populace in particular regions will or will not be able to cope with the adverse effects of damage.

Table 11. Social Vulnerability Components [after Peacock (2007)]

Social Vulnerability		
1st order	**2nd Order**	**3rd Order**
1.1. Poverty (% persons below poverty)	**2.1 Potential child care needs**	**3.1 Vulnerability Hot-Spot Projection**
1.2 Female Headed Households (% female Headed households)		
1.3 Children (% persons below 17)		
1.4 Elders (% persons above 65)	**2.2 Elder care needs**	
1.5 Elder Poverty (% Elders below poverty level)		
1.6 Public Transportation dependency (% workers using Public Transportation)	**2.3 Public transportation needs**	
1.7. Travel Time (Aggregate travel time by Public Transportation /Total Pop.)		
1.8 Unemployment (% unemployed over 16)	**2.4 Temporary Shelter and Housing Recovery needs**	
1.9 Renters (% renters)		
1.10 Minorities (% non-White)		
1.11 Income (Per capita income)		

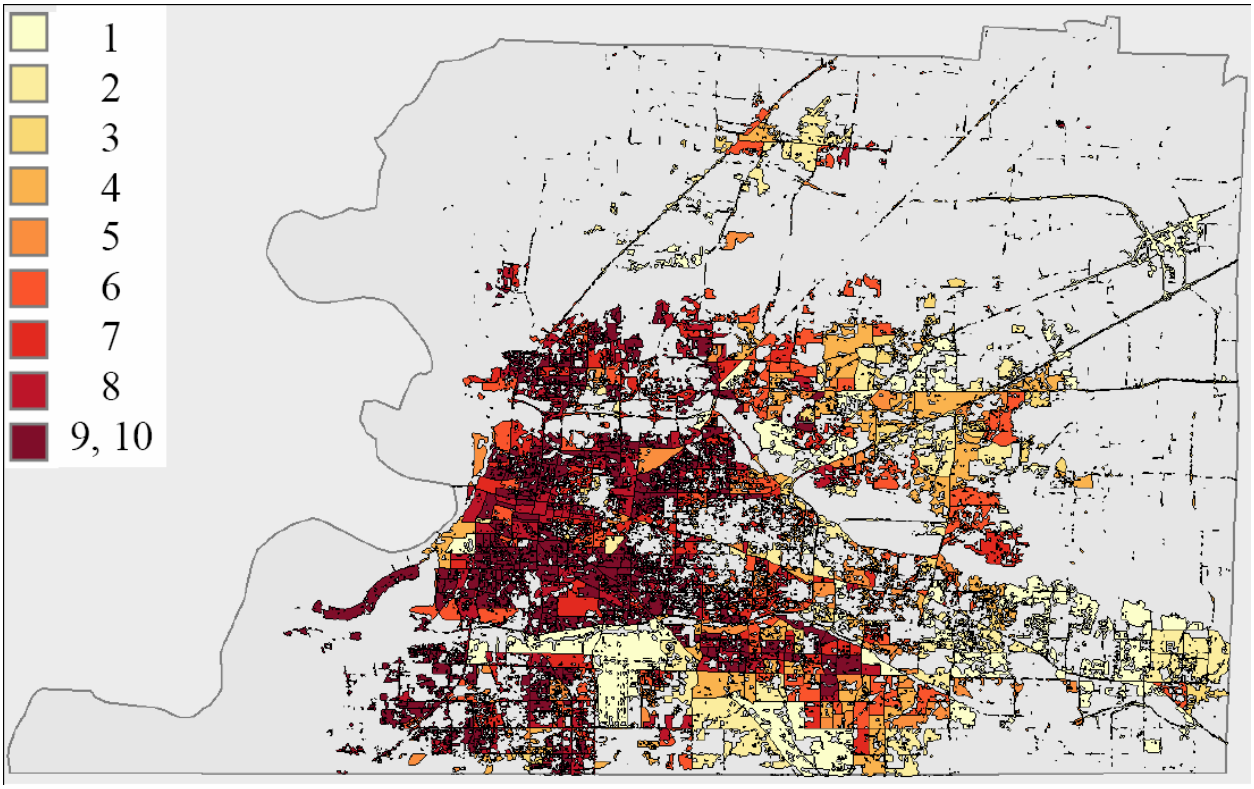

Figure 85. Social Vulnerability Aggregated to Block Groups

6.10 Multi-Layered Loss Visualization

The specific components of loss described in the previous sections may be layered and rendered within a GIS framework to pinpoint regions which will sustain particularly heavy damage from multiple sources, or to highlight zones of increased risk resulting from multiple factors. For example, consider the combined effect on injuries requiring hospitalization of not only direct building damage that initially causes the likely injuries, but also whether hospitals will sustain too much damage to be able to treat all of the injuries, whether bridges and transportation routes will be open to allow easy access to medical facilities, and whether social vulnerability would imply that injured persons will not be able to transport themselves to medical centers without the support of others. Overlaying the four associated datasets yields a map as shown in Figure 86. This map overlays injuries aggregated to tracts, hospital damage (crosses, with darker color representing more damage), bridge functionality immediately after the earthquake, and social vulnerability. In the simplest terms, darker areas on the map have greater risk. However, the map does not explicitly relate bridge damage or hospital functionality to risk, as a result of a lack of data to define likely routes or a detailed transportation network mapping individual residences and commercial and industrial buildings to hospitals. Inclusion of those considerations presently requires estimation and intuition on the part of a planner.

A second multilayered representation is provided in Figure 87 to represent areas of major social and economic disruption. In this case, business interruption is combined with shelter requirements to determine which areas are subject to the most significant risk of population redistribution. A visitor to the areas that are darkest red just after a major seismic event would be likely to see several shops and stores closed. The construction industry may find attractive contracts in these areas, but that is not guaranteed. Business owners may also decide to attempt to relocate to more attractive areas where less damage was sustained, where the customer base is larger and more likely to have greater disposable assets than in an area with a large percentage of displaced households and persons requiring shelter following destruction of property. Here, as with the previous figure, data would ideally be available to map customers to businesses, and to establish routes so that estimates could be made of which customers would be likely to change buying habits and where cash flow could be expected to be redirected.

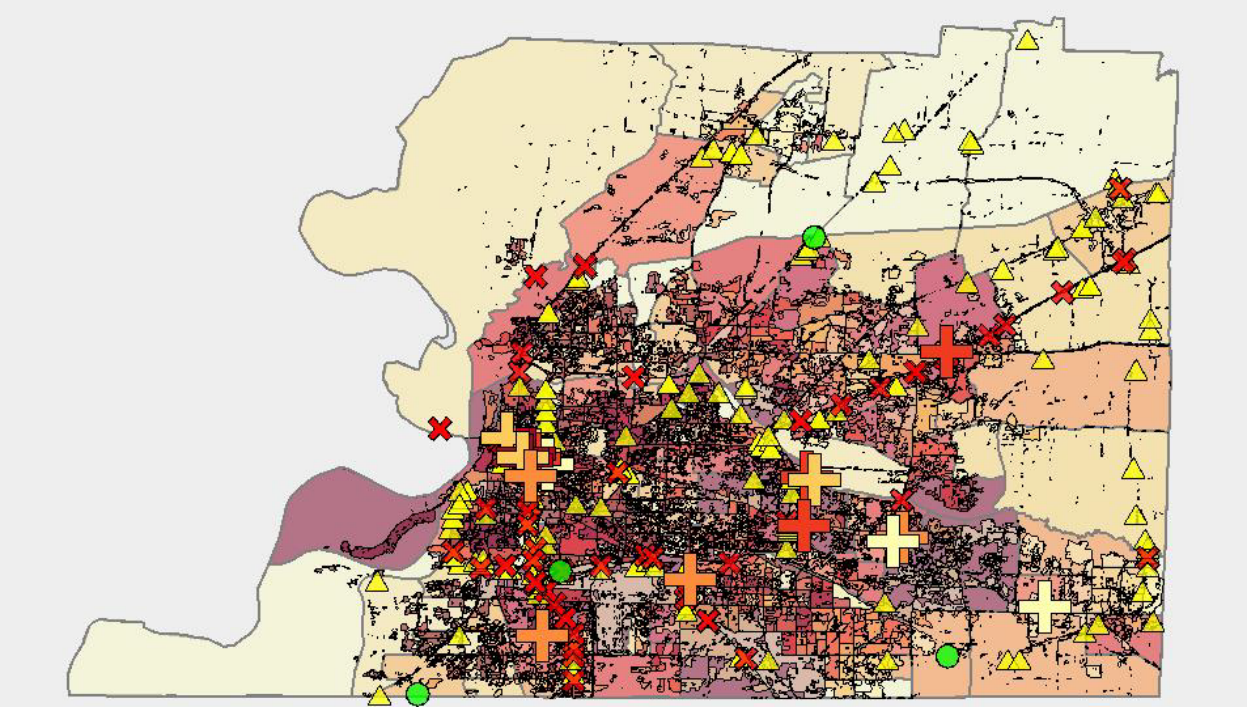

Figure 86. Higher-Order Representation of Risk of Injuries

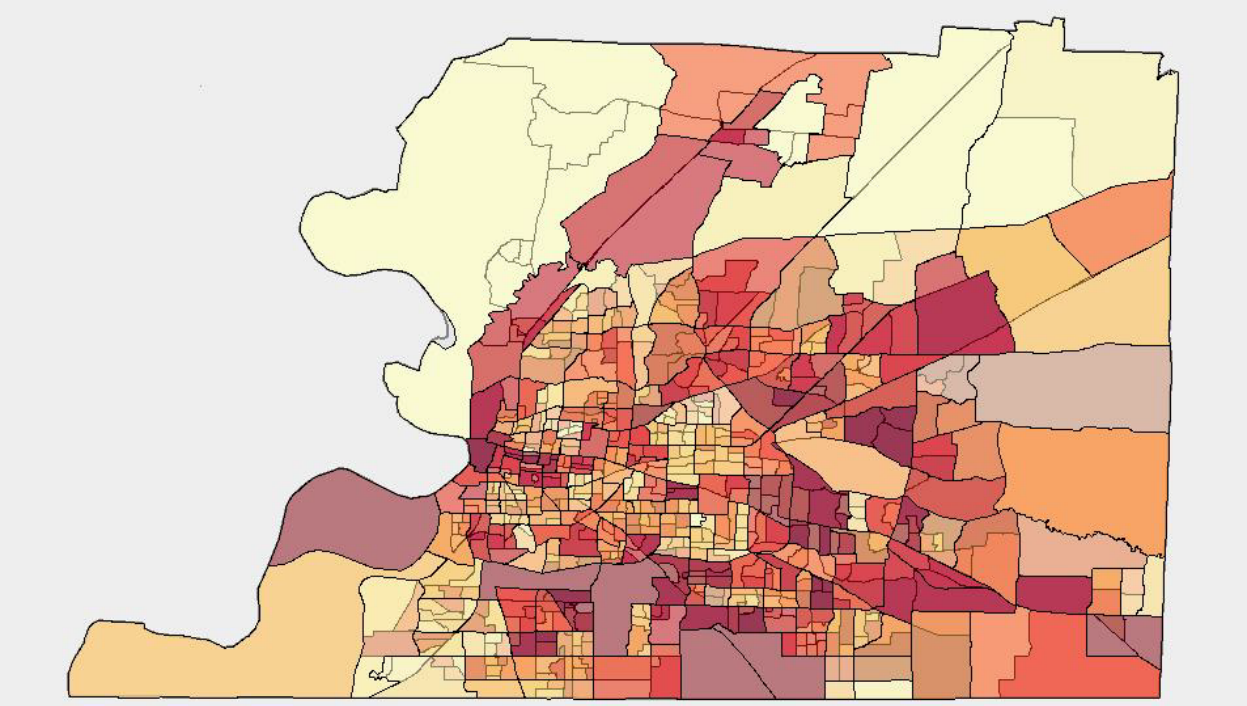

Figure 87. Business Interruption and Shelter Requirements

7 DECISION SUPPORT

The aggregate results of risk assessment algorithms developed within the MAE Center provide useful information to decision makers with regard to disaster planning. Additional algorithms have also been implemented specifically to assist decision-makers, as detailed in this section. The algorithms generally seek to assist decision-makers in determining the most advantageous distribution of mitigation funds to install retrofits.

There are two approaches available for determining an optimized retrofit scheme: equivalent cost analysis (ECA), and multi-attribute utility analysis (MAUA). Both of these approaches are detailed in Park (2004). The ECA relies upon quantification of all losses, including casualties and loss of functionality of essential facilities, in terms of dollar values. By comparison, the MAUA establishes utility functions to measure success of a particular retrofit scheme.

For an ECA analysis of the building stock, values of death and injuries resulting from building damage are estimated at $8.5 million and $1 million, respectively (Dillingham, 1985; Hahn, 1996; Karels, 2003; Miller, 1990; Viscusi, 1993). The equivalent dollar value for loss of function is more challenging to quantify, and so an ECA has been conducted multiple times, assuming values of $50,000, $100,000, and $250,000 per day per 10,000 square feet.

For an MAUA analysis of the building stock, there are two required user inputs: utility functions and weights to apply to individual utility checks. As in Park (2004), two sets of utility functions are considered: risk-seeking and risk-averse. Also, in each case, four utility checks are evaluated: economic loss, deaths, injuries, and loss of function. Unlike the ECA approach, dollar values are not required for the utility checks other than economic loss. Instead, a tolerance must be specified for each utility check to establish a value of zero utility, such as the number of acceptable fatalities as a result of the event.

For this study, estimates were obtained for thresholds of acceptable losses in terms of monetary losses and casualties by using Northridge as a baseline. According to Reis et al. (2001), the documented direct economic losses for buildings in the Northridge event were $26 billion, and the count of deaths and injuries were 57 and 1,616 persons, respectively. Dividing these losses by the building stock exposure and the population of the study region supplied on the HAZUS-MH MR2 default data DVDs, and multiplying by the dollar exposure and population estimate for the study region in Shelby County yields values of approximately $1.7 billion for direct economic loss, 13 deaths, and 365 injuries. Furthermore, since the total monetary loss estimate includes other losses in addition to direct economic losses (e.g., inventory losses, business interruption losses), the threshold value for direct economic losses was increased to $2.125 billion (based on scaling the initial value to reflect the relationship of the total sum of all economic losses to repair and replacement costs reported in the previous sections of this paper).

The acceptable disruption to essential facilities is not easily quantified. In this study, it is assumed that a disruption of half of the essential facilities space for 3 days establishes the

tolerable threshold. The total floor area of essential facilities for Shelby County is 9,543,908 ft^2. Thus, the threshold for disruption to essential facilities is approximately 1400 days*(units of 10,000 ft^2). As in Park (2004), the utility function for a risk-seeking approach follows an exponential form, as

$$U(X) = \exp\left(\frac{X \ln(U_{\min})}{X_{\lim}}\right) \tag{14}$$

Where

$U(X)$ = utility (1 is optimum, 0 is failing)

X = decision attribute value (e.g., number of fatalities)

$X_{\lim}$ = limiting value for decision attribute value (e.g. tolerance for number of fatalities)

$U_{\min}$ = utility value at $X = X_{\lim}$, taken as 0.001 in this study

Also as in Park (2004), the risk-averse approach follows a cubic form, as

$$U(X) = 1 - \left(\frac{X}{X_{\lim}}\right)^3 \tag{15}$$

in which the terms are defined identically to the risk-seeking function. The general forms of the utility functions are shown in Figure 88. The final component of the MAUA which must be specified is the set of weighting factors to be applied to the various utility checks. Four sets of utility weights are considered for this analysis, as shown in Table 12. In Table 12, the weighting factors correspond to monetary losses, deaths, injuries, and essential facility loss of function, in order from 1 to 4. The final utility value is determined by a weighted linear combination of the four individual decision attribute utilities, as

$$\overline{U} = \sum_{i=1}^{4} w_i U_i \tag{16}$$

Where

$\overline{U}$ = total utility (1 is optimum, 0 is failing)

w_i = weight of decision attribute i

U_i = utility of decision attribute i

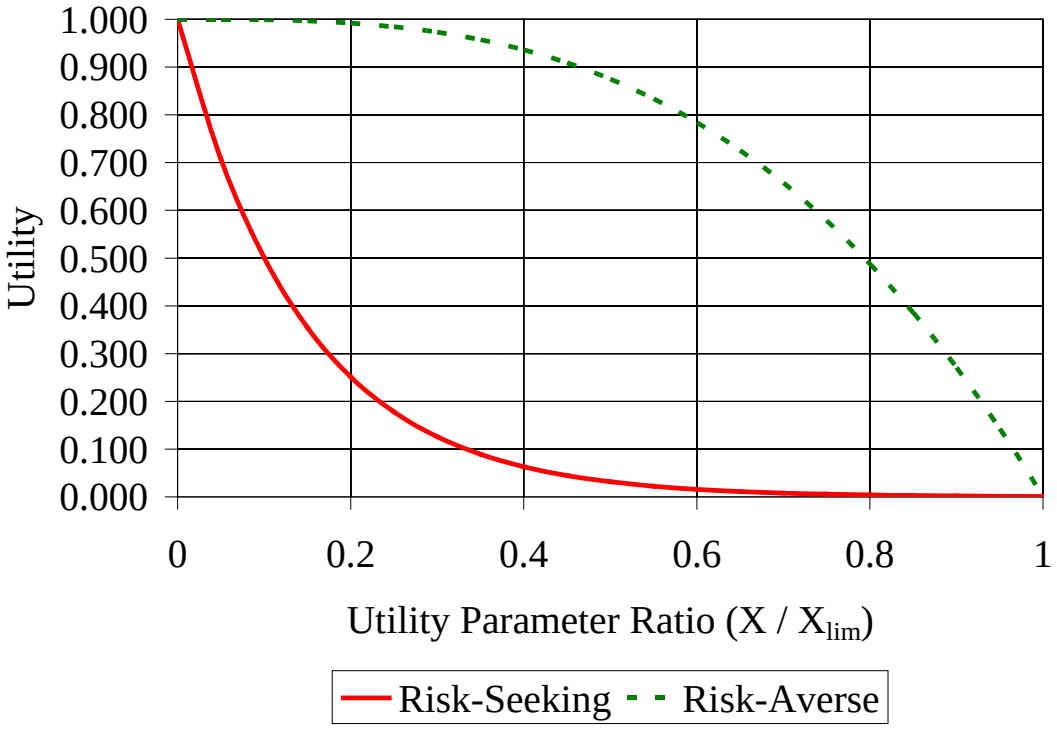

Figure 88. Generalized Utility Functions

Table 12. Weighting Factors for MAUA Cases

Case	Description	w_1	w_2	w_3	w_4
1	Evenly Weighted	0.25	0.25	0.25	0.25
2	Focus on Monetary Loss	0.85	0.05	0.05	0.05
3	Focus on Casualties	0.05	0.45	0.45	0.05
4	Focus on Functionality of Essential Facilities	0.05	0.05	0.05	0.85

In all instances, retrofit vulnerabilities are established by applying the parameterized fragility method with parameters obtained from HAZUS-MH MR2 and the adjustments mentioned previously (FEMA, 2006; Jeong and Elnashai, 2007; Steelman and Hajjar, 2008) to develop fragility sets for higher code levels that are not represented in the body of MAE Center research. When a retrofit is applied, it is assumed that the work has been performed to reduce structural damage only, and therefore as-built nonstructural fragility sets were employed for all retrofit cases.

The costs associated with installation of retrofits were based on values obtained from FEMA 156/157 (FEMA, 1994; FEMA, 1995). Initial values for estimated retrofit costs per unit floor area were taken from FEMA 156 for the various structure types, and each value was increased by $13 per square foot to account for additional nonstructural work required to expose and then

cover building structural components, as recommended in FEMA 157. Buildings were sorted by floor area and tabulated to determine the prevalence of small, medium, large, and very large buildings in the study region inventory. The area adjustment factors in FEMA 156 were then weighted and combined for each structure type category based on the tabulated building counts. A location adjustment factor of 0.86 was applied in accordance with FEMA 156 for Tennessee, and a time factor of 1.52 was applied to adjust the values from 1993 dollars to an inflated present day amount. Finally, factors were selected to meet the Life Safety performance objective for Low, Moderate, High, and Very High seismicity regions.

Based on the HAZUS-MH MR2 Technical Manual (FEMA, 2006), the seismicity categories in FEMA 156 map directly to Pre-, Low-, Moderate-, and High-Code construction, and therefore each retrofit cost was mapped directly to a code level classification for fragility sets. As a final calibration to determine retrofit costs for buildings, the retrofit cost for Pre-Code structures was normalized to zero, and the estimated cost for Pre-Code was subtracted from each of the other Code level retrofit cost estimates. This adjustment was performed to reflect the assumption that all buildings should meet at least this performance level, even if the structure was only designed for wind loading.

Results of the ECA and MAUA analyses are shown in the following figures. For the ECA analyses, the equivalent value of losses was calculated for each building and for each applicable Code level, using the dollar value equivalents mentioned previously for casualties and loss of functionality for essential facilities, where applicable Code levels are only as-built and higher. The value for "benefit" is then calculated by subtracting the equivalent value of losses in the retrofit condition from the equivalent value of losses in the as-built condition. That is, for buildings that are Low-Code in the as-built condition, the benefit-cost ratio is zero for a Low-Code level, and benefit values are calculated for Moderate-Code and High-Code levels. Costs are calculated by subtracting the value for retrofit installation cost per unit floor area in the as-built condition from the value for a retrofit level of interest, and multiplying by the floor area recorded in the inventory database.

For each building, if the maximum benefit-cost ratio is less than 1, the optimum Code level is considered to be the as-built condition. Otherwise, the Code level corresponding to the maximum benefit-cost ratio was identified, and the results were tabulated and plotted in 100% stacked columns in Figure 89 through Figure 91. In some cases, the results are skewed by inaccuracies in the building stock inventory database. Essential facilities, in particular, are susceptible to such issues, since the building stock inventory relies heavily on the Tax Assessor's database, and essential facilities typically are not taxable assets. For example, the buildings classified as Fire Stations show a tendency to remain in the as-built condition. However, this result is misleading, since many fire stations have zeros recorded for floor area in the inventory database, which results in a retrofit cost of zero, and if retrofit costs were equal to zero, that Code level was not considered as a viable option in the analysis. If all optimum retrofits were installed,

the total cost would be about $602 million, and the benefit would be $2,000 million to $3,700 million, depending on the value of essential facility functionality selected for the analysis.

The results shown in Figure 89 through Figure 91 represent a broad view at the regional level, however, the resolution of the inventory permits the investigation and selection of retrofits for a subset of structures to achieve a maximum benefit-cost ratio. For the Blytheville scenario, a subset of 8 structures may be selected such that the cost is approximately $10.5 million, but the projected benefit is about $555.6 million. The driving characteristics to define the selected subset were the vulnerability associated with older steel frame structures, the nature of the structures as essential facilities, and the projected benefit available to that structure type relative to capital investment. All of the selected structures are hospitals, and all are classified as steel frame (S1) structure types. A range of heights are included in the selected subset, from 2 to 19 stories. The selected structures were all constructed between 1920 and 1989, and are therefore expected to include little, if any, seismic consideration in the as-built condition. The locations of the structures are shown as white circles superimposed on a map of hospitalizations aggregated to tracts in Figure 92.

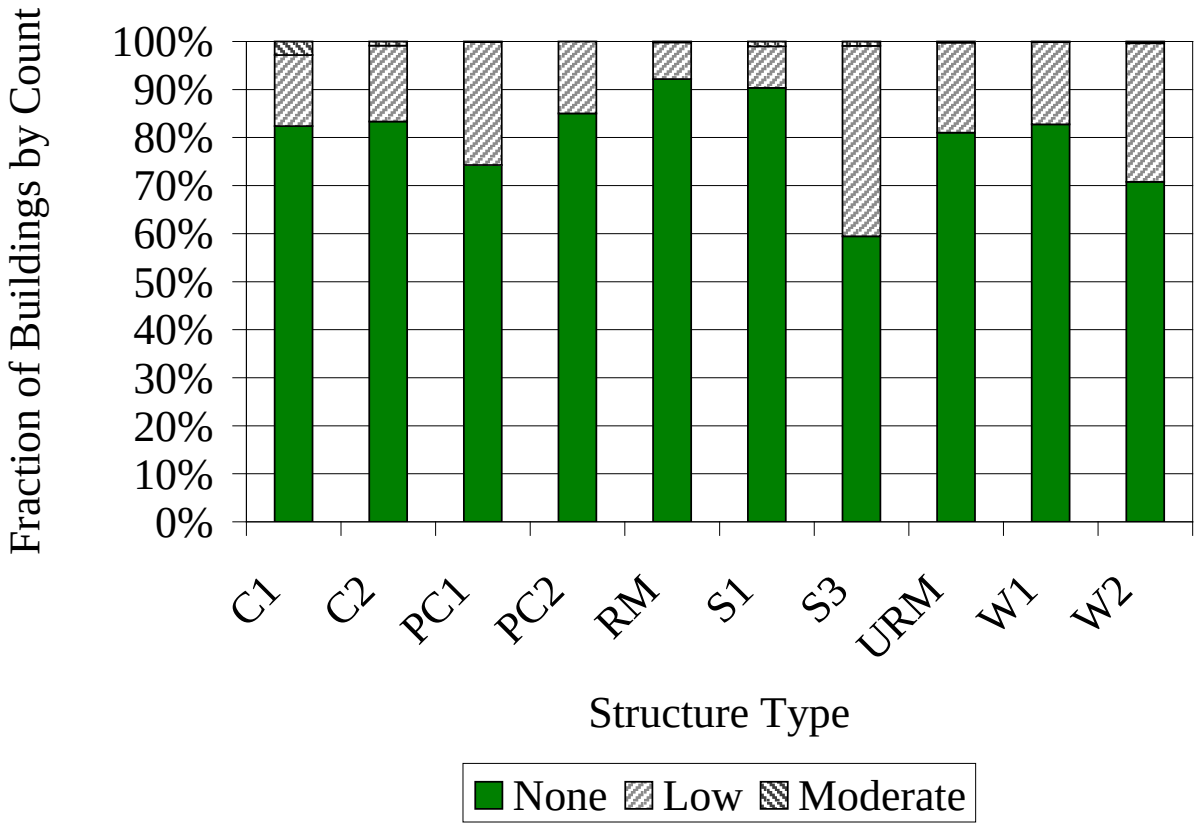

Figure 89. Optimum Retrofit According to ECA by Structure

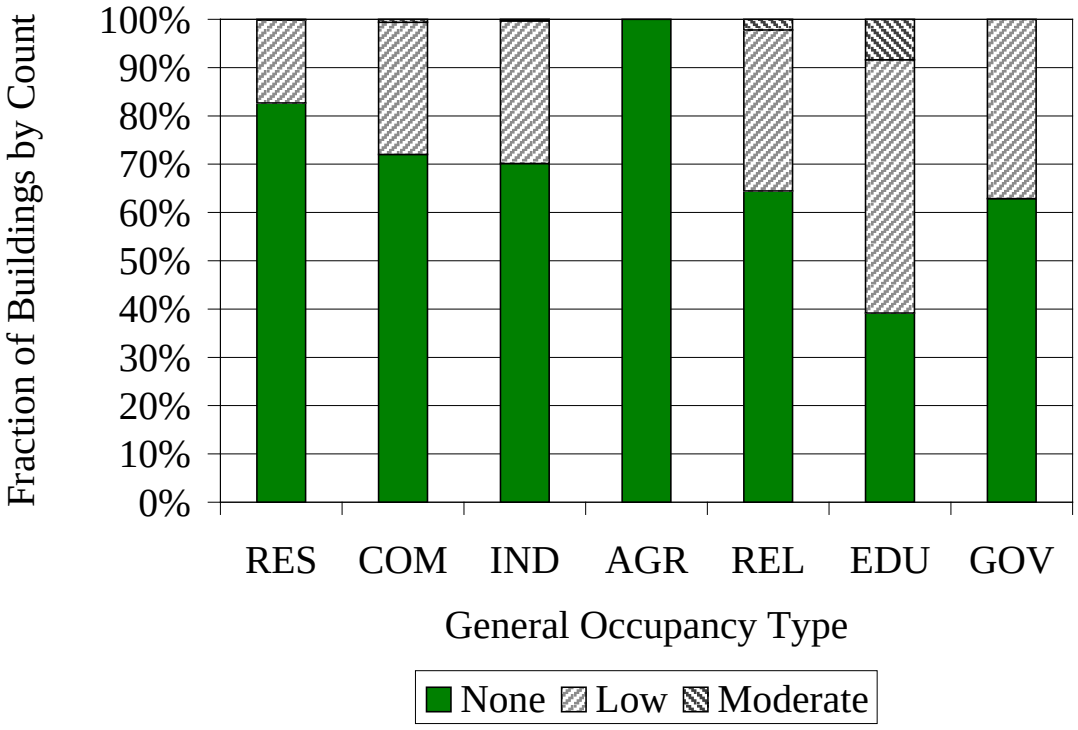

Figure 90. Optimum Retrofit According to ECA by Occupancy

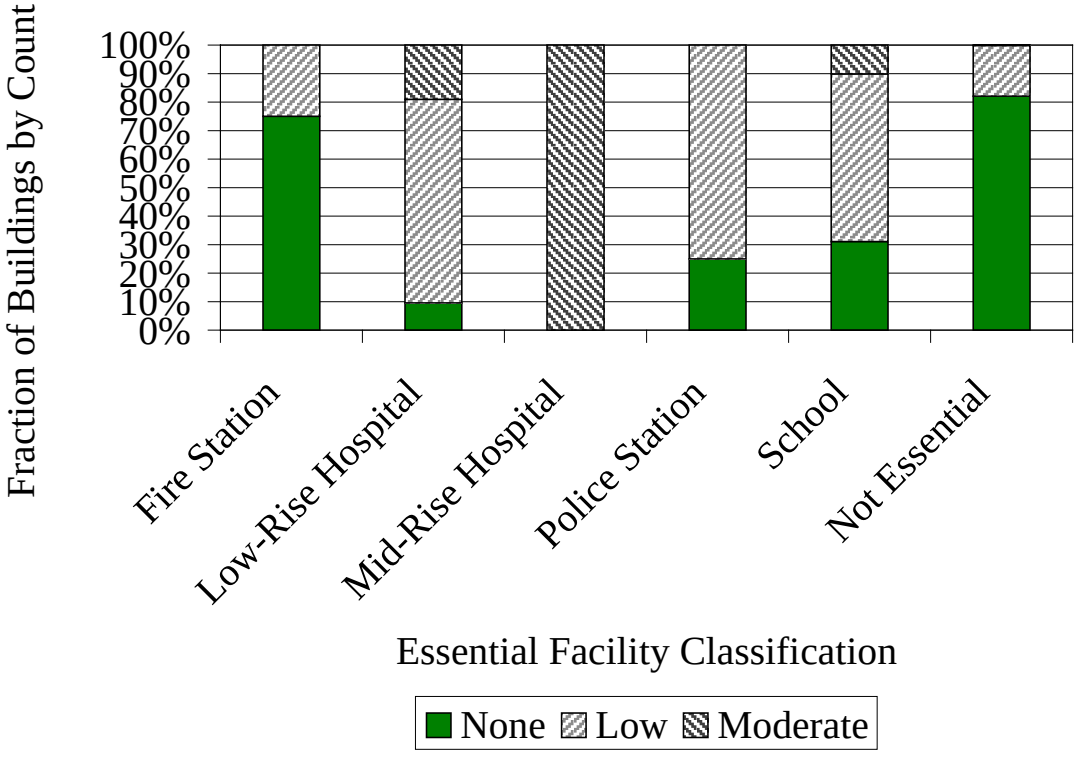

Figure 91. Optimum Retrofit According to ECA by Essential Facility Classification

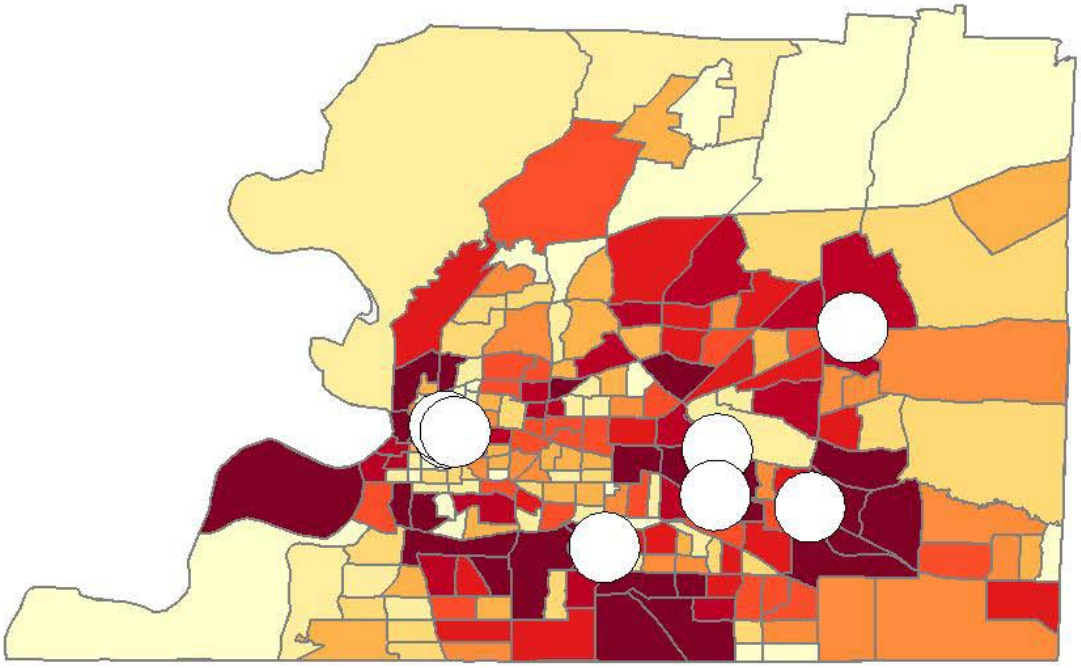

Figure 92. Prioritized Retrofit Selections by ECA

As mentioned previously, one of the fundamental differences between ECA and MAUA is that MAUA requires limiting values to be specified for each decision attribute, rather than converting non-currency values to currency equivalents. As an initial excursion into the decision methodology of MAUA, values were selected based on scaling Northridge losses to account for differences in dollar exposure and population for the study regions, as described in previous sections. The outcome of the use of the scaled Northridge thresholds is shown in Figure 93 and Figure 94. Regardless of the decision-maker's risk attitude, the proposed thresholds cannot be met. To interpret the values shown in the figures, recall that utility is defined such that a value of 1 is a perfectly functioning system (e.g., zero dollar losses or casualties). As the system damage increases, the utility of the retrofit scheme degrades. When the utility reaches a value of zero, or very near zero in the case of a risk seeking decision-maker, the losses have risen to a level which is considered unacceptable according to the standards defined by the decision-maker. Thus, the option with the maximum utility is preferred, and any retrofit scheme with a utility of approximately zero or less has exceeded the tolerance for loss established for the scenario. These results indicate that if a large magnitude event were to occur, the study region can be expected to sustain more severe losses than those observed at Northridge, in a relative sense, regardless of the mitigation efforts employed in the building stock. This interpretation is supported by the observation that all schemes and cases for the risk-averse decision-maker are negative, and the utilities are no higher than 0.00006 for a risk-seeking decision-maker, where the risk-seeking function can only approach, but never reach, a value of zero.

Confronted with this outcome, the thresholds were redefined to bring them closer to the predicted losses for the study region in the as-built condition. The thresholds were adjusted to 621 persons killed, 3,249 persons injured, 27,225 days*(units of 10,000 ft^2 area), and $4.8 billion. The results obtained when using the revised thresholds are shown in Figure 95 and Figure 96,

which confirm that with these more relaxed tolerances, acceptable retrofit or non-retrofit options are available. To determine which retrofit scheme is most attractive, the cost to install retrofits also needed to be considered. To this end, Figure 97 and Figure 98 were generated to show the change in utility from an as-built condition to each retrofitted condition, normalized by the cost required to achieve the respective retrofit levels. These plots show that, when normalized by cost, the Low-Code level is generally preferred, regardless of the weighting scheme chosen for the individual utility checks. The lone exception occurs when limitation of monetary loss is heavily weighted in the decision process for a risk-averse decision maker, in which case the as-built condition is optimum.

Similarly to the ECA approach, the high resolution of the inventory was used to determine a subset of 8 buildings with maximum utility gradients with respect to capital investment. Subsets of buildings were selected for each of the four weighting cases and for each of the decision attitudes considered in the analysis. For both the Risk-Seeking and Risk-Averse attitudes, when applying the Case 4 weighting scheme (essential facility functionality), the selected buildings were identical to the ECA analysis. The same buildings were also selected for Case 1 (equal weighting) of the Risk-Averse attitude, and only two exceptions were made for Case 3 (casualties). The Case 3 Risk-Averse results included two concrete moment frame structures in place of two steel frames. Both the frames being replaced and the additions to the prioritized retrofit selections were low-rise and built in the 1970's. The Risk-Averse results for Case 2 (economic loss) indicated that the maximum normalized utility gradient would be achieved by primarily retrofitting low-rise, single-family, wood frame structures. However, the computed normalized gradient was more uniform throughout the building stock for this Case, so the mandate indicated for this particular subset of 8 buildings is relatively weak, compared to other Cases. The Risk-Seeking results were consistent for Cases 1, 2, and 3, with single-story concrete moment frame office buildings populating the top 8 positions for Cases 1 and 3, and 7 of the top 8 for Case 2. As with the Risk-Averse Case 2 results, the variation of normalized utility gradient was lower for this case, and a single-story, wood frame, single-family residence replaced one of the concrete frame buildings in the priority list. Selections are shown in Figure 99 and Figure 100. In Figure 99, the selections for Risk-Averse Case 3 include the two concrete frames shown as shaded triangles. Figure 100 shows the selections for Cases 1, 2, and 3 for the Risk-Seeking attitude, with the exception of the added wood frame in Case 2. The two shaded markers are shared choices between Risk-Averse Case 3 and the Risk-Seeking Cases.

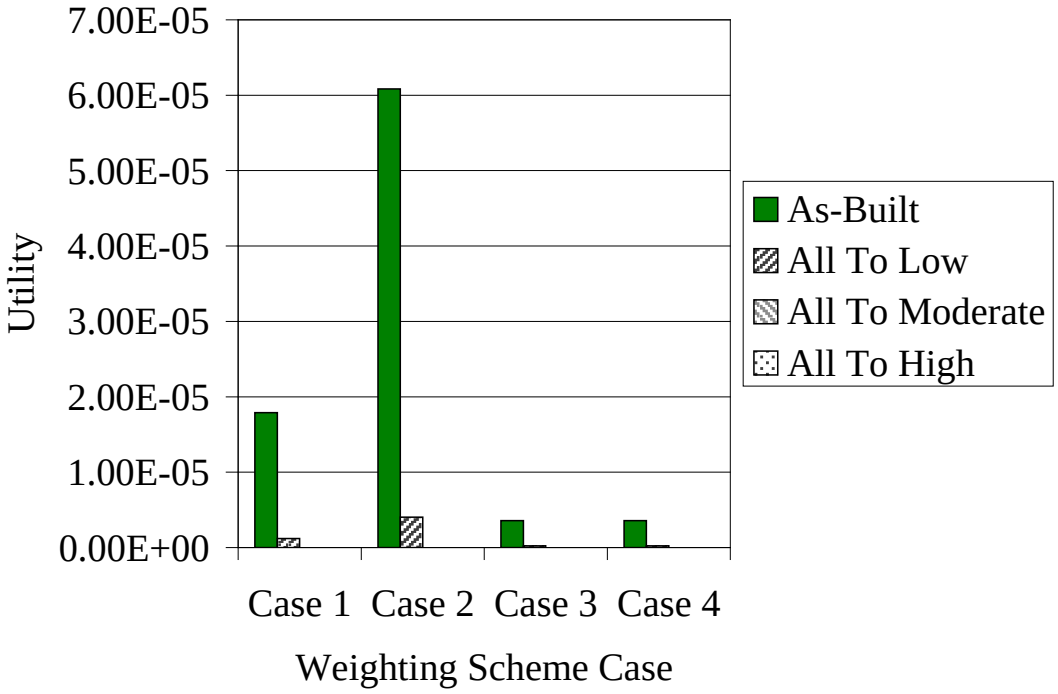

Figure 93. Utility by Retrofit and Weighting Case for Scaled Northridge Thresholds (Risk-Seeking Decision-Maker)

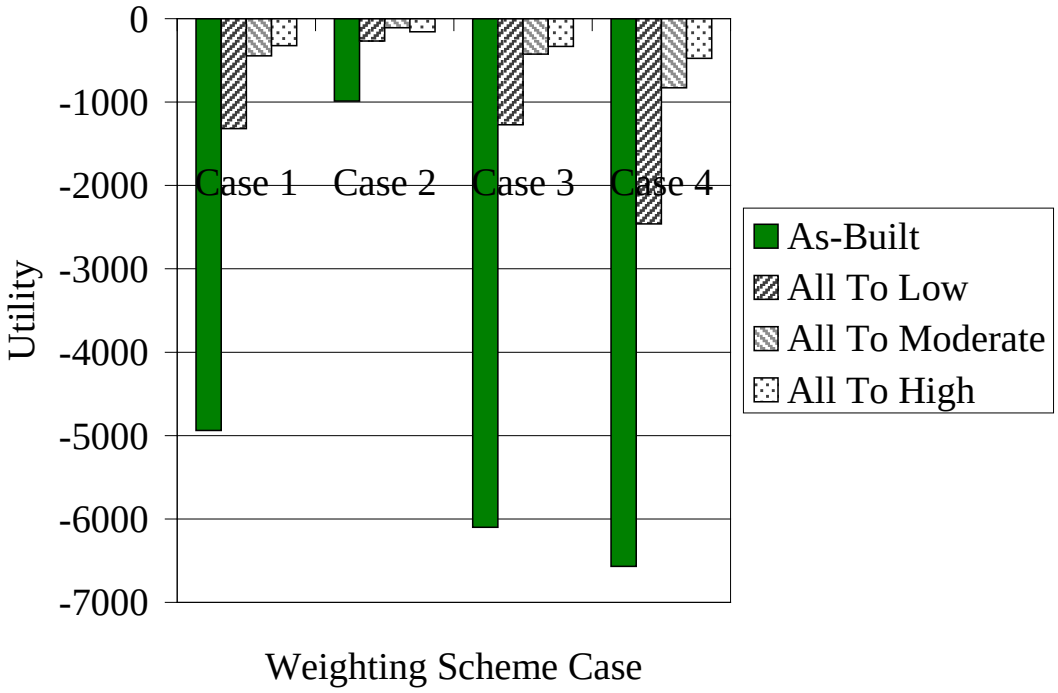

Figure 94. Utility by Retrofit and Weighting Case for Scaled Northridge Thresholds (Risk-Averse Decision-Maker)

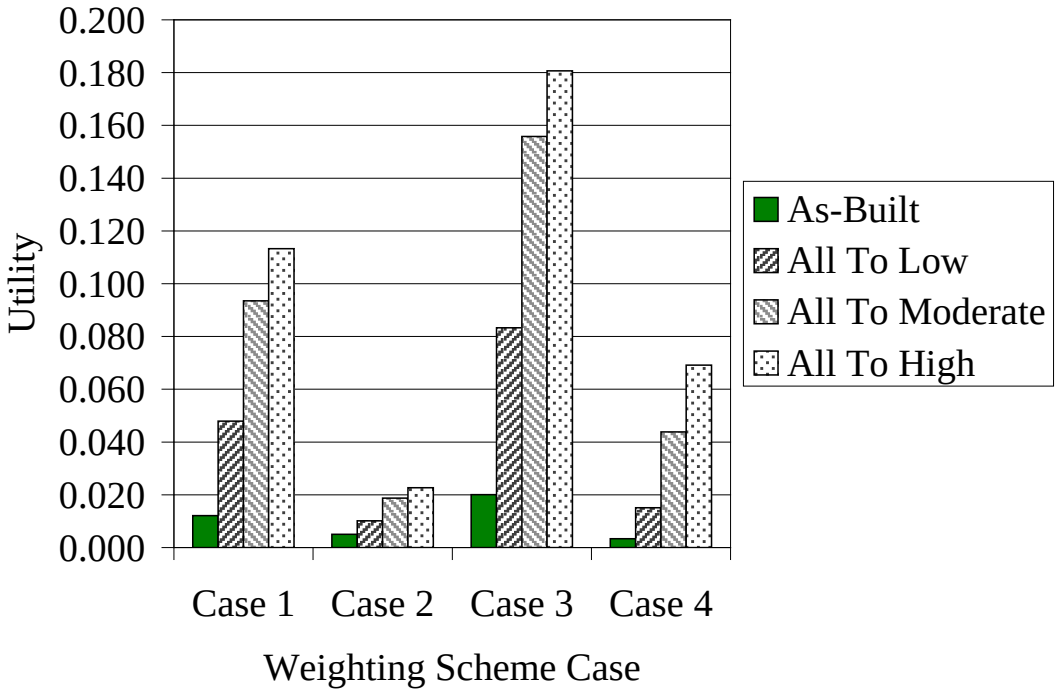

Figure 95. Utility by Retrofit and Weighting Case for Revised Thresholds (Risk-Seeking Decision-Maker)

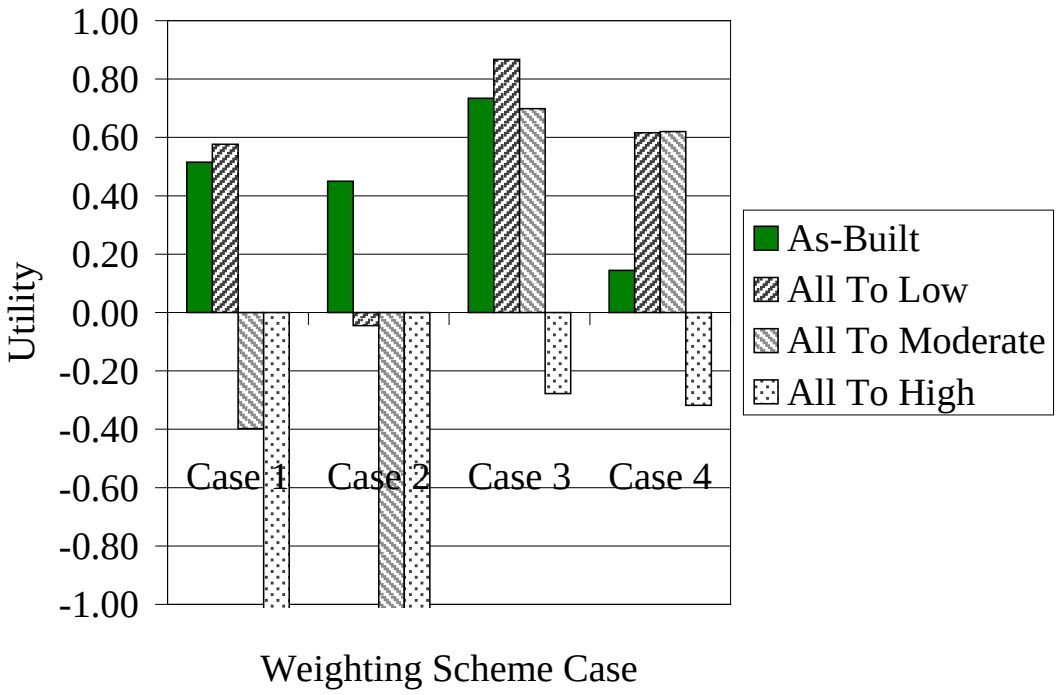

Figure 96. Utility by Retrofit and Weighting Case for Revised Thresholds (Risk-Averse Decision-Maker)

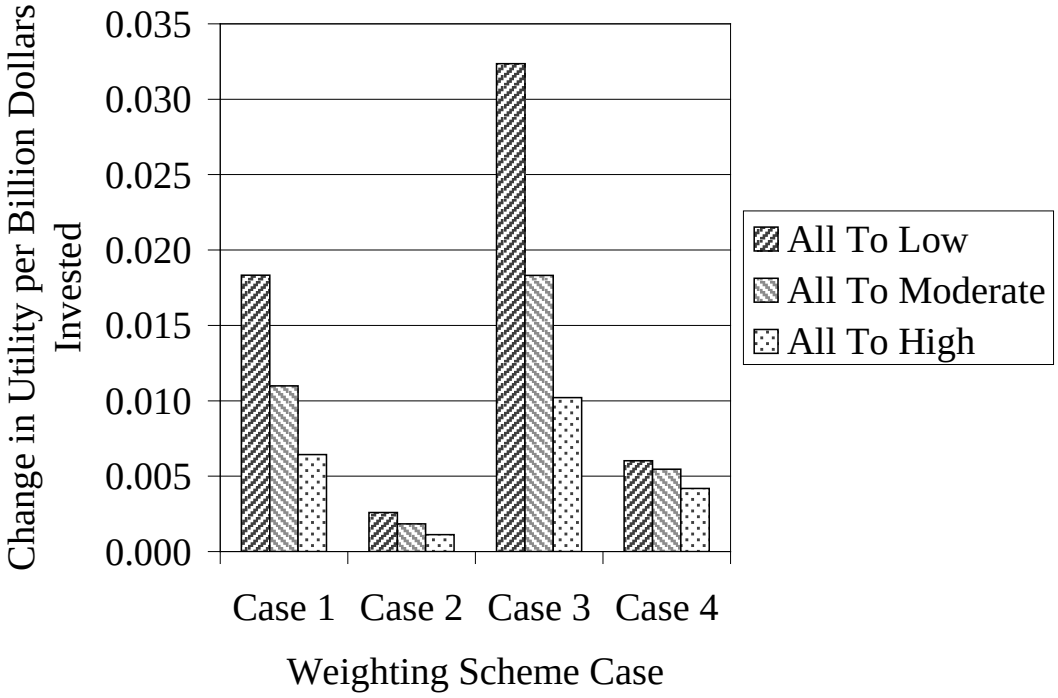

Figure 97. Change in Utility by Retrofit and Weighting Case, Normalized by Cost (Risk-Seeking Decision-Maker)

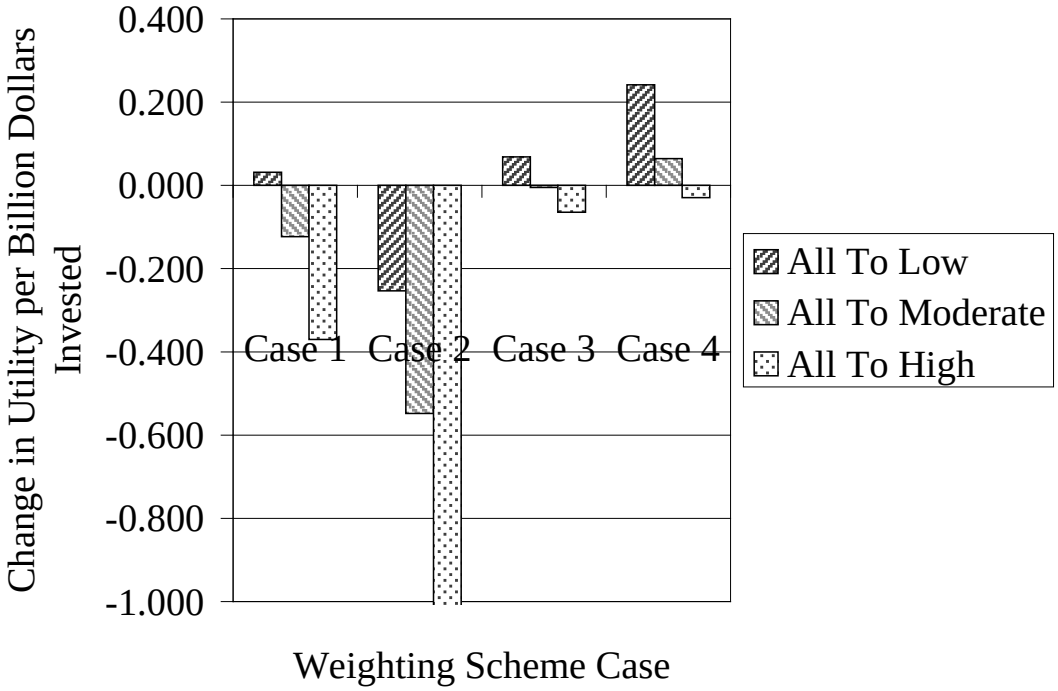

Figure 98. Change in Utility by Retrofit and Weighting Case, Normalized by Cost (Risk-Averse Decision-Maker)

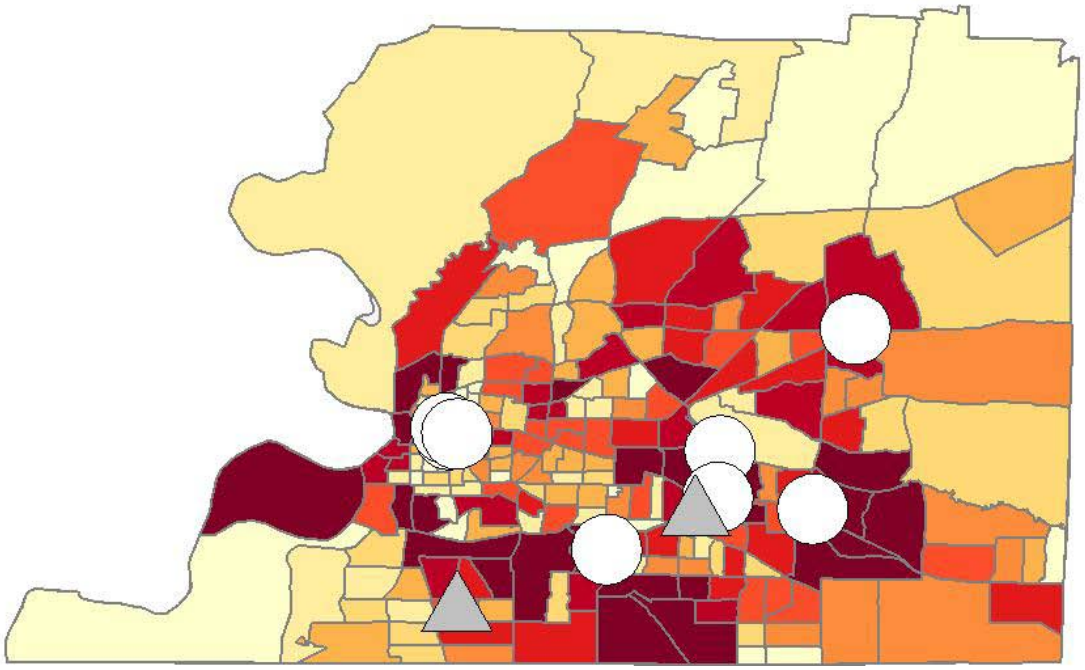

Figure 99. Prioritized Retrofit Selections by MAUA with Risk-Averse Attitude

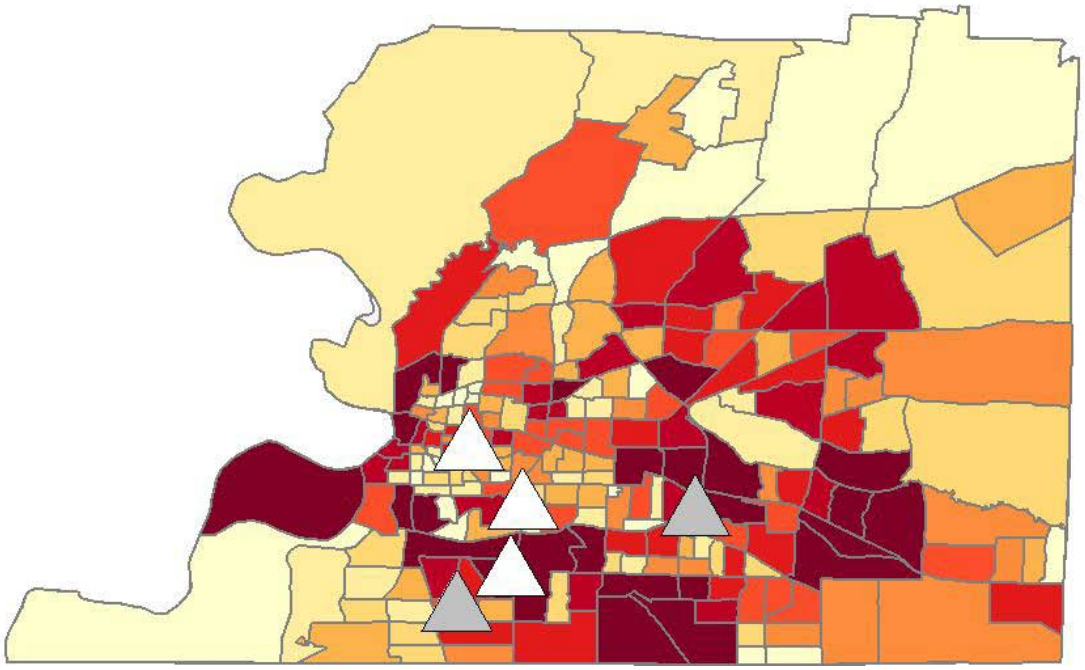

Figure 100. Prioritized Retrofit Selections by MAUA with Risk-Seeking Attitude

The foregoing charts represent general trends for the building stock, and assume that all buildings will receive retrofits to a specified Code level. However, by calculating the effect of retrofits building by building and assessing the change in utility per retrofit cost investment, individual buildings can be classified according to optimum retrofit level. This was performed

using each of the four weighting scheme cases mentioned previously (Table 12), and also with each of the two risk attitude utility functions. The results of the analyses are shown in 100% stacked bars by grouping buildings according to structure type, occupancy type, and essential facility classification in Figure 101 through Figure 124.

Certain trends become immediately apparent when reviewing the figures. A non-intervention strategy is preferable for Case 2 (Table 12), regardless of structure type, occupancy type, or risk attitude. This is a generally expected pattern, as the costs of installing retrofits are typically not justified solely on the basis of reduced physical damage and mitigation of resulting repair and replacement costs. Generally, the justification for retrofit installation is found in reduction of other effects, such as casualties, as seen in Case 3. The pattern for Case 3, with a 90% weighting applied to the casualty component of utility, is the opposite of Case 2, so that regardless of structure type, occupancy type, or risk attitude, a non-intervention approach is generally not attractive. The pattern for Case 4, focusing on loss of function of essential facilities, does generally follow a pattern of encouraging retrofit installation more strongly at essential facilities. The pattern is forced by the analysis algorithm, which considers "loss of function" at non-essential facilities to cause an economic impact (e.g., business disruption), but when utility is being calculated, the value is taken as zero.

With regard to structure type, light steel frame structures (S3) are the most attractive candidates for retrofit in virtually all cases, which is usually followed by URM, concrete frame (C1), and precast concrete (PC1 and PC2) structures. With regard to general observations for occupancies, although there is variation within the groups, the commercial (COM) and industrial (IND) structures are expected to receive the most benefit per investment. The RES4 and RES5 occupancies may also be attractive candidates. Agricultural buildings (AGR) are the least attractive candidates, which is reasonable considering that, in general, structures in this category are lightly constructed, relatively easily replaced, and generally unlikely to cause casualties in the event of severe damage. The GOV2 occupancy may initially appear to be of similarly little attention, but the results are skewed by the inclusion of essential facilities, primarily police and fire stations, and suffer from the data reliability issues mentioned in the discussion of ECA. About half of structures in the GOV2 occupancy have recorded floor areas of zero, which leads to a default selection of a non-retrofit option as optimum. In general, the appeal of a particular occupancy as a recipient of retrofit measures is dependent on its constitution in terms of structure types. Thus, occupancies with S3 or URM structures generally appear more attractive for retrofit.

One final point that should be considered is the general reliability of the data obtained from this analysis, given that the results represent an amalgamation of vulnerability predictions from various sources, depending on structure type. For URM and S3 structures, for example, all fragilities are determined by the parameterized fragility method, and are therefore relatively homogeneous, depending only on the reliability of the input parameters such as strength ratios and periods. For some other types, such as concrete (C1) or steel frames (S1), however, the entire set of fragility sets for all Code levels includes a combination of parameterized fragilities and other fragilities derived by other MAE Center researchers, which may be derived based on analytical variations which are not easily compared, such as alternate ground motion record suites or constitutive modeling of structural components. There is a fundamental difference in the global modeling of parameterized versus non-parameterized fragilities, as the parameterized fragilities simplify structures to SDOF oscillators, while non-parameterized models include consideration of an assemblage of elements into a structural system. This lack of homogeneity

can lead to perturbations in results, so that the "optimum" retrofit may not be consistent with the result of the exclusive use of fragilities from a single source. This effect is particularly pronounced when the fragility in the as-built condition estimates less vulnerability than would be obtained by a similar parameterized fragility. In such a case, if the non-parameterized MAE Center fragility is, for example, a Pre-Code level fragility, and the estimate of vulnerability is lower than for a parameterized Pre-Code level fragility, then the parameterized fragilities used for Low- and possibly Moderate-Code levels may estimate vulnerability to be higher in the retrofitted case than in the non-retrofitted case, leading to a selection of a High-Code retrofit as the only option with a positive gradient of utility normalized by cost. For this reason, the results of the decision support algorithms should be viewed as particularly uncertain estimations, and decision makers employing the results of such an analysis must maintain the nature of the prediction in its proper perspective.

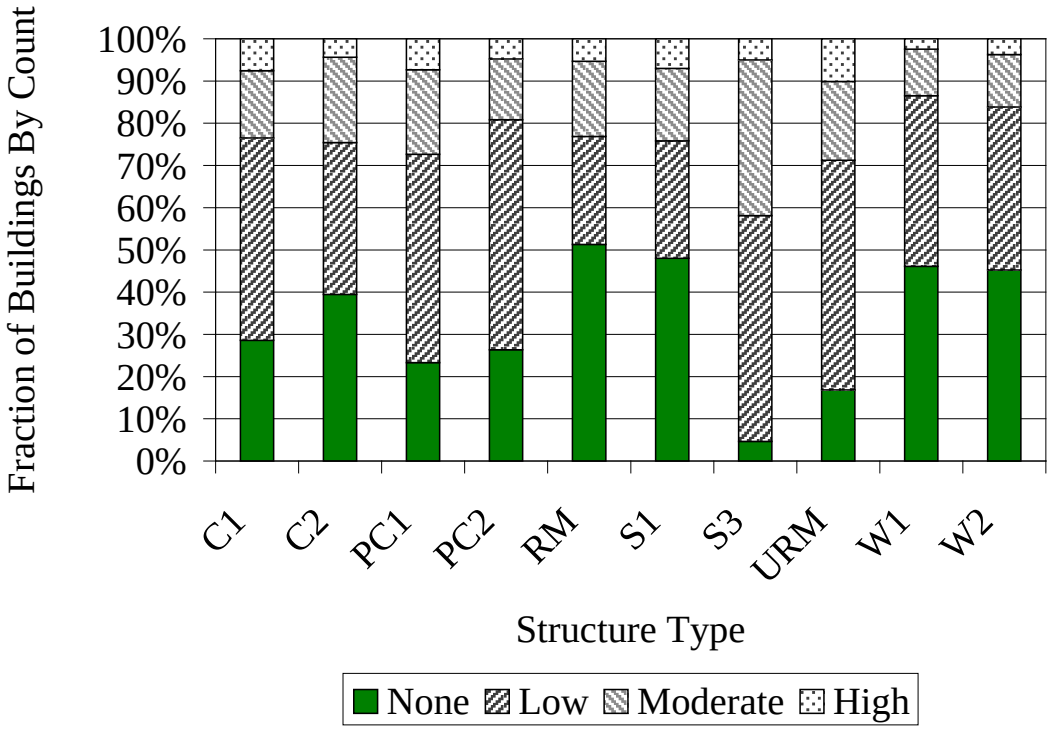

Figure 101. Optimum Retrofit for Weighting Scheme Case 1, Sorted By Structure Type (Risk-Seeking Decision-Maker)

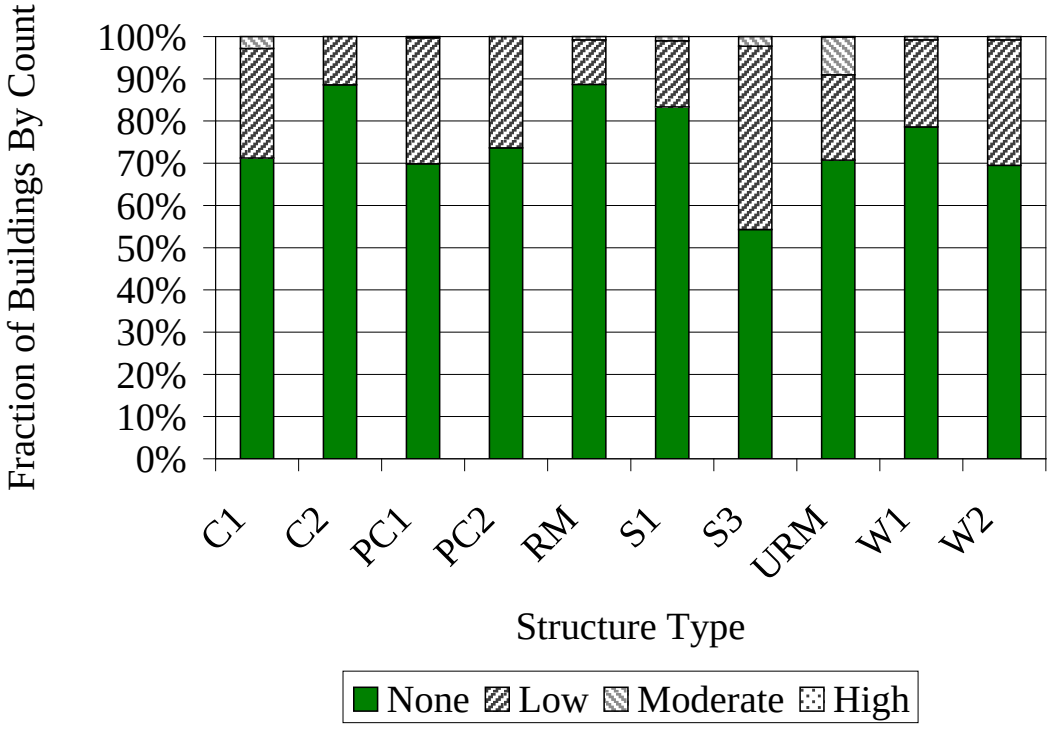

Figure 102. Optimum Retrofit for Weighting Scheme Case 2, Sorted By Structure Type (Risk-Seeking Decision-Maker)

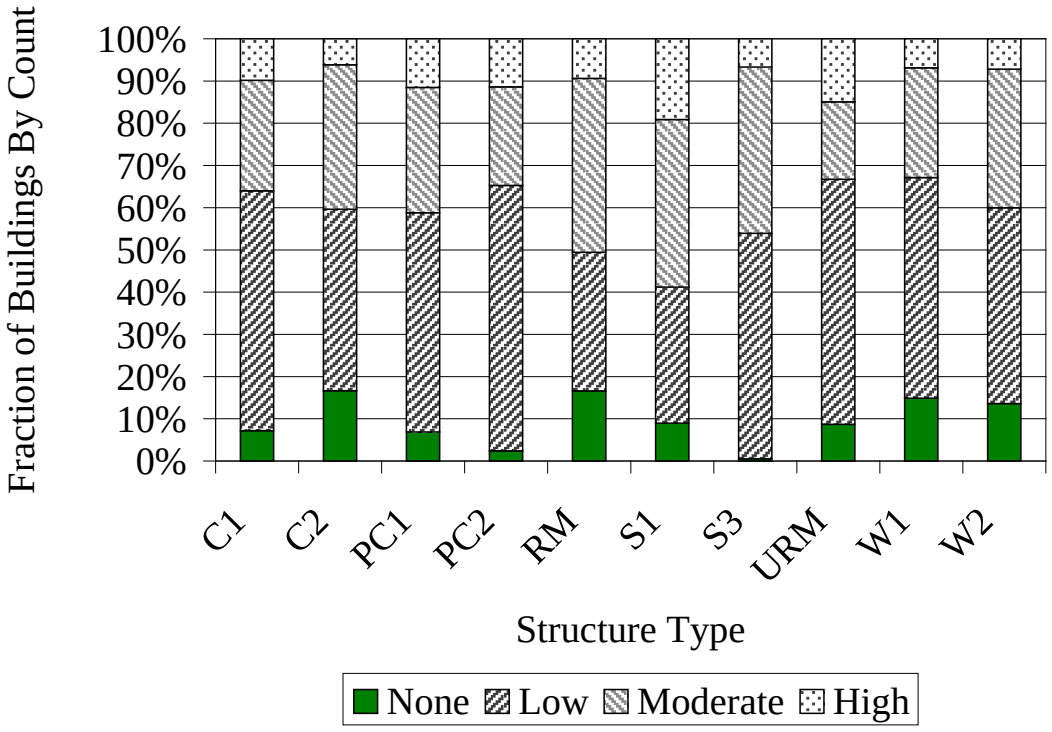

Figure 103. Optimum Retrofit for Weighting Scheme Case 3, Sorted By Structure Type (Risk-Seeking Decision-Maker)

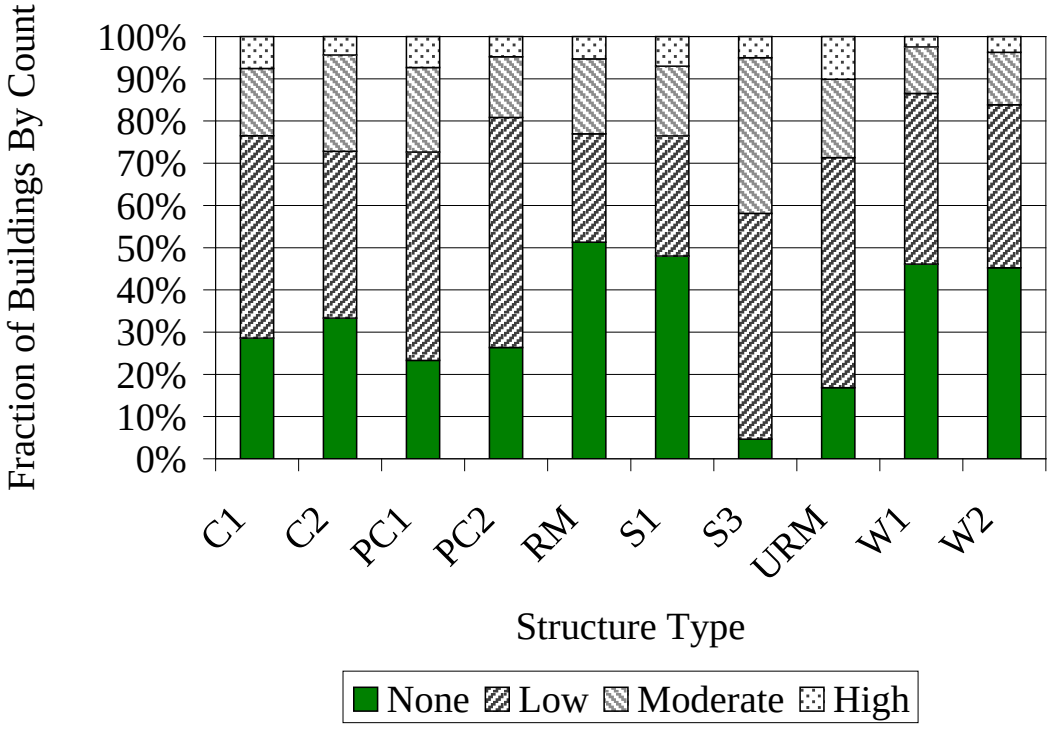

Figure 104. Optimum Retrofit for Weighting Scheme Case 4, Sorted By Structure Type (Risk-Seeking Decision-Maker)

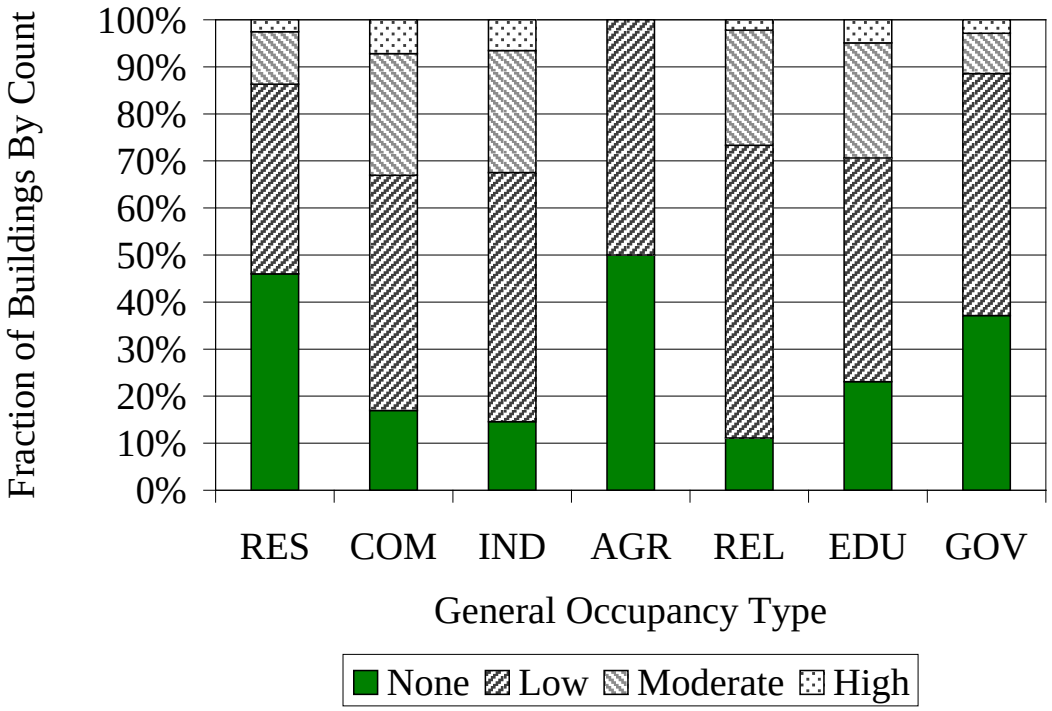

Figure 105. Optimum Retrofit for Weighting Scheme Case 1, Sorted By Occupancy Type (Risk-Seeking Decision-Maker)

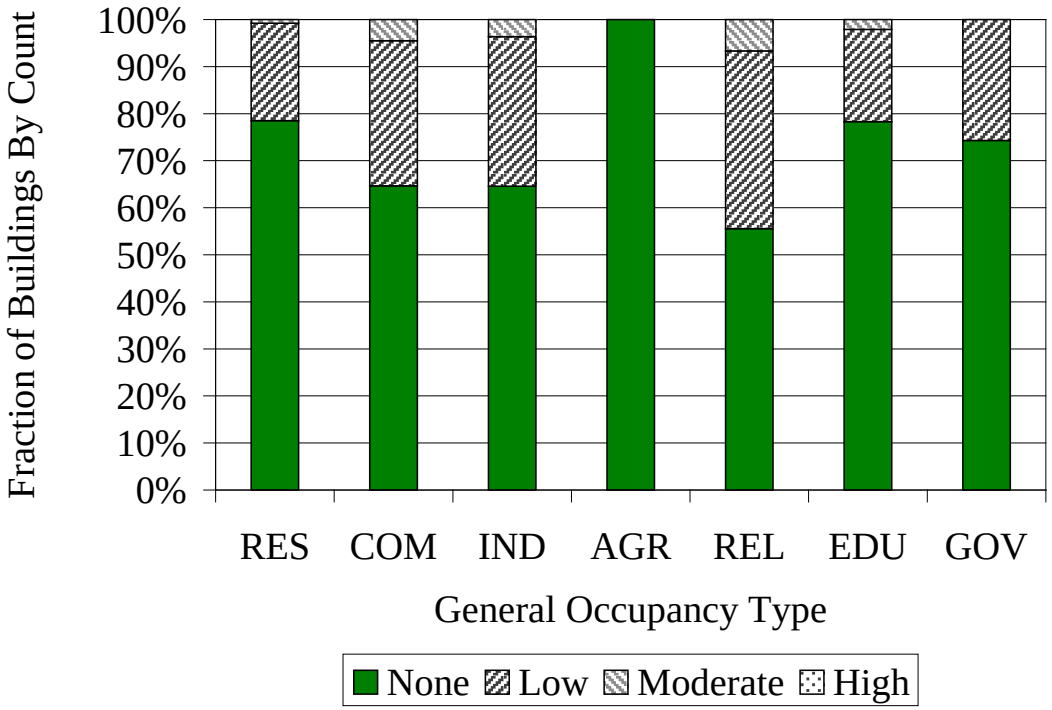

Figure 106. Optimum Retrofit for Weighting Scheme Case 2, Sorted By Occupancy Type (Risk-Seeking Decision-Maker)

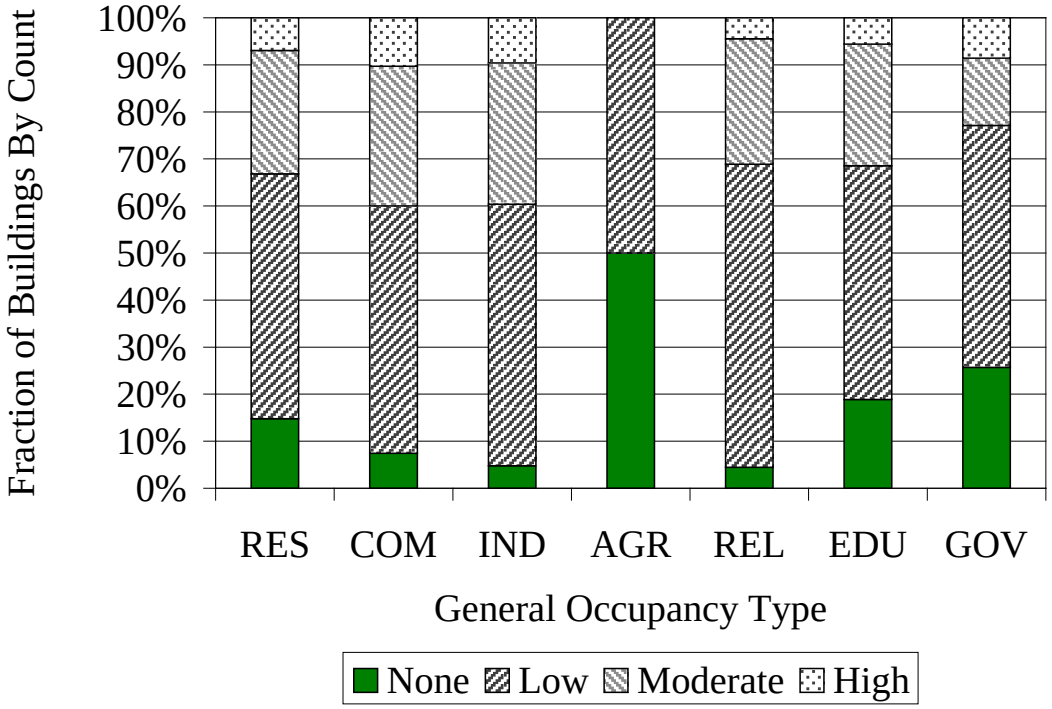

Figure 107. Optimum Retrofit for Weighting Scheme Case 3, Sorted By Occupancy Type (Risk-Seeking Decision-Maker)

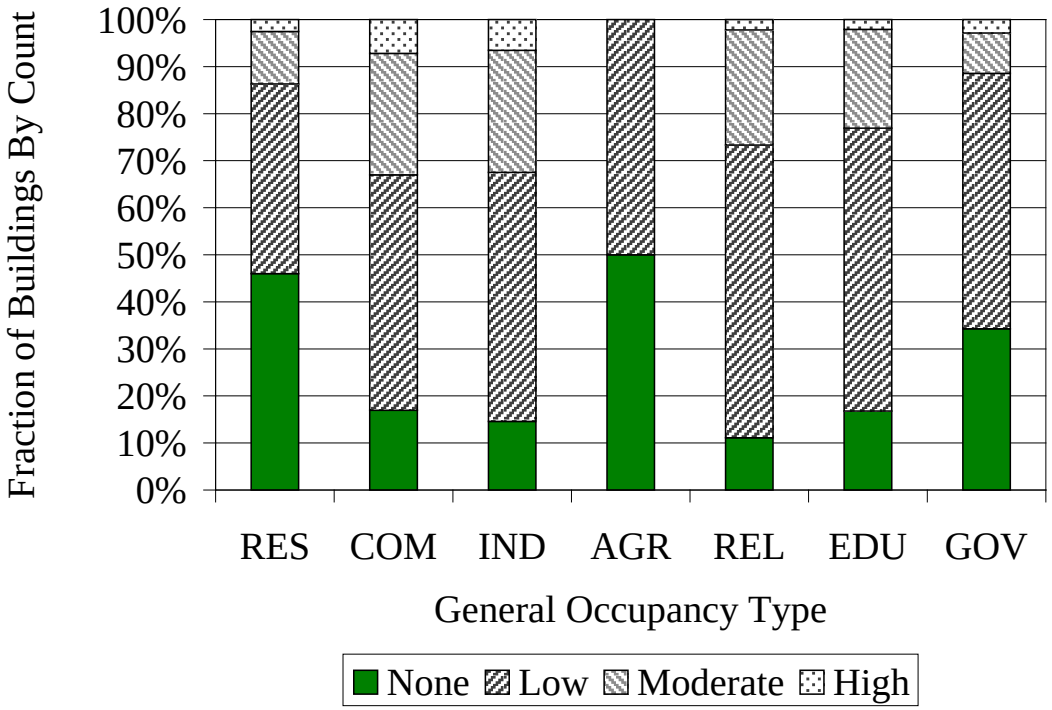

Figure 108. Optimum Retrofit for Weighting Scheme Case 4, Sorted By Occupancy Type (Risk-Seeking Decision-Maker)

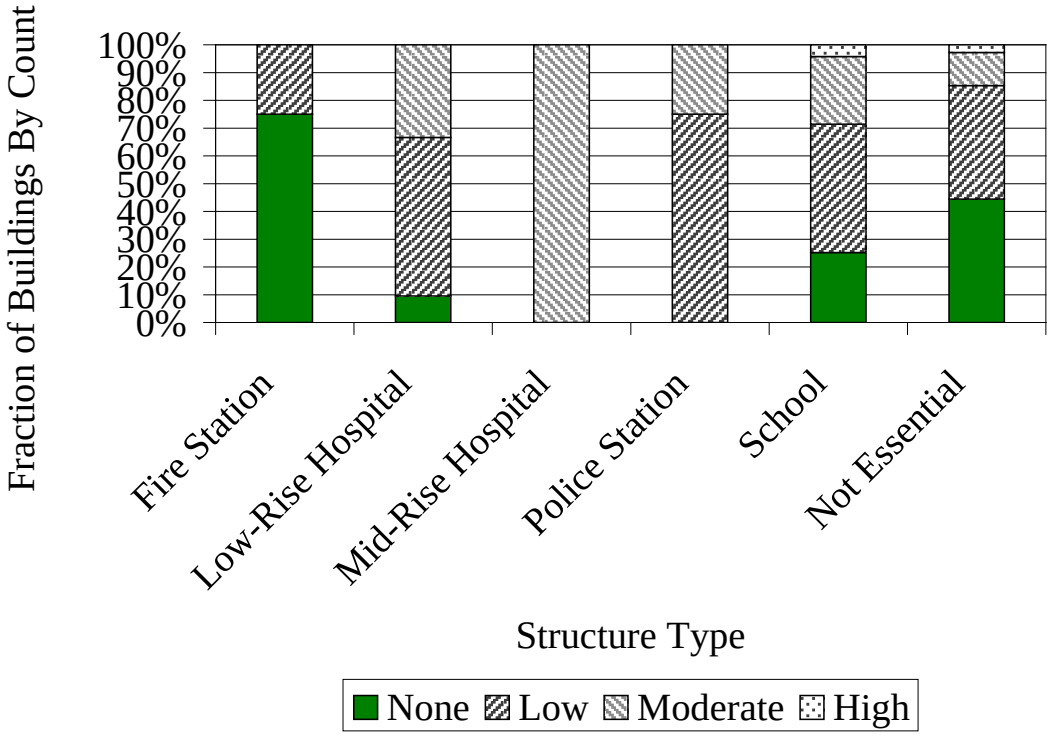

Figure 109. Optimum Retrofit for Weighting Scheme Case 1, Sorted By Essential Facility Class (Risk-Seeking Decision-Maker)

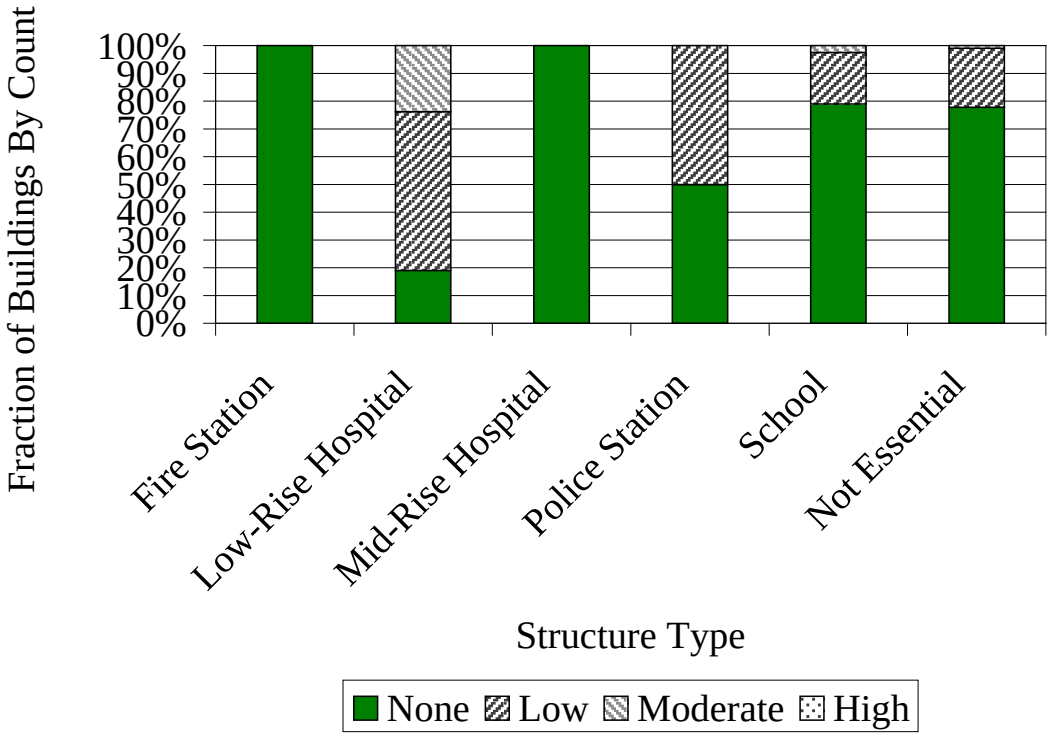

Figure 110. Optimum Retrofit for Weighting Scheme Case 2, Sorted By Essential Facility Class (Risk-Seeking Decision-Maker)

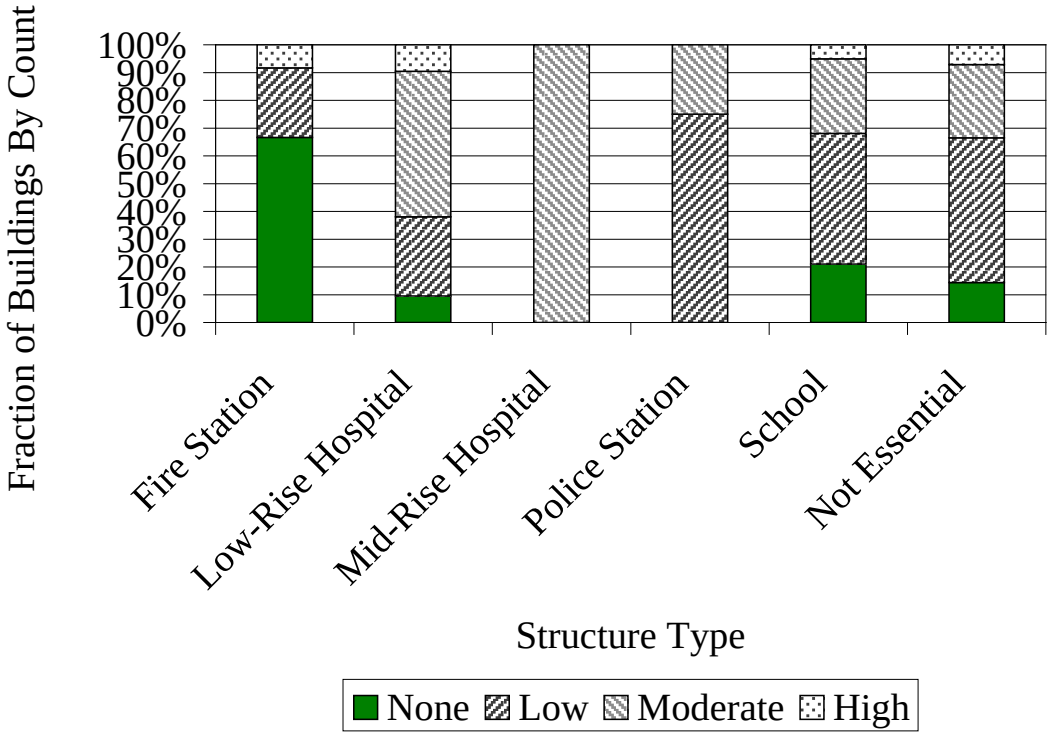

Figure 111. Optimum Retrofit for Weighting Scheme Case 3, Sorted By Essential Facility Class (Risk-Seeking Decision-Maker)

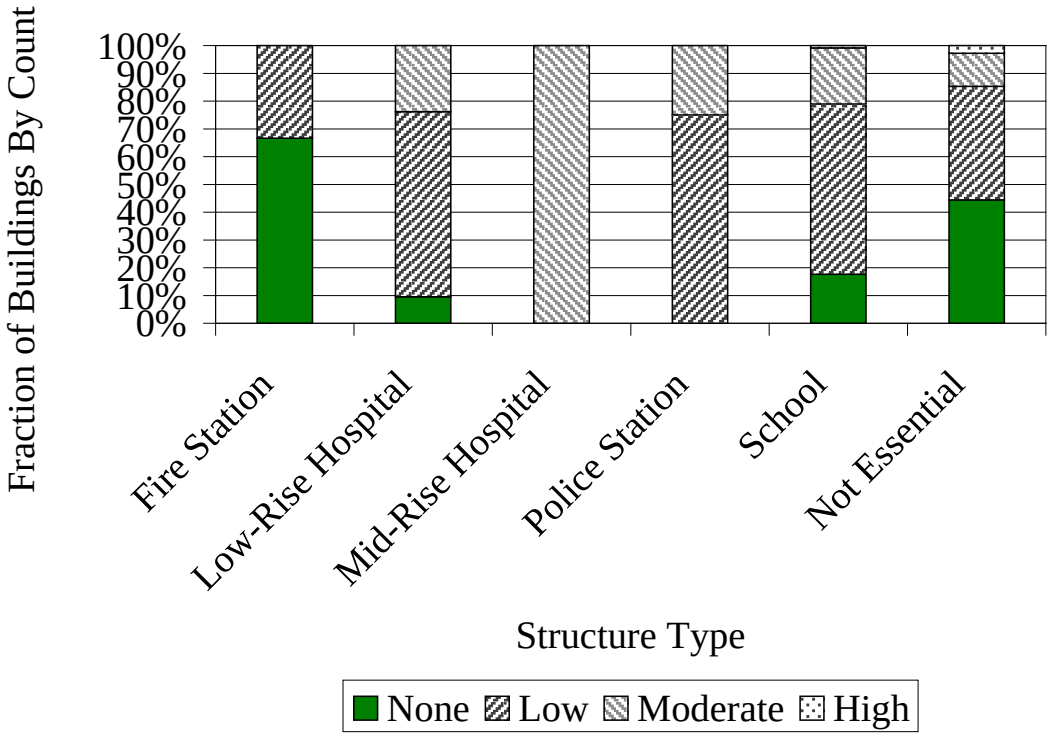

Figure 112. Optimum Retrofit for Weighting Scheme Case 4, Sorted By Essential Facility Class (Risk-Seeking Decision-Maker)

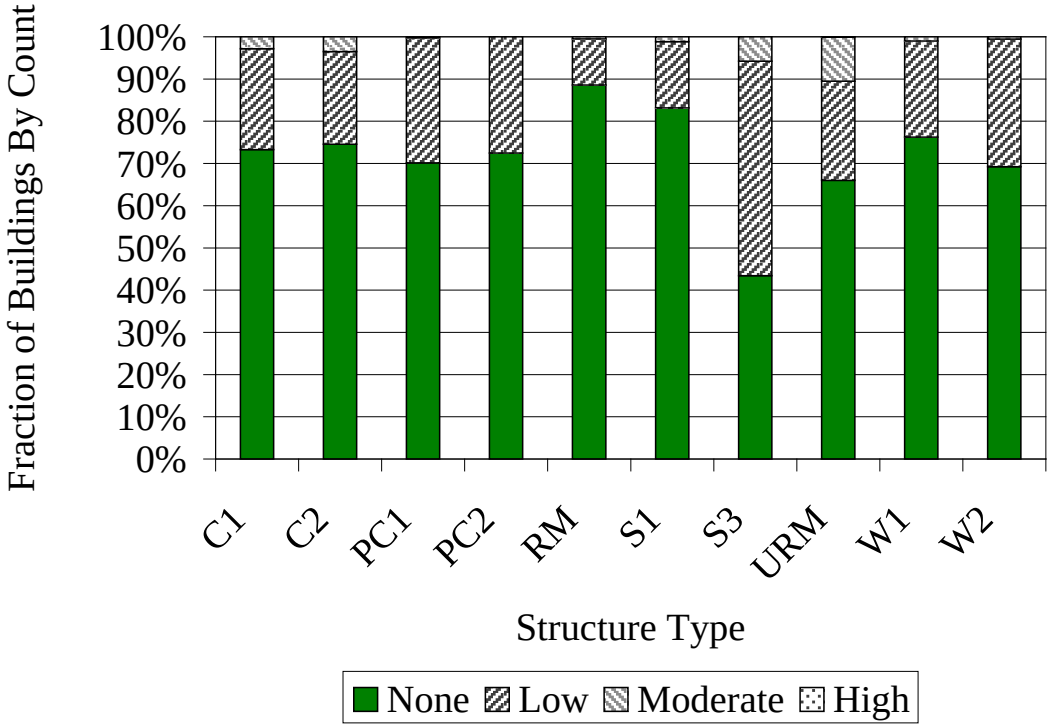

Figure 113. Optimum Retrofit for Weighting Scheme Case 1, Sorted By Structure Type (Risk-Averse Decision-Maker)

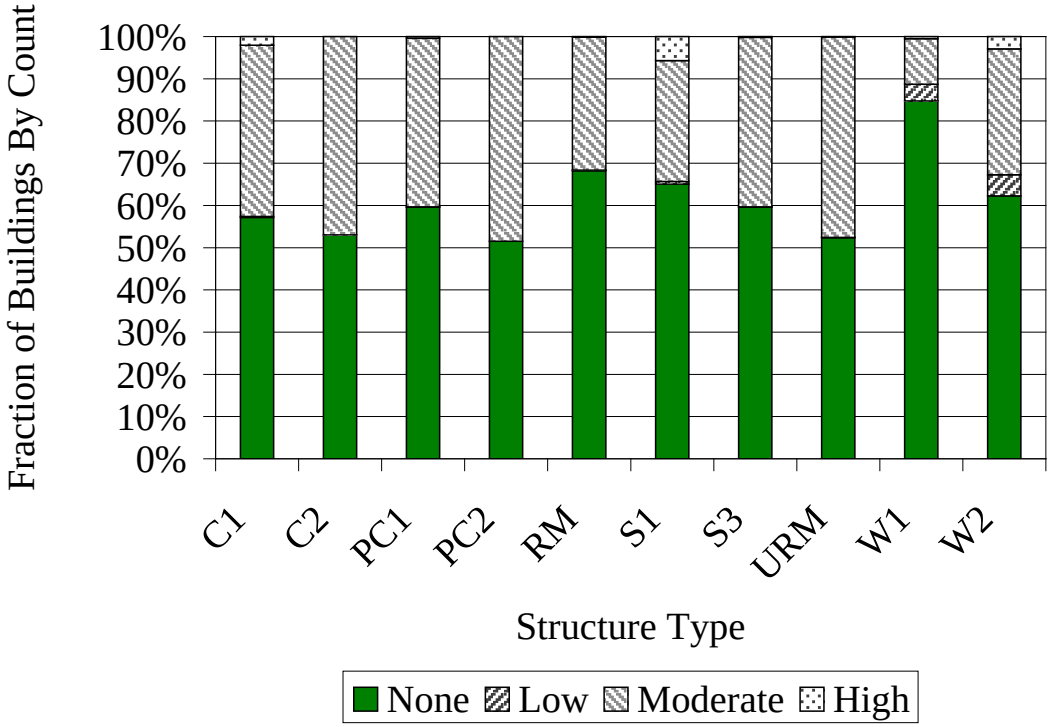

Figure 114. Optimum Retrofit for Weighting Scheme Case 2, Sorted By Structure Type (Risk-Averse Decision-Maker)

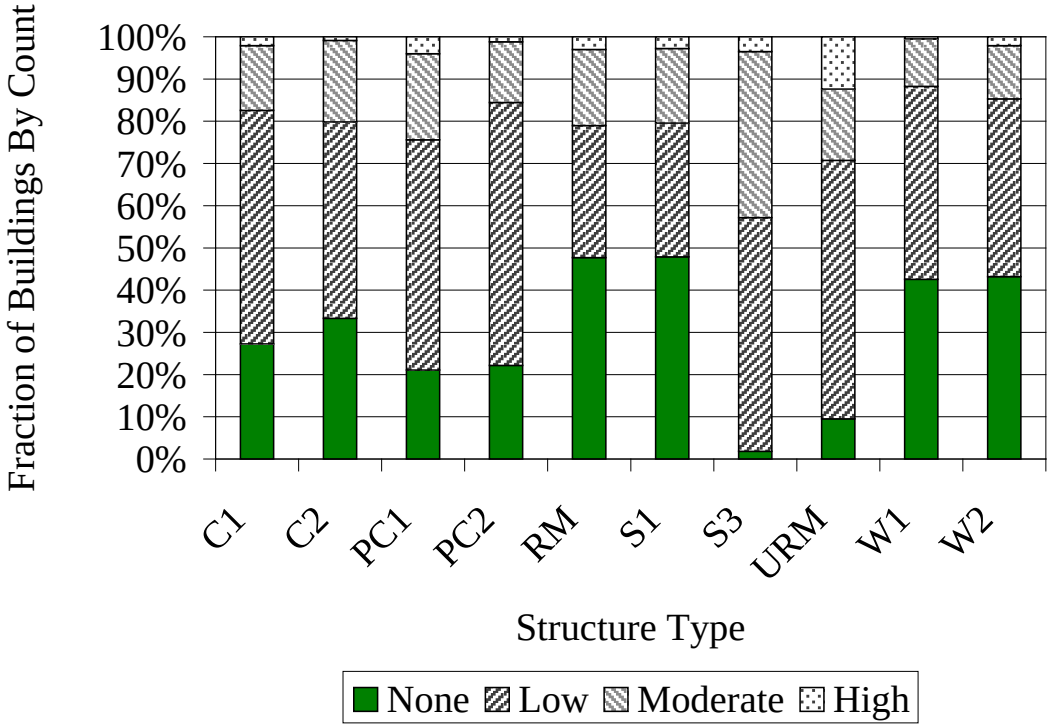

Figure 115. Optimum Retrofit for Weighting Scheme Case 3, Sorted By Structure Type (Risk-Averse Decision-Maker)

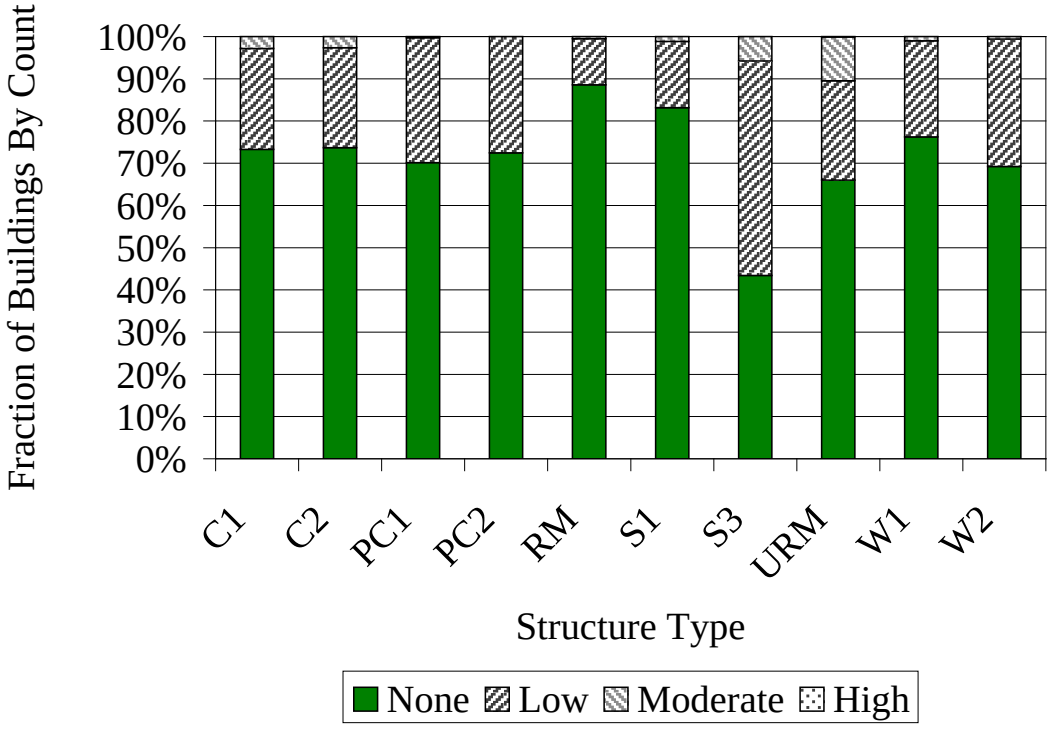

Figure 116. Optimum Retrofit for Weighting Scheme Case 4, Sorted By Structure Type (Risk-Averse Decision-Maker)

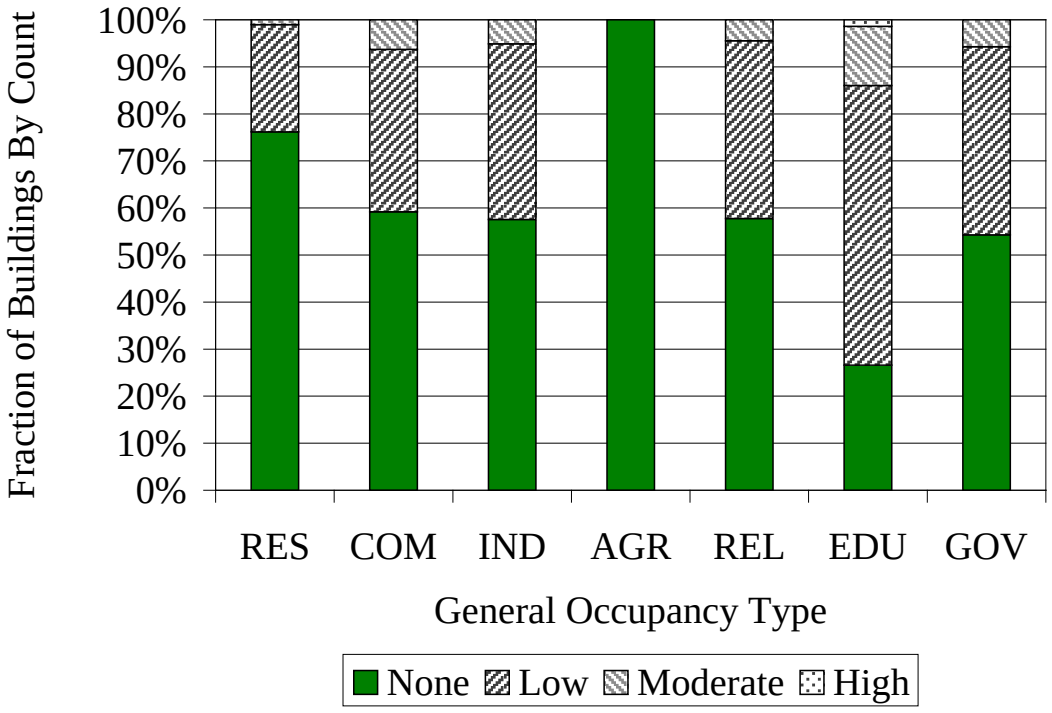

Figure 117. Optimum Retrofit for Weighting Scheme Case 1, Sorted By Occupancy Type (Risk-Averse Decision-Maker)

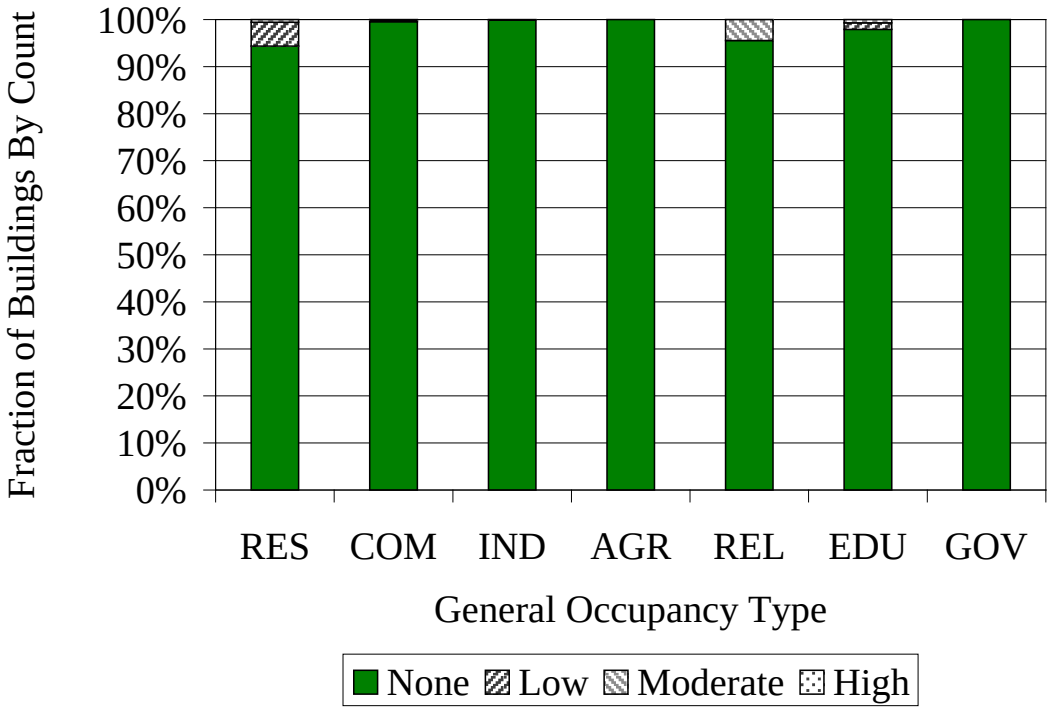

Figure 118. Optimum Retrofit for Weighting Scheme Case 2, Sorted By Occupancy Type (Risk-Averse Decision-Maker)

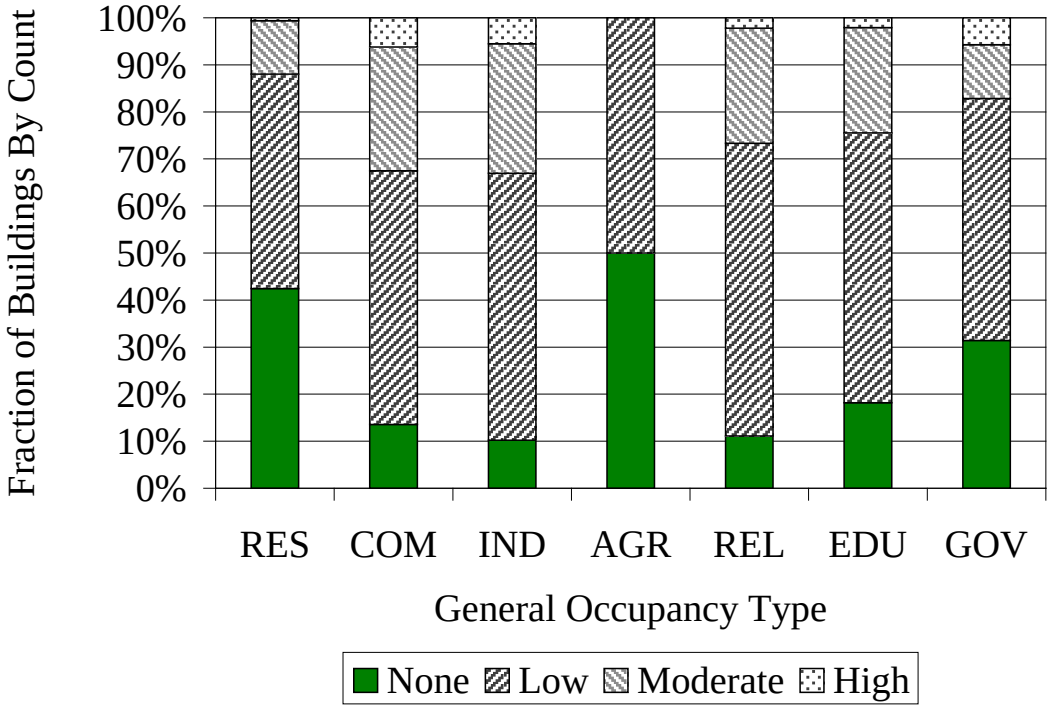

Figure 119. Optimum Retrofit for Weighting Scheme Case 3, Sorted By Occupancy Type (Risk-Averse Decision-Maker)

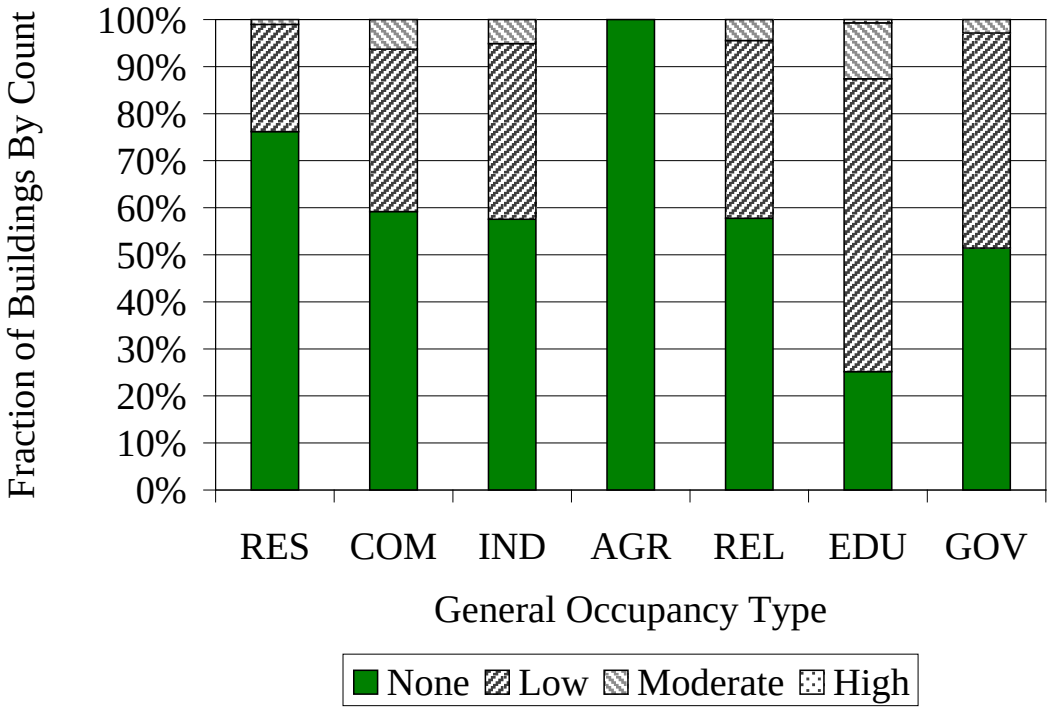

Figure 120. Optimum Retrofit for Weighting Scheme Case 4, Sorted By Occupancy Type (Risk-Averse Decision-Maker)

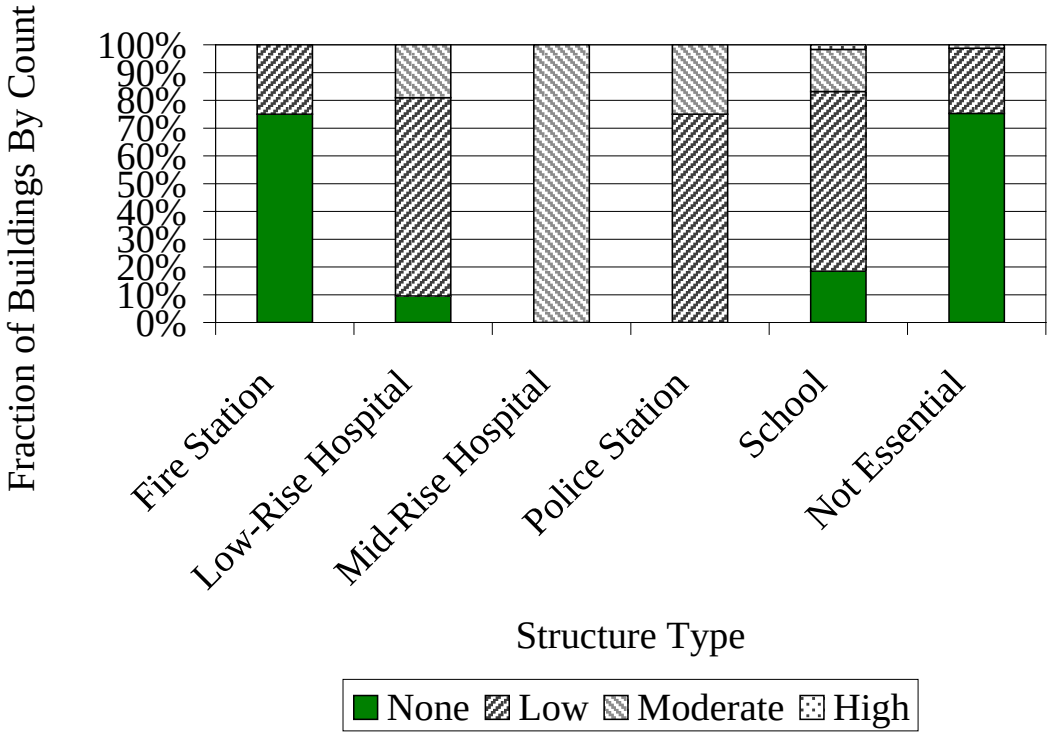

Figure 121. Optimum Retrofit for Weighting Scheme Case 1, Sorted By Essential Facility Class (Risk-Averse Decision-Maker)

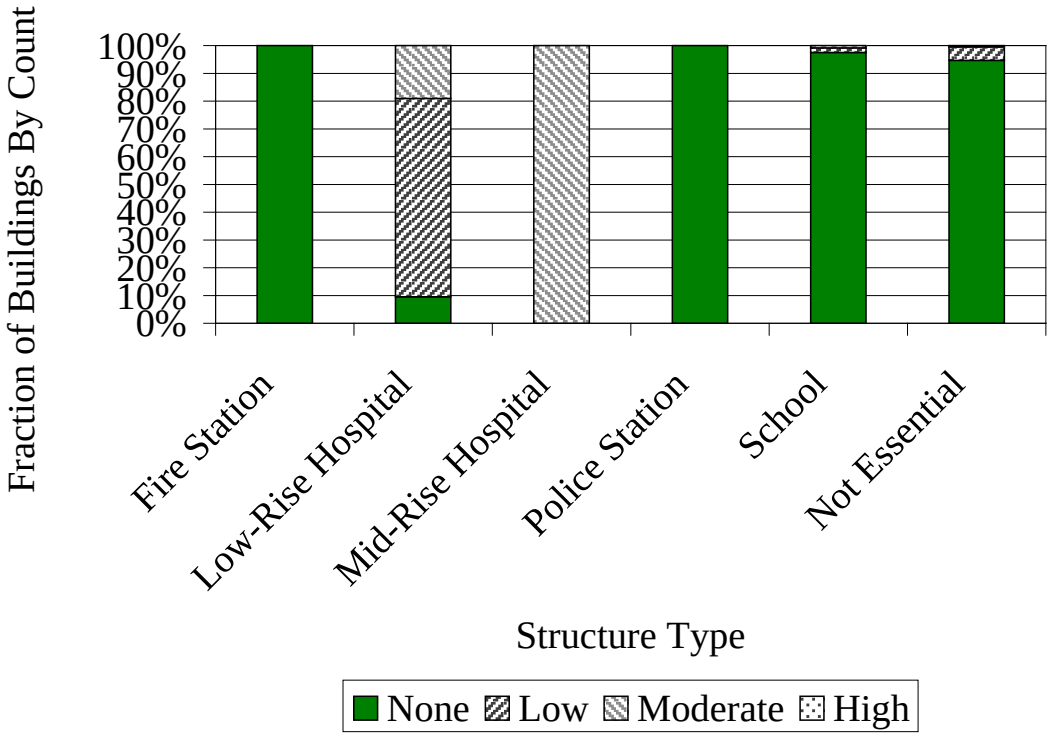

Figure 122. Optimum Retrofit for Weighting Scheme Case 2, Sorted By Essential Facility Class (Risk-Averse Decision-Maker)

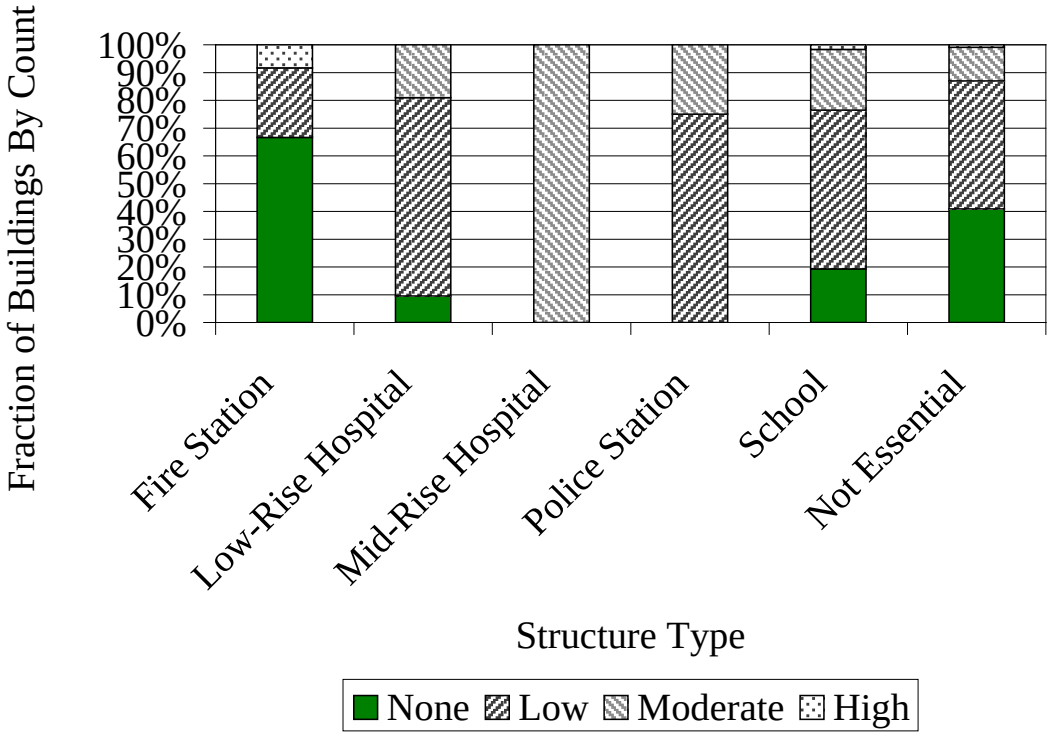

Figure 123. Optimum Retrofit for Weighting Scheme Case 3, Sorted By Essential Facility Class (Risk-Averse Decision-Maker)

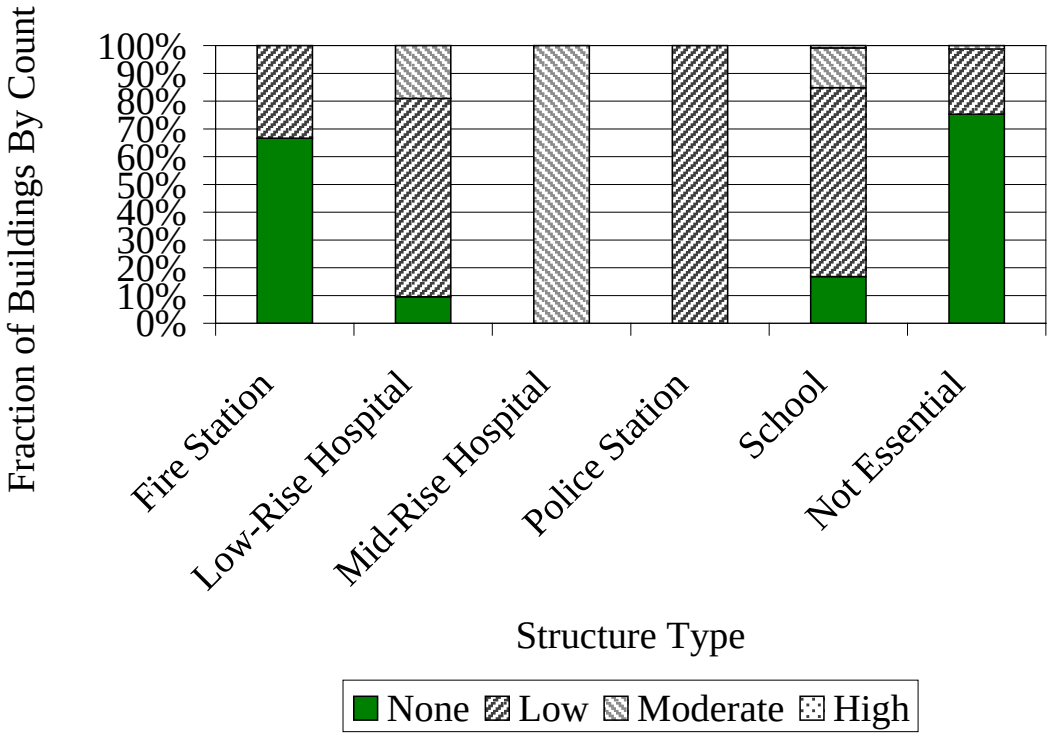

Figure 124. Optimum Retrofit for Weighting Scheme Case 4, Sorted By Essential Facility Class (Risk-Averse Decision-Maker)

8 UNCERTAINTY OF AGGREGATED RESULTS

The algorithms currently implemented in MAEViz propagate hazard uncertainty through the estimate of each loss measure, such as structural repair cost and acceleration-sensitive nonstructural repair cost. The general procedure for each loss measure typically includes estimation of damage to structures in terms of probabilities of damage states, and then correlation of physical damage to economic and social loss metrics. Damage state probabilities are estimated using Equation (1), which has the appearance of a closed form equation or a table look-up to evaluate the cumulative density function. However, when incorporating the adjustment shown in Equation (2) to account for hazard uncertainty, the result of Equation (1) represents an accumulation of damage estimates for all lognormally distributed hazard intensities. When aggregating the results of multiple loss measures, the individual measures are correlated through the hazard, but that correlation is not presently incorporated in MAEViz algorithms.

To investigate the effect of this characteristic of loss estimation uncertainty, structural, nonstructural, and contents repair costs were numerically evaluated and aggregated for four example hazard distributions and for each of the common low-rise structure types that constitute the clear majority of the building stock inventory, as described in previous sections. The calculations were performed assuming a distribution of replacement value consistent with the RES1 occupancy class. That is, as fractions of total structural and nonstructural replacement cost, 23.4%, 50%, 26.6%, and 50% of total structural and nonstructural value are assumed to be associated with structural, drift-sensitive nonstructural, acceleration-sensitive nonstructural, and contents components, respectively. Note that when a "total" damage factor is discussed, the factor is relative to total replacement cost including contents (i.e., for the example calculations, loss relative to 150% of structural and nonstructural value). Figure 125 through Figure 128 show mean and confidence bounds of damage factors for individual components of loss for a W1 structure. In the figures, a beta distribution was assumed to correspond to the damage factor distributions. Figure 129 then shows the aggregation of the data presented in the component plots.

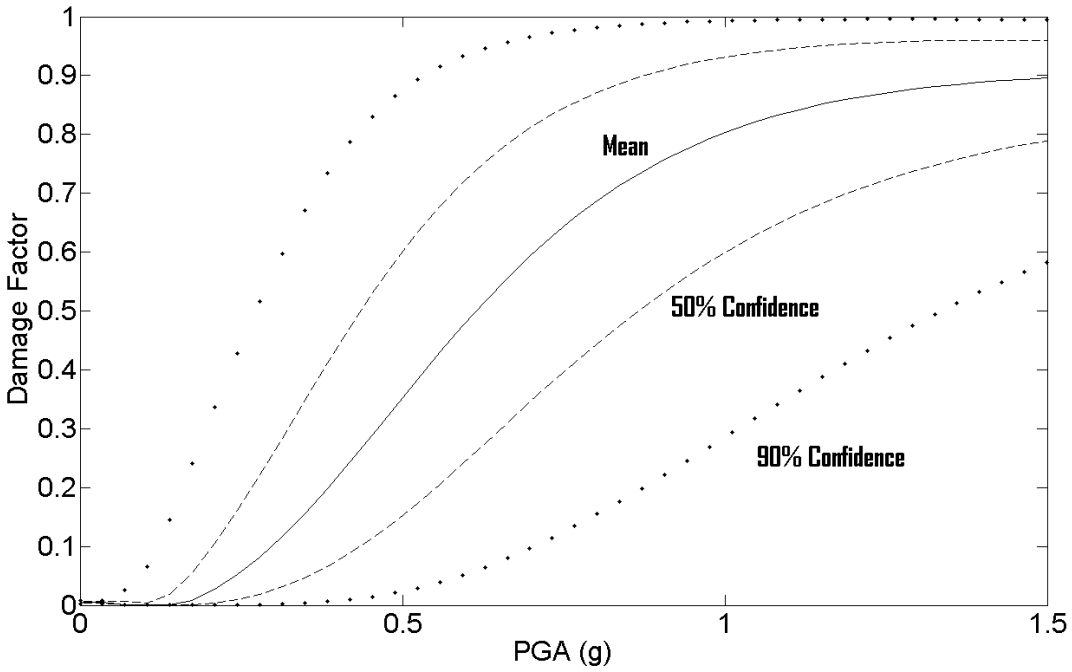

Figure 125. Structural Damage Factor versus PGA

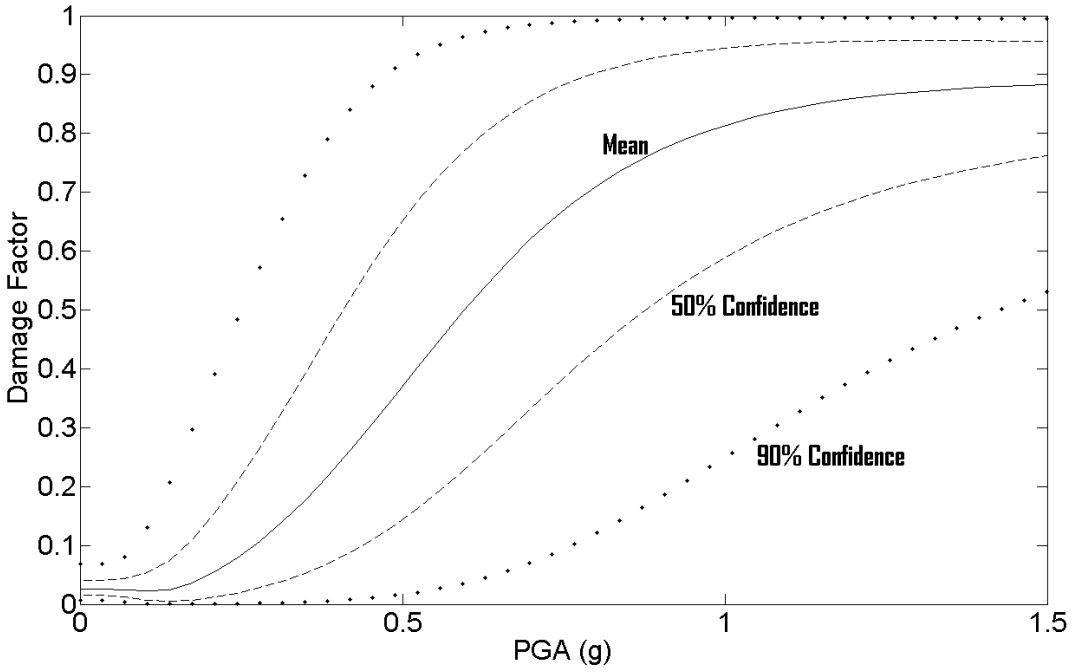

Figure 126. Drift-Sensitive Nonstructural Damage Factor versus PGA

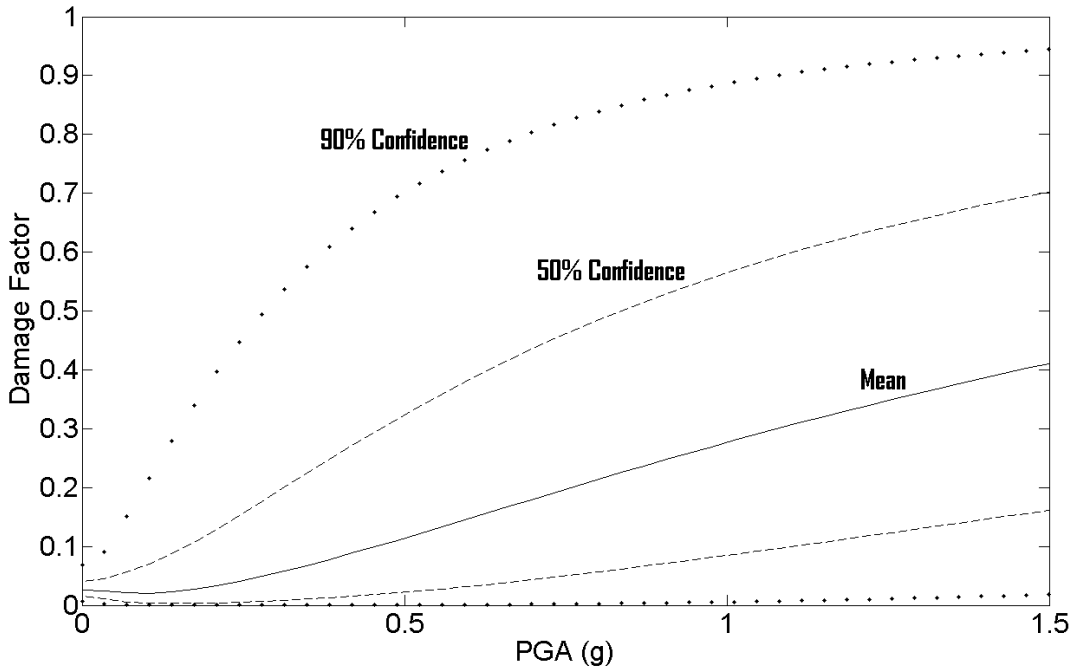

Figure 127. Acceleration-Sensitive Nonstructural Damage Factor versus PGA

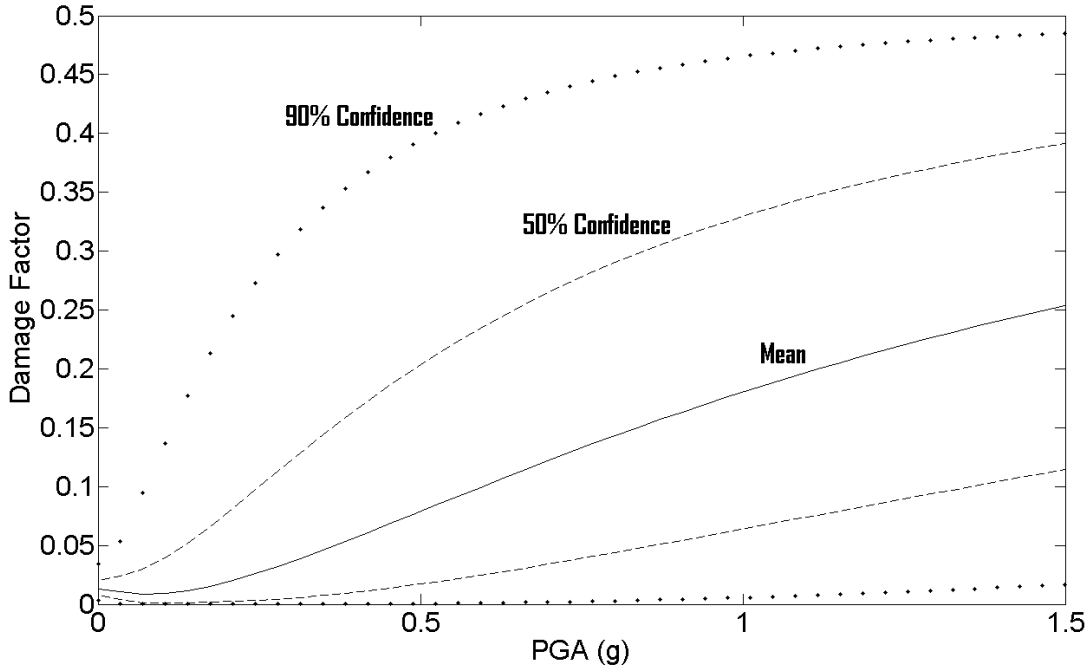

Figure 128. Contents Damage Factor versus PGA

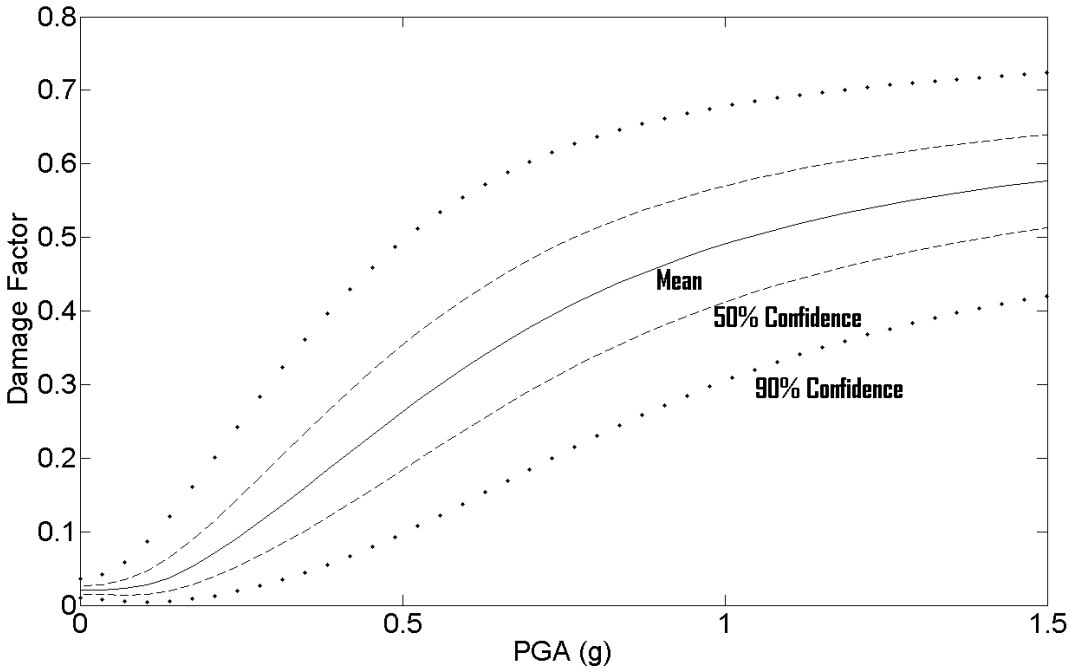

Figure 129. Total Aggregated Damage Factor versus PGA

In each of the plots, PGA is taken as a parameter of evaluation, rather than a random variable. Uncertainty at each value of PGA is dependent on the vulnerability functions and the damage factor distributions for each damage type. Figure 130 shows three representations of total aggregated damage factor distributions for a scenario based on a prediction of median and lognormal standard deviation of PGA equal to 0.43g and 0.674, respectively, consistent with USGS attenuation functions and NEHRP class D soil for a M_w 7.9 event at Blytheville, AR. The MAEViz Prediction curve represents the distribution that would be obtained from MAEViz by aggregating loss distributions from different damage types (e.g., structural, acceleration-sensitive non structural, etc.) while ignoring statistical dependence between component damages. The Numerical Integration curve is obtained by evaluating total damage factor distributions for a range of PGA hazard inputs and combining the probability of the hazard value with the damage factor probability distribution to arrive at a joint probability density in terms of hazard intensity and damage factor. The probability density values are then condensed through numerical integration for a range of damage factors, resulting in a probability distribution dependent only on damage factor. The last distribution is a fitted beta distribution representation of the Numerical Integration distribution, using the same mean and variance, and represents the distribution that a MAEViz user may be capable of generating if the only available data is mean and variance, rather than a full range probability densities for particular sampled damage factors, as was used to generate the Numerical Integration plot. Although the distributions appear to be clearly different, the mean of each prediction is similar, with the Numerical Integration and

Fitted Beta Distribution means deviating only -0.25% from the MAEViz result. However, the variance of the Numerical Integration and Fitted Beta Distribution results increased from 0.019 for the MAEViz prediction with uncorrelated hazard, to a value of 0.035, or an increase of 85%. The discrepancy in mean values is primarily a consequence of truncating part of the hazard distribution (rather than evaluating all hazard values up to a PGA of infinity), along with the relatively minor influence of applying a trapezoidal numerical integration rule to a nonlinear function.

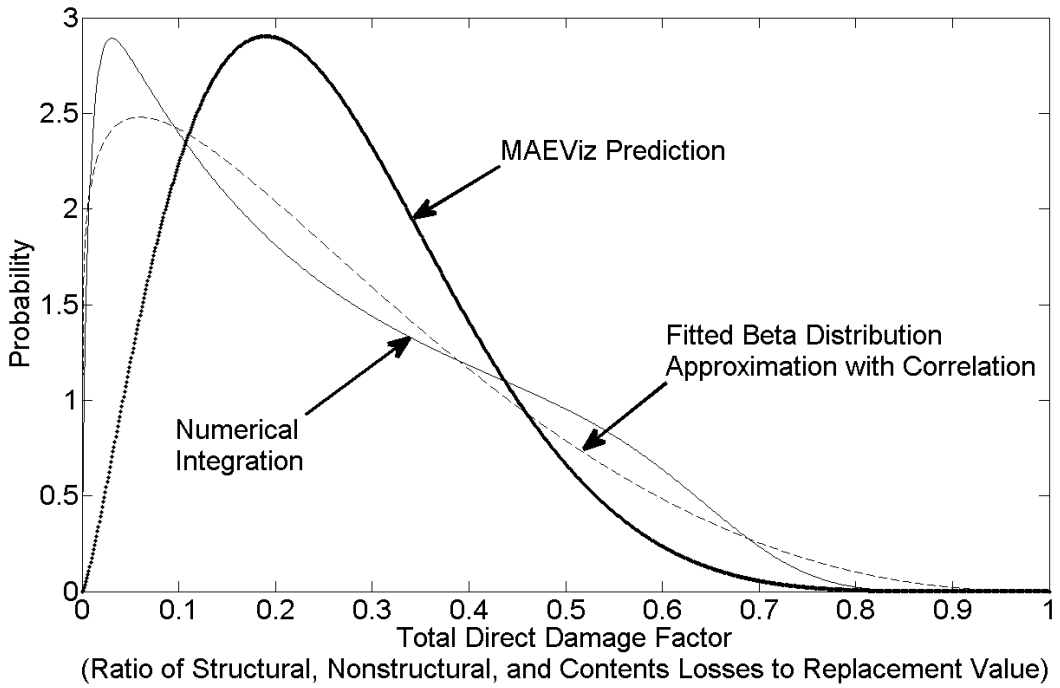

Figure 130. Damage Factor Probabilistic Distribution for Scenario with Median and Lognormal Standard Deviation of PGA = 0.43g and 0.674

The result obtained in Figure 130 is influenced by the selection of hazard parameters. Larger hazard uncertainty will naturally result in increased uncertainty in loss prediction. The effect on damage estimation uncertainty is not clear as a result of a continuous variation from zero at very small hazard medians (tending to certainty of negligible or very light damage) to some maximum at an intermediate value of hazard, and then reducing to zero again for very large hazard as damage prediction converges to certainty of complete damage. Larger hazard medians will also result in increased influence of damage factors for heavy damage, which tend to be more uncertain by their nature. The influence of these parameters is seen in Figure 131 through Figure 139, where mean losses and loss distributions are calculated for three methods and for four scenarios defined by distance and attenuations. The three methods were to first neglect hazard uncertainty entirely, then to use the MAEViz algorithm, and finally to apply numerical integration to account for hazard correlation between damage types. The scenarios are combinations of “Near” and “Far” cases, representing locations within Shelby County nearest to

(59.5 km) and farthest from (107 km) Blytheville, AR, and using either Rix-Fernandez attenuations for an Uplands soil profile or USGS attenuations modified for NEHRP Site Class D. All scenarios used a M_w 7.9 source event at Blytheville, AR.

Table 13. Scenario Definitions and Hazard Distribution Parameters

Attenuations	Soil	Distance (km)	Median PGA (g)	Lognormal Std Dev
Rix-Fernandez	Uplands	59.5	0.177	0.313
Rix-Fernandez	Uplands	107	0.154	0.331
USGS	NEHRP D	59.5	0.430	0.674
USGS	NEHRP D	107	0.273	0.719

All analyses were carried out using low-rise, pre-code structures, based on fragilities obtained by applying the parameterized fragility method (Jeong and Elnashai, 2007; Steelman and Hajjar, 2008). Figure 131 through Figure 134 are provided to illustrate the effect on mean damage factors associated with each structure type. The figures provide verification that the numerical integration solution and the MAEViz algorithm are in agreement, with respect to a shift in the mean damage factors expected when considering a hazard distribution. Figure 135 provides a legend for the following figures, Figure 136 through Figure 139, which show 90% confidence ranges of damage factor distributions (assumed to follow a beta distribution) for all structure types for each of the three methods and each of the four combinations of scenario parameters. The ranges are overlaid, as shown in Figure 135, to form a composite bar chart and allow visual comparison of the distributions resulting from all methods.

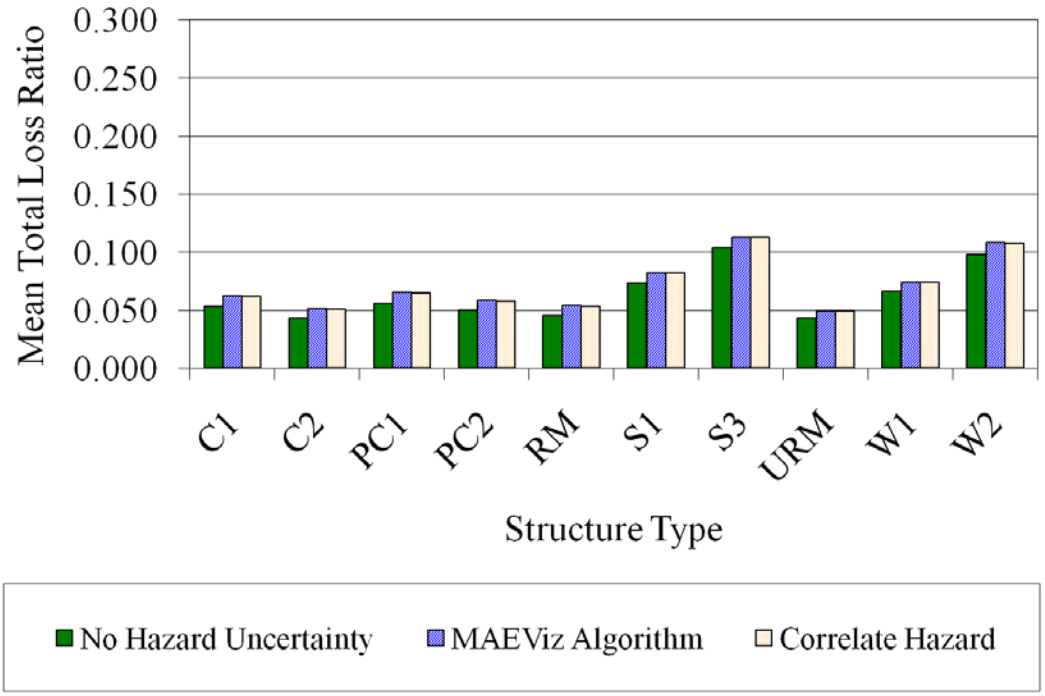

Figure 131. Mean Loss Ratio by Structure Type for Near/Rix-Fernandez Scenario

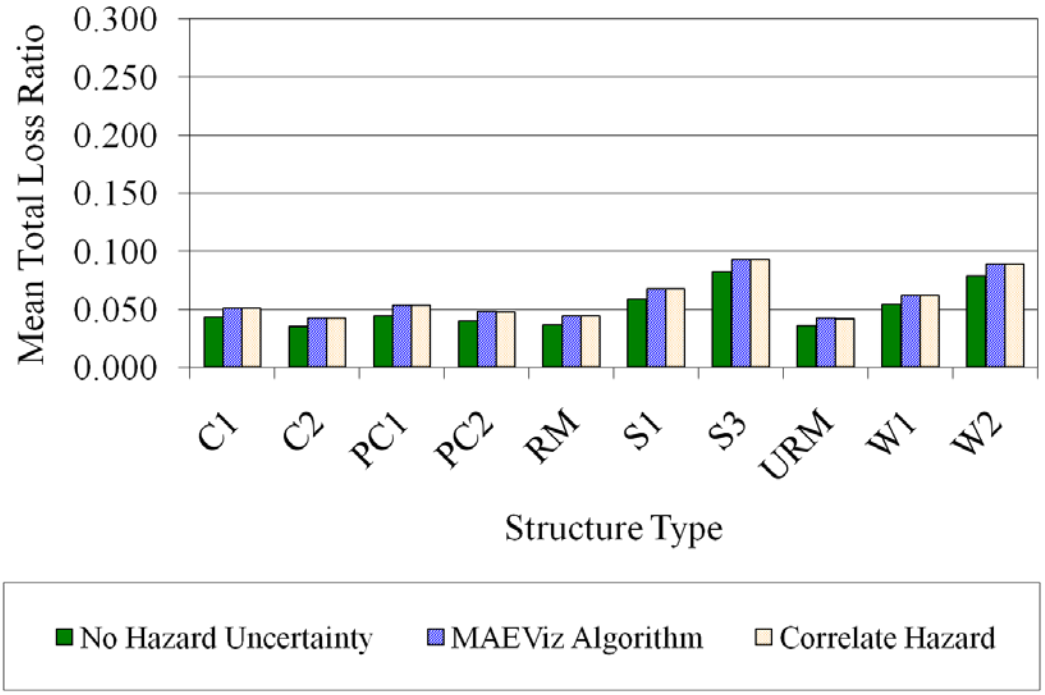

Figure 132. Mean Loss Ratio by Structure Type for Far/Rix-Fernandez Scenario

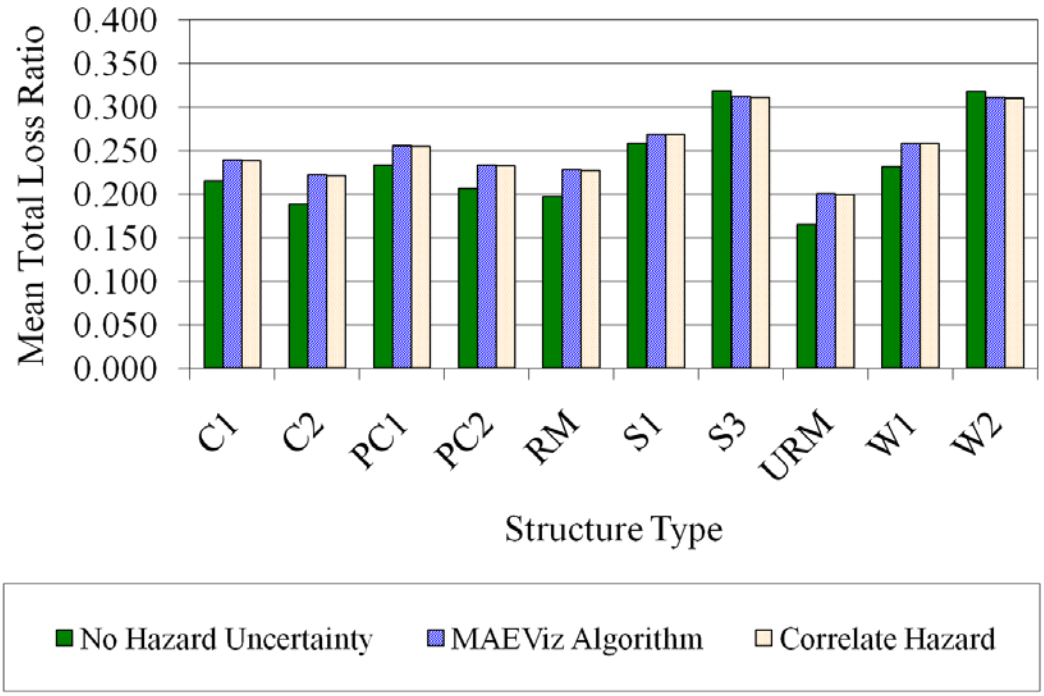

Figure 133. Mean Loss Ratio by Structure Type for Near/USGS-NEHRP Scenario

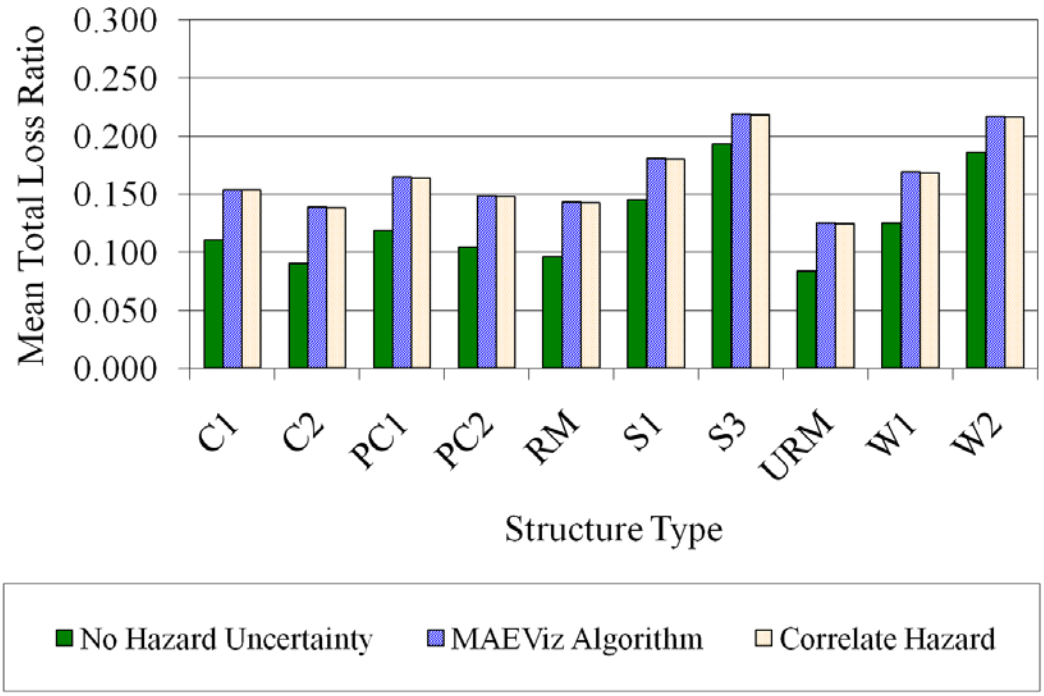

Figure 134. Mean Loss Ratio by Structure Type for Far/USGS-NEHRP Scenario

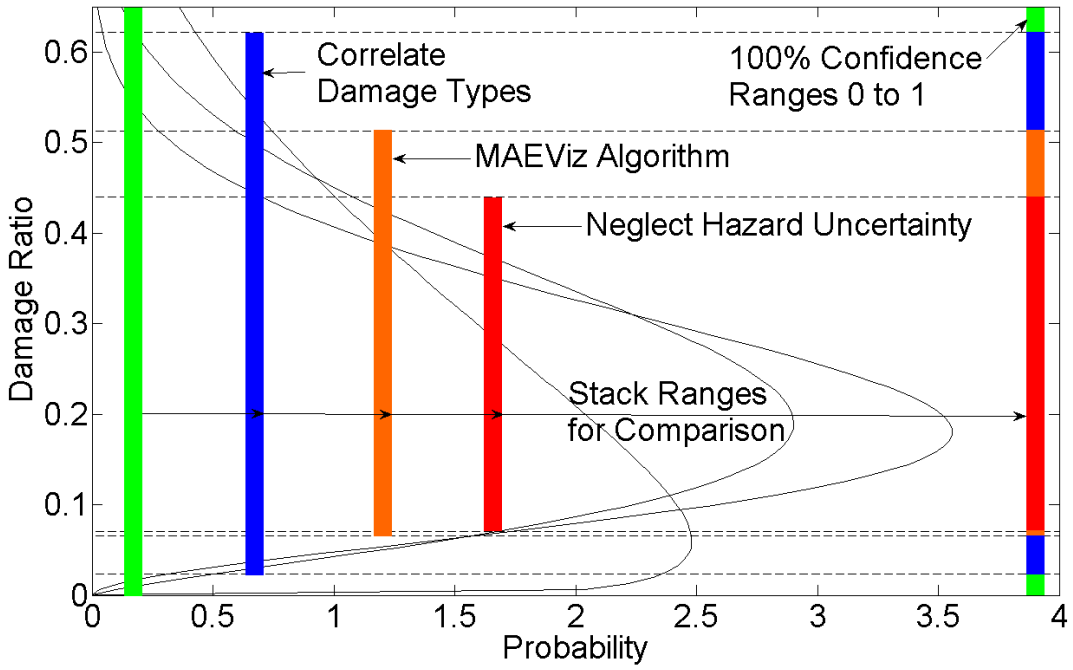

Figure 135. Legend for Composite Representations of 3 Methods of Loss Ratio 90% Confidence Range

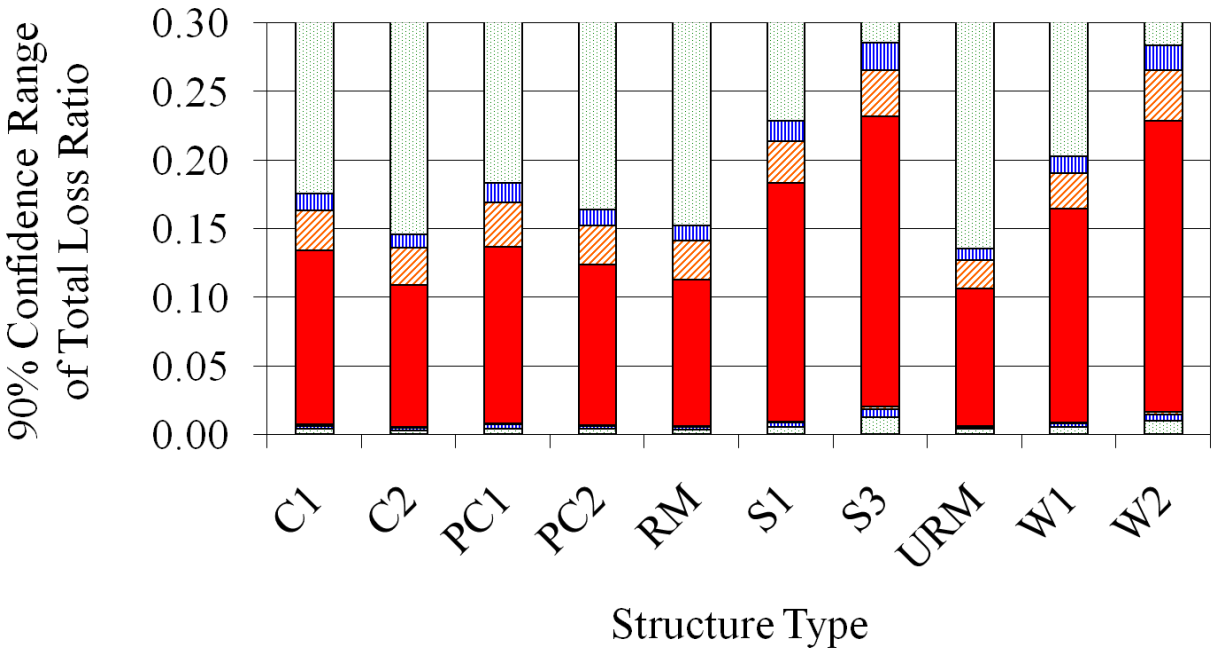

Figure 136. Composite Loss Ratio 90% Confidence Range by Structure Type for Near/Rix-Fernandez Scenario

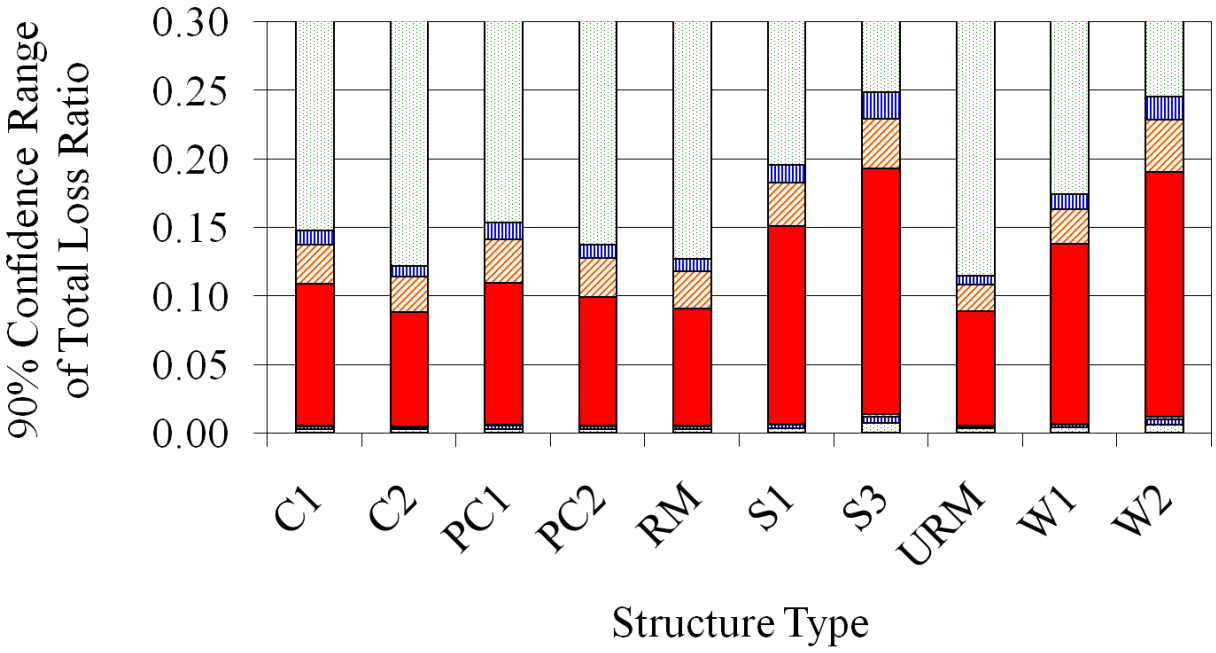

Figure 137. Composite Loss Ratio 90% Confidence Range by Structure Type for Far/Rix-Fernandez Scenario

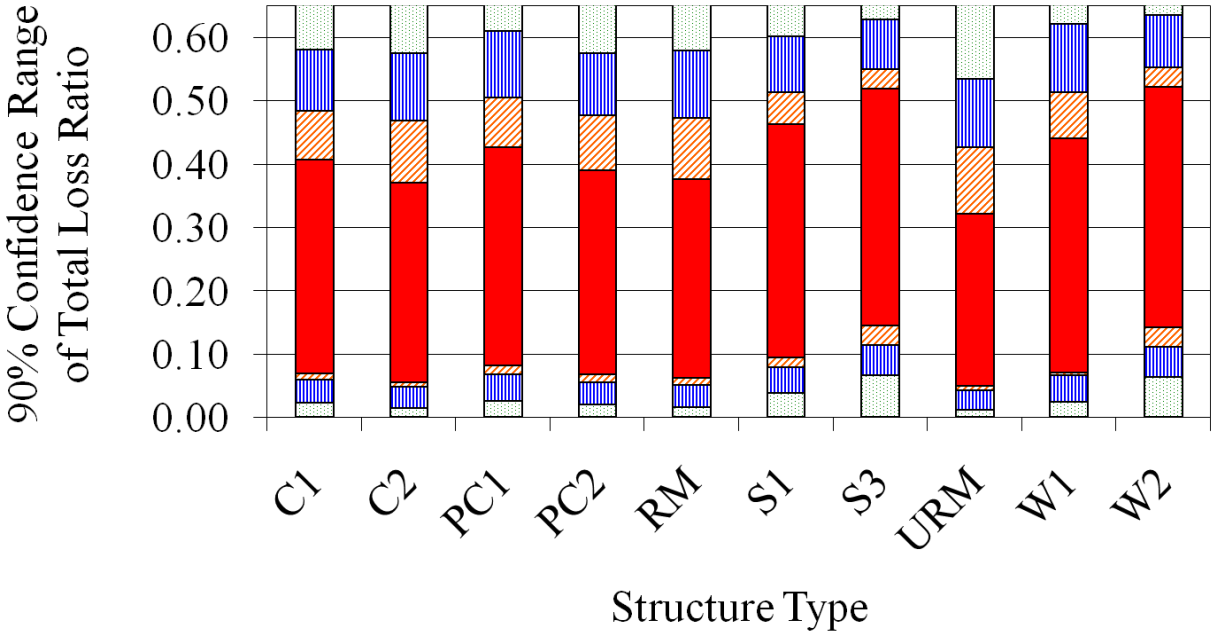

Figure 138. Composite Loss Ratio 90% Confidence Range by Structure Type for Near/USGS-NEHRP Scenario

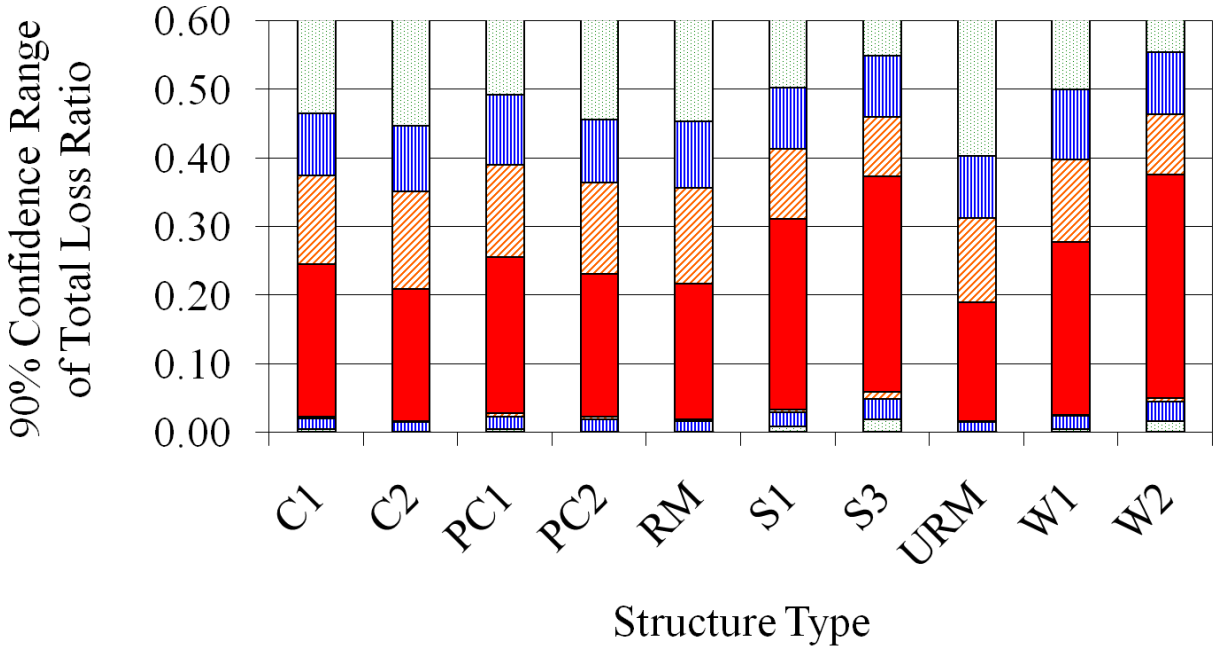

Figure 139. Composite Loss Ratio 90% Confidence Range by Structure Type for Far/USGS-NEHRP Scenario

The effect on the uncertainty of the loss prediction depends on the hazard distribution and the probabilistic parameters defining the vulnerability functions. A generalized analysis was performed in which the hazard median and lognormal standard deviation were varied, and the variance of the prediction was calculated for total economic loss both with and without consideration of correlation between damage types. The hazard parameters were varied relative to the fragility parameters associated with the threshold between Moderate and Heavy structural damage states. The range of consideration extended from a multiple of 0.1 to 2 times each of the fragility median and lognormal standard deviation parameters. The results of this analysis for a ratio of variance of total loss with and without considering correlation are shown in Figure 140 for a light wood frame structure (W1) structure with a single-family residential (RES1) occupancy. The occupancy must also be specified, since different occupancies will have different distributions of value among components. The data shown in Figure 140 are observed to approximately follow a bilinear pattern, with a primary dependence on the ratio of lognormal standard deviations. However, as hazard medians decrease, the bilinear assumption loses validity as the uncertainty tends rapidly to zero for small hazard medians. Therefore, this approach is not likely to be appealing for small hazard medians, but in such situations, damage will be likely to be light, with a small variance. For moderate to large hazard medians, a plane can be fitted to the data, as shown in Figure 141.

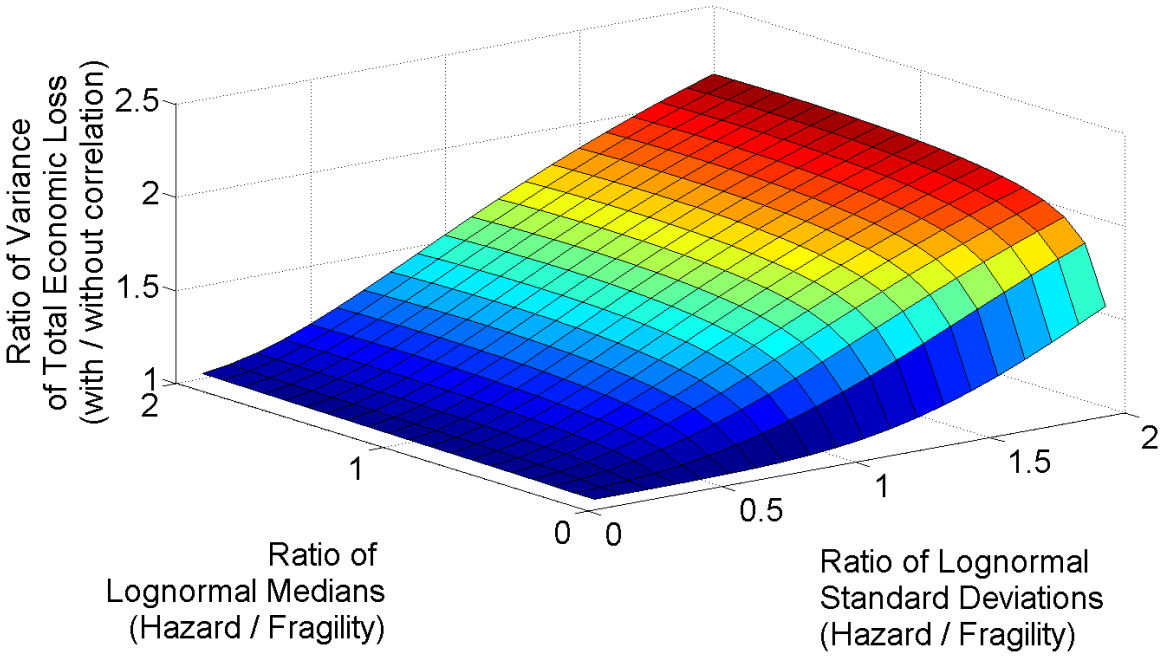

Figure 140. Surface of Ratio of Total Economic Loss Variance With and Without Considering Correlation of Component Damage

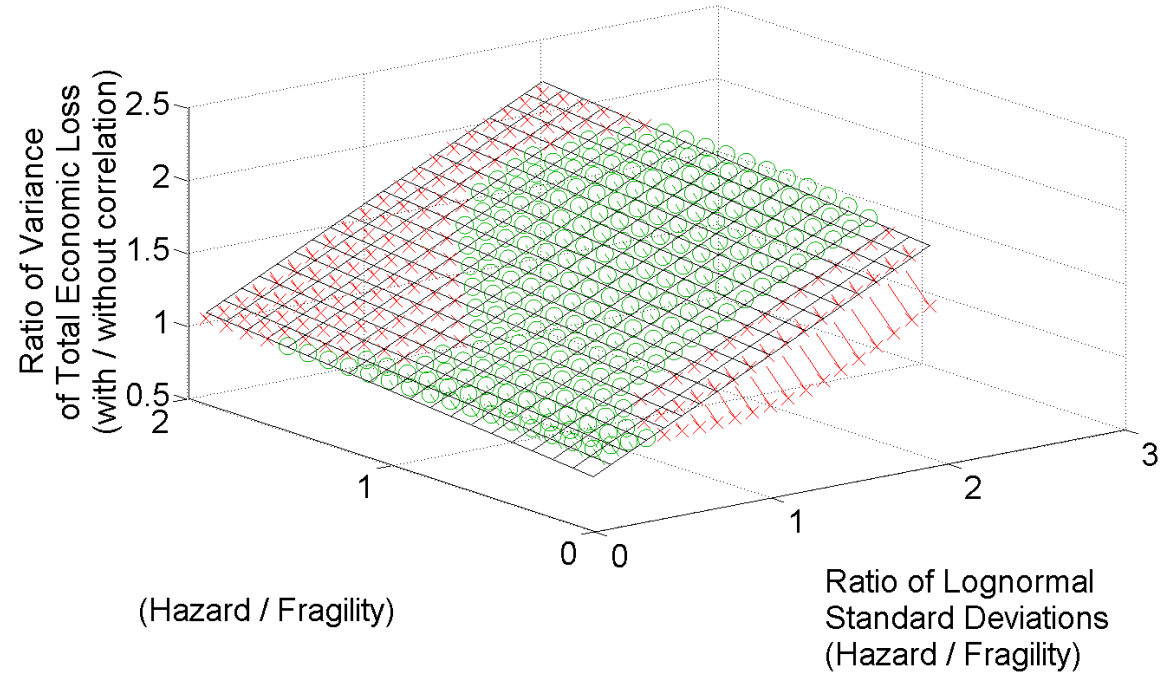

Figure 141. Planar Fit of Ratio of Total Economic Loss Variance With and Without Considering Correlation of Component Damage

The planar fit is shown with "o" markers for data lying above the fitted plane, and with "x" markers for data lying below the fitted plane. The square root of the sum of errors, normalized by the sample size of data points (20 PGA steps x 20 standard deviation steps = 400 samples) is 0.0063. The fit could be improved for moderate to large hazard medians by omitting points with median ratios less than 0.3. For the planar fit shown in Figure 141, the mathematical definition of the fit is given by

$$\frac{VAR_{CORR}}{VAR_{UNCORR}} = \gamma_1 \left(\frac{\overline{PGA}_{hazard}}{\overline{PGA}_{fragility}} \right) + \gamma_2 \left(\frac{\beta_{hazard}}{\beta_{fragility}} \right) + \gamma_3 \qquad (17)$$

Where

γ_1 = 0.1349 (determined by fitting)

γ_2 = 0.6013 (determined by fitting)

γ_3 = 0.7358 (determined by fitting)

$\overline{PGA}_{hazard}$ = median PGA of lognormal hazard distribution (g)

$\overline{PGA}_{fragility}$ = median PGA parameter for probability of at least heavy structural damage (g), 0.488 g in this example

β_{hazard} = lognormal standard deviation of PGA hazard distribution

$\beta_{fragility}$ = lognormal standard deviation PGA parameter for probability of at least heavy structural damage, 0.448 in this example

This fitted plane may now be used to estimate the increase in uncertainty for spatially disturbed individual structures without the need for performing numerical integration for each structure. The process should be repeated for other structure types and occupancy classes to maximize the reliability of the fit. When calculations were performed for other structure types and occupancy class combinations, the maximum and minimum ratios of γ_2 / γ_1 were 6.34 and 1.59, maximum and minimum values of γ_2 were 0.684 and 0.277, and maximum and minimum values of γ_1 were 0.213 and 0.051.

To investigate how this additional consideration may affect the results presented in previous sections, which only reported results obtained from MAEViz, and did not account for correlation of damage for individual structures, consider a single building, with a mean damage factor and variance taken equal to the average of the RES1 W1 structure results presented previously for "Near" and "Far" cases using Rix-Fernandez hazard distributions and USGS/NEHRP hazard distributions separately. For the Rix-Fernandez hazard distributions, the mean and variance of the total damage factor are 0.0677 and 0.0030, respectively. For the USGS/NEHRP hazard distributions, the values increase to 0.2133 and 0.0164, as a result of both increased median and dispersion parameters for the USGS/NEHRP distributions. For these example calculations, the

values are held constant for each building, and the number of buildings is scaled. Results of the analysis are shown in Figure 142. In order to provide a normalized measure for comparison of the different cases, coefficient of variation is calculated and plotted with respect to building count. As the number of buildings increases, the coefficient of variation decreases, resulting from the linear increase of both mean and variance of loss, and the relation between standard deviation and variance, as mentioned previously in the section on direct economic loss. Consideration of correlation of damage types within a structure is clearly of greatest importance to individual structures, or for a small set of structures. For the building stock in this study region, numbering approximately $3x10^5$, the impact on the aggregate result is minimal. However, for strategically critical structures, such as essential facilities, consideration of this aspect of uncertainty can have an appreciable influence.

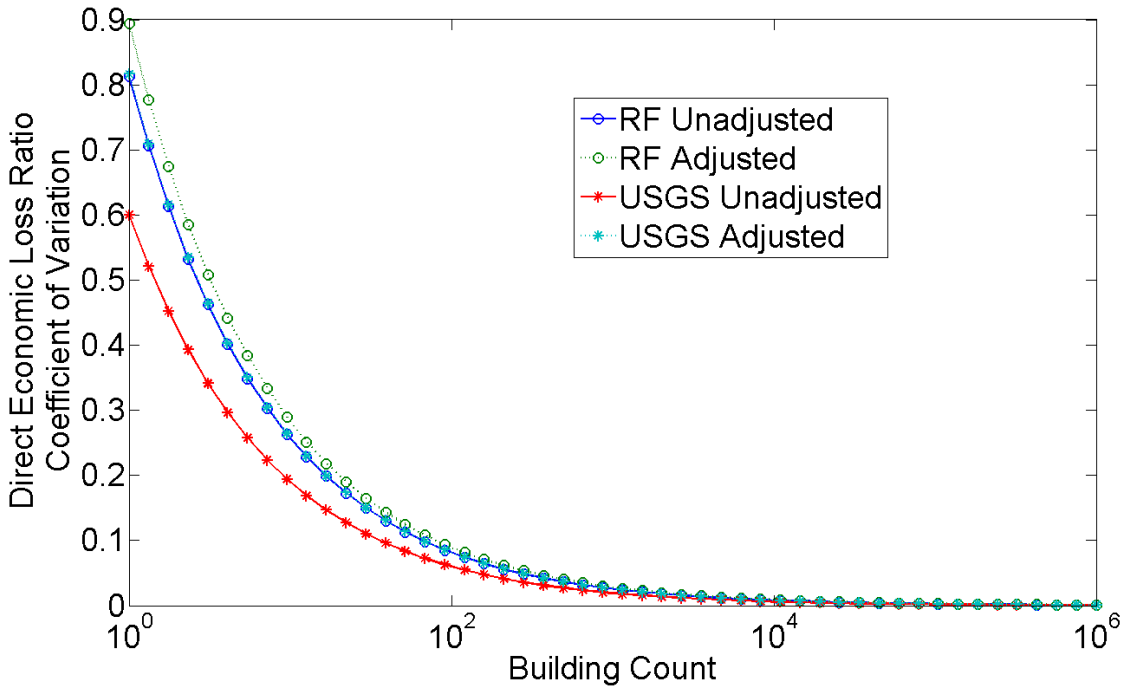

Figure 142. Effect of Correlation of Damage within a Structure on Coefficient of Variation of Direct Economic Loss Ratio with respect to Building Count

As one final consideration, it should be noted that ground motion correlation has thus far been ignored in the analysis. The most significant difficulty associated with such considerations for this scenario is that ground motion correlation is generally developed empirically, using ground motion records from multiple recording sites to account for the various unknowns inherent in the estimation of ground motion effects at any given location. Augmenting the calculations performed to obtain Figure 142 permits an investigation of direct economic loss

correlation arising from correlation in ground motions between spatially distributed sites for postulated correlations. The expression evaluated to generate the plots takes the form

$$c.o.v._{REGION} = \frac{\sqrt{n\ \bar{\gamma}\ VAR_{UNCORR} + \rho_{TDELR}\ n\ (n-1)\ \bar{\gamma}\ VAR_{UNCORR}}}{n\ \mu}$$

$$c.o.v._{REGION} = \frac{\sqrt{n\ + \rho_{TDELR}\ n\ (n-1)}}{n} \sqrt{\bar{\gamma}}\ c.o.v._{BUILDING} \quad (18)$$

Where

$c.o.v._{REGION}$ = coefficient of variation of regional direct economic loss prediction

n = number of buildings in study region

$\bar{\gamma}$ = multiplier equal to $VAR_{CORR} / VAR_{UNCORR}$ from Equation (17)

VAR_{UNCORR} = variance of total direct economic loss ratio neglecting correlation of damage types

μ = mean of total direct economic loss ratio

$c.o.v._{BUILDING}$ = coefficient of variation of direct economic loss prediction for an individual structure

ρ_{TDELR} = correlation of total direct economic loss ratio

To establish estimates of correlation coefficients, the results of investigations conducted by Goda and Hong (2008) using California and Chi-Chi records were reviewed. The data suggested that there was very weak correlation for the California records, dropping to only 2 or 3% for separation distances of greater than 10 km. For the Chi-Chi records, however, there was relatively strong correlation, with a value of about 50% near 20 km separation distance. Realistically, the correlation should and will vary from one building site pair to another, however, given the relatively small region size, and given that many of the buildings are clustered in the city of Memphis, rather than distributed uniformly throughout Shelby County, a value of 50% was selected for example calculations. The results are presented in Figure 143. For the example calculations, the correlation of economic loss between buildings is taken equal to the spatial correlation of the ground shaking intensity. In the extreme, with a maximum value of 100%, the coefficient of variation for the region does not change with the number of buildings. Even with 50%, the uncertainty of the result is far greater than the assumed statistically independent condition would indicate. The value of spatial ground motion correlation is clearly a key parameter in describing the uncertainty associated with the regional loss estimate. It should also be noted that if there is significant ground motion correlation, the importance of correlation of damage types for individual structures becomes more important as well. As the number of

structures in the study region tends to infinity, the correlation coefficient will be influenced equally by each consideration, as in Equation (19).

$$\lim_{n\to\infty} c.o.v._{REGION} = \sqrt{\rho_{TDELR}}\,\sqrt{\gamma}\; c.o.v._{BUILDING} \tag{19}$$

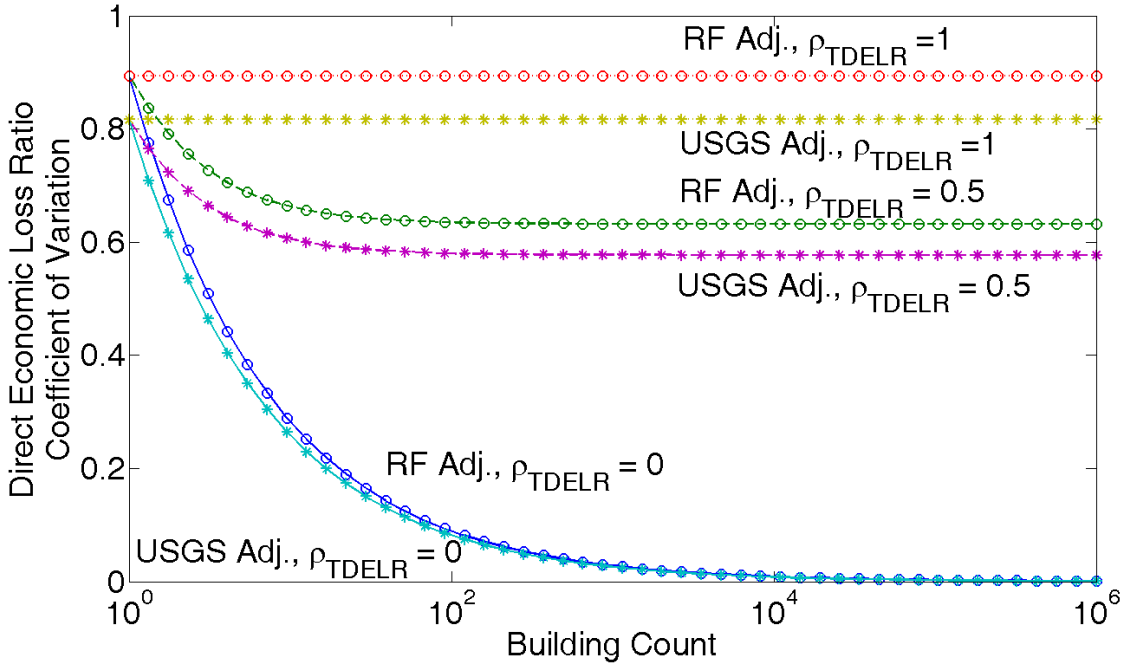

Figure 143. Effect of Correlation of Peak Ground Motion on Coefficient of Variation of Direct Economic Loss Ratio with respect to Building Count

9 CONCLUSION

This report summarizes a capstone scenario assessment of regional loss in Shelby County, Tennessee due to a scenario earthquake on the New Madrid seismic zone. The capstone scenario simulations illustrate the breadth and depth of research performed within the MAE Center to address the special considerations required for an area of low- to moderate-seismicity, and highlight the capabilities of MAEViz. Individual models were developed to represent the study region in great detail and to realistically assess both the expected effects of potential hazards as well as the ranges expected in the loss estimates. Shelby County is shown to be a region with substantial risk from future large magnitude events, which are expected to recur periodically after long periods of low seismic activity, based on the historical seismic behavior in the New Madrid Seismic Zone.

As part of this study, uncertainty was propagated systematically through the risk assessment. Uncertainty in ground shaking hazard intensity was brought into the vulnerability assessment of exposed assets by adjusting the dispersion parameters of the lognormal fragility curves. Uncertainty in the reliability of prediction of structure types was also considered by assigning alternate fragility sets to individual assets and conducting parallel analyses, and finally using a weighted combination of structure type results. The uncertainty in the hazard was found to be far more significant than the uncertainty in assignment of a structure type inventory attribute. This is likely due to the nature of the two uncertainties. When structure type is uncertain, that uncertainty will likely be applied throughout the study region, so that some buildings will experience an increase and others will experience a decrease in predicted loss, resulting little net change for the aggregated results of the study region. When hazard is uncertain, however, and especially in a case such as the capstone scenarios where the median hazard predicts relatively light damage, the uncertain hazard will act similarly on all structure types, resulting in either an approximately uniform increase or decrease in predicted losses. When the median hazard is less than a fragility median, as in this case, considering the full range of hazard increases the likelihood of exceeding the fragility threshold.

Uncertainty in direct costs of repair and replacement of assets associated with various damage states were combined with the uncertainties obtained from the fragility assessment to arrive at a comprehensive estimate of both expected loss and variation of loss for individual structures in the built environment. Regional loss assessments commonly provide “best estimates” for loss predictions as deterministic values, and this approach is not unreasonable for large numbers of buildings and bridges, as long as the underlying presumption of statistical independence of ground motion intensity is valid. To investigate the implications of this assumption, calculations were performed with respect to the effects of correlation of losses, both locally (i.e., types of losses within a particular inventory asset), and at a regional level. Both types of correlation are important considerations when attempting to capture the uncertainty of prediction for large quantities of assets. In particular, the uncertainty of the total loss prediction

is highly sensitive to correlation of ground motions across a region, especially with increasing study region size.

As in many of the recent studies performed using HAZUS, the majority of the economic impact on the region is expected to be driven by the cost of repair and replacement of building stock assets. Specifically, for the losses estimated in this study as a result of a M_w 7.9 event at Blytheville, direct loss due to repair and replacement was estimated to be $4.80 billion, out of a total of about $5.90 billion, or about 81% of the economic loss. Furthermore, as a consequence of both the inherent vulnerability and the large proportion of the building stock accounted for with wood frame structures, such structures are expected to dominate the direct economic loss for the region. These structures also are significant to dislocation estimation, where they account for about 27,000 of the projected 38,000 displaced persons, or about 10,000 out of 15,000 displaced households, since they account for the vast majority of housing units, and to casualty estimation, where they account for about 333 out of 984 injuries requiring hospitalization and about 28 out of 188 fatalities, since their aggregate square footage leads to the expectation that many people would be within wood frame buildings at the onset of a seismic event. In keeping with commonly observed patterns in other earthquakes, unreinforced masonry is found to have a high casualty rate when normalized by floor area. Tilt-up concrete buildings were also predicted to be similarly hazardous to occupants during an earthquake event with respect to fatalities (about 99% of the casualty rate when normalized by floor area), but not for hospitalizations (about 60% of the casualty rate when normalized by floor area, similar to most other structure types) when compared to unreinforced masonry.

As part of the decision support investigations to explore mitigation strategies, it is seen that although the predicted economic loss is lower for Shelby County, compared to the 1994 Northridge, CA event, when subjected to a seismic event comparable to a repeat of one of the main shocks of the 1811-1812 sequence, the losses relative to the economic exposure and population density of the study region are more severe. Furthermore, the impact on the study region should be expected to be compounded by surrounding damage, which was not addressed in this study. It should be noted that the estimates provided in this report are premised on the accuracy of hazard models, which expect soft soils to dampen ground shaking effects and effectively reduce ground failure hazard. Alternate models employed for seismic design in the region, promoted by the United States Geological Survey, tend to predict much larger ground shaking hazards. Unfortunately, it is only after a major event occurs that there will be any means of verifying which of the two model approaches is more representative of the seismic hazard in the region.

While decision-makers and disaster planners face daunting challenges in preparing for a repeat of a large magnitude earthquake, the research performed within the MAE Center and implemented in MAEViz provides a flexible methodology capable of supplying useful information for developing mitigation strategies to optimize efficiency, within the bounds of the

reliability of the input data, as well as constructing post-event response strategies to target the most severely impacted and vulnerable members of society.

10 REFERENCES

Abrams, D. P. and Shinozuka, M. (eds.) (1997). "Loss Assessment of Memphis Buildings," Technical Report No. NCEER-97-0018, National Center for Earthquake Engineering Research, State University of New York at Buffalo, Buffalo, New York.

Atkinson, G.M. and D. M. Boore (1995). "Ground Motion Relations for Eastern North America," *Bulletin of the Seismological Society of America*, Vol. 85, pp. 17-30.

Bai, J.-W. and Hueste, M. D. (2006) "Seismic Fragility Analysis for a Retrofitted Five-Story Reinforced Concrete Building," Draft Internal Report, Mid-America Earthquake Center Report, University of Illinois at Urbana-Champaign, Urbana, Illinois.

Bai, J. W., Hueste, M., and Gardoni, P. (2007). "Probabilistic Assessment of Structural Damage due to Earthquakes for Buildings in Mid-America," *Journal of Structural Engineering*, ASCE, submitted for publication.

Bal, I. E., Crowley, H., and Pinho, R. (2008) "Development of a Displacement-Based Earthquake Loss Assessment Method for Turkish Buildings," Proceedings of the 14th World Conference on Earthquake Engineering, Beijing, China, October 12-17, 2008, International Association of Earthquake Engineering, Beijing, China.

Ballantyne, D., Bartoletti, S., Chang, S., Graff, B., MacRae, G., Meszaros, J., Pearce, I., Pierepiekarz, M., Preuss, J., Stewart, M., Swanson, D., and Weaver, C. (2005). *Scenario for a Magnitude 6.7 Earthquake on the Seattle Fault*, Earthquake Engineering Research Institute, Oakland, California.

Borcherdt, R. D. (1994). "Estimates of Site-Dependent Response Spectra for Design (Methodology and Justification)," *Earthquake Spectra*, Vol. 10, pp. 617-653.

Central United States Earthquake Consortium (CUSEC) (1985). "An Assessment of Damage and Casualties for Six Cities in the Central United States Resulting from Earthquakes in the New Madrid Seismic Zone," Internal Report, Federal Emergency Management Agency, Washington, DC.

Central United States Earthquake Consortium (CUSEC) (2003). "Comparison Study of the 1985 CUSEC Six Cities Study Using HAZUS," Internal Report, Central United States Earthquake Consortium, Memphis, Tennessee.

Choi, E., DesRoches, R., and Nielson, B. (2004). "Seismic Fragility of Typical Bridges in Moderate Seismic Zones," *Engineering Structures*, Vol. 26, No. 2, pp. 187-199.

Crowley, H., Pinho, R., and Bommer, J. (2004). "A Probabilistic Displacement-based Vulnerability Assessment Procedure for Earthquake Loss Estimation," *Bulletin of Earthquake Engineering*, Vol. 2, pp. 173-219.

DesRoches, R., Leon, R. T., and Dyke, S. (2003). "Response Modification of Bridges," Internal Report, CD Release 03-08, Mid-America Earthquake Center, Urbana, Illinois.

DesRoches, R., Padgett, J. E., Elnashai, A. S., Kin, Y. S., and Reed, D. (2006) "MAE Center Transportation Test Bed," Proceedings of the 8th U.S. National Conference on Earthquake Engineering, San Francisco, California, April 18-22, 2006, Earthquake Engineering Research Institute, Oakland, California.

Dillingham, A. E. (1985). "The Influence of Risk Variable Definition on Value-of-Life Estimates," *Economic Inquiry*, Vol. 23, No. 2, pp. 277-294.

Dobry, R., Borcherdt, R. D., Crouse, C. B., Idriss, I. M., Joyner, W. B., Martin, G. R., Power, M. S., Rinne, E. E., and Seed, R. B. (2000). "New Site Coefficients and Site Classification System Used in Recent Building Seismic Code Provisions," *Earthquake Spectra*, Vol. 16, pp. 41-67.

Elnashai, A. S., and Hajjar, J. F. (2006). "Mid-America Earthquake (MAE) Center Program in Seismic Risk Management," Proceedings of the 8th U.S. National Conference on Earthquake Engineering, San Francisco, California, April 18-22, 2006, Earthquake Engineering Research Institute, Oakland, California.

Elnashai, A. S., Cleveland, L. J., Jefferson, T., and Harrald, J. (2008). "Impact of Earthquakes on the Central USA," Mid-America Earthquake Center, University of Illinois at Urbana-Champaign, Urbana, Illinois.

Ellingwood, B.R., (2006). "Wood and Steel Frame Fragility Parameters," School of Civil and Environmental Engineering, Georgia Institute of Technology, Atlanta, Georgia, personal communication.

Ellingwood, B.R., Rosowsky, D.V., and Pang, W.C. (2008). "Performance of Light-Frame Wood Residential Construction Subjected to Earthquakes in Regions of Moderate Seismicity," *Journal of Structural Engineering*, Vol. 134, No. 8, pp. 1353-1363.

Erberik, M. A., and Elnashai, A. S. (2006). "Loss Estimation Analysis of Flat-Slab Structures," *Natural Hazards Review*, Vol. 7, No. 1, pp. 26-37.

Erdik, M., Cagnan, Z., Zulfikar, C., Sesetyan, K., Demircioglu, M.B., Durukal, E., and Kariptas, C. (2008) "Development of Rapid Earthquake Loss Assessment Methodologies for Euro-Med Region," Proceedings of the 14th World Conference on Earthquake Engineering, Beijing, China, October 12-17, 2008, International Association of Earthquake Engineering, Beijing, China.

Federal Emergency Management Agency (FEMA) (1994). "FEMA-156, Typical Costs for Seismic Rehabilitation of Existing Buildings, Second Edition. Volume 1 – Summary," Federal Emergency Management Agency, Washington, D.C.

Federal Emergency Management Agency (FEMA) (1995). “FEMA-157, Typical Costs for Seismic Rehabilitation of Existing Buildings, Second Edition. Volume 2 – Supporting Documentation,” Federal Emergency Management Agency, Washington, D.C.

Federal Emergency Management Agency (FEMA) (2001). “HAZUS99 SR2 Technical Manual,” Federal Emergency Management Agency, Washington, D.C.

Federal Emergency Management Agency (FEMA) (2005). “HAZUS-MH MR1 Users and Technical Manual,” Federal Emergency Management Agency, Washington, D.C.

Federal Emergency Management Agency (FEMA) (2006). “HAZUS-MH MR2 Users and Technical Manual,” Federal Emergency Management Agency, Washington, D.C.

Fernandez, J. A. (2007). “Numerical Simulation of Earthquake Ground Motions in the Upper Mississippi Embayment,” Ph.D. Dissertation, School of Civil and Environmental Engineering, Georgia Institute of Technology, Atlanta, Georgia.

Fernandez, J.A. and Rix, G.J. (2006). "Soil Attenuation Relationships and Seismic Hazard Analyses in the Upper Mississippi Embayment". Proceedings of the 8th U.S. National Conference on Earthquake Engineering, San Francisco, California, April 18-22, 2006, Earthquake Engineering Research Institute, Oakland, California.

Frankel, A., C. Mueller, T. Barnhard, D. Perkins, E. Leyendecker, N. Dickman, S. Hanson, and M. Hopper (1996). “National Seismic-Hazard Maps: Documentation June 1996,” *U.S. Geological Survey, Open-file Report 96-532*, U.S. Geological Survey, Denver, Colorado.

French, S. P., and Muthukumar, S. (2006). “Memphis Building Stock Inventory Shapefiles and Databases, Version 4,” Center for Geographic Information Systems, Georgia Institute of Technology, Atlanta, Georgia, personal communication.

French, S. P., and Muthukumar, S. (2006). “Advanced Technologies for Earthquake Risk Inventories,” *Journal of Earthquake Engineering*, Vol. 10, No. 2, pp. 207-236.

Goda, K. and Hong, H. P. (2008). “Spatial Correlation of Peak Ground Motions and Response Spectra,” *Bulletin of the Seismological Society of America*, Vol. 98, No. 1, pp. 354-365.

Green, T., and Feser, E. (2007) “Business Interruption Loss Modeling by a Modified HAZUS Approach,” Department of Urban and Regional Planning, University of Illinois at Urbana-Champaign, Urbana, Illinois, personal communication.

Green, T., and Feser, E. (2007) “Business Inventory Loss Modeling by a Modified HAZUS approach,” University of Illinois at Urbana-Champaign, Urbana, Illinois, personal communication.

Hahn, R. W. (1996). *Risks, Costs, and Lives Saved: Getting Better Results from Regulation*, American Enterprise Institute, Washington, D.C.

Hajjar, J. F, and Elnashai, A. S. (2006). "Models for Seismic Vulnerability in the Mid-America Earthquake Center," Proceedings of the 8th U.S. National Conference on Earthquake Engineering, San Francisco, California, April 18-22, 2006, Earthquake Engineering Research Institute, Oakland, California.

Hueste, M. D., and Bai, J.-W. (2003). "Predicting the Seismic Performance of a RC Building in the Central U.S.," Proceedings of the Fifth US-Japan Workshop on Performance-Based Earthquake Engineering Methodology for Reinforced Concrete Building Structures, Moehle, J. P. and Kabeyasawa, T. (eds.), September 9-11, 2003, Hakone, Japan, Earthquake Research Institute, University of Tokyo, Tokyo, Japan.

Jeong, S. H., and Elnashai, A. S. (2007). "Probabilistic Fragility Analysis Parameterized by Fundamental Response Quantities," *Engineering Structures*, Vol. 29, pp. 1238-1251.

Karels, Terrance R. (2003). "Economic Considerations --- AFCI Replacements," Memorandum, United States Consumer Product Safety Commission, Washington, D.C.

Kueht, E., (2006). "Historical Adoption of Building and Seismic Codes in Memphis, TN," Texas A&M University, College Station, Texas, personal communication.

MAEviz (2008). "MAEviz Software," Mid-America Earthquake Center, University of Illinois at Urbana-Champaign, Urbana, Illinois, "http://maeviz.ce.uiuc.edu/software and tools/maeviz.html" February 12.

Memphis Light, Gas & Water (MLGW) (2005). "Memphis Cast-Iron Pipeline Database," Memphis, Tennessee, personal communication.

Mid-America Earthquake Center (2007). "Comprehensive Seismic Loss Modeling for the State of Illinois: Final Report," University of Illinois at Urbana-Champaign, Urbana, Illinois.

Miller, T. R. (1990). "The Plausible Range for the Value of Life – Red Herrings Among the Mackerel," *Journal of Forensic Economics*, Vol. 3, No. 3, pp. 17-29.

Myers, J. D. and Spencer, B. F. (2005). "Cyberinfrastructure in Support of Earthquake Loss Assessment: The MAEViz Cyberenvironment," Proceedings of the First International Workshop on An Earthquake Loss Estimation Program for Turkey, HAZTURK-2005, Istanbul, Turkey, December 1-2, 2005, Istanbul Technical University, Istanbul, Turkey.

National Institute of Building Sciences (NIBS) (1999). "Development of a Standardized Earthquake Loss Estimation Methodology," Technical Manual, Federal Emergency Management Agency, Washington, DC.

Padgett, J. E., (2006). "Unit Replacement Costs for Bridges in the Mid-America Earthquake Center Transportation Testbed (Charleston, SC)," School of Civil and Environmental Engineering, Georgia Institute of Technology, Atlanta, Georgia, personal communication.

Padgett, J. E., and DesRoches, R. (2007). "Bridge Functionality Relationships for Improved Seismic Risk Assessment of Transportation Networks," *Earthquake Spectra*, Vol 23, No. 1, pp. 115-130.

Park, J. (2004). "Development and Application of Probabilistic Decision Support Framework for Seismic Rehabilitation of Structural Systems," Ph.D. Thesis, School of Civil and Environmental Engineering, Georgia Institute of Technology, Atlanta, Georgia.

Peacock, W. (2007) "Displaced Household Algorithm 1: A Modified HAZUS Approach," Hazard Reduction and Recovery Center, Texas A&M University, College Station, Texas, personal communication.

Peacock, W. (2007) "Short Term Shelter Requirements," Hazard Reduction and Recovery Center, Texas A&M University, College Station, Texas, personal communication.

Peacock, W. (2007) "Social Vulnerability Algorithm," Hazard Reduction and Recovery Center, Texas A&M University, College Station, Texas, personal communication.

Pezeshk, S. (2005). "Comparative Analysis of HAZUS-MH Runs for Shelby County, TN and Tate County, MO," Internal Report, Department of Civil Engineering, University of Memphis, Memphis, Tennessee.

Pinho, R., Crowley, H., and Bommer, J. (2008) "Open-Source Software and Treatment of Epistemic Uncertainties in Earthquake Loss Modelling," Proceedings of the 14th World Conference on Earthquake Engineering, Beijing, China, October 12-17, 2008, International Association of Earthquake Engineering, Beijing, China.

Office of Americas/North America & Homeland Security Division (PMH) (2006). "Homeland Security Infrastructure Program (HSIP) GOLD Dataset," Department of Homeland Security, Washington, D.C.

Pruess, J. and Godfrey, J. (2006). "Guidelines for Developing an Earthquake Scenario," Earthquake Engineering Research Institute, Oakland, California.

Ramamoorthy, S.K., Gardoni, P., and Bracci, J.M. (2006) "Seismic Fragility and Confidence Bounds for Gravity Load Designed Reinforced Concrete Frame of Varying Height," *Journal of Structural Engineering*, Vol. 134, No. 4, pp. 639-650.

Reis, E., Comartin, C., King, S., and Chang, S. (2001). "HAZUS99-SR1 Validation Study," Federal Emergency Management Agency, Washington, D.C.

Silva, W., Gregor, N., and Darragh, R. (2003). "Development of Regional Hard Rock Attenuation Relations for Central and Eastern North America, Mid-Continent and Gulf Coast Areas," Pacific Engineering and Analysis, El Cerrito, California.

Spence, R., So, E., Cultrera, G., Ansal, A., Pitilakis, K., Costa, A.C., Tonuk, G., Argyroudis, S., Kakderi, K., and Sousa, M.L. (2008) "Earthquake Loss Estimation and Mitigation in Europe: A

Review and Comparison of Alternative Approaches," Proceedings of the 14th World Conference on Earthquake Engineering, Beijing, China, October 12-17, 2008, International Association of Earthquake Engineering, Beijing, China.

Spencer, B. F., Myers, J. D., and Yang, G. (2005). "MAEViz/NEESgrid and Applications Overview," Proceedings of the First International Workshop on An Earthquake Loss Estimation Program for Turkey, HAZTURK-2005, Istanbul, Turkey, December 1-2, 2005, Istanbul Technical University, Istanbul, Turkey.

Steelman, J., and Hajjar, J. (2008). "Systemic Validation of Consequence-Based Risk Management for Seismic Regional Losses," Mid-America Earthquake Center, University of Illinois at Urbana-Champaign, Urbana, Illinois.

Steelman, J., Song, J., and Hajjar, J. (2006). "Integrated Data Flow and Risk Aggregation for Consequence-Based Risk Management of Seismic Regional Losses," Internal Report, Mid-America Earthquake Center, University of Illinois at Urbana-Champaign, Urbana, Illinois.

Strasser, F., Stafford, P., Bommer, J., and Erdik, M. (2008) "State-of-the-art of European Earthquake Loss Estimation Software," Proceedings of the 14th World Conference on Earthquake Engineering, Beijing, China, October 12-17, 2008, International Association of Earthquake Engineering, Beijing, China.

Teramo, M., Crowley, H., Lopez, M., Pinho, R., Cultrera, G., Cirella, A., Cocco, M., Mai, M., and Teramo, A. (2008) "A Damage Scenario for the City of Messina, Italy, Using Displacement-Based Loss Assessment," Proceedings of the 14th World Conference on Earthquake Engineering, Beijing, China, October 12-17, 2008, International Association of Earthquake Engineering, Beijing, China.

United States Geological Survey (USGS) (2006). "Memphis Hazards Mapping Project," United States Geological Survey, Reston, Virginia.

URS Corporation (2001). "Comprehensive Seismic Risk and Vulnerability Study for the State of South Carolina," Internal Report, South Carolina Emergency Preparedness Division, West Columbia, South Carolina.

Viscusi, W. K. (1993). "The Value of Risks to Life and Health, Journal of Economic Literature," *Journal of Economic Literature*, Vol. 31, No. 4, pp. 1912-1946.

Wong, I., Bouabid, J., Graf, W., Huyck, C., Porush, A., Silva, W., Siegel, T., Bureau, G., Eguchi, R., and Knight, J. (2005). "Potential Losses in a Repeat of the 1886 Charleston, South Carolina Earthquake," *Earthquake Spectra*, Vol. 21, No. 4, pp. 1157-1184.

APPENDIX A – INVENTORY CLASSIFICATION NOMENCLATURE

This appendix contains descriptions of the structure and occupancy ID codes used in the text, figures, and tables in the main body of the paper. Table A.1 provides descriptions of the 10 structure types assigned by the neural network model for the study region building stock inventory (French and Muthukumar, 2006). Table A.2 defines the mappings used in this study to correlate the structure types in the building stock inventory with the structure types employed by HAZUS-MH MR2 (FEMA, 2006). The mappings in A.2 were required to establish which fragility parameters were considered to be appropriate for particular combinations of structure type and other inventory attributes, which were then used to define fragility functions for nonstructural building damage and retrofit performance. Table A.3 lists the occupancy categories employed in this study. The Tax Assessor's database included sufficient data so that a total of 86 detailed occupancy categories could be defined, but the level of detail provided in those cases was not necessary for the algorithms employed in this study. Therefore, only the selected 25 HAZUS-MH MR2 (FEMA, 2006) occupancy categories were employed in the study.

Table A.1. Structure Type Descriptions

General Structure Type ID	Structure Type Description	Code	Number	Percent
C	Concrete Moment Resisting Frame	C1	528	0.18%
	Concrete Frame with Concrete Shear Wall	C2	114	0.04%
	Concrete Tilt-up	PC1	1,078	0.37%
	Precast Concrete Frame	PC2	167	0.06%
S	Steel Frame	S1	612	0.21%
	Light Metal Frame	S3	6,668	2.28%
M	Reinforced Masonry	RM	2,586	0.88%
	Unreinforced Masonry	URM	6,302	2.15%
W	Light Wood Frame	W1	269,725	92.23%
	Commercial Wood Frame	W2	4,658	1.59%
Total			**292,438**	**100.00%**

Table A.2. Structure Type HAZUS – MAEViz Mappings

Structure Type Description	MAEViz Code	Number of Stories	Essential Facility	HAZUS Code
Concrete Moment Resisting Frame	C1	1-3	ANY	C1L
		4-7	ANY	C1M
		8+	ANY	C1H
Concrete Frame with Concrete Shear Wall	C2	1-3	ANY	C2L
		4-7	ANY	C2M
		8+	ANY	C2H
Concrete Tilt-up	PC1	ANY	ANY	PC1
Precast Concrete Frame	PC2	1-3	ANY	PC2L
		4-7	ANY	PC2M
		8+	ANY	PC2H
Steel Frame	S1	1-3	ANY	S1L
		4-7	ANY	S2M
		8+	ANY	S2L
Light Metal Frame	S3	ANY	ANY	S3
Reinforced Masonry	RM	1-3	NOT Schools (EFS1)	RM1L
		4-7	NOT Schools (EFS1)	RM1M
		1-3	Schools (EFS1)	RM2L
		4-7	Schools (EFS1)	RM2M
		8+	ANY	RM2H
Unreinforced Masonry	URM	1-2	ANY	URML
		3+	ANY	URMM
Light Wood Frame	W1	1	ANY	W1
		2+	ANY	W2
Commercial Wood Frame	W2	1	ANY	W1
		2+	ANY	W2

Table A.3. Occupancy Type Descriptions

General Occupancy ID	HAZUS Occupancy Type	HAZUS Occupancy Description	Number of Structures	Percent
AGR	AGR1	Agriculture	2	0.00%
COM	COM1	Retail Trade	3,885	1.33%
	COM2	Wholesale Trade	20	0.01%
	COM3	Personal and Repair Services	3,872	1.32%
	COM4	Professional/Technical Services	1,110	0.38%
	COM5	Banks	2,904	0.99%
	COM6	Hospital	173	0.06%
	COM7	Medical Office/Clinic	43	0.01%
	COM8	Restaurants and Bars	314	0.11%
	COM9	Theaters	965	0.33%
	COM10	Parking Garages	16	0.01%
EDU	EDU1	Education (Schools/Colleges)	143	0.05%
GOV	GOV1	General Government Services	17	0.01%
	GOV2	Emergency Services (Police/Fire/EOC)	18	0.01%
IND	IND1	Heavy Industrial	1,547	0.53%
	IND2	Light Industrial	502	0.17%
	IND3	Food/Drugs/Chemicals	21	0.01%
	IND4	Metals/Minerals Processing	37	0.01%
REL	REL1	Place of Worship	45	0.02%
RES	RES1	Single-family Residential	266,618	91.17%
	RES2	Mobile Home	24	0.01%
	RES3	Multi-family Residential	10,068	3.44%
	RES4	Temporary Lodging (Hotel/Motel)	10	0.00%
	RES5	Institutional Dormitory	4	0.00%
	RES6	Nursing Home	80	0.03%
Total			**292,438**	**100.00%**